NASA TECHNICAL MEMORANDUM

NASA TM X-1647

NASA TM X-1647

PERFORMANCE EVALUATION OF ATLAS-CENTAUR RESTART CAPABILITY IN EARTH ORBIT

Lewis Research Center
Cleveland, Ohio

NATIONAL AERONAUTICS AND SPACE ADMINISTRATION • WASHINGTON, D. C. • SEPTEMBER 1968

NASA TM X-1647

PERFORMANCE EVALUATION OF ATLAS-CENTAUR RESTART CAPABILITY IN EARTH ORBIT

Lewis Research Center
Cleveland, Ohio

NATIONAL AERONAUTICS AND SPACE ADMINISTRATION

For sale by the Clearinghouse for Federal Scientific and Technical Information
Springfield, Virginia 22151 – CFSTI price $3.00

ABSTRACT

The flight of Atlas-Centaur launch vehicle AC-9 on October 26, 1966 was the final flight in the Centaur research and development program. The vehicle carried a mass model of the Surveyor spacecraft. The mass model was boosted into a simulated lunar intercept trajectory using a parking-orbit mode of ascent. This mode of ascent placed the Centaur in a circular orbit. After coasting under low-gravity conditions, the Centaur main engines were restarted to supply energy to attain the proper simulated lunar intercept trajectory. This report includes a flight performance evaluation of the Atlas-Centaur systems for the total launch vehicle mission.

FOREWORD

The launching of an Atlas-Centaur-Surveyor requires the close team work of hundreds of scientists and engineers. The Centaur Project Office in the role of launch vehicle manager is responsible for the design, development, production, launching, and performance of the vehicle. This report describes one phase of the total activity - evaluation of the flight performance of Atlas-Centaur vehicle, AC-9. If the reader is interested in performance of previous Atlas-Centaur flights, the formal postflight reports published for these earlier missions should be consulted.

The material presented in this document reflects the close cooperation and efforts of the authors, staff supervisors, technical review committee members, and staff editors, all of whom are to be commended for their dedicated efforts.

Edmund R. Jonash
Manager, Centaur Project

CONTENTS

I. SUMMARY

The Atlas-Centaur vehicle AC-9 was successfully launched from Eastern Test Range Complex 36B on October 26, 1966 at 0612:02.6 hours eastern standard time. The launch vehicle carried a mass model of the Surveyor spacecraft. This 1750-pound (794-kg) model was injected into a 90-nautical-mile (167-km) parking orbit. The vehicle then coasted under low-gravity conditions for about 24 minutes. The Centaur engines then were restarted, and the Surveyor mass model was accurately placed in a simulated lunar transfer trajectory. This flight was the first to demonstrate successfully the restart of a cryogenic stage in Earth orbit.

The AC-9 flight was the final research and development flight in the Centaur program and the second of two vehicles designed to demonstrate the indirect (parking-orbit) mode of ascent. This capability increases the opportunity available for launch of lunar or interplanetary spacecraft. Another significant achievement of the flight was the completely successful control of the cryogenic propellants. Propellants were retained in a settled condition throughout the 24-minute, low-gravity coast period and fully supported restart of the main engines. A performance evaluation of the Atlas and Centaur vehicle systems in support of this flight is covered in this report.

II. INTRODUCTION

by John J. Nieberding

The flight of Atlas-Centaur vehicle AC-9 on October 26, 1966 was the final flight in the Centaur research and development program. It was the second of two vehicles designed to boost a mass model of the Surveyor into a simulated lunar intercept trajectory using an indirect (parking orbit) mode of ascent. This ascent mode included (1) launching the Centaur and the mass model into a nearly 90-nautical-mile (167-km), circular parking orbit, (2) coasting under low-gravity conditions, and (3) restarting the Centaur main engine (second burn) to supply the necessary energy to attain the proper simulated lunar intercept trajectory.

Centaur was first developed by the Convair Division of General Dynamics as a second stage for a modified Atlas D missile. Vehicles AC-1 to AC-6 were direct-ascent (one-burn) research and development flights. AC-7 and AC-10 followed as operational direct-ascent flights. The AC-8 and AC-9 vehicles were indirect-ascent research and development flights.

The development of the indirect, or two-burn, mode of ascent was undertaken to provide greater launch flexibility for certain missions than can be provided by the direct-ascent, or one-burn, mode. For example, direct-ascent lunar launches are restricted to the summer months. Indirect ascent permits launches every month of the year and allows more launch time on each available day.

The seventh Atlas-Centaur research and development vehicle, AC-8, was the first of two vehicles specifically assigned to support the Centaur indirect-ascent flight program. Launched on April 7, 1966, the flight of AC-8 successfully demonstrated the ability of several newly incorporated modifications to provide the propellant control during the coast phase essential for a Centaur main engine restart. However, the second firing of the main engines was not successful. A leak in the hydrogen peroxide system depleted the supply, required by the boost pumps, to support main engine operation. Extensive analysis resulted in corrective action for AC-9.

The overall objective of the AC-9 mission was to inject the Surveyor mass model into the proper, simulated lunar trajectory. A further requirement was to verify the overall function of the inertial guidance system, including its ability to provide proper discretes and steering signals to the Atlas and Centaur flight control systems for an indirect-ascent mission. This report presents a final evaluation of the AC-9 vehicle system performance.

III. LAUNCH VEHICLE DESCRIPTION

by Eugene E. Coffey

The Atlas-Centaur AC-9 was a two-stage launch vehicle consisting of an Atlas first stage and a Centaur second stage. Both stages were 10 feet (3.05 m) in diameter and were connected by an interstage adapter. The composite vehicle was 113 feet (34.44 m) in length and weighed 303 000 pounds (137 000 kg) at lift-off. The basic structure of the Atlas and the Centaur stages utilized thin-wall, pressurized, main propellant tank sections of monocoque construction.

The first-stage Atlas vehicle, shown in figure III-1, was 65 feet (19.81 m) long. It was powered by a standard Rocketdyne MA-5 propulsion system that provided 389 000 pounds (1730.27×10^3 N) of thrust at lift-off. This system consisted of two booster engines with a total thrust of 330 000 pounds (14.7×10^5 N), a single sustainer engine of 57 000 pounds (25.4×10^4 N) of thrust, and two small vernier engines of 1000 pounds (4.5×10^3 N) of thrust each. All engines burned liquid oxygen and kerosene (RP-1) and were ignited simultaneously on the ground. The booster engines were gimbaled for roll and directional control during the booster phase of the flight. This phase was completed when the vehicle acceleration equaled 5.7 ± 0.08 g's and the booster engines were cut off. The booster engines were jettisoned 3.5 seconds after booster engine cutoff. The sustainer and the vernier engines continued to burn after booster engine cutoff for the Atlas sustainer phase of the flight. During this phase, the sustainer engine was gimbaled for directional control only while the vernier engines were gimbaled for roll control only. The sustainer and vernier engines burned until propellant depletion, which terminated the sustainer phase. The Atlas was then separated from the Centaur by the firing of a shaped-charge severance system. The firing of a retrorocket system, to back the Atlas and the interstage adapter away from the Centaur, completed the separation of these stages. Other major systems of the Atlas first stage included flight control, structures, separation, propellant utilization, telemetry and instrumentation, range safety command (vehicle destruct), and electrical.

The second-stage Centaur vehicle is shown in figure III-2. This stage, including the nose fairing, is 48 feet (14.63 m) long. Centaur is a high-performance stage (specific impulse, 443 sec). It is powered by two Pratt & Whitney YRL-10A-3 engines which generated a total thrust of 30 000 pounds (133.45×10^3 N). These engines burn liquid hydrogen and liquid oxygen. The Centaur main engines are gimbaled to provide directional and roll control during Centaur powered flight. Fourteen hydrogen peroxide engines of various thrust levels provide thrust for attitude control, propellant settling and retention, and vehicle reorientation. The Centaur hydrogen tank is insulated with four 1-inch- (2.54-cm-) thick panels. These panels consist of glass fabric lamination

with a polyurethane foam core. A fiberglass nose fairing is used to provide an aerodynamic shield for the spacecraft mass model, guidance equipment, and electronic packages during ascent. The insulation panels and nose fairing are jettisoned during the Atlas sustainer phase. Additional major systems of the Centaur include the flight control, structures, separation, propellant utilization, telemetry and instrumentation, range safety command (vehicle destruct), C-band radar tracking beacon, inertial guidance, and electrical.

The AC-9 vehicle was designed for indirect-ascent trajectory. As such, the hydrogen tank was equipped with a slosh baffle and energy-dissipating devices on the propellant return lines to inhibit disturbances in the liquid propellants at engine shutdown. Suppression of liquid disturbance after main engine first cutoff and the retention of the liquid propellants during the low-gravity coast period were provided by continuous thrust from the hydrogen peroxide engines.

AC-9 was similar to AC-8 (see ref. 1) in that both were designed and developed to demonstrate indirect-ascent mission capability.

The major systems, as they were configured for the Atlas-Centaur launch vehicle AC-9, are delineated in the subsequent sections of this report.

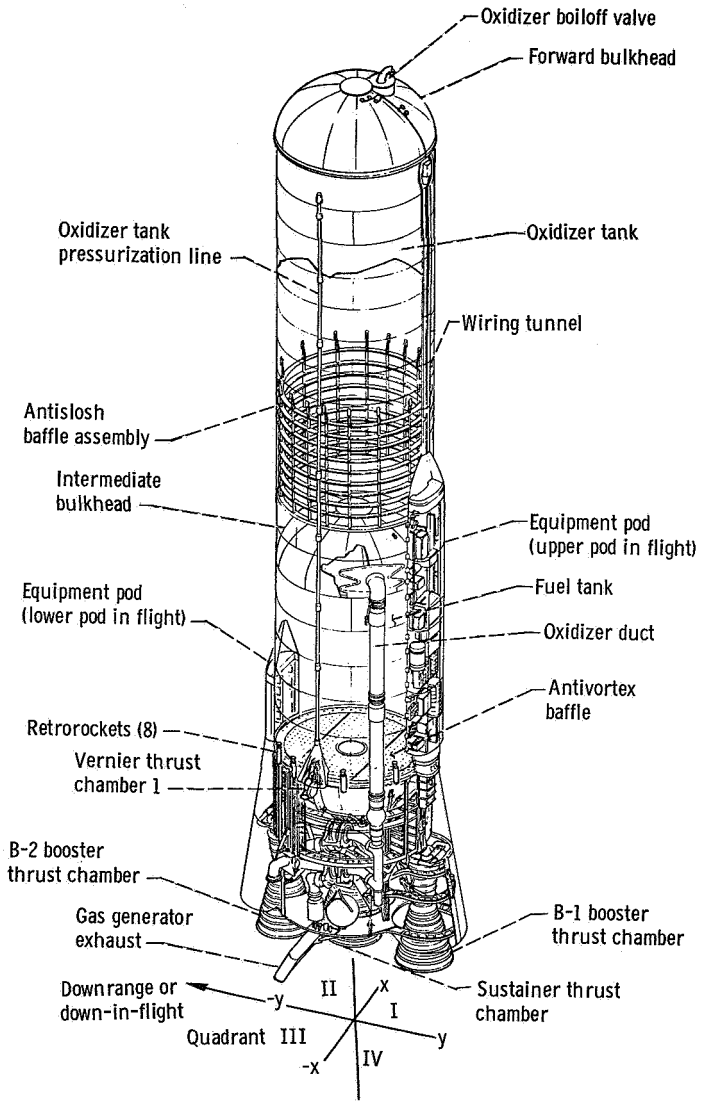

Figure III-1. - General arrangement of Atlas launch vehicle, AC-9.

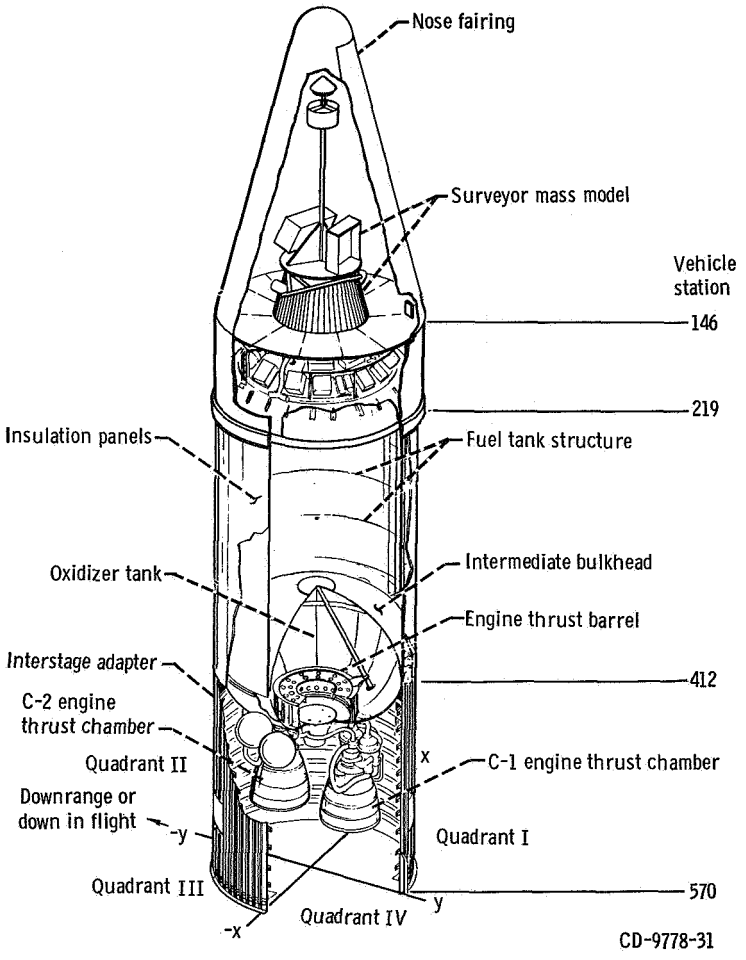

Figure III-2. - General arrangement of Centaur vehicle, AC-9.

IV. MISSION PERFORMANCE

by William A Groesbeck

The Atlas-Centaur vehicle AC-9, carrying a 1750-pound (794-kg) mass model of the Surveyor, was launched from Eastern Test Range Complex 36B on October 26, 1966 at 0612:02.6 hours eastern standard time. The flight successfully achieved the programmed objective by placing the Centaur and mass model of Surveyor into a nearly 90-nautical-mile (167-km) parking orbit, coasting for 24 minutes, restarting main engines, and injecting the mass model into the planned simulated lunar-transfer orbit.

A compendium of the AC-9 mission profile and the simulated lunar transfer trajectory are shown in figures IV-1 and IV-2. For reference also, a listing of the atmospheric sounding data, trajectory data, launch windows and countdown history, Centaur postflight weight summary, Atlas postflight weight summary, comparison of preflight and actual event times, are presented in appendix A. The Centaur performance calculations are given in appendix B.

ATLAS FLIGHT PHASE

Atlas engine ignition and thrust buildup were normal, and the vehicle lifted off (T + 0 sec) with a combined vehicle weight of 303 000 pounds (137 000 kg). Two seconds after lift-off, the vehicle began a programmed roll from the fixed launcher azimuth of 115^{o} to the required flight azimuth of 99.69^{o}. At T + 15 seconds, the vehicle began a preprogrammed pitchover maneuver which lasted through booster engine cutoff. Guidance-generated steering commands were issued after this time.

The preset Atlas pitch program used to steer the vehicle during the booster phase of flight was augmented for the first time by supplemental pitch and yaw inputs which acted to reduce vehicle bending loads due to wind. This supplemental program, one of a series selected on the basis of prelaunch upper air soundings, was stored in the airborne computer. The incremental values were algebraically summed with the fixed program stored in the Atlas programmer. With this modified pitch program, the maximum engine gimbal angle required to control the vehicle during the atmospheric ascent was only 2.36^{o} or 50 percent of the control capability.

Vehicle acceleration during the boost phase was normal. Centaur guidance properly issued the booster engine cutoff signal (at T + 143.1 sec) when the vehicle acceleration reached 5.68 g's. About 3.5 seconds later, the Atlas programmer issued the staging command to separate the booster engine stage from the vehicle. Staging transients were negligible, and momentary vehicle rate excitation in pitch, yaw, or roll did not exceed 1.76 degrees per second.

Vehicle steering by the inertial guidance system was initiated about 4 seconds following Atlas booster staging. At the start of guidance steering, slight errors due to differences in vehicle attitude and the desired steering vector required corrections of about 13^{o} nose up in pitch and about 1^{o} nose right in yaw. These corrections were completed in about 9 seconds. The guidance system then issued commands to continue the pitch-over maneuver during the Atlas sustainer phase.

The insulation panels were jettisoned during the sustainer phase at T + 177.3 seconds. The shaped-charge separation system functioned normally and the panels fell away from the vehicle. The nose fairing unlatch command was given at T + 203.3 seconds, and the thruster bottles, firing 0.5 second later, rotated the fairing halves away from the vehicle. Vehicle angular rates due to the jettisoning of the insulation panels and nose fairing were negligible. Maximum rates in pitch yaw or roll did not exceed 1.4 degrees per second.

Sustainer and vernier engine performance was normal for about 60 seconds into the sustainer flight phase. Engine performance then started to deteriorate, and the engines shut down about 7 seconds early at T + 229.1 seconds. This earlier-than-expected shutdown was caused by a helium leak which developed in the vernier oxygen bleed valve at booster engine cutoff. Because of this leak, the reference pressure to the sustainer gas generator liquid oxygen regulator gradually dropped below the regulator range. In turn, the liquid oxygen flow to the gas generator was reduced; the turbopumps slowed; and the propellant supply pressures decreased and activated the propellant depletion pressure switches located in the fuel injector manifold. This was the normal method for engine shutdown except that it was earlier than expected. At engine shutdown, the vehicle had accelerated to an Earth-referenced velocity of 11 235 feet per second (3425 m/sec).

Coincident with sustainer engine cutoff, the guidance steering commands to flight control were discontinued, and the vehicle was allowed to coast in a noncontrolled flight mode. Steering commands were discontinued to prevent gimbaling of the Centaur engines under nonthrusting conditions and to allow the engines to be centered to maintain clearance between the engines and the interstage adapter during staging.

The Atlas staging command from the flight programmer was given at T + 231.0 seconds and the shaped charge was fired separating the two vehicles. Eight retrorockets on the Atlas then fired to push the Atlas stage away from the Centaur. Staging transients were negligible, and the maximum angular rate imparted to the vehicle was 2.6 degrees per second in roll.

CENTAUR FLIGHT PHASE

Centaur Main Engine First Firing

Centaur stage boost pumps were started prior to sustainer engine cutoff and were operated in a recirculating mode until main engine prestart. To maintain the required net positive suction pressure at the boost pump inlets, during the near-zero-gravity period from sustainer engine cutoff until main engine start, propellant tank pressures were increased by injection of helium gas into the ullage. Ullage pressures were increased 1.10 psi (0.76 N/cm^2) in the hydrogen tank and 10.3 psi (7.1 N/cm^2) in the oxygen tank.

Eight seconds prior to main engine start, the Centaur programmer issued preparatory commands for main engine firing. Engine pump inlet valves were opened to allow liquid propellants to flow through the lines and chill down the engine turbopumps. Chilldown of the turbopumps ensured against cavitation during pump acceleration and made possible a uniform and rapid thrust buildup after engine ignition. The ignition command was given by the flight control programmer at T + 240.5 seconds, and engine thrust increased to full flight levels within 2 seconds.

Guidance steering for the Centaur stage was initiated at T + 244.5 seconds, after the engine thrust was fully established. No guidance steering commands were permitted during the main start sequence to prevent excessive vehicle angular rates induced by correction of vehicle position errors. During this interval, angular rates induced by staging and engine start transients resulted in only a slight vehicle drift off the steering vector. This attitude drift was corrected within 4 seconds after start of guidance steering. Through the remainder of the Centaur engine firing period, the guidance steering commands provided the required pitchdown rate to attain the injection velocity vector. At T + 577.7 seconds the required injection velocity was attained and the engines were shut down. The Centaur engine firing time was about 10 seconds longer than predicted. The longer burn time was necessary to compensate for the early sustainer engine shutdown and also a slightly lower-than-expected Centaur engine thrust. Orbital insertion at an altitude of 90 nautical miles (167 km) occurred approximately 1200 nautical miles (2220 km) southeast of Cape Kennedy at a velocity of 24 148 feet per second (7360 m/sec).

The propellant utilization system performed normally during the first engine firing sequence. At main engine first cutoff, the liquid level in the hydrogen tank was at station 331, with about 1365 pounds (620 kg) of residual liquid hydrogen. The liquid level in the oxygen was at station 426, with about 6420 pounds (2910 kg) of residual liquid oxygen.

Centaur Coast Phase

At main engine cutoff, the vehicle began a 24-minute orbital coast. Guidance generated steering commands to the flight control system were discontinued at this time, but vehicle attitude control was maintained by the hydrogen peroxide attitude control system. Coincident with main engine first cutoff, two of the four 50-pound (222-N) thrust engines were fired for 76 seconds. This provided 100 pounds (444 N) of thrust, or an acceleration of 7×10^{-3} g's, to settle the residual propellants and to suppress any disturbances of the liquids induced by the main engine cutoff transient.

Excursions of the liquid hydrogen in the tank caused by the engine shutdown transient were small. Energy-dissipation devices, including slosh baffles and energy-dissipating diffusers on return flow lines into the tank, restricted the forward movement of the liquid to about 15 inches (38.1 cm) above the normally settled liquid surface. After about 20 seconds, the liquid was resettled, and it remained quiescent throughout the remainder of the coast phase. After 76 seconds of coast, the thrust level was reduced to 6 pounds (26.7 N), or an acceleration of 4×10^{-4} g's.

Attitude control of the vehicle through the coast phase was normal. Roll torques caused by jet exhaust impingement (from the 50-lb (222-N) thrust engines) against the main engine were again noted, as experienced previously on the AC-8 flight (see ref. 1). These disturbances were well within the capability of the attitude control system. Hydrogen tank venting started after 300 seconds of coast as tank pressures increased to the regulating range of the primary valve. Tank pressures were regulated normally, and there was no indication of liquid entrainment during venting. The balanced thrust vent system performance was satisfactory, as there was no evidence of the vent gasses producing torques on the vehicle.

Forty seconds prior to engine restart, the thrust level on the vehicle was increased again to 100 pounds (444 N) by firing two of the 50-pound (222-N) thrust hydrogen peroxide engines. The tank vent valves were also closed and the propellant tank pressures were increased by injecting helium gas into the ullage. Twenty-eight seconds prior to engine restart, the propellant boost pumps were started, and 11 seconds later the engine prestart valves were opened to allow propellants to flow through the lines and chill down the engine turbopumps.

Centaur Main Engine Second Firing

The Centaur engines were successfully restarted at T + 2034.7 seconds, and engine performance was normal throughout the main engine second firing. Coast phase attitude control was terminated at engine restart, and 4 seconds later, Centaur guidance steering was resumed to steer the vehicle toward the required velocity vector. The

propellant utilization system performed normally in controlling propellant consumption for minimum residuals.

At T + 2140.9 seconds, after a firing period of 106 seconds, the required guidance-computed velocity for the lunar-transfer orbit was attained and the engines were shut down. Burnable propellants remaining were sufficient for about 5 more seconds of engine firing. This indicated an adequate propellant reserve and satisfactory vehicle performance.

SPACECRAFT SEPARATION

Coincident with main engine second cutoff, the guidance-generated steering commands were temporarily discontinued, and the hydrogen peroxide attitude control system was again activated. Angular rates imparted to the vehicle by engine shutdown transients were small and were quickly damped to less than the control threshold of 0.2 degree per second. The residual vehicle motion below the rate threshold allowed only a negligible drift in vehicle attitude. This drift did not interfere with the subsequent spacecraft separation.

The Centaur and mass model of Surveyor coasted under near-zero-gravity conditions for about 70 seconds. This coast allowed for canceling out any residual vehicle rates in preparation for the spacecraft separation. Commands were given by the Centaur programmer to the spacecraft mass model to turn on the spacecraft high-power transmitter and to arm spacecraft separation pyrotechnics. Commands were also given to simulate extending landing gear and omniantennas. All commands were received by the spacecraft.

Spacecraft separation was commanded at T + 2210.8 seconds. The hydrogen peroxide attitude control system was turned off, the pyrotechnically operated latches were fired, and the separation springs pushed the mass model away from the Centaur. Separation velocity was about 0.75 foot per second (0.228 m/sec), and full extension of all three springs occurred nearly simultaneously. As a result, angular rates imparted to the mass model after separation were small and did not exceed 0.5 degree per second. This rate was well below an established allowable of 3.0 degrees per second.

CENTAUR RETROMANEUVER

The Centaur vehicle was commanded to turn around and perform a retrothrust maneuver after spacecraft separation. This type of maneuver on an operational (Surveyor) spacecraft is necessary (1) to increase the separation distance in order to

eliminate the possibility of the Surveyor star sensor acquiring the reflected light from Centaur rather than the star Canopus, and (2) to avoid impact of the Centaur on the lunar surface.

The guidance steering vector selected for the turnaround was the reciprocal of the velocity vector at main engine second cutoff. The turnaround was commanded 5 seconds after spacecraft separation. The guidance system accounted for any vehicle drift after main engine cutoff by the steering commands which rotated the vehicle in the shortest arc from its actual position to the new vector. Angular rates during the turnaround were limited, for structural considerations, to a maximum of 1.6 degrees per second.

About halfway through the turnaround at T + 2251 seconds, two 50-pound (222-N) thrust hydrogen peroxide engines were fired for 20 seconds to impart lateral as well as additional longitudinal separation from the spacecraft. The lateral separation was necessary to minimize the impingement of frozen propellant particles on the spacecraft during the subsequent discharge of residual Centaur propellants through the main engines. While the 50-pound (222-N) thrust engines were firing, the exhaust plumes produced large impingement forces on the vehicle causing a clockwise roll disturbing torque. To correct this disturbing roll torque, the 3.5-pound (15.5-N) thrust hydrogen peroxide attitude control engines were required to operate 50 percent of the time.

The turnaround maneuver was completed at T + 2310 seconds after rotating the vehicle through 167^{o}. Once the retrovector was acquired, the attitude control maintained the vehicle position on the vector within 1.5^{o}.

At T + 2451 seconds, the retrothrust portion of the retromaneuver was commanded by the Centaur programmer. The main engines were gimbaled to aline the thrust vector with the newly acquired steering vector, the engine prestart valves were opened, and residual propellants were discharged through the engines. The propellant discharge provided sufficient thrust to alter the Centaur trajectory in order to avoid impact on the simulated lunar target and to increase Centaur-Surveyor separation distance. The relative separation distance between the spacecraft and the Centaur at the end of 5 hours was 1194 kilometers. This distance was more than 3.5 times an established minimum requirement.

At completion of the retromaneuver at T + 2701 seconds, the hydrogen and oxygen tank vent valves were enabled to the normal regulating mode. A postmission experiment was then conducted to determine the amount of hydrogen peroxide remaining. Two of the 50-pound (222-N) thrust engines were fired until the hydrogen peroxide was depleted about 40 seconds later.

SURVEYOR MASS MODEL TRANSIT PHASE

The Surveyor mass model was accurately injected into a simulated lunar-transfer orbit, as shown in figure IV-2, and would have impacted the imaginary Moon position without further trajectory correction. The simulated trajectory was chosen to prevent an actual lunar impact. The injection accuracy was such that a midcourse correction of only 6.5 meters per second for miss only, and 7.5 meters per second for miss-plus-time-of-flight errors, would have been required to impact the selected aiming point. This injection accuracy would have been well within the 50-meter-per-second midcourse-correction capability of the Surveyor spacecraft. The mass model of the Surveyor was about 400 pounds (181 kg) lighter than an actual Surveyor, but this weight difference was more than offset by the added instrumentation weight on the Centaur.

The Atlas-Centaur flight of AC-9 was considered a complete success. The flight demonstrated the capability of Centaur to place an operational Surveyor spacecraft in a lunar orbit by an indirect mode of ascent.

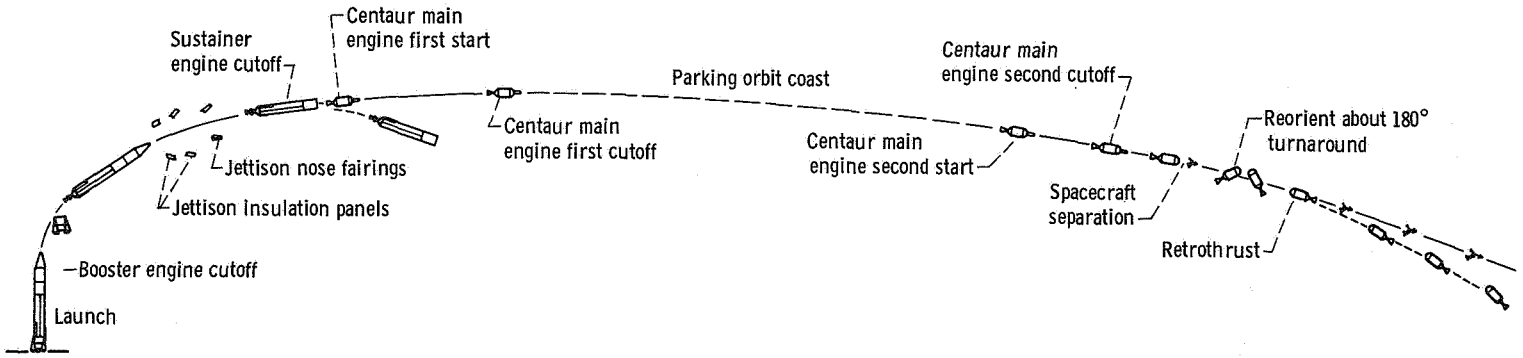

Figure IV-1. - Atlas-Centaur flight compendium for indirect-ascent mode, AC-9.

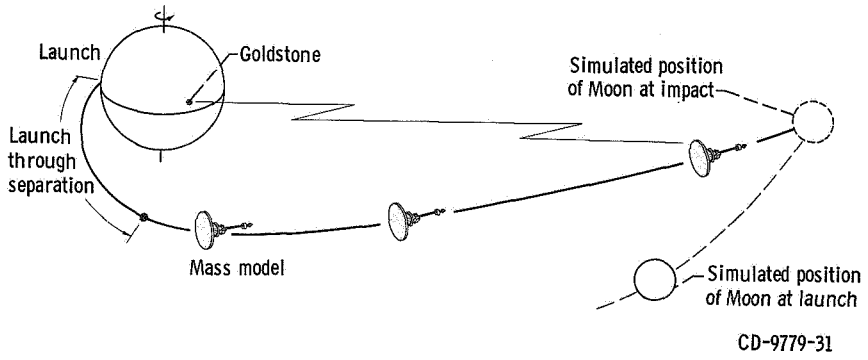

Figure IV-2. - Simulated Earth-Moon trajectory of Surveyor mass model, AC-9.

V. LAUNCH VEHICLE SYSTEM ANALYSIS

PROPULSION SYSTEMS

by Steven V. Szabo, Jr., Ronald W. Ruedele,
Kenneth W. Baud, and Donald B. Zelten

Atlas

System description. - The Rocketdyne MA-5 system utilized by the Atlas consisted of a booster engine system, a sustainer engine system, a vernier engine system, an engine start system, a logic control subsystem, and an electric subsystem. The systems are shown schematically in figure V-1.

All engines were the single-start type, using liquid oxygen as the oxidizer and kerosene (RP-1) as the fuel cartridges. The pyrophoric fuel preceded the RP-1 into the combustion chambers and initiated ignition by reacting with the liquid oxygen. Combustion was then sustained by the RP-1 and liquid oxygen. All thrust chambers were regeneratively cooled with RP-1. The rated thrust values of the engines are given in the following table:

Engine	Number of chambers	Thrust	
		lb	N
Booster	2	332 000	14.7×10^5
Sustainer	1	57 000	25.4×10^4
Vernier	2	2 000	9×10^3

The booster engine system consisted of two gimbaled thrust chambers and a common power package consisting of a gas generator and two turbopumps, and a supporting control system. The sustainer engine was a gimbaled engine assembly consisting of a thrust chamber, gas generator, turbopump, and supporting control system. The two vernier engines consisted of thrust chambers, propellant valves, gimbal bodies, and mounts. The self-contained engine start system consisted of an oxidizer start tank, a fuel start tank, and the associated controls.

System performance. - Engine start and thrust buildup transients were normal, and engine operation was satisfactory up to booster engine jettison. However, during the sustainer flight, engine performance was not normal, and engine shutdown occurred about 7 seconds earlier than expected.

At booster engine jettison, an abrupt decrease in chamber pressure occurred on both vernier engines. The number 1 vernier engine chamber pressure dropped 32 psi (22 N/cm^2) and the number 2 vernier chamber pressure dropped 17 psi (12 N/cm^2). At this time, the sustainer engine helium control bottle pressure began to decay sharply (see PNEUMATIC SYSTEMS section) indicating a leak in the pneumatic system. The helium leak has been attributed to a broken line supplying closing pressure to a vernier liquid-oxygen bleed valve. This allowed the bleed valve to be partly open, resulting in a decrease in the vernier engine chamber pressures.

The partial opening of the vernier liquid-oxygen bleed valve further affected engine

TABLE V-1. - ATLAS ENGINE SYSTEM PERFORMANCE, AC-9

Engine parameter	Flight time, sec		
	T + 10	Booster engine cutoff, T + 143.1	Sustainer engine cutoff, T + 229.1
Number 1 booster engine:			
Chamber pressure (absolute), psi; N/cm^2	564; 388	568; 391	----------
Pump speed, rpm	6 281	6 252	----------
Oxidizer pump inlet pressure (absolute), psi; N/cm^2	57.5; 40	79; 54	----------
Fuel pump inlet pressure (absolute), psi; N/cm^2	70; 48	54; 37	----------
Number 2 booster engine:			
Chamber pressure (absolute), psi; N/cm^2	562; 387.2	(a)	----------
Pump speed, rpm	6 160	6 230	----------
Oxidizer pump inlet pressure (absolute), psi; N/cm^2	58; 40	82; 57	----------
Fuel pump inlet pressure (absolute), psi; N/cm^2	69; 48	54; 37	----------
Booster gas generator:			
Combustion chamber pressure (absolute), psi; N/cm^2	526; 362	529; 364	----------
Booster liquid oxygen regulator reference pressure (absolute), psi; N/cm^2	639; 440	639; 440	----------
Sustainer:			
Chamber pressure (absolute), psi; N/cm^2	688; 474	678; 467	566; 390
Pump speed, rpm	10 080	9 958	<9 000
Oxidizer injector manifold pressure (absolute), psi; N/cm^2	791; 550	816; 562	649; 447
Fuel pump discharge pressure (absolute), psi; N/cm^2	920; 634	942; 649	790; 544
Oxidizer regulator reference pressure (absolute), psi; N/cm^2	811; 559	806; 555	629; 433
Gas generator discharge pressure (absolute), psi; N/cm^2	608; 419	608; 419	487; 336
Fuel pump inlet pressure (absolute), psi; N/cm^2	68; 46.8	63; 43.4	43; 29.6
Oxidizer pump inlet pressure (absolute), psi; N/cm^2	64; 44	85; 59	41; 28
Oxidizer pump inlet temperature, ^oF, ^oK	-284; 102	-281; 99	-281; 99
Number 1 vernier chamber pressure (absolute), psi; N/cm^2	347; 239	347; 239	283; 195
Number 2 vernier chamber pressure (absolute), psi; N/cm^2	346; 238	350; 241	297; 205

[a]No data

performance by causing a reduction in the sustainer gas generator liquid-oxygen regulator reference pressure. The reference pressure dropped below the normal regulator range and thereby caused a decrease in the liquid-oxygen flow to the gas generator. The reduced flow to the gas generator decreased the energy to the pump turbine and slowed down the turbopump. The pump slowdown caused the fuel discharge pressure to drop. When the pressure in the fuel injector manifold decreased to the range of the pressure switches, the switches initiated engine shutdown. Engine shutdown occurred at T + 229.1 seconds and was 7 seconds earlier than expected. This shutdown time, however, was within the predicted limits of T + 235.8 plus 9.6 minus 9.2 seconds and the successful completion of the flight was not compromised.

Engine system flight measurements near sustainer engine cutoff are shown in figure V-2. All the parameters, with the exception of the sustainer turbopump speed and liquid-oxygen pump inlet pressure, are characteristic of a normal engine shutdown by oxygen depletion. The sustainer turbopump speed, however, exhibited a marked decrease, and the sustainer liquid-oxygen pump inlet pressure remained nearly constant, as is characteristic of a fuel depletion shutdown. A liquid-oxygen depletion shutdown increases pump speed and sharply decreases liquid-oxygen pump inlet pressure.

Significant propulsion system data are summarized in table V-1. With the exception of the early sustainer engine shutdown and decrease in vernier engine chamber pressure, all other engine system measurements indicated satisfactory operation.

Centaur Main Engines

System description. - Two Pratt & Whitney YRL10A-3-3 engines were used to provide thrust for the Centaur stage. A schematic drawing of the Centaur main engine is shown in figure V-3. Each was a regeneratively cooled and turbopump-fed engine with a single thrust chamber. Engine rated thrust was 15 000 pounds (66.7×10^3 N) at an altitude of 200 000 feet (61 000 m). Propellants were liquid oxygen and liquid hydrogen injected at a nominal oxidizer to fuel mixture ratio of 5.0 to 1. Rated engine thrust was achieved at a design combustion chamber absolute pressure of 400 psi (275.5 N/cm^2). The thrust chamber nozzle expansion area ratio was 57 with a nominal specific impulse of 444 seconds.

These engines used a unique bootstrap process. Pumped fuel, after cooling the thrust chamber, was expanded through the turbine to rotate the propellant pumps. The fuel was then injected into the combustion chamber. The pumped oxidizer was supplied directly to the propellant injector through the propellant utilization valve. This valve controlled the propellant mixture ratio supplied to the thrust chamber.

Thrust control was achieved by regulating the amount of fuel bypassed around the turbine as a function of combustion chamber pressure. The turbopump speed varied thereby controlling engine thrust. Ignition was accomplished by a spark igniter recessed in the propellant injector face. Starting and stopping were controlled by pneumatic valves. Helium pressure to these valves was supplied through engine mounted solenoid valves which were controlled by electrical signals from the flight programmer.

System performance. - An engine chilldown sequence of 8.0 seconds duration was initiated immediately prior to first main engine start to ensure adequate precooling of the engine turbopumps. Main engine start was commanded at T + 240.5 seconds. Engine thrust chamber pressures during the first engine start transient are presented in figure V-4. Engine acceleration times to 90 percent of rated thrust were 1.42 seconds for the C-1 engine and 1.60 seconds for the C-2 engine. Total impulse from engine start to start plus 2 seconds was calculated to be 9640 pound-seconds (43 000 N-sec) for the C-1 engine and 8780 pound-seconds (39 300 N-sec) for the C-2 engine. The differential of 860 pound-seconds (3820 N-sec) between engines was well within previous experience.

Liquid hydrogen and liquid oxygen pump inlet pressure and temperature data for the first 90 seconds of main engine operation are presented in figures V-5 to V-8. The pump inlet pressures remained well above saturation during this time period. The margin between the steady-state operating limit and the actual inlet conditions ensured satisfactory values of net positive suction pressure.

Steady-state operating conditions for the first firing are summarized and compared with corresponding predicted values in table V-2. The C-1 chamber pressure was approximately 11 psi (7.6 N/cm^2) below that of the engine acceptance test. This would correspond to a calculated decrease in thrust of approximately 420 pounds (1870 N). A slight decrease in all system pressures downstream of the turbopump, accompanied by a decrease in turbopump speed and an increase in fuel turbine inlet temperature, substantiated a shift in engine performance. The data also indicated that the decrease in thrust was caused by the engine thrust controller.

A thorough review was conducted to determine the cause for the thrust controller performance shift. This investigation revealed that the engines used on AC-9 had been subjected to a thrust control contamination inspection following the final acceptance tests. It is believed that this inspection caused the performance shift. A series of tests was conducted following this flight to determine the effects of repeated disassemblies for inspection. These tests were conducted with different combinations of thrust control housings and metering orifices (the type which had been removed during the contamination inspection). Certain combinations, when assembled with varying levels of installation torque, resulted in performance shifts comparable to that noted on AC-9.

Main engine performance in terms of thrust, specific impulse, and mixture ratio is presented in figures V-9 and V-10. Figures V-9 and V-10 describe engine perform-

TABLE V-2. - DATA SUMMARY FOR MAIN ENGINE FIRST FIRING, AC-9

Parameter	Range of expected values	Time from main engine start, sec					
		90		200		335	
		Engine					
		C-1	C-2	C-1	C-2	C-1	C-2
Fuel pump:							
Total inlet pressure (absolute), psi; N/cm^2	37.3 to 17.2; 25.7 to 11.9	30.8; 21.2	31.3; 21.6	29.5; 20.3	30.0; 20.7	26.8; 18.5	26.8; 18.3
Inlet temperature, ^oR, ^oK	43.0 to 37.4; 23.9 to 20.8	38.6; 21.4	38.8; 21.6	38.2; 21.2	38.2; 21.2	37.3; 20.7	37.2; 20.7
Oxidizer:							
Pump total inlet pressure (absolute), psi; N/cm^2	77.9 to 52.2; 53.7 to 36.0	63.1; 43.5	63.6; 43.9	62.9; 43.4	65.5; 45.2	65.3; 45.0	63.8; 44.0
Pump inlet temperature, ^oR, ^oK	183.8 to 172.0; 102.1 to 95.6	176.7; 98.2	176.5; 98.1	176.0; 97.8	176.1; 97.8	174.8; 97.1	175.0; 97.2
Pump speed, rpm	[a]12 005±183	11 890	12 080	11 993	12 092	11 878	12 042
Fuel venturi upstream pressure (absolute), psi; N/cm^2	[a]724±17; 499.2±11.7	709.9; 489.5	727.4; 501.5	719.0; 495.7	731.5; 504.4	718.1; 495.1	731.0; 504.0
Fuel turbine inlet temperature, ^oR, ^oK	[a]361.0±21.0; 200.6±11.7	376.7; 209.3	374.8; 208.2	363.4; 201.9	365.4; 203.0	364.9; 202.7	361.1; 200.6
Oxidizer Injector differential pressure, psi; N/cm^2	[a]54±26.3; 37.2±18.1	46.9; 32.3	50.3; 34.7	43.6; 30.1	46.6; 32.1	46.0; 31.7	46.6; 32.1
Engine chamber pressure (absolute), psi; N/cm^2	[a]392±4; 270.2±2.8	381.4; 263.0	389.2; 268.3	382.5; 263.7	392.8; 270.8	384.4; 265.0	392.9; 270.9
Fuel pump discharge pressure (absolute), psi; N/cm^2	[a]964±18; 664.6±12.4	943.3; 650.4	966.4; 666.3	958.1; 660.6	961.5; 662.9	964.2; 664.8	966.5; 666.4
Oxidizer pump discharge pressure (absolute), psi; N/cm^2	[a]571±26; 393.7±17.9	573.8; 395.6	573.1; 395.1	577.0; 397.8	578.1; 398.6	579.3; 399.4	573.9; 399.1

[a]Expected value with nominal inlet conditions and nulled propellant utilization valve angle.

ance for the entire flight based on the Pratt & Whitney characteristic velocity (C*) iteration technique. An explanation of this technique is given in appendix B.

Main engine first cutoff was commanded at T + 577.7 seconds. The engine thrust decay appeared normal. Vehicle cutoff impulse was calculated to be 3110 pound-seconds (13 820 N-sec). This value compares favorably with the predicted value of 3175±175 pound-seconds (14 110±779 N-sec).

Main engine first firing was 337.2 seconds duration compared with a predicted value of 326.9 seconds. Approximately 4.2 seconds of the time difference was attributed to the early Atlas sustainer engine shutdown. Low thrust of the C-1 engine accounted for an additional 4.6 seconds. The remaining 1.5 seconds are unaccounted for but are well within the allowable tolerance. The firing time dispersion is plus 9.6 and minus 9.2 seconds from the predicted value.

The C-1 engine fuel pump inlet pressure measurement failed to return to zero following main engine first cutoff. All values of the C-1 engine fuel pump inlet pressure recorded during the coast phase and during the second main engine firing were approximately 13 psi (57.9 N/cm^2) higher than expected. A transient pressure peak, exceeding the transducer range, normally occurs during engine shutdown. It is believed that this pressure surge permanently deformed the transducer wiper arm.

Fuel and oxidizer pump housing and fuel turbine inlet temperatures for the entire flight are presented in figures V-11 to V-13. Temperature trends immediately following main engine first cutoff are compared with those following main engine second cutoff in table V-3. The higher warming rates following main engine first cutoff are considered to be the result of jet impingement from the exhaust of the 50-pound (222-N) hydrogen peroxide engines. These engines fired for the 76-second period immediately following main engine first cutoff. Data obtained from comparable measurements on the AC-8 flight are also presented in table V-3 for purposes of comparison. AC-9 represented a near-maximum heating condition because of a daytime launch, whereas AC-8 represented a minimum heating condition because of a night launch.

Engine pump inlet temperatures prior to main engine second start are presented in figure V-14. The oxidizer temperature at the C-1 pump inlet indicated liquid following actuation of the 50-pound (222-N) thrust hydrogen peroxide engines at main engine second start minus 40 seconds. The temperature at the C-2 pump inlet indicated liquid prior to actuation of the 50-pound (222-N) thrust engines. Both temperatures went off scale high temporarily prior to main engine prestart. This was caused by high heat input from the boost pump combined with low oxidizer outflow from the tank. The hydrogen temperatures at both pump inlets indicated liquid within 2 seconds following the initiation of main engine prestart. These data indicated that the propellant feed ducts were chilled satisfactorily prior to main engine second start.

TABLE V-3. - TEMPERATURE TRENDS FOLLOWING CENTAUR MAIN ENGINE CUTOFF, AC 9

Flight	Event	Temperature, ^{o}R, ^{o}K							
		Fuel pump housing		Oxidizer pump housing		Fuel turbine inlet		Thrust chamber jacket	
		Engine							
		C-1	C-2	C-1	C-2	C-1	C-2	C-1	C-2
AC-8	Main engine first cutoff:								
	Main engine cutoff	40.0; 22.2	71.0; 39.4	211.0; 117.2	181.0; 100.6	219.7; 122.0	224.5; 124.8	148.2; 82.4	140.3; 78.0
	Main engine cutoff + 76 sec	90.0; 50.0	82.0; 45.5	285.0; 158.2	160.0; 88.9	206.0; 113.4	206.0; 113.4	212.0; 117.9	218.7; 121.7
AC-9	Main engine first cutoff:								
	Main engine cutoff	58.1; 32.2	88.0; 48.9	198.5; 110.1	208.0; 115.6	374.3; 208.0	370.3; 205.9	176.6; 98.0	178.6; 99.1
	Main engine cutoff + 76 sec	131.0; 72.8	131.6; 73.0	349.0; 193.9	337.6; 187.2	361.3; 200.5	356.5; 198.0	345.4; 191.8	341.0; 189.3
	Main engine second cutoff:								
	Main engine cutoff	74.4; 41.3	90.2; 50.1	189.9; 105.3	205.3; 104.0	363.6; 213.0	383.5; 213.0	176.6; 98.0	191.3; 106.2
	Main engine cutoff + 76 sec	99.3; 55.1	108.7; 60.3	176.8; 98.0	219.5; 121.9	364.8; 202.8	362.8; 201.8	278.5; 154.9	303.0; 168.2

Fuel pump housing temperature during the main engine second start transient decreased more slowly than during the main engine first start transient (see figs. V-15 and V-16). At main engine second start, the fuel pump housing temperatures were approximately 132° and 116° R (73.5° and 63.5° K) for the C-1 and C-2 engines, respectively. These values compare with approximate values of 124° and 80° R (69° and 44° K) at main engine first start. There was concern that the warmer housing temperatures at main engine second start may have been the result of severe impingement heating from the 50-pound (222-N) thrust hydrogen peroxide engines. Two of these engines were commanded on for 40 seconds immediately prior to main engine second start.

An engine chilldown sequence was initiated 17 seconds prior to main engine second start. This sequence was 9 seconds longer than the first to provide added cooling of the engine turbopumps. The additional cooling duration was provided to counteract the warmer component temperatures anticipated after the coast phase of flight. Main engine second start was commanded at T + 2034.7 seconds. System performance was normal except for a momentary decrease in oxidizer pump discharge pressure which occurred at approximately 7000 rpm while the pump was accelerating. The momentary decrease in oxidizer pump discharge pressure probably resulted from the oxidizer rich propellant utilization valve position at main engine second start. Similar operations have been noted during engine ground testing. Oxidizer and fuel pump discharge pressures during the start transient are plotted as a function of pump speed in figures V-17 and V-18, respectively. For purposes of comparison, the same curves are presented for the main engine first start transient in figures V-19 and V-20.

Engine thrust chamber pressures for the main engine start transient are presented in figure V-21. Engine acceleration times to 90 percent of rated thrust were approximately 1.56 seconds for both engines. Total impulse from engine start to engine start plus 2 seconds was calculated to be 10 400 and 9950 pound-seconds (46 200 and 44 200 N-sec) for the C-1 and C-2 engines, respectively. The start total impulse differential was well within previous experience limits.

Liquid-hydrogen and liquid-oxygen pump inlet pressure and temperature data for the first 90 seconds of main engine second firing are presented in figures V-22 to V-25. The pump inlet pressures remained above the steady-state operating limit during this time period.

Steady-state operating conditions are compared with corresponding predicted values in table V-4. The C-1 engine thrust chamber pressure was approximately 7 psi (4.8 N/cm^2) below that of the engine acceptance test. The remaining C-1 engine system data again substantiated a shift in engine performance. Engine performance in terms of thrust, specific impulse, and mixture ratio is described in figures V-9 and V-10.

Main engine second cutoff was commanded at T + 2140.9 seconds. The thrust decay again appeared normal. Engine shutdown total impulse was calculated to be 2927 pound-

TABLE V-4. - DATA SUMMARY FOR MAIN ENGINE SECOND FIRING, AC-9

Parameter	Range of expected values	Time from main engine start, sec					
		50		100		105	
		Engine					
		C-1	C-2	C-1	C-2	C-1	C-2
Fuel pump:							
Total inlet pressure (absolute), psi; N/cm^2	39.3 to 17.7; 27.1 to 12.2	35.7; 24.6	35.6; 24.5	33.6; 23.2	33.5; 23.1	33.2; 22.9	33.3; 23.0
Inlet temperature, ^oR, ^oK	43.4 to 37.6; 24.1 to 20.9	38.9; 21.6	39.0; 21.7	39.3; 21.8	39.4; 21.9	39.3; 21.8	39.3; 21.8
Oxidizer pump:							
Total inlet pressure (absolute), psi; N/cm^2	78.2 to 51.4; 53.9 to 35.4	64.6; 44.5	65.6; 45.2	61.3; 42.3	62.4; 43.0	60.1; 41.4	61.6; 42.5
Inlet temperature, ^oR, ^oK	184.4 to 172.5; 102.4 to 95.8	175.2; 97.3	175.3; 97.4	174.0; 96.7	174.1; 96.7	173.8; 96.6	173.7; 96.5
Speed, rpm	[a]12 005±183	11 989	12 139	11 927	12 099	11 879	12 017.8
Fuel venturi upstream pressure (absolute), psi; N/cm^2	[a]724±17; 499.2±11.7	723.5; 498.8	738.7; 509.3	711.8; 490.8	725.3; 500.1	711.7; 490.7	726.5; 500.9
Fuel turbine inlet temperature, ^oR, ^oK	[a]361±21; 200.6±11.7	364.3; 202.4	360.1; 200.1	380.7; 211.5	376.4; 209.1	380.7; 211.5	378.0; 210.0
Oxidizer injector differential pressure, psi; N/cm^2	[a]54±26.3; 37.2±18.1	47.2; 32.5	47.8; 33.0	47.7; 32.9	51.7; 35.6	47.1; 32.5	51.5; 35.5
Engine chamber pressure (absolute), psi; N/cm^2	[a]392±4; 270.3±2.8	387.1; 266.9	396.0; 273.0	386.2; 266.3	396.1; 273.1	386.6; 266.6	395.1; 272.4
Fuel pump discharge pressure (absolute), psi; N/cm^2	[a]964±18; 664.6±12.4	963.1; 664.0	974.2; 671.7	944.1; 650.9	964.6; 665.1	933.7; 643.8	964.0; 664.7
Oxidizer pump discharge pressure (absolute), psi; N/cm^2	[a]571±26; 393.7±17.9	590.1; 406.9	599.4; 413.3	577.6; 398.2	608.9; 419.8	580.0; 399.9	579.2; 399.3

[a]Expected value with nominal inlet conditions and nulled propellant utilization valve angle.

seconds (13 000 N-sec). This value is outside the predicted range of 3186±175 pound-seconds (13 800±777 N-sec) but is not outside the previous experience band. This impulse error did not significantly increase the requirement for the midcourse correction. (See section on GUIDANCE AND FLIGHT CONTROL SYSTEMS.) Main engine second firing duration was 106.2 seconds which compared favorably with a predicted value of 107.2 plus 2.2 minus 2.7 seconds.

Main engine system temperatures following main engine second cutoff are shown in figures V-11 to V-13. The increase in oxidizer pump housing temperature at T + 2250 seconds was caused by a 20-second firing of two of the 50-pound (222-N) thrust hydrogen peroxide engines for the vehicle retromaneuver. Hydrogen and oxygen pressures and temperatures at the engine turbopump inlets during the main engine retrothrust operation are presented in figures V-26 and V-27. The data indicated that liquid conditions were present at the oxidizer pump inlets during the entire retrothrust operation. The change in rate of fuel pressure decrease between 50 and 100 seconds following initiation of retrothrust indicated the inception of two-phase flow. The rise in fuel temperature at and after 200 seconds of retrothrust operation indicated that the liquid supply was depleted at that time.

Centaur Boost Pumps

System description. - Boost pumps were used in the liquid-oxygen and liquid-hydrogen tanks on Centaur to supply propellants to the main engine turbopumps at the required inlet pressures. Both boost pumps were mixed-flow, centrifugal types, and were powered by hot-gas-driven turbines. The hot gas consisted of superheated steam and oxygen from catalytic decomposition of hydrogen peroxide. Constant turbine input power on each unit was maintained by metering hydrogen peroxide through fixed orifices upstream of a catalyst bed. A speed-limiting control system was provided on each unit to prevent pump overspeed under abnormal operating conditions. Illustrations of the complete boost pump and hydrogen peroxide supply systems are shown in figures V-28 to V-31.

Boost pump performance. - Performance of the boost pumps was satisfactory during the entire flight. Boost pump first start command was initiated at T + 204.8 seconds and was terminated simultaneously with main engine first cutoff at T + 577.7 seconds. Boost pump second start was initiated at T + 2007.0 seconds and was terminated simultaneously with main engine second cutoff at T + 2140.9 seconds. First indications of turbine inlet pressures were evident less than 1 second after boost pump start command for both engine firings. Steady-state turbine inlet pressures were within 3 psi (2.07 N/cm^2) of expected values for both engine firings. Expected absolute pressure values of 95 psi (65.5 N/cm^2) for the liquid-oxygen unit, and 100 psi (69.0 N/cm^2) for

the liquid-hydrogen unit were established from prelaunch test data.

Turbine speed data for both boost pumps are shown in figures V-32 to V-35 for the first and second engine firings. Steady-state speeds for both turbines were from 500 to 2500 rpm higher than the values obtained during prelaunch tests. Differences between the ground test data and flight values were within the accuracy tolerance of the instrumentation and telemetry systems. A slight unexplained drop in turbine speed was noticed on the oxidizer unit 17 seconds after boost pump first start. A similar small drop in turbine speed was noted on a preceding Atlas-Centaur flight, AC-7. This drop in turbine speed (AC-9) had no effect on overall system performance.

Oxidizer and fuel boost pump differential pressure rise data are shown in figures V-36 to V-39 for both engine firings. Steady-state fuel boost pump pressure rise was approximately 0.5 psi (0.345 N/cm^2) higher than the prelaunch test value. Similarly, the oxidizer boost pump pressure rise was approximately 6 psi (4.13 N/cm^2) higher than expected. Differences between ground test data and the flight values were within the accuracy tolerances of the instrumentation and telemetry systems. A slight drop in the oxidizer unit differential pressure occurred at exactly the same time as the turbine speed drop mentioned previously (boost pump start plus 17 sec). This pressure drop combined with the turbine speed verified that either a reduction in available pump power occurred or there was an increase in volumetric flow rate through the pump.

Both the oxidizer and fuel boost pump differential pressure data exhibited a more rapid decrease following main engine first cutoff than was experienced on Atlas-Centaur flight, AC-8. The differential pressure decreases on AC-8 were smooth exponential curves which were consistent with the corresponding turbine speed decrease curves. Turbine speed and pump differential pressure decrease times (time required to reach zero) on AC-8 were approximately 70 seconds. This is expected for a two-burn (indirect-ascent) vehicle which utilizes small-thrust hydrogen peroxide engines to settle and retain the propellants following main engine first cutoff. No attempt was made to retain the propellants settled after main engine cutoff on previous single-burn vehicles. This allowed liquids to move away from the boost pump inlets resulting in rapid loss of pump differential pressure and linear turbine speed decrease rates with corresponding decay times of 115 to 180 seconds.

On AC-9, the turbine speed rates of decrease and times to stop rotating appeared normal (approximately 70 sec), but the pump differential pressure for both boost pumps dropped to zero in a short time. The normal speed decrease times (as well as other liquid-vapor sensor instrumentation in the propellant tanks) indicated that the propellants remained settled following main engine first cutoff. The only plausible explanation for the rapid decrease in pump differential pressure on AC-9 is pump cavitation. Pump cavitation may result from gas bubble ingestion, or loss of net positive suction pressure at the pump inlet. Gas bubbles may be generated by boiling of propellants, mixing ullage

gas with the liquid, or from engine backflow at shutdown. Boiling of propellants occurs when sufficient heat is supplied to the liquid to increase the bulk temperature to the saturation temperature, or if the inlet pressure is reduced to the local saturation pressure.

AC-8 was a night launch with low space heating, whereas AC-9 was a daytime launch with near-maximum space heating. The high heat flux resulted in a higher heat transfer from surrounding metal into the liquid residuals after main engine first cutoff. This is the most plausible explanation for the rapid loss of pump differential pressures on AC-9. The high heat input on AC-9, combined with the sudden termination of vehicle acceleration at main engine first cutoff, resulted in loss of the required net positive suction pressure and the occurrence of pump cavitation.

Boost pump inlet temperature and pressure and boost pump discharge temperature data are shown in figures V-40 to V-42 for the entire flight. Tank pressurization prior to each main engine start was sufficient to supply the necessary net positive suction pressure for proper boost pump operation. The oxidizer inlet and discharge temperatures and the fuel inlet temperature remained in the liquid temperature range through engine second cutoff. The fuel boost pump discharge temperature from T + 850 to T + 2010 seconds indicated that the liquid-hydrogen supply lines were dry. This was caused by liquid-hydrogen vaporization resulting from space heating. Of particular significance was the reestablishment of liquid temperatures within 3 seconds after boost pump start, well in advance of main engine second start.

During the retrothrust operation, both the fuel boost pump inlet and discharge temperatures reflected the migration of the residual liquid hydrogen, as venting and changes in vehicle thrust levels occurred. The inlet temperature rose rapidly 60 seconds after start of retrothrust, as the liquid level dropped below the temperature sensor. The temperature decreased after completion of retrothrust, as residual liquid covered the sensor.

Boost pump component temperature data are shown in figure V-43. All temperatures indicated approximately 70° F (294° K) at lift-off, which is within the expected range of 50° to 100° F (283° to 311° K) established by previous launch experience. The fuel boost pump overspeed sensor temperature at main engine second cutoff was 189° F (361° K) against a predicted value of 182° F (357° K).

Hydrogen Peroxide Supply and Engine System

System description. - The hydrogen peroxide engines were used during the nonpowered portions of flight for attitude control, propellant settling and retention, and to provide the initial thrust for the retromaneuver (see table V-21, in the section

GUIDANCE AND FLIGHT CONTROL SYSTEMS). The attitude control system consisted of four 3.0-pound (13-N) thrust engines, four 50-pound (222-N) thrust engines, and two clusters each of two 3.5-pound (15.6-N) and one 6.0-pound (26.8-N) thrust engines. Propellant was fed to the engines from a positive-expulsion bladder-type storage tank which was pressurized by the pneumatic system to about 300 psi (207 N/cm^2) absolute. The hydrogen peroxide was decomposed in the engine catalyst beds, and the hot decomposition products expanded through converging-diverging nozzles to provide thrust. Hydrogen peroxide was also provided to drive the boost pump turbines. The system is shown in figures V-28 and V-44. AC-9 was the first vehicle to incorporate the welded joint engine design on the cluster engines and 3.0-pound (13-N) thrust engines. The welded joint design replaced a large aluminum B-nut joint which was suspected of leaking during the AC-8 flight.

System performance. The hydrogen peroxide supply and engine system was extensively instrumented with special temperature measurements to detect any leakage within the system. In space, hydrogen peroxide leakage would cause temperatures to decrease due to evaporative cooling. The instrumentation was installed as a result of leakage which caused a premature depletion of hydrogen peroxide during the AC-8 flight. All the temperature data reflected normal system performance with no indication of hydrogen peroxide leakage. Based on the engine firing commands, all engines performed their programmed function and operated as expected.

A postmission experiment was performed on AC-9 to provide data for determining hydrogen peroxide consumption. The experiment consisted of firing the 50-pound (222-N) engines in the V "half on" mode (see table V-21 in GUIDANCE AND FLIGHT CONTROL SYSTEMS) until the hydrogen peroxide supply was depleted. The firing time was 40.4 seconds, which, for estimated consumption rates, corresponded to 29 pounds (13 kg) of hydrogen peroxide. This amount of residual propellant verified that the existing hydrogen peroxide tank capacity was adequate for indirect-ascent Surveyor missions.

The hydrogen peroxide consumption was calculated for the various flight sequence times (see table V-5). This calculation was made by using the hydrogen peroxide commands (see fig. V-115 in the GUIDANCE AND FLIGHT CONTROL SYSTEMS section) to establish the total engine firing times. Propellant flow rates for the individual engines were estimated.

TABLE V-5. - CALCULATED HYDROGEN PEROXIDE CONSUMPTION

Sequence	Duration, sec	Mass	
		lb	kg
Boost pumps; first firing of main engines	373.1	31.7	14.4
Main engine first cutoff to vernier engine cutoff (V engines in half on mode[a])	76.0	54.1	24.5
Vernier engine cutoff to main engine second start minus 40 sec (S engines in half on mode)	1340.9	56.9	25.8
Main engine second start minus 40 sec to main engine second start (V engines in half on mode)	40.0	28.8	13.0
Boost pumps; main engine second firing	133.1	11.3	5.1
Main engine second cutoff to blowdown (attitude control and vehicle turnaround, excluding lateral thrust time)	289.8	2.6	1.2
Lateral thrust (V engines in half on mode)	20.0	14.7	6.7
Blowdown of propellant tanks	250.0	2.6	1.2
Hydrogen peroxide experiment (V engines in half on mode)	40.4	29.7	13.5
Total consumption	------	232.4	105.4
Total tanked	------	236.9	107.4
Unusable residual	------	4.5	2.0
Total usable	------	232.4	105.4

[a]See table V-21 in GUIDANCE AND FLIGHT CONTROL SYSTEMS section for description of firing modes.

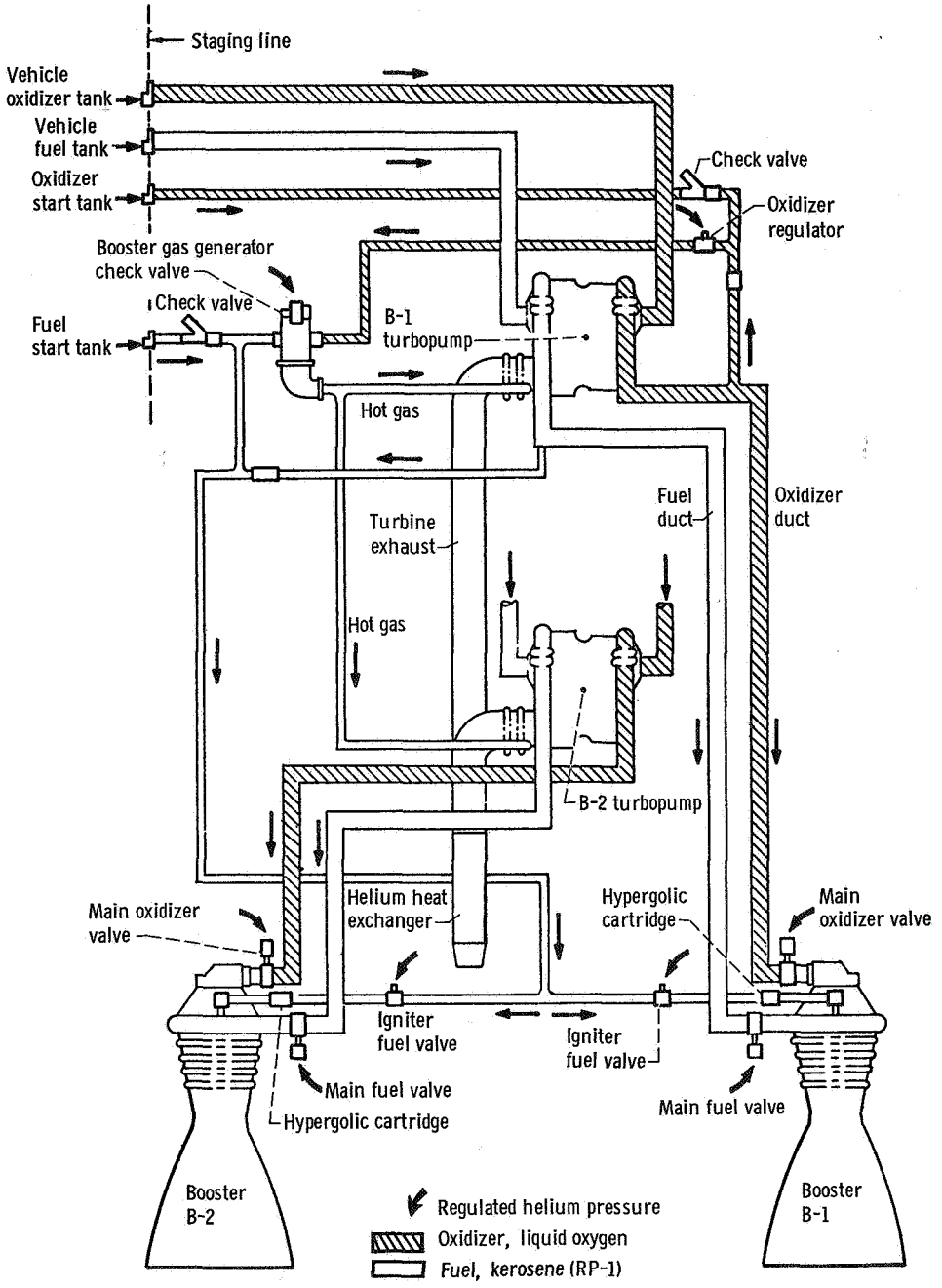

(a) Atlas vehicle booster engine.

Figure V-1. - Engine system schematic drawing AC-9.

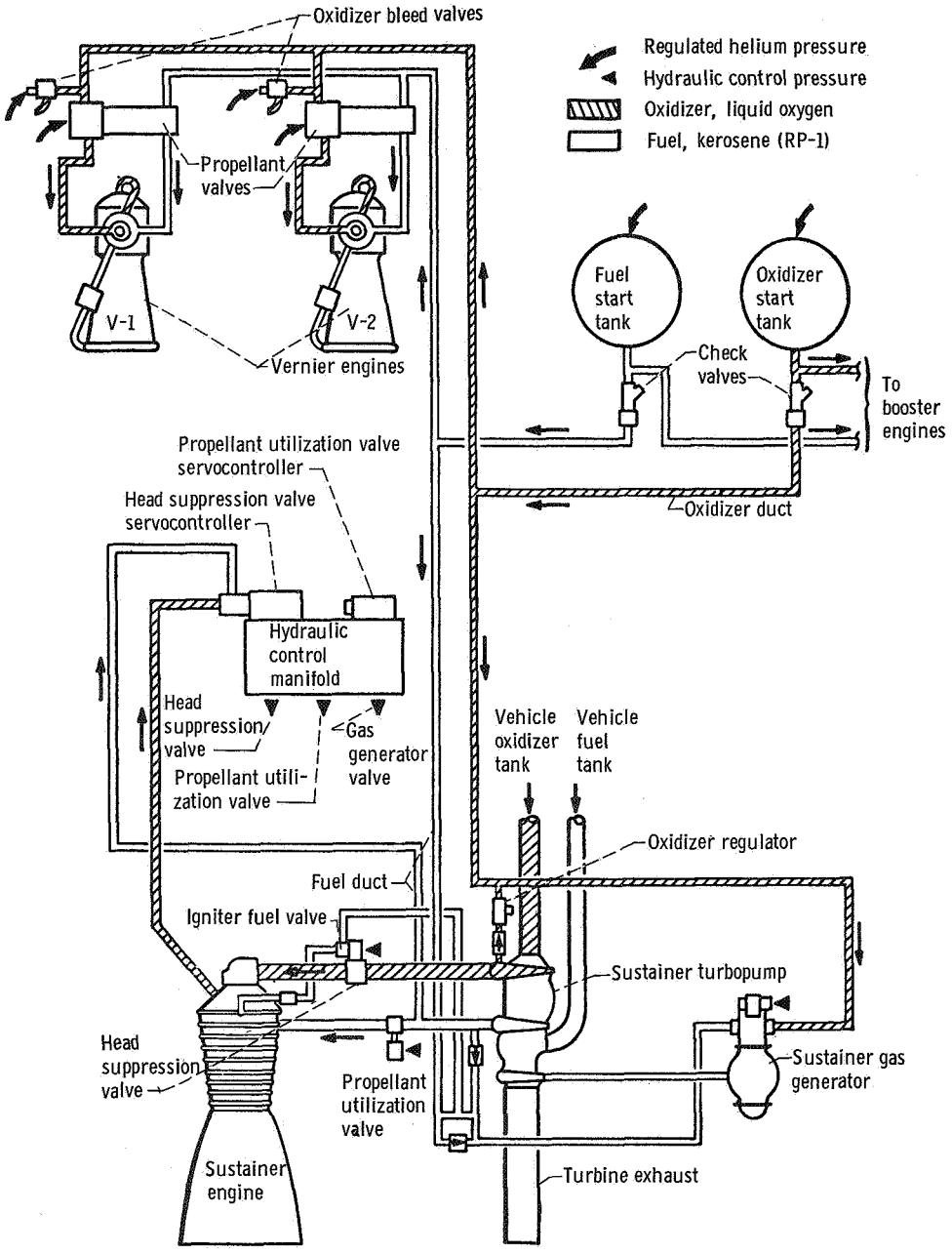

(b) Atlas vehicle sustainer and vernier engines.

Figure V-1. - Concluded.

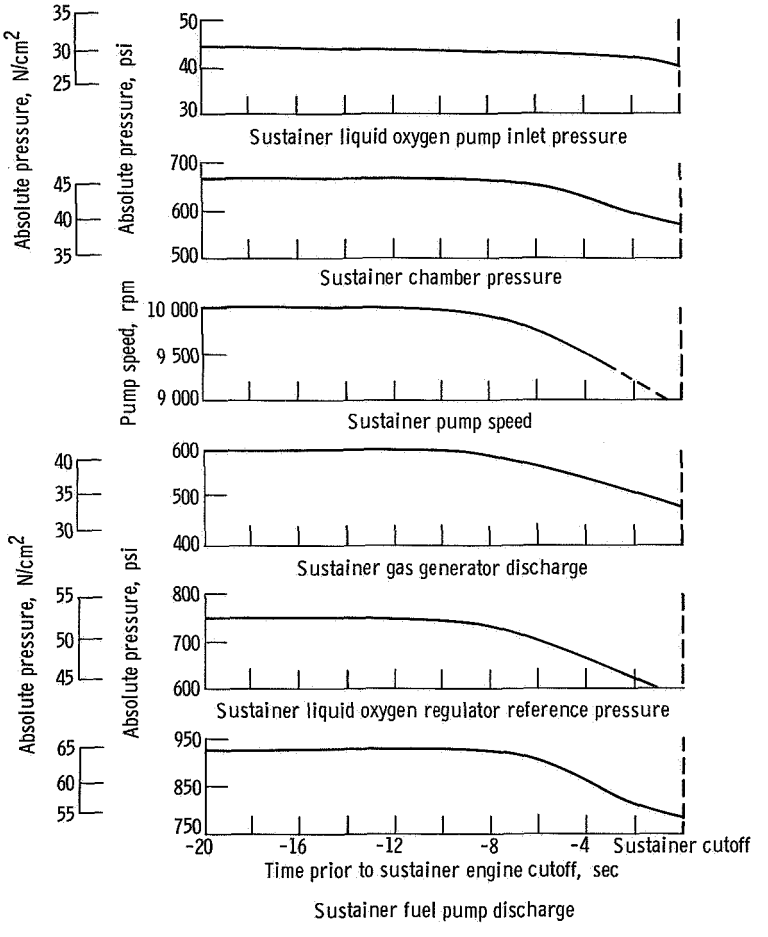

Figure V-2. - Atlas sustainer engine operation, AC-9.

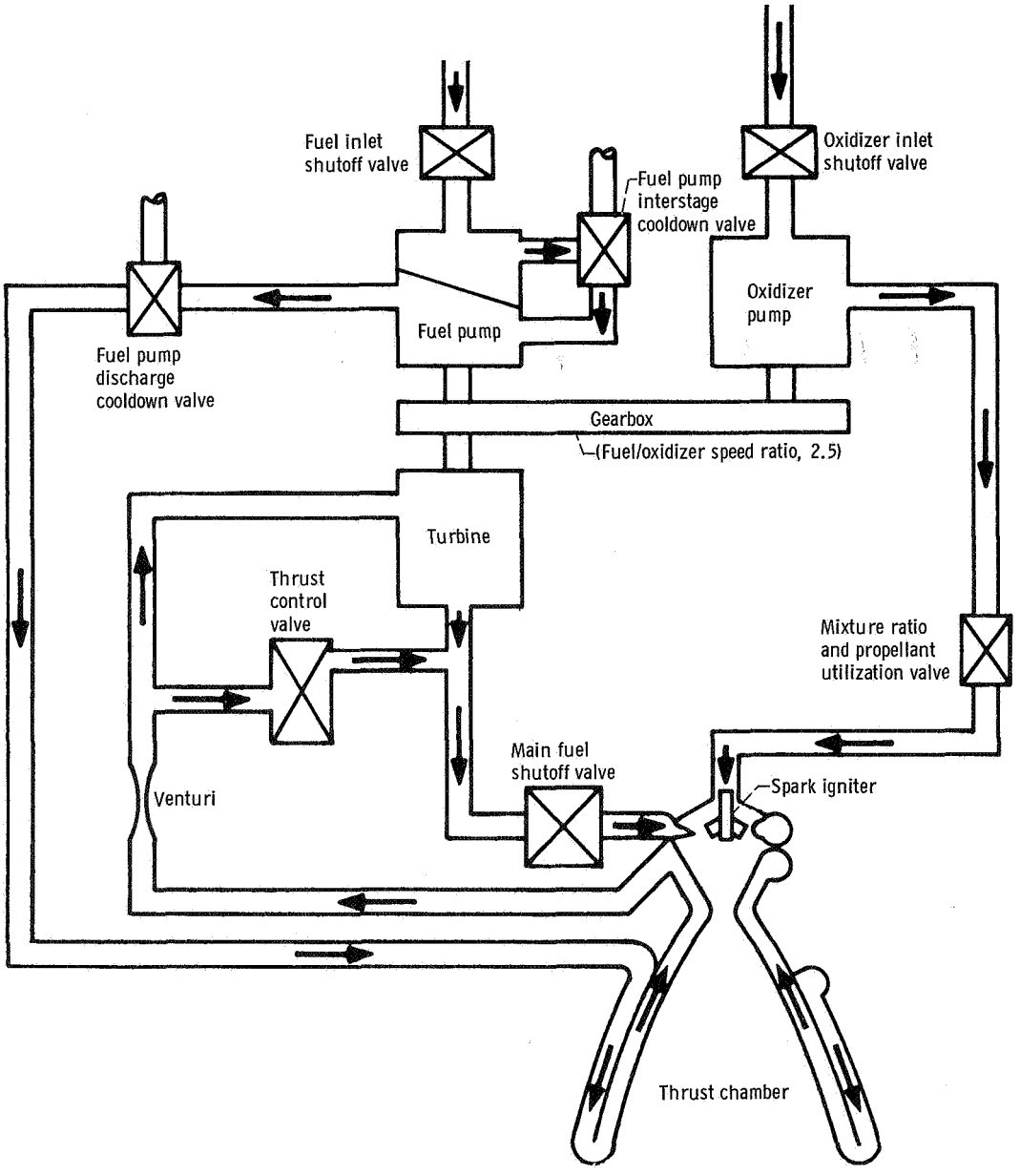

Figure V-3. - Centaur main engine schematic drawing, AC-9.

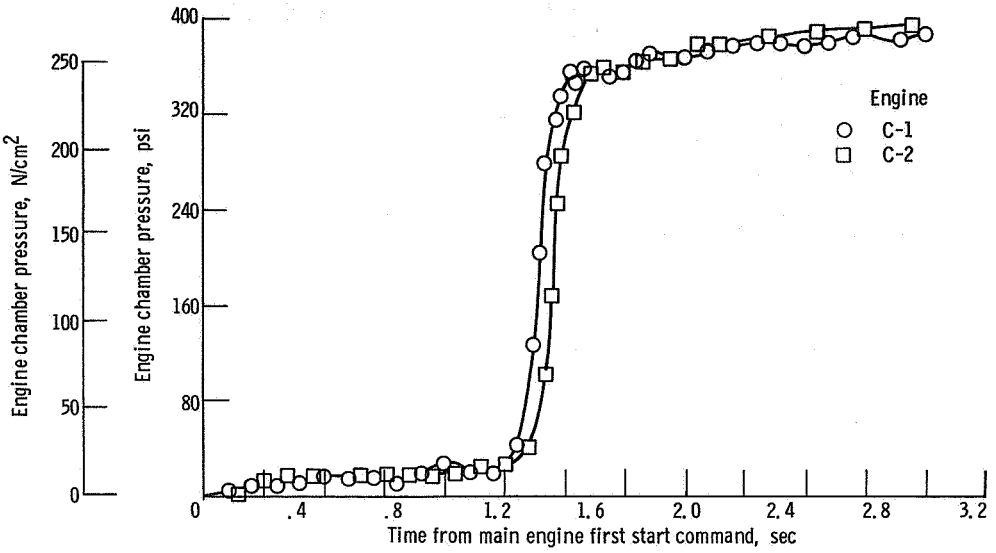

Figure V-4. - Centaur engine thrust chamber absolute pressure during start transient, AC-9.

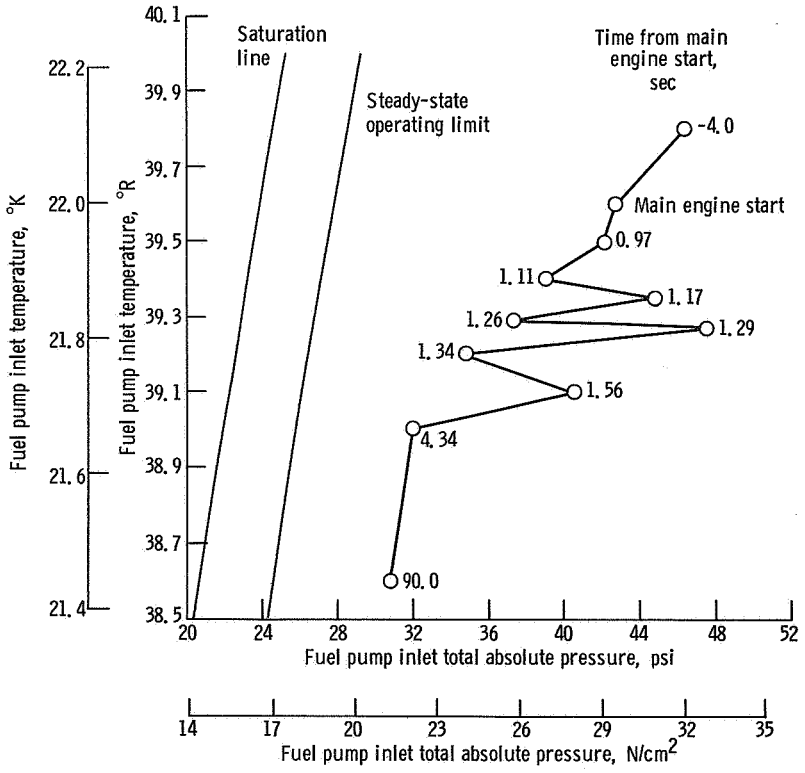

Figure V-5. - Centaur C-1 engine fuel pump inlet conditions during engine first start and initial steady-state operation, AC-9.

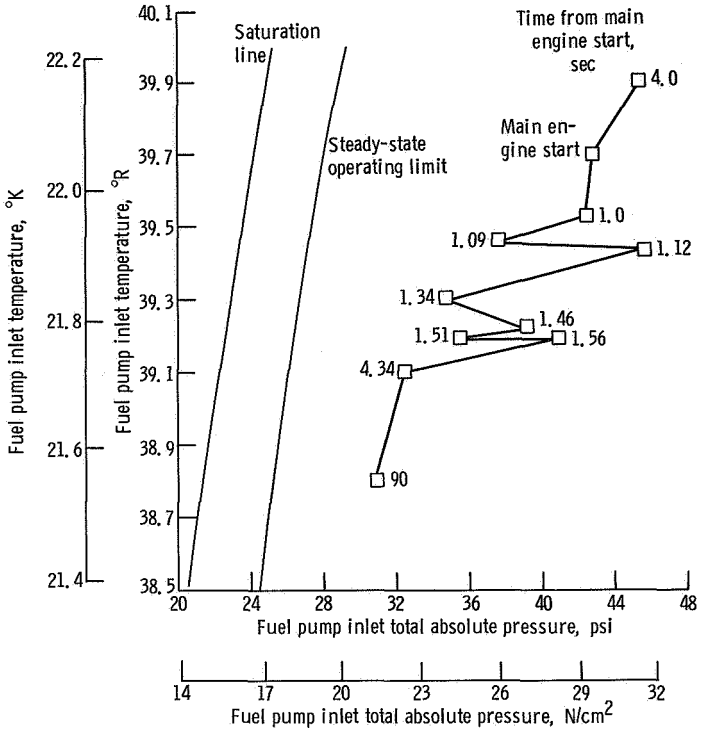

Figure V-6. - Centaur C-2 engine fuel pump inlet conditions during engine first start and initial steady-state operation, AC-9.

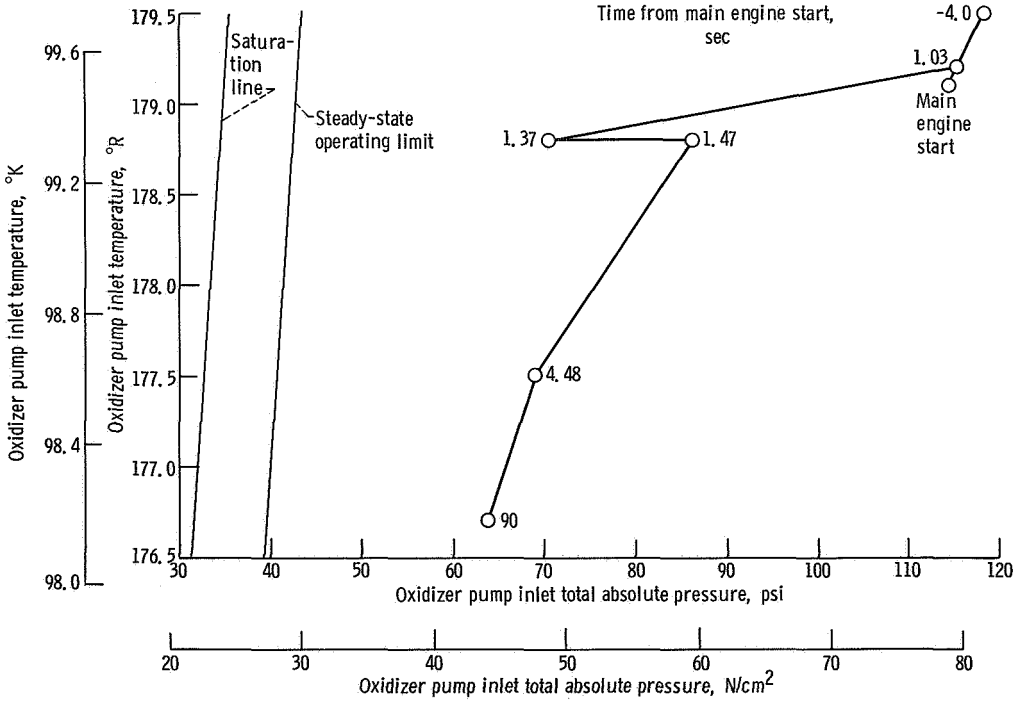

Figure V-7. - Centaur C-1 engine oxidizer pump inlet conditions during engine first start and initial steady-state operation, AC-9.

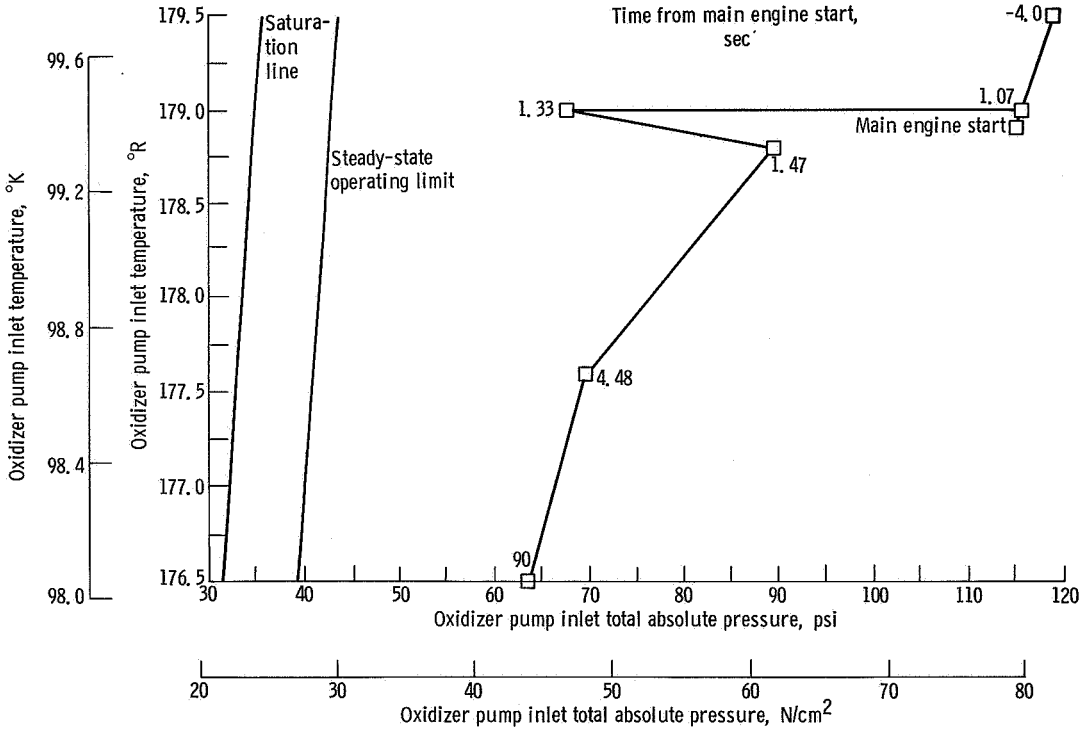

Figure V-8. - Centaur C-2 engine oxidizer pump inlet conditions during engine first start and initial steady-state operation, AC-9.

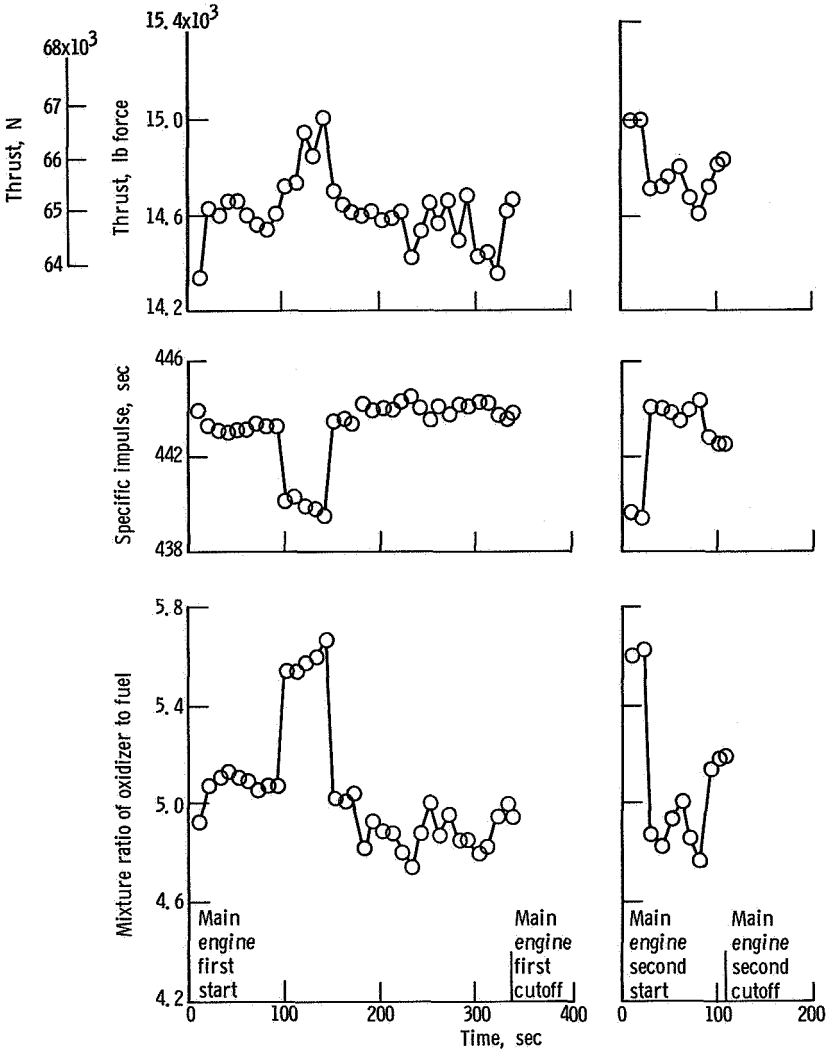

Figure V-9. - Centaur C-1 main engine performance, AC-9.

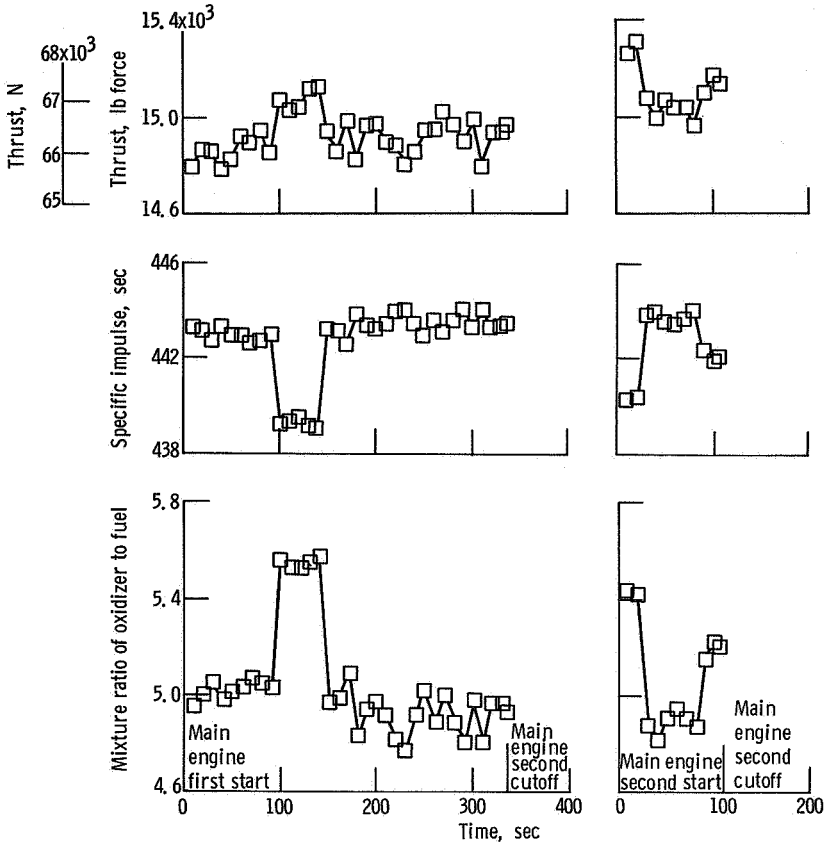

Figure V-10. - Centaur C-2 main engine performance, AC-9.

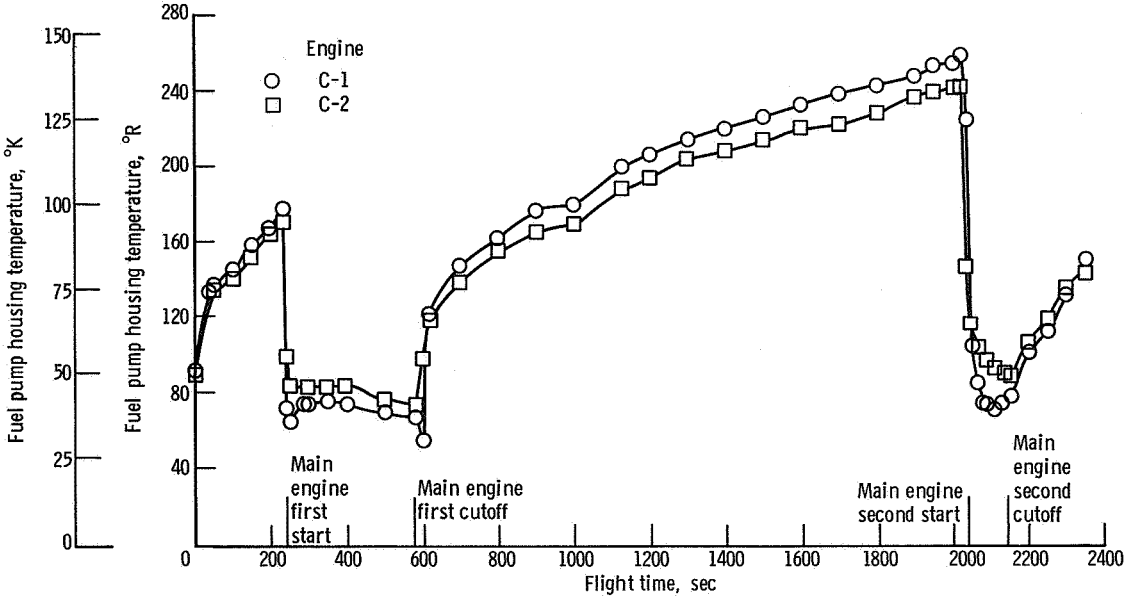

Figure V-11. - Centaur fuel pump housing temperatures, AC-9.

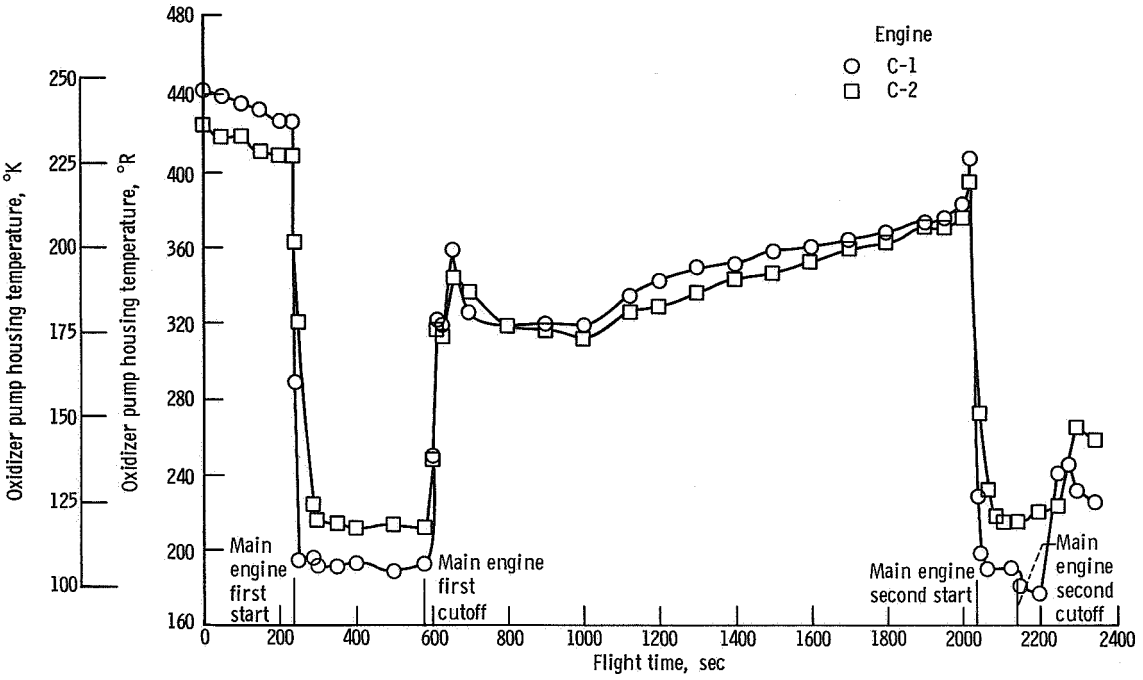

Figure V-12. - Centaur oxidizer pump housing temperatures, AC-9.

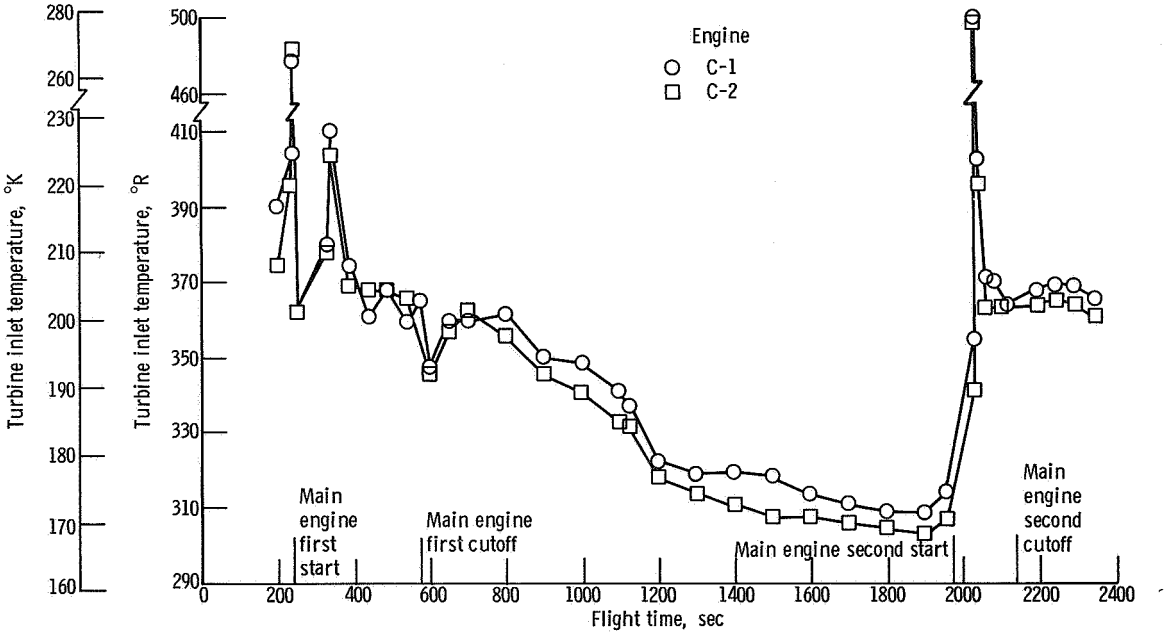

Figure V-13. - Centaur turbine inlet temperatures, AC-9.

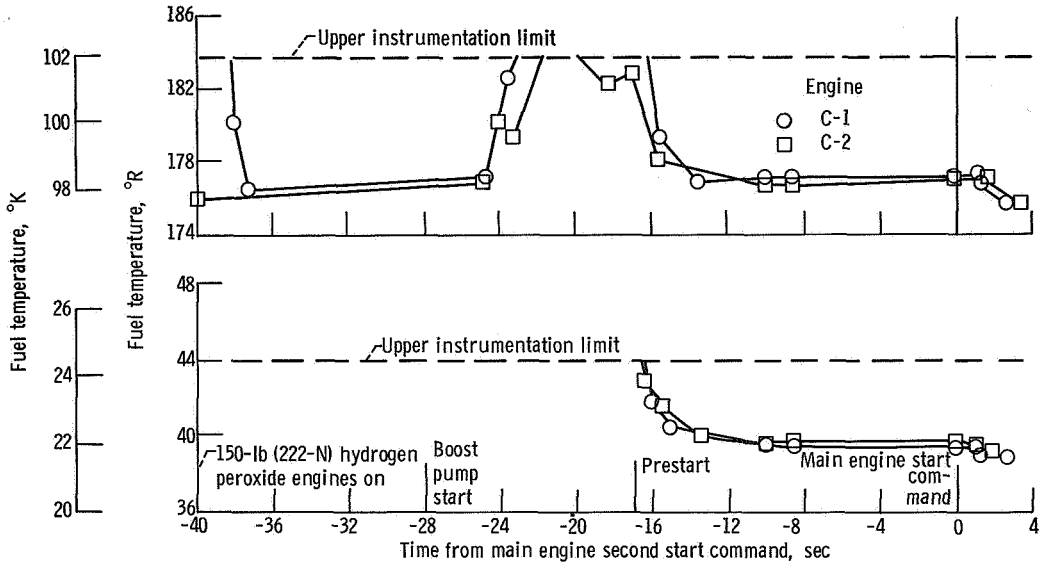

Figure V-14. - Centaur fuel and oxidizer pump inlet temperatures, AC-9.

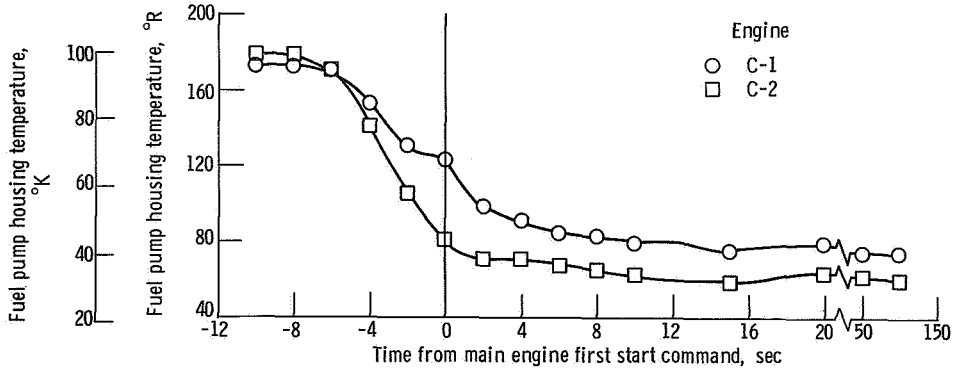

Figure V-15. - Centaur fuel pump housing temperatures at main engine first start, AC-9.

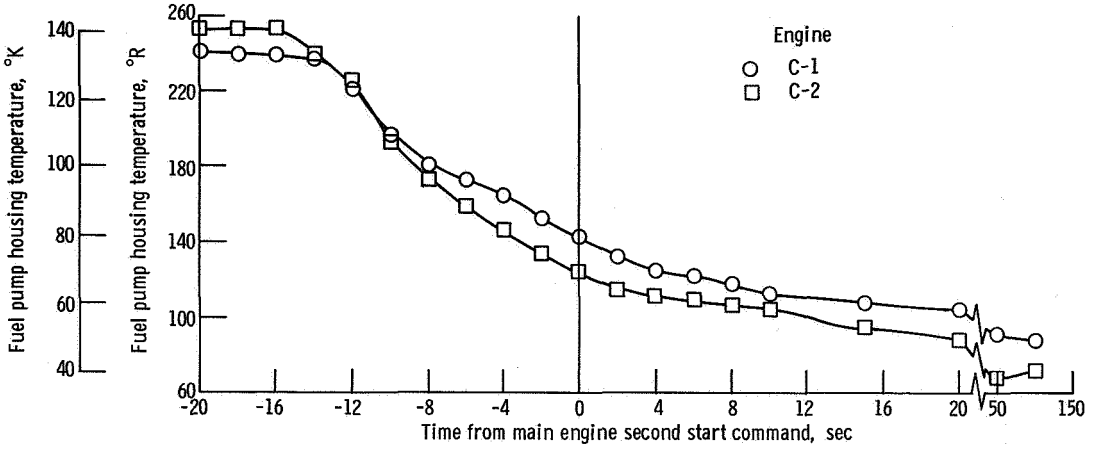

Figure V-16. - Centaur fuel pump housing temperatures at main engine second start, AC-9.

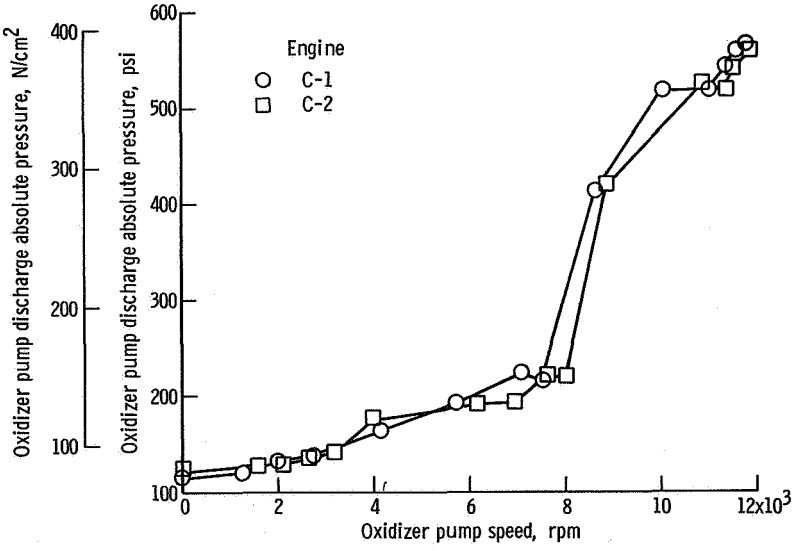

Figure V-17. - Centaur oxidizer pump characteristics during main engine second start, AC-9.

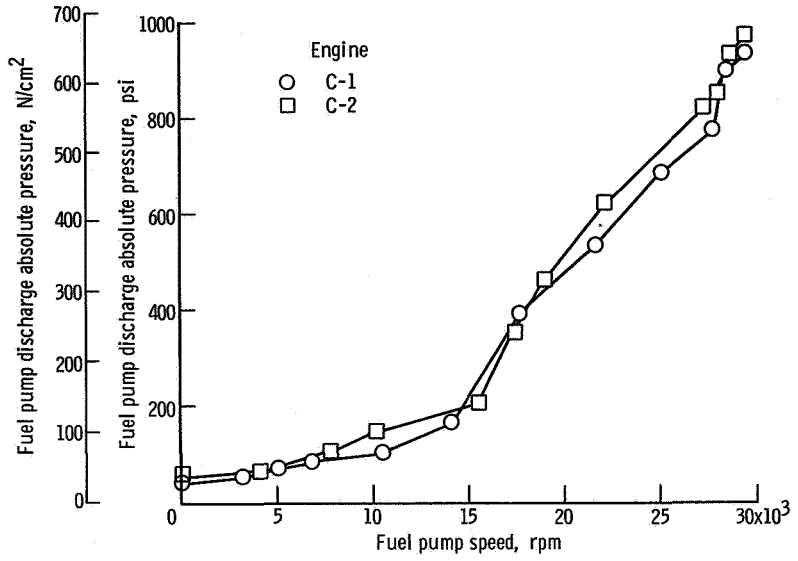

Figure V-18. - Centaur fuel pump characteristics during main engine second start, AC-9.

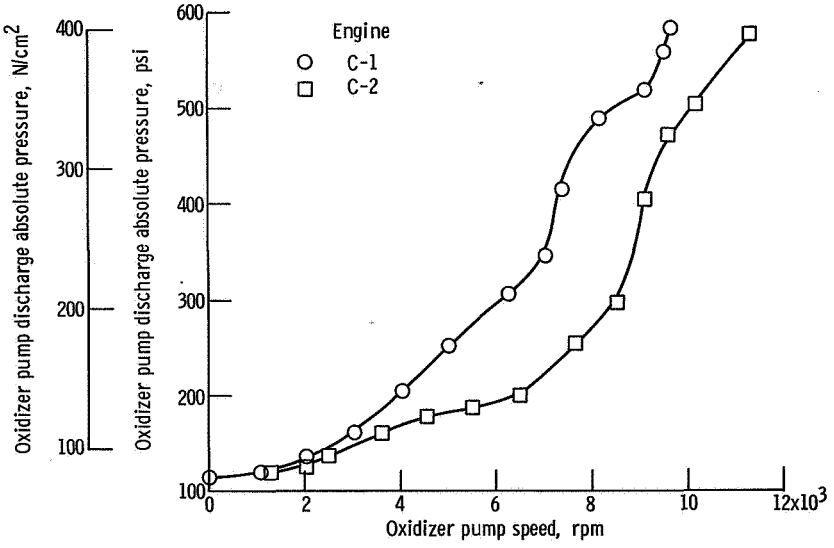

Figure V-19. - Centaur oxidizer pump characteristics during main engine first start, AC-9.

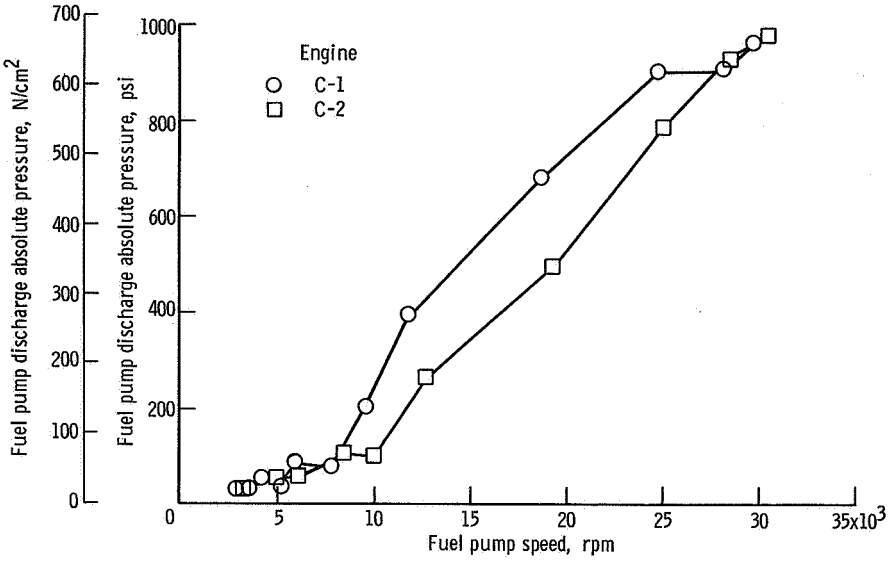

Figure V-20. - Centaur fuel pump characteristics during main engine first start, AC-9.

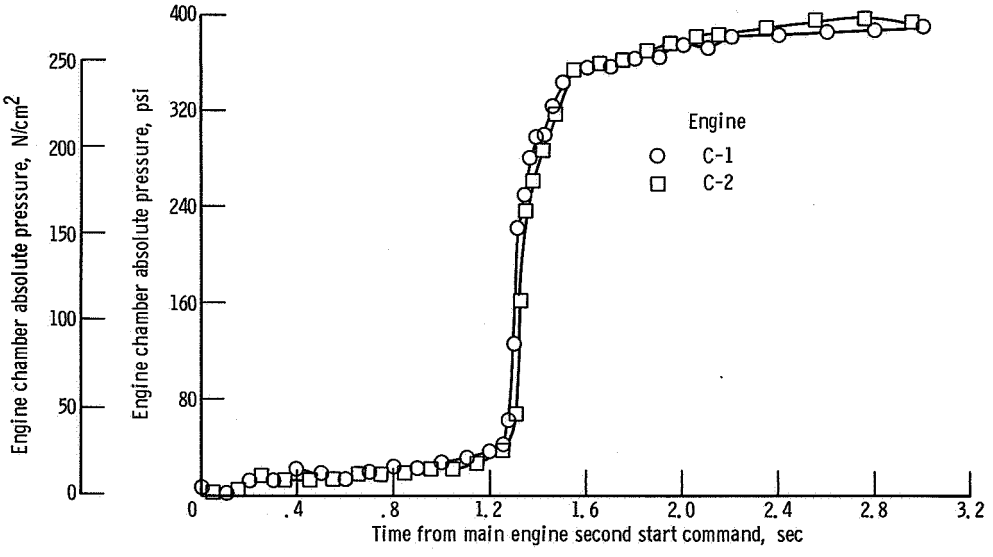

Figure V-21. - Centaur engine chamber pressure during start transient, AC-9.

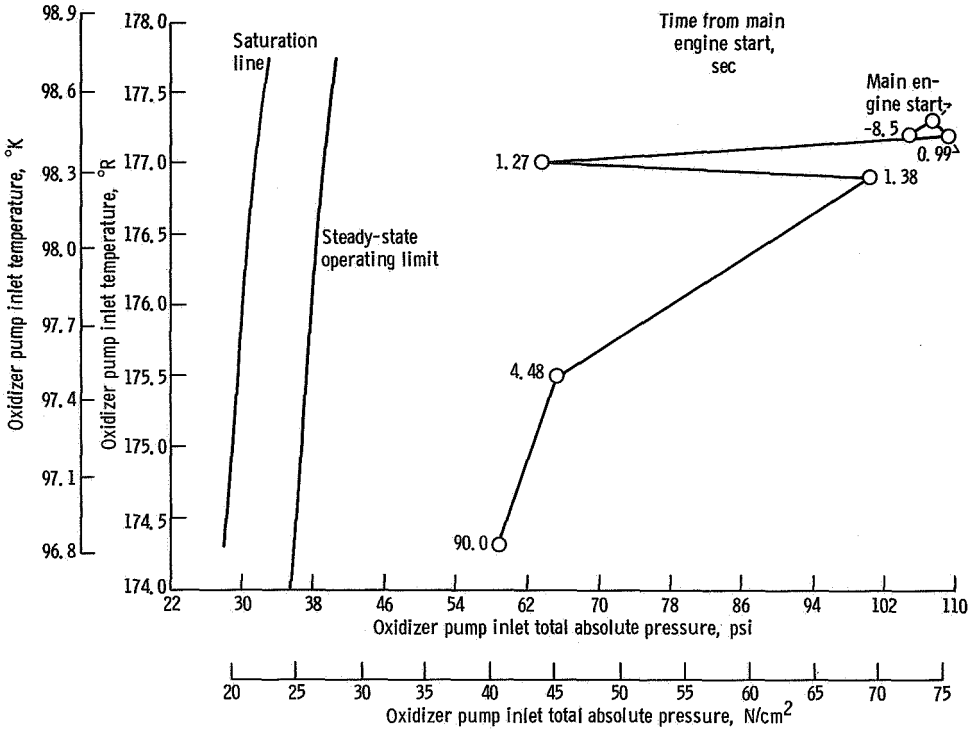

Figure V-22. - Centaur C-1 engine oxidizer pump inlet conditions during engine second start and initial steady-state operation, AC-9.

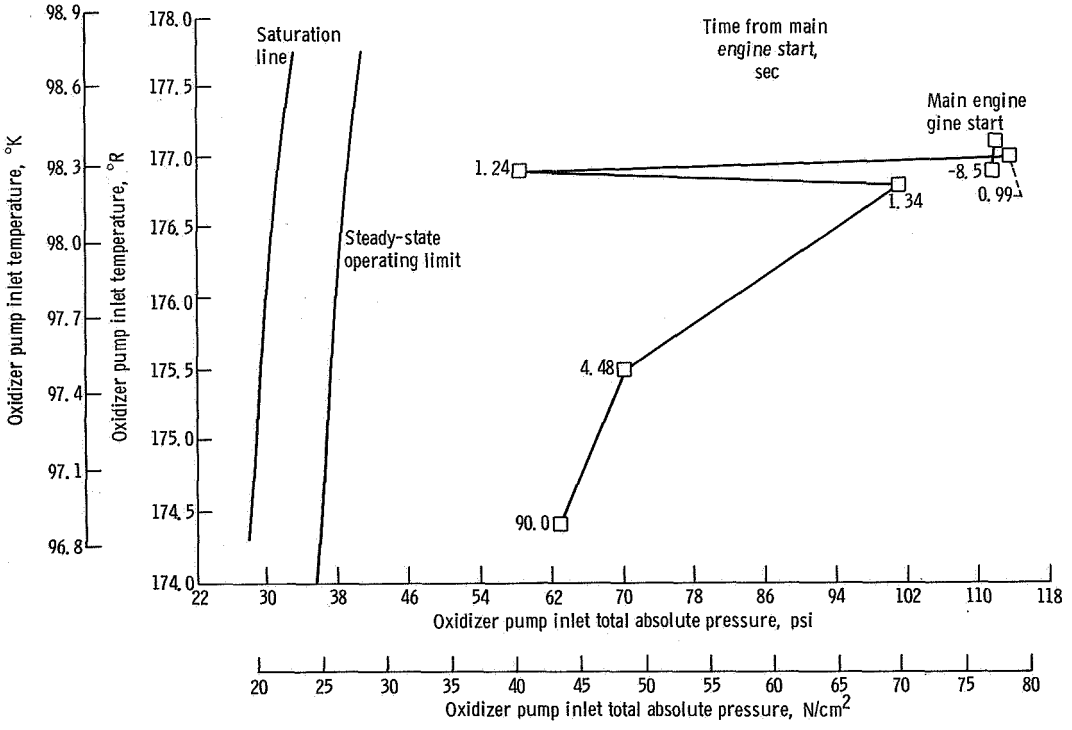

Figure V-23. - Centaur C-2 engine oxidizer pump inlet conditions during engine second start and initial steady-state operation, AC-9.

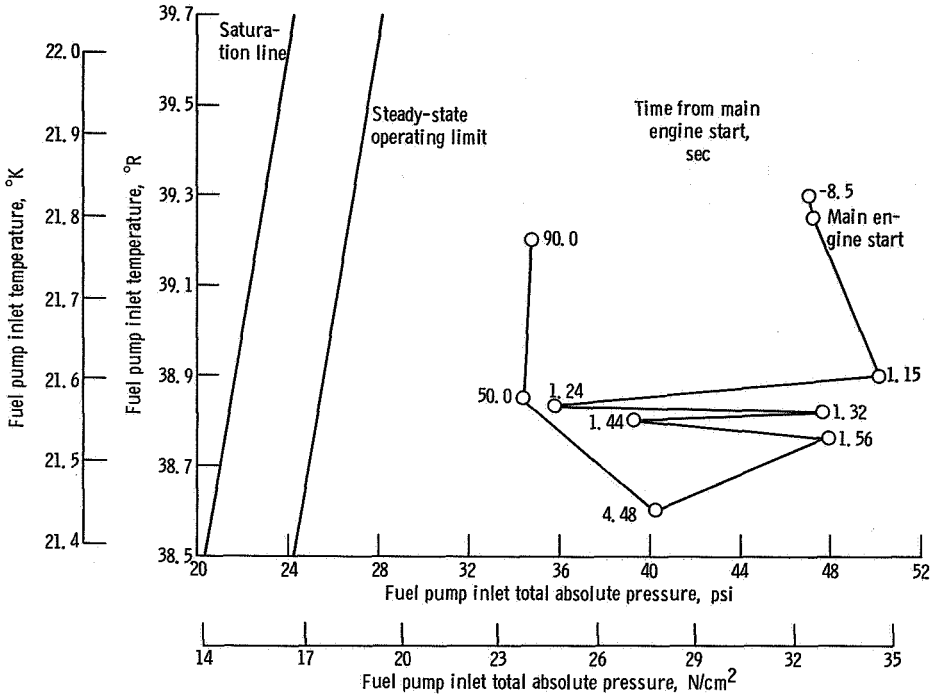

Figure V-24. - Centaur C-1 engine fuel pump inlet conditions during engine second start and initial steady-state operation, AC-9.

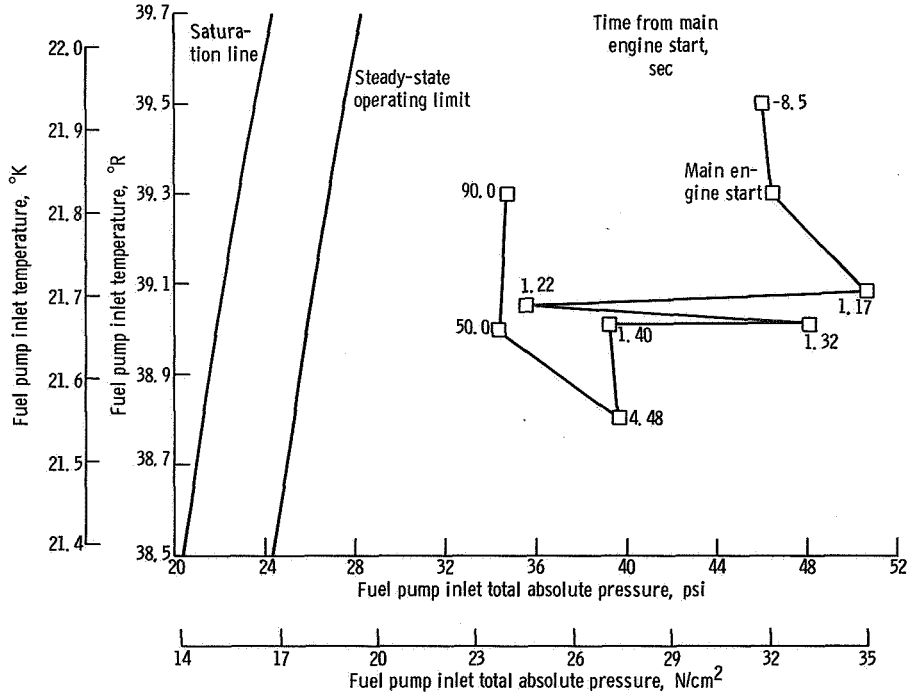

Figure V-25. - Centaur C-2 engine fuel pump inlet conditions during engine second start and initial steady-state operation, AC-9.

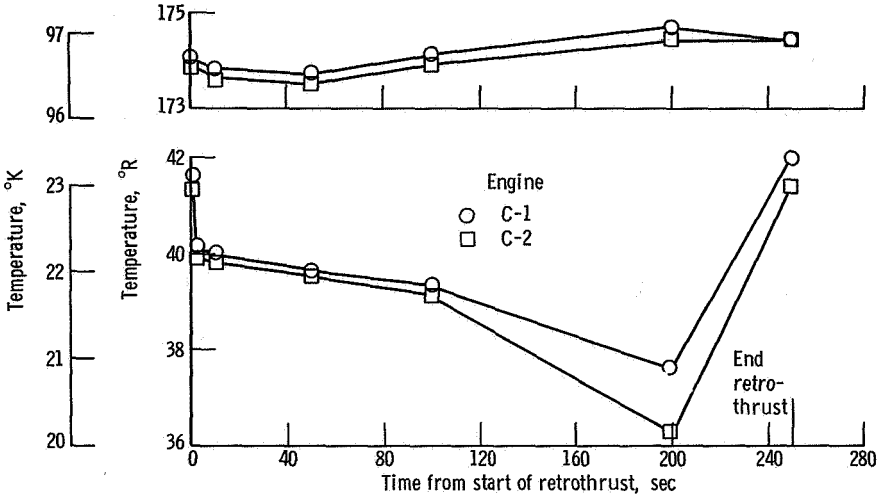

Figure V-26. - Centaur fuel and oxidizer inlet temperatures during retrothrust, AC-9.

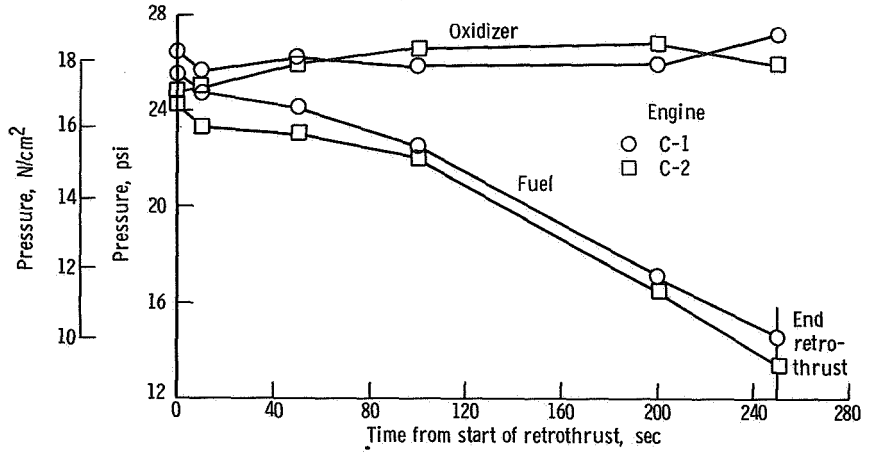

Figure V-27. - Centaur fuel and oxidizer inlet absolute pressures during retrothrust, AC-9.

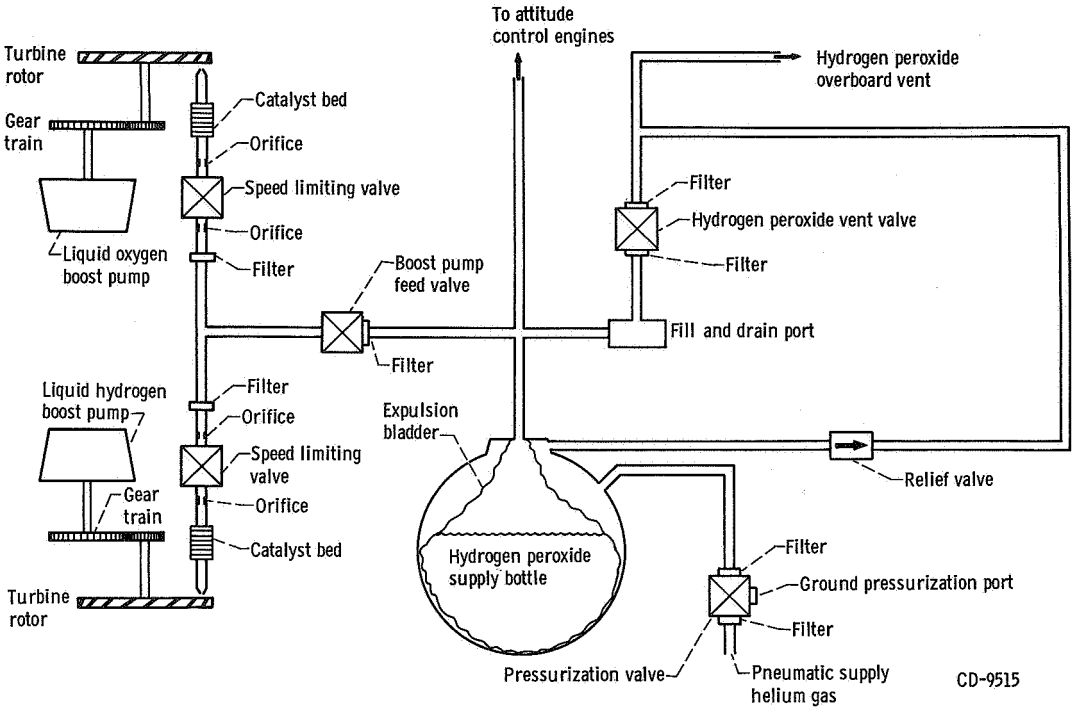

Figure V-28. - Schematic drawing of Centaur boost pump hydrogen peroxide supply, AC-9.

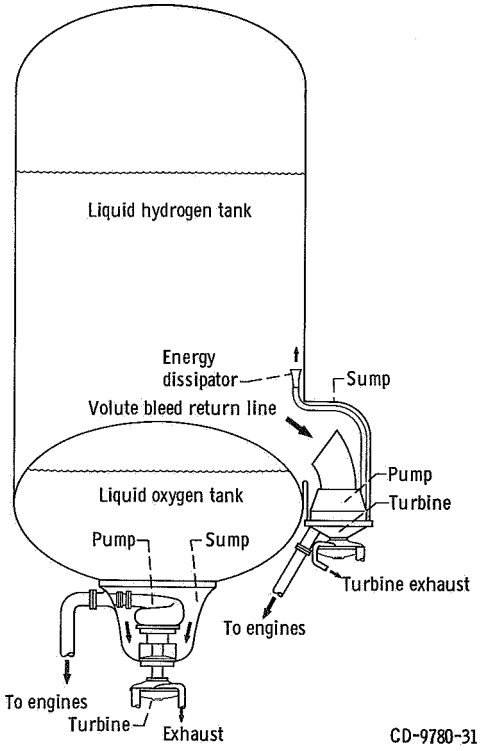

Figure V-29. - Centaur tank-mounted boost pumps, AC-9.

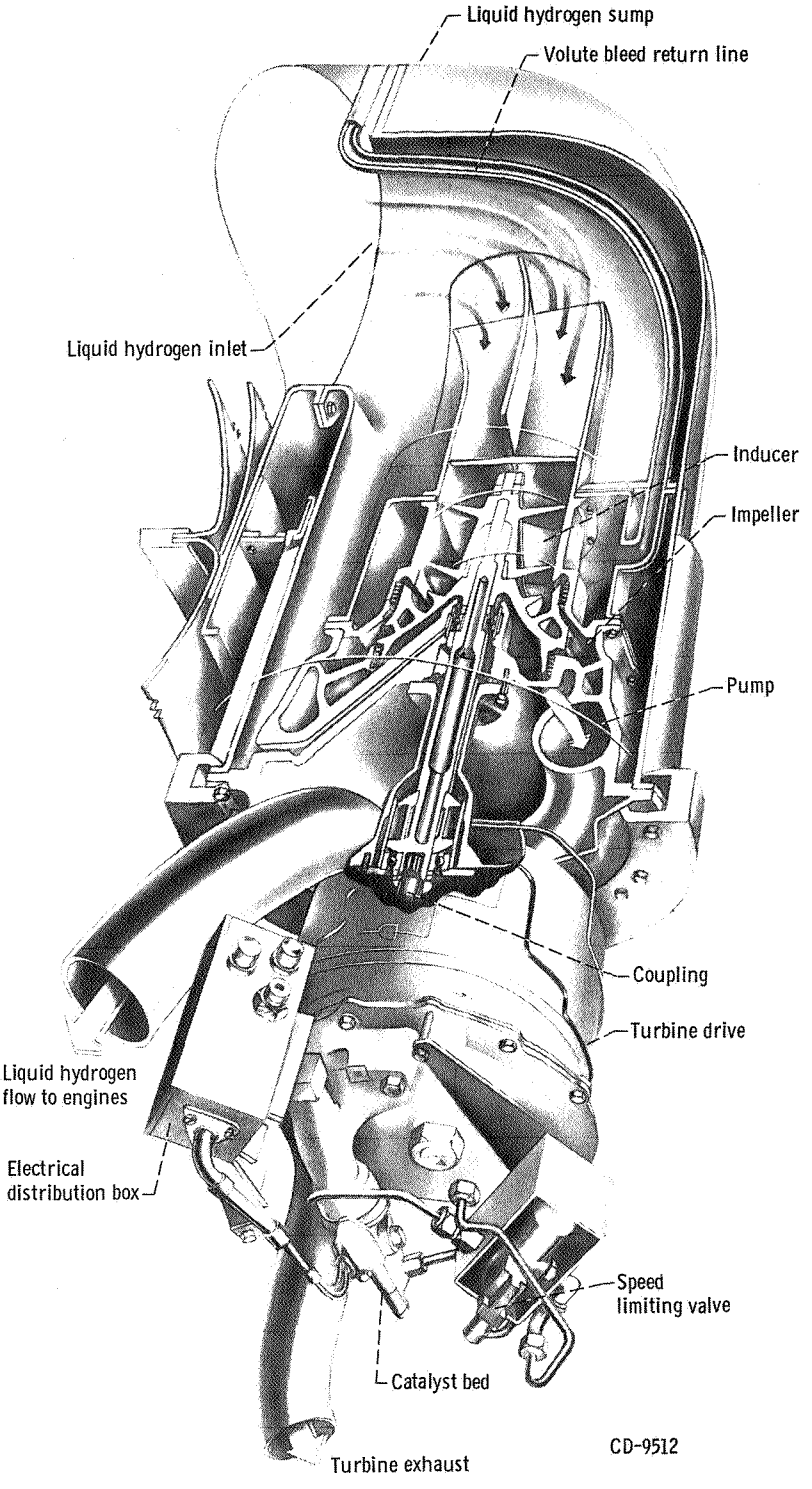

Figure V-30. - Centaur liquid hydrogen boost pump cutaway, AC-9.

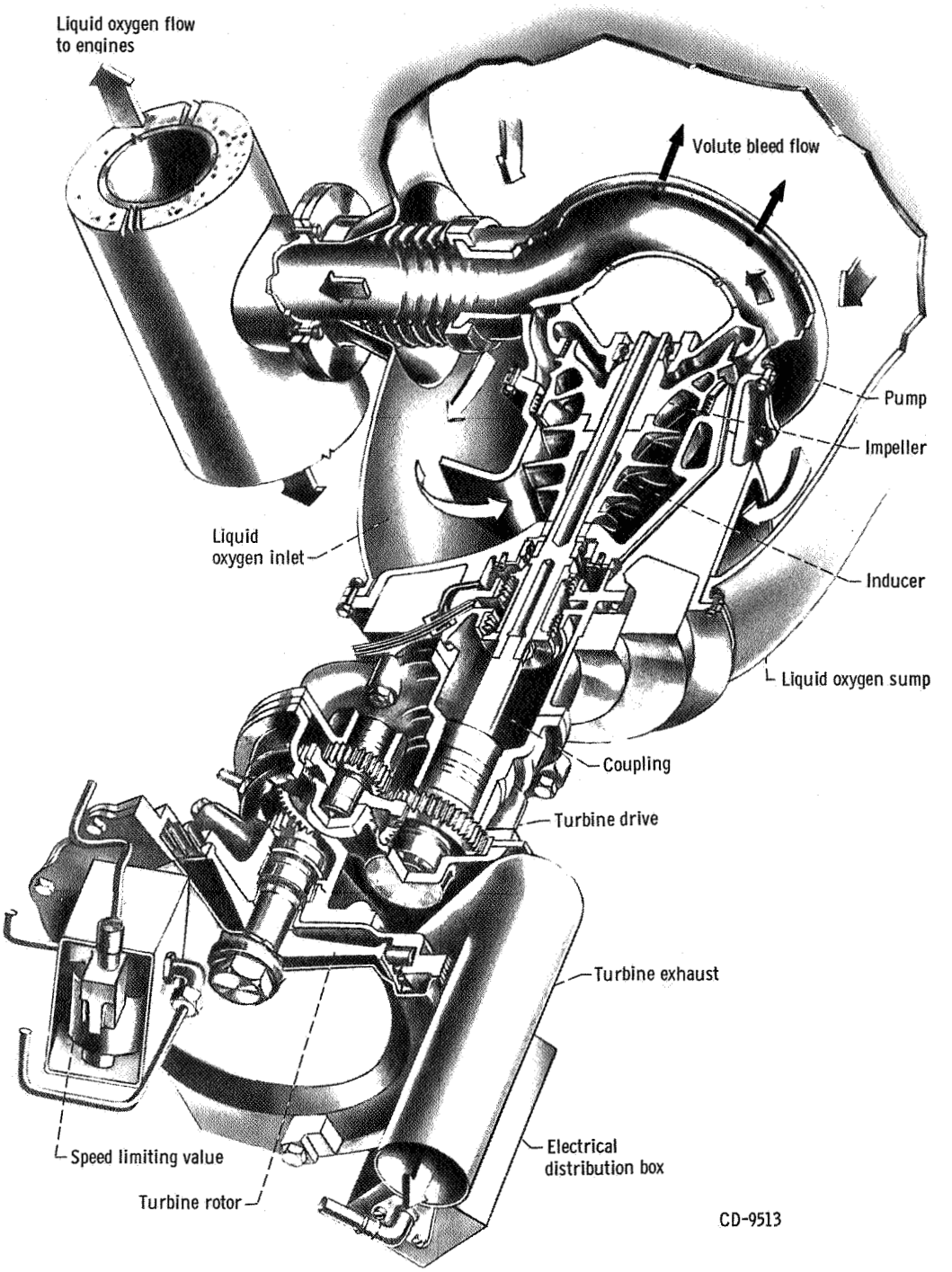

Figure V-31. - Centaur liquid oxygen boost pump cutaway, AC-9.

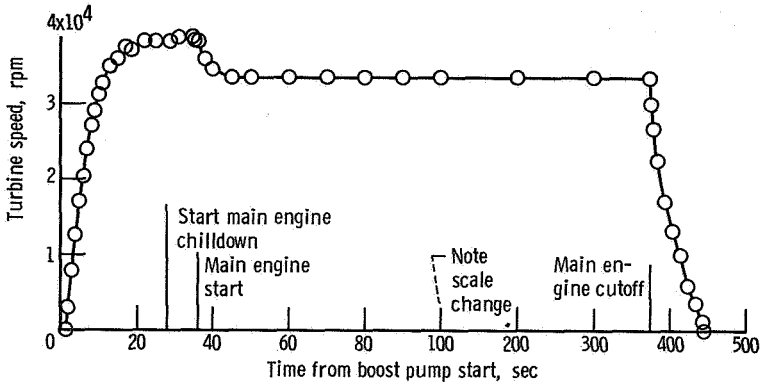

Figure V-32. - Centaur oxidizer boost pump turbine speed for main engine first firing, AC-9.

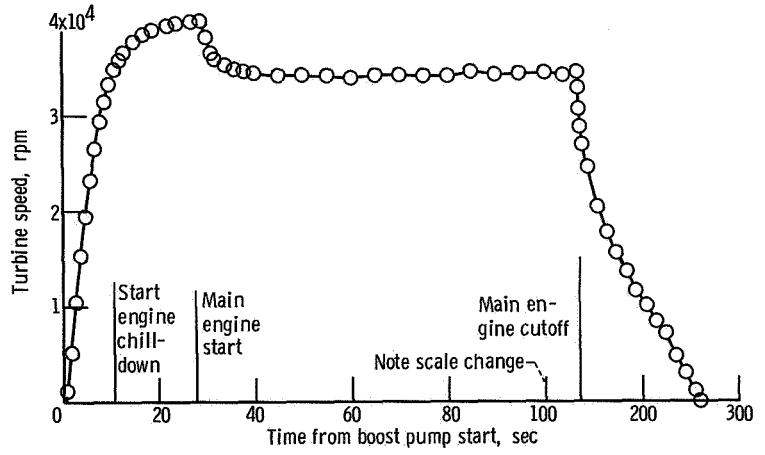

Figure V-33. - Centaur oxidizer boost pump turbine speed for main engine second firing, AC-9.

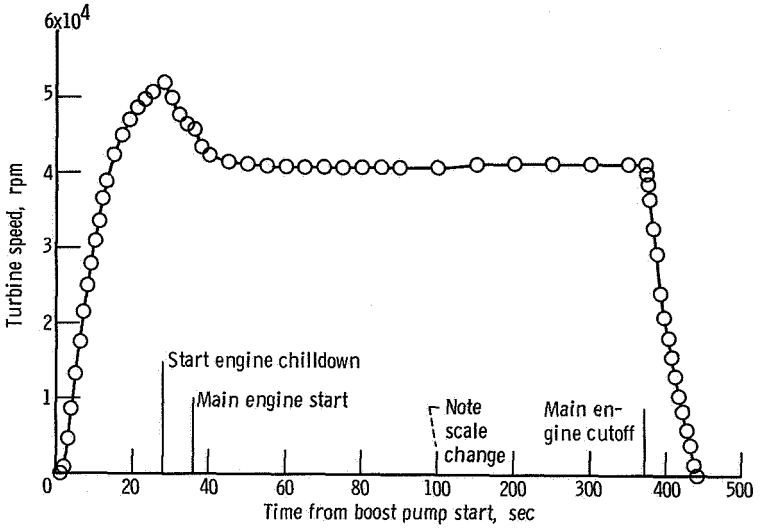

Figure V-34. - Centaur fuel boost pump turbine speed for main engine first firing, AC-9.

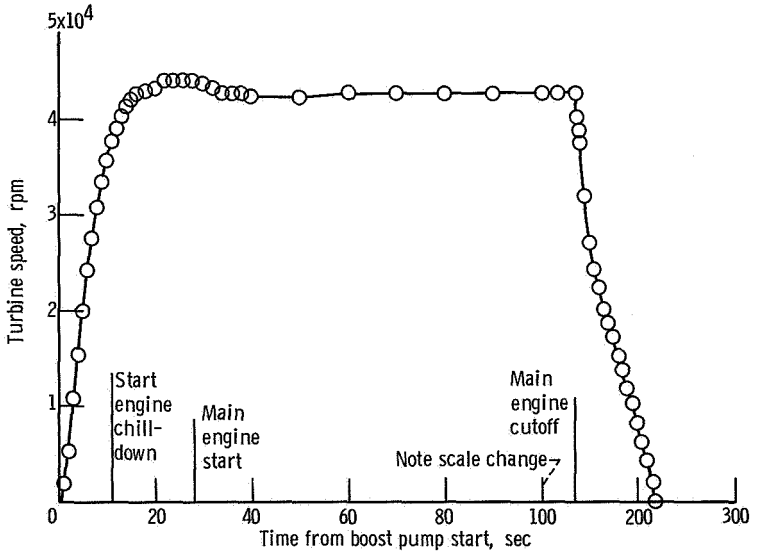

Figure V-35. - Centaur fuel boost pump turbine speed for main engine second firing, AC-9.

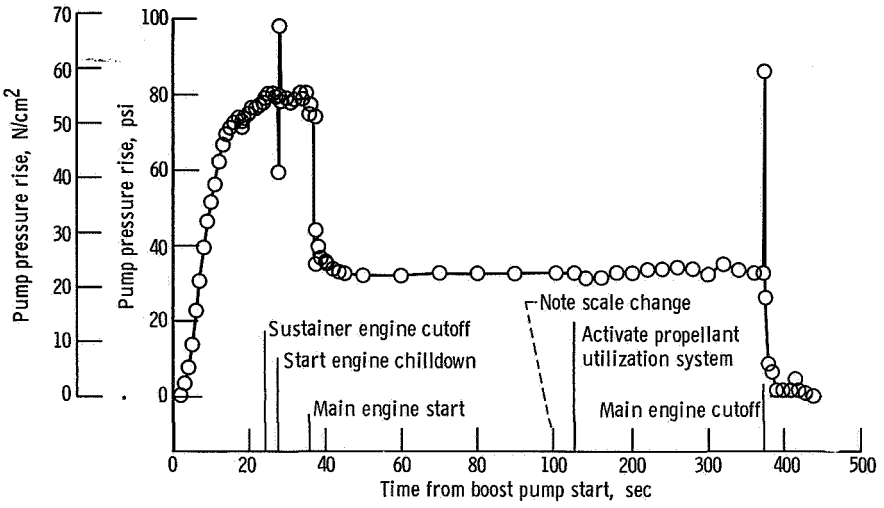

Figure V-36. - Centaur oxidizer boost pump pressure rise for main engine first firing, AC-9.

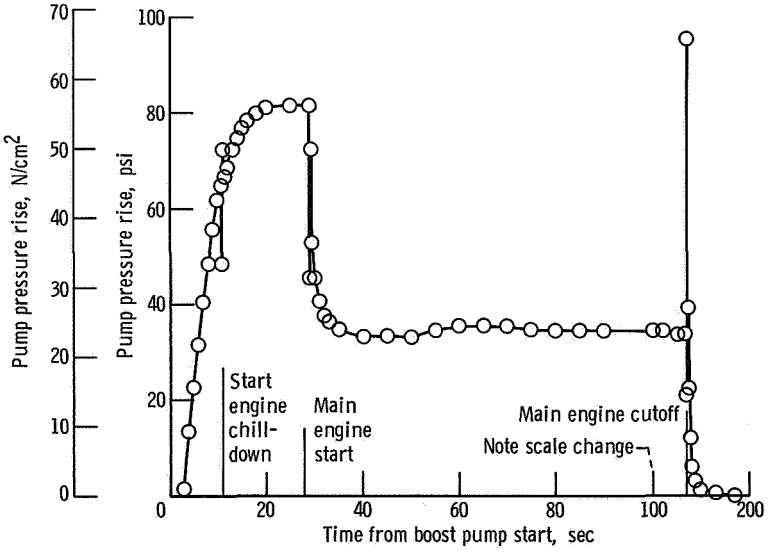

Figure V-37. - Centaur oxidizer boost pump pressure rise for main engine second firing, AC-9.

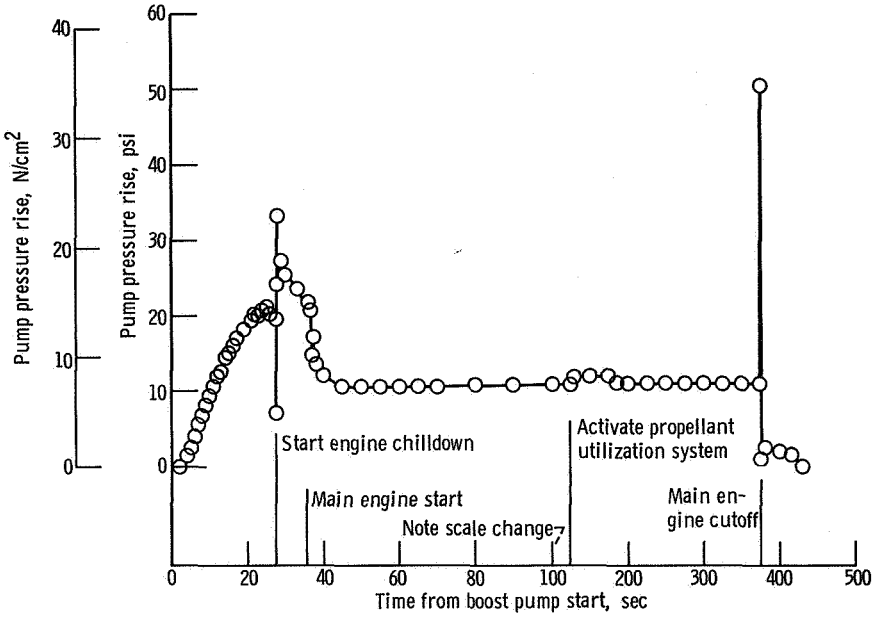

Figure V-38. - Centaur fuel boost pump pressure rise for main engine first firing, AC-9.

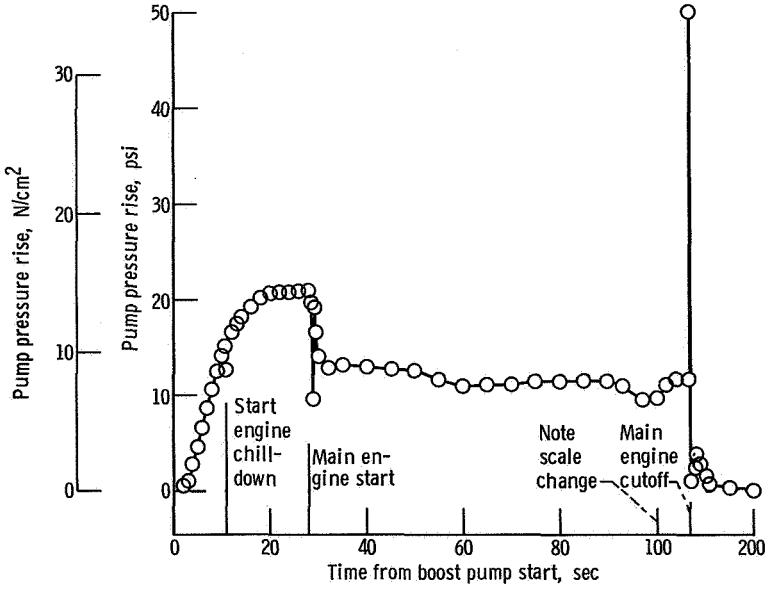

Figure V-39. - Centaur fuel boost pump pressure rise for main engine second firing, AC-9.

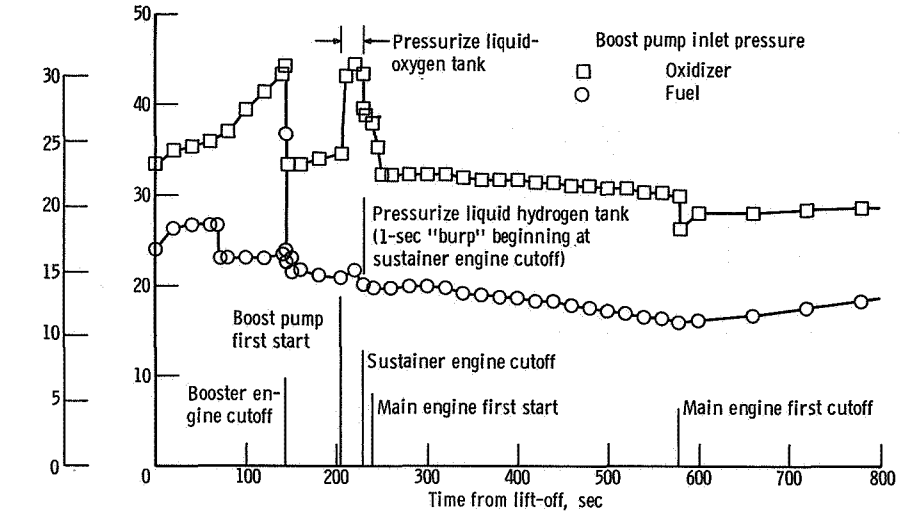

(a) T - 0 to T - 800 seconds.

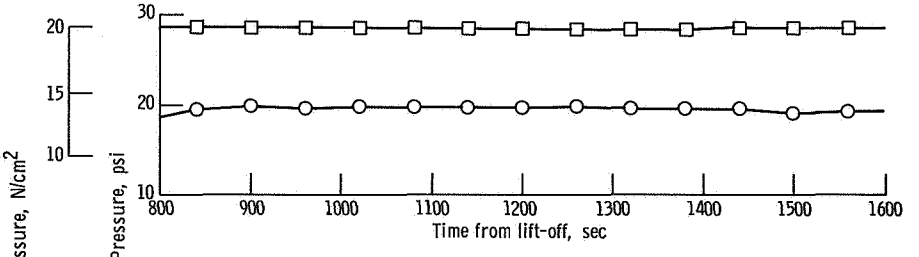

(b) T + 800 to T + 1600 seconds.

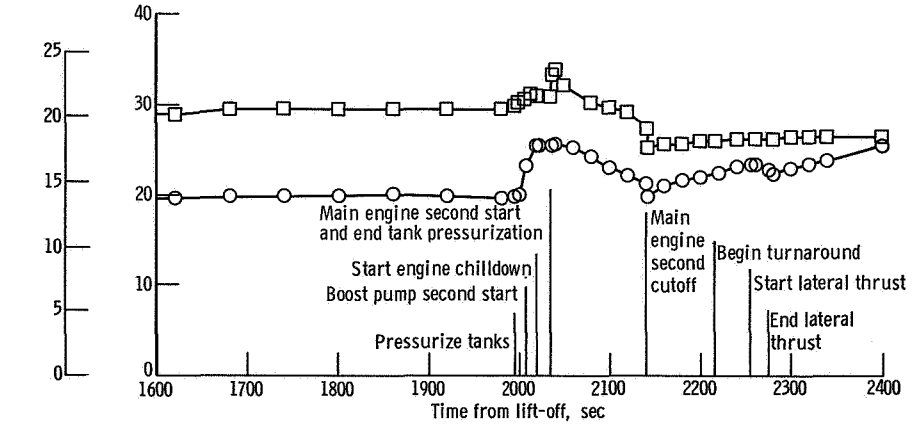

(c) T + 1600 to T + 2400 seconds.

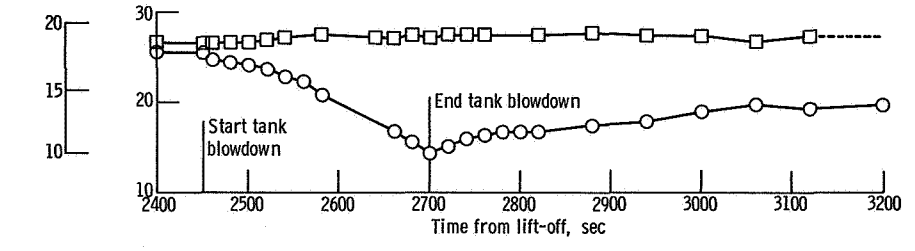

(d) T + 2400 to T + 3200 seconds.

Figure V-40. - Centaur oxidizer and fuel boost pump inlet absolute pressures, AC-9.

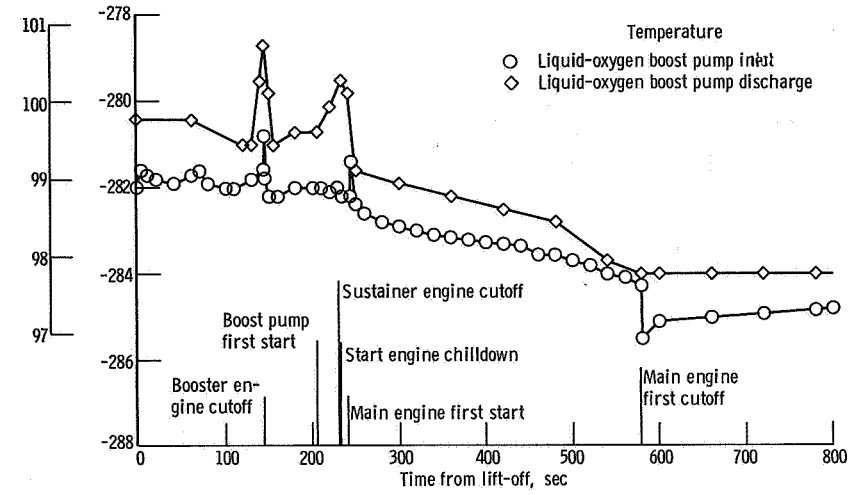

(a) T - 0 to T + 800 seconds.

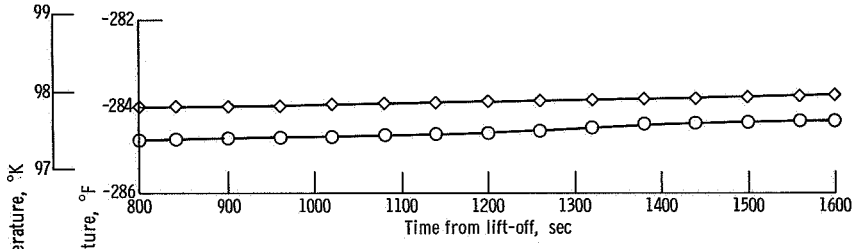

(b) T + 800 to T + 1600 seconds.

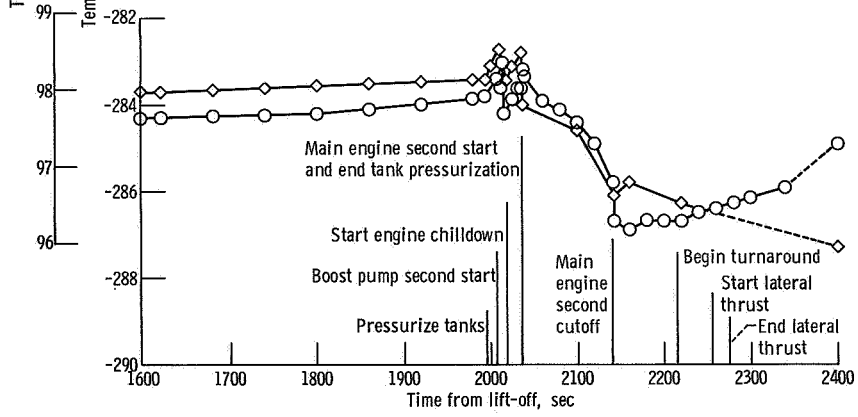

(c) T + 1600 to T + 2400 seconds.

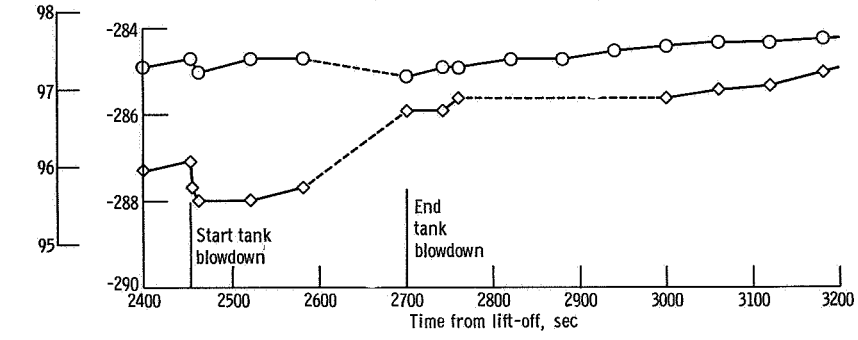

(d) T + 2400 to T + 3200 seconds.

Figure V-41. - **Centaur oxidizer** boost pump inlet and discharge temperatures, AC-9.

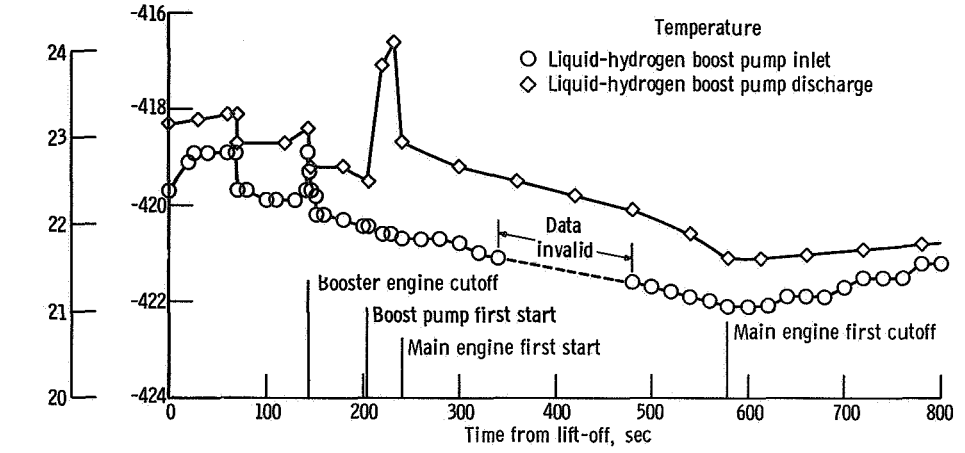

(a) T - 0 to T + 800 seconds.

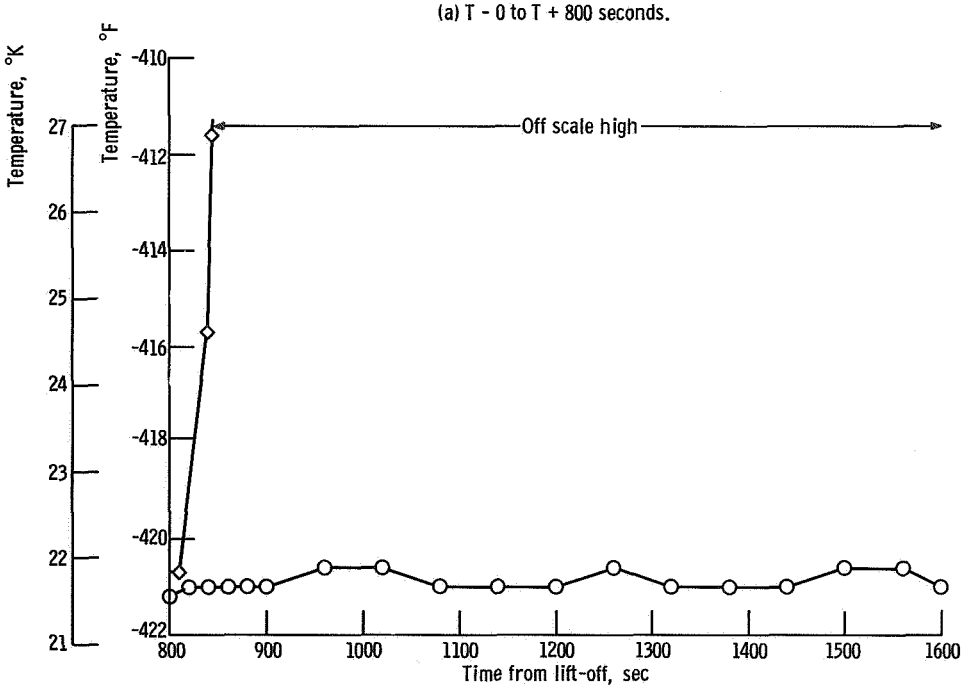

(b) T + 800 to T + 1600 seconds.

Figure V-42. - Centaur fuel boost pump inlet and discharge temperatures, AC-9.

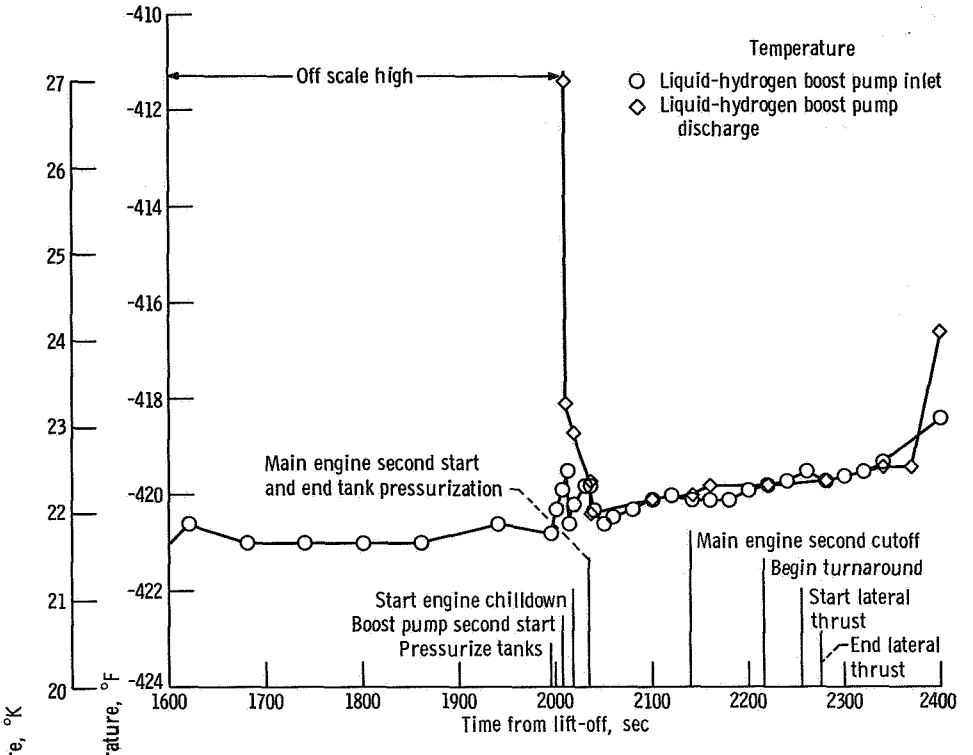

(c) T + 1600 to T + 2400 seconds.

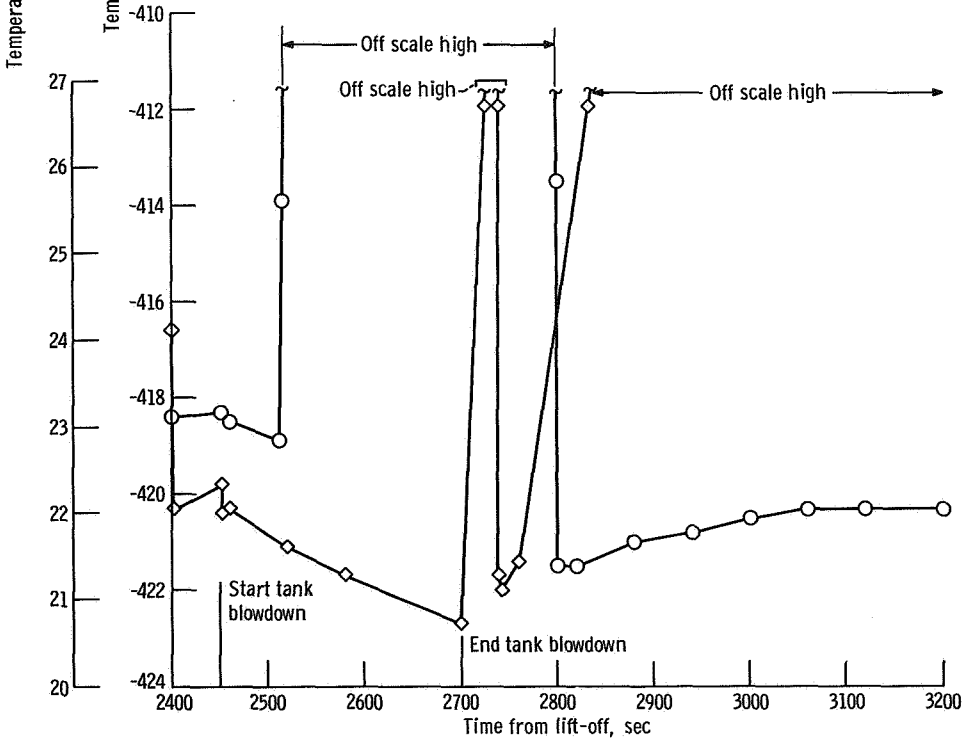

(d) T + 2400 to T + 3200 seconds.

Figure V-42. - Concluded.

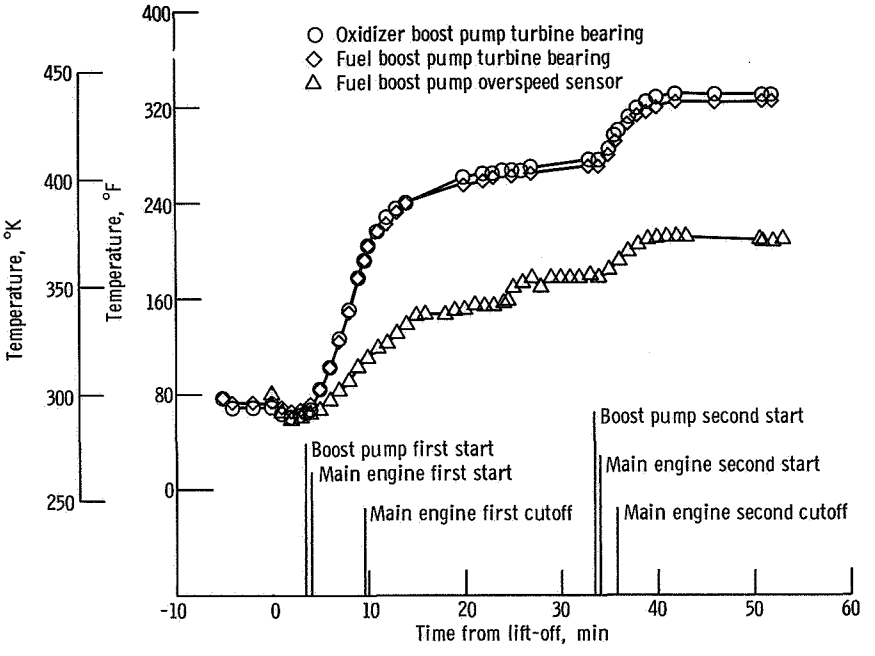

Figure V-43. - Centaur boost pump component temperatures, AC-9.

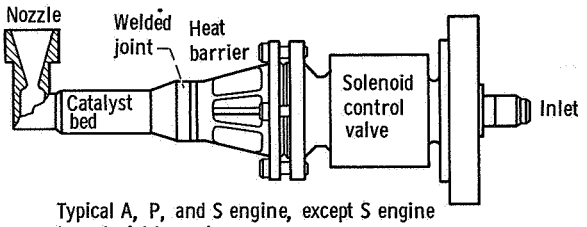

Typical A, P, and S engine, except S engine has straight nozzle

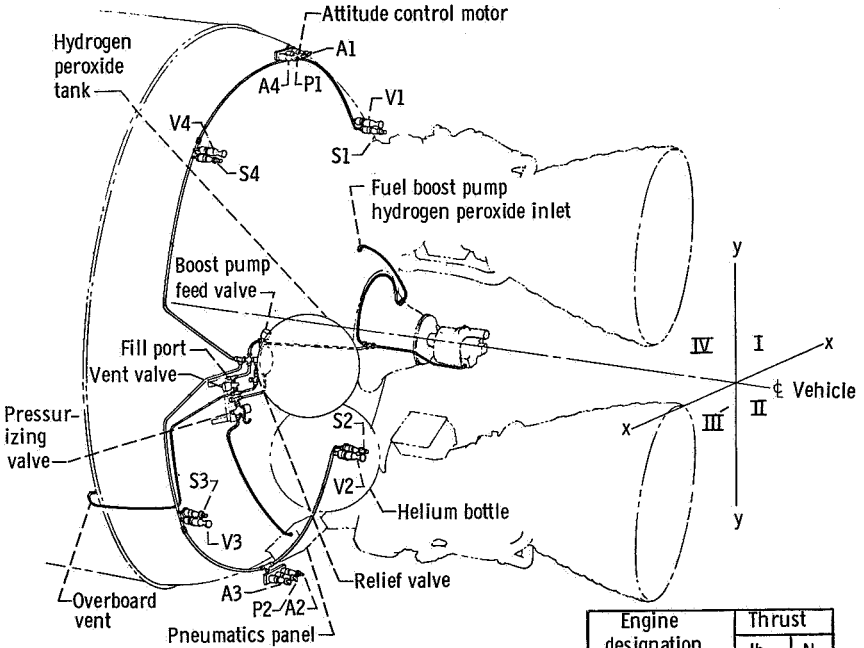

Hydrogen peroxide control system

Engine designation	Thrust	
	lb	N
V1, V2, V3, V4	50	222
S1, S2, S3, S4	3	13
A1, A2, A3, A4	3.5	16
P1, P2	6	27

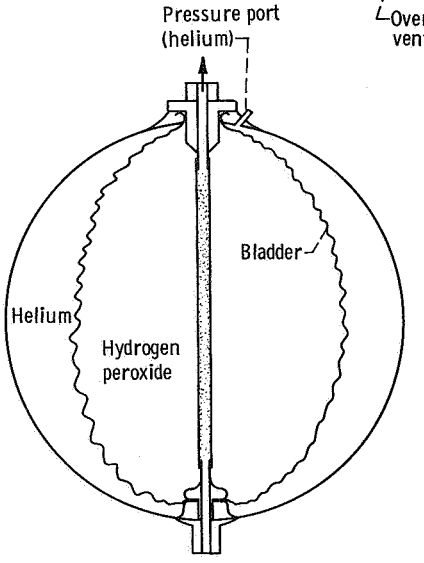

Hydrogen peroxide positive expulsion bladder type storage bottle

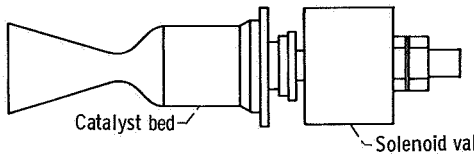

50-lb (222-N) thrust engine

CD-9517

CD-9781-31

Figure V-44. - Hydrogen peroxide system isometric, AC-9.

PROPELLANT LOADING AND PROPELLANT UTILIZATION

by Steven V. Szabo, Jr.

Propellant Level Indicating System for Propellant Loading

System description. - Atlas propellant levels for flight were determined from liquid level sensors located at discrete points in the fuel (RP-1) and liquid-oxygen tanks, as shown in figure V-45. The sensors in the fuel tank were the vibrating piezoelectric crystal type. The sensors in the liquid-oxygen tank were the platinum hot-wire type.

The control circuitry for the fuel level sensors was a piezoelectric oscillator. When the sensor was immersed in liquid, the crystal was damped, causing the oscillations to stop. This cessation of oscillations operated a relay and provided a signal for the propellant loading operator.

The control unit for the platinum hot-wire liquid-oxygen sensors was an amplifier that detected a change in voltage level. The amplified signal was applied to an electronic trigger circuit. The liquid-oxygen sensors were supplied with a nearly constant current of approximately 200 milliamperes. The voltage drop across a sensor reflected the resistance value of the sensor. The sensing element was a 1-mil (0.254-mm) platinum wire which had a linear resistance temperature coefficient. When dry, the wire has a high resistance and therefore a high voltage drop. When immersed in a cryogenic fluid, it had a low resistance and voltage drop. When the sensor was wetted, a control relay was deenergized and a signal was sent for the propellant loading operator.

The Centaur propellant level indicating system is shown in figure V-46. It utilized hot-wire level sensors in both the liquid-oxygen and liquid-hydrogen tanks. These sensors were similar in operation to the ones used in the Atlas liquid-oxygen tank.

Propellant weights. - Atlas fuel (RP-1) weight at lift-off was calculated to be 77 000 pounds (34 900 kg) based on a density of 49.8 pounds per cubic foot (797 kg/cu m). Atlas liquid oxygen tanked was calculated to be 175 500 pounds (79 580 kg) based on a density of 69.3 pounds per cubic foot (1108 kg/cu m).

Centaur propellant loading was satisfactorily accomplished. Calculated propellant weights at lift-off were 5253 pounds ±3.2 percent (2383 kg) of liquid hydrogen and 25 477 pounds ±1.5 percent (11 553 kg) of liquid oxygen. Data used to calculate these propellant weights are given in table V-6.

TABLE V-6. - CENTAUR PROPELLANT LOADING DATA, AC-9

Quantity or event	Propellant tank	
	Hydrogen	Oxygen
Sensor required to be wet at T - 90 sec, percent	99.8	----------
Sensor required to be wet at T - 75 sec, percent	----------	100.2
Sensor location (vehicle station number)	175	373
Tank volume at sensor[a], ft^3; m^3	1257; 35.6	371; 10.5
Ullage volume at sensor, ft^3; m^3	11.2; 0.32	6.6; 0.19
Liquid hydrogen 99.8 percent sensor dry at-, sec	T - 28	----------
Liquid oxygen 100.2 percent sensor dry at-, sec	----------	T - 65
Ullage absolute pressure at time sensor goes dry, psi; N/cm^2	22.6; 15.6	31.0; 21.4
Density[b] at time sensor goes dry, lb mass/ft^3; kg/m^3	4.18; 70.0	68.7; 1100
Weight in tank at sensor dry, lb mass; kg	5259; 2385	25 498; 11 563
Liquid-hydrogen boiloff[c] to vent valve close, lb mass; kg	6; 3	----------
Liquid-oxygen boiloff[c] to lift-off, lb mass; kg	----------	21; 10
Ullage volume at lift-off, ft^3; m^3	12.7; 0.4	7; 0.2
Weight[d] at lift-off, lb mass; kg	5253±3.2%; 2382±3.2%	25 477±1.5%; 11 553±1.5%

[a]Volumes include 1.85 ft^3 (0.5 m^3) liquid oxygen and 2.53 ft^3 (0.72 m^3) liquid hydrogen for lines from boost pumps to engine turbopump inlet valves.

[b]Liquid-hydrogen density taken from ref. 2; liquid-oxygen density taken from ref. 3.

[c]Boiloff rates determined from tanking test to be 0.31 lb mass/sec (0.14 kg/sec) liquid hydrogen and 0.33 lb mass/sec (0.15) kg/sec) liquid oxygen.

[d]Preflight estimates were 5301 lb (2404 kg) of liquid hydrogen and 25 447 lb (11 543 kg) liquid oxygen.

Atlas Propellant Utilization System

System description. - The Atlas propellant utilization system (fig. V-47) was used to ensure nearly simultaneous depletion of the propellants and minimum propellant residuals at sustainer engine cutoff. This was accomplished by controlling the propellant mixture ratio (ratio of oxidizer flow rate to fuel flow rate) to the sustainer engine. The system consisted of two mercury manometer assemblies, a computer-comparator, a hydraulically actuated propellant utilization (fuel) valve, sensing lines, and associated electrical harnessing. During flight, the manometers sensed propellant head pressures which were indicative of propellant mass. The mass ratio was then compared with a reference ratio in the computer-comparator, and if needed, a correction signal was sent to the valve controlling the main fuel flow to the sustainer engine (the propellant utilization valve). The oxidizer flow was regulated by the head suppression valve. This valve sensed propellant utilization valve movement and moved in a direction opposite to that of the propellant utilization valve. This opposite movement thus altered the propellant

mixture ratio but maintained a constant total propellant mass flow to the engine. The system flown on AC-9 was modified slightly from previous vehicles. The head sensing manometer cross sections were recontoured to match the Centaur flight profile more closely.

System performance. - The Atlas propellant utilization system operation was satisfactory. However, because of the early sustainer engine cutoff, propellant residuals were not minimized.

The system error signal (error demodulator output) and the propellant utilization valve angle during flight are shown in figure V-48. The valve responded properly to the error signal. The fuel and liquid-oxygen head sensing ports uncovered within 1.25 seconds of each other, with the liquid-oxygen port uncovering first. This small time difference in port uncovery indicates satisfactory system performance.

Atlas propellant residuals. - The premature sustainer engine cutoff resulted in calculated propellant residuals of 891 pounds (404 kg) of liquid oxygen and 528 pounds (240 kg) of fuel above the sustainer engine pump inlet. These calculations were based on the propellant utilization head sensing port uncovery times and volumes below the ports. Sustainer engine flow-rate decay, based on propellant utilization valve angles, was also included in the residual calculations.

Centaur Propellant Utilization System

System description. - The Centaur propellant utilization system was used during flight to control propellant consumption by the main engines to provide minimum propellant residuals. The system is shown schematically in figure V-49. It was also used during tanking to indicate propellant levels. The mass of propellant remaining in each tank was sensed by a capacitance probe and compared in a bridge circuit. If the mass ratio of propellants remaining varied from a predetermined value (ratio of oxidizer to fuel, 5 to 1), an error signal was sent to the proportional servopositioner which controlled the liquid-oxygen flow control valve. If the mass ratio was greater than 5 to 1, the liquid oxygen flow was increased to reestablish the 5 to 1 ratio. If the ratio was less than 5 to 1, the liquid-oxygen flow was decreased. Since the sensing probes to not extend to the top of the tanks, system control was not commanded "on" until approximately 90 seconds after main engine first start. For this 90 seconds of engine firing, the bridge is nulled, locking the liquid-oxygen flow-control valves at a propellant mixture ratio of 5 to 1.

System performance. - Prelaunch checks and calibrations of the system were all within specification. The in-flight operation of the system was satisfactory during both engine firing periods. The system liquid-oxygen flow-control-valve positions during the

engine firings are shown in figure V-50. The system was commanded on by the vehicle programmer at main engine first start plus 89.1 seconds. The valves then moved to the oxygen-rich stop and remained there for approximately 40 seconds. During this time, the system corrected for 287 pounds (130 kg) of excess oxygen. This correction was necessary because of

(1) Engine consumption error during the first 90 seconds of engine firing
(2) Tanking errors
(3) System bias to ensure that liquid oxygen depleted first
(4) System bias to compensate for differential propellant boiloff during coast; the liquid-oxygen boiloff is zero and, if this compensation was not made, the mass ratio at main engine second start would not be 5 to 1

The system commanded the valve to control mainly in a hydrogen-rich position during the remainder of the first engine firing period. The maximum valve angle was approximately 35^{o}. At main engine first cutoff, the valves moved to the oxygen-rich stop. Approximately 10 seconds after engine shutoff, the system bias for the coast phase differential propellant boiloff was removed from the bridge, and the valves moved to the hydrogen-rich stop in response to the hydrogen-rich condition existing in the tanks. After main engine first cutoff, the propellants began to rise in the sensing probes due to capillary action. In approximately 100 seconds, the propellants had filled the probes, and the system began to sense a liquid-oxygen-rich condition. At this time the valves moved to the oxygen-rich stop and remained there for the remainder of the coast period. The valves remained at the oxygen-rich stop through the main engine start transient. Approximately 17 seconds after engine start, the valves moved from the stop and controlled in a hydrogen-rich position. Approximately 25 seconds prior to main engine second cutoff, the valves were placed in a mixture ratio position of 5 to 1 because the probes do not extend to the bottom of the tanks and system control is eliminated at this time.

Centaur propellant residuals. - The propellant residuals were calculated by using data obtained from the propellant utilization system. Liquid propellants remaining at engine first cutoff were calculated by using the times that the propellant levels passed the tops of the sensing probes as reference points. The gaseous-hydrogen residual at main engine first cutoff was based on the temperature profile in the tank as shown in figure V-51. This temperature profile was established from ullage temperature sensors located as shown in figure V-56. These calculations established the liquid-hydrogen level at main engine first cutoff as station 331. This level corresponds to the level indicated by the in-tank liquid-vapor sensors, as shown in figure V-52. The gaseous-oxygen residual was calculated assuming saturated oxygen gas in the tank. The liquid-oxygen level was calculated to be station 425.8 at main engine first cutoff. The propellants remaining in the tanks at main engine first cutoff are given in the following table:

Propellant remaining at main engine first cutoff	Propellant	
	Hydrogen	Oxygen
Liquid residual, lb; kg	1420; 644	6417; 2904
Gaseous residual, lb; kg	68; 31	140; 64

The liquid-hydrogen level at main engine second cutoff was calculated at station 379.5. This station number was also determined from in-tank liquid-vapor sensors, as shown in figure V-52. The liquid-oxygen level, calculated from propellant utilization system data, was station 449.8 at main engine second cutoff. The propellant residuals remaining at main engine second cutoff were calculated by using the times that the propellant levels passed the bottoms of the probes as reference points. The residuals were as shown in the following table:

Residuals at main engine second cutoff	Propellant	
	Oxygen	Hydrogen
Total propellants, lb; kg	340; 154	149; 68
Burnable propellants, lb; kg	272; 123	76; 34
Remaining burn time to depletion, sec	4.8	6.7

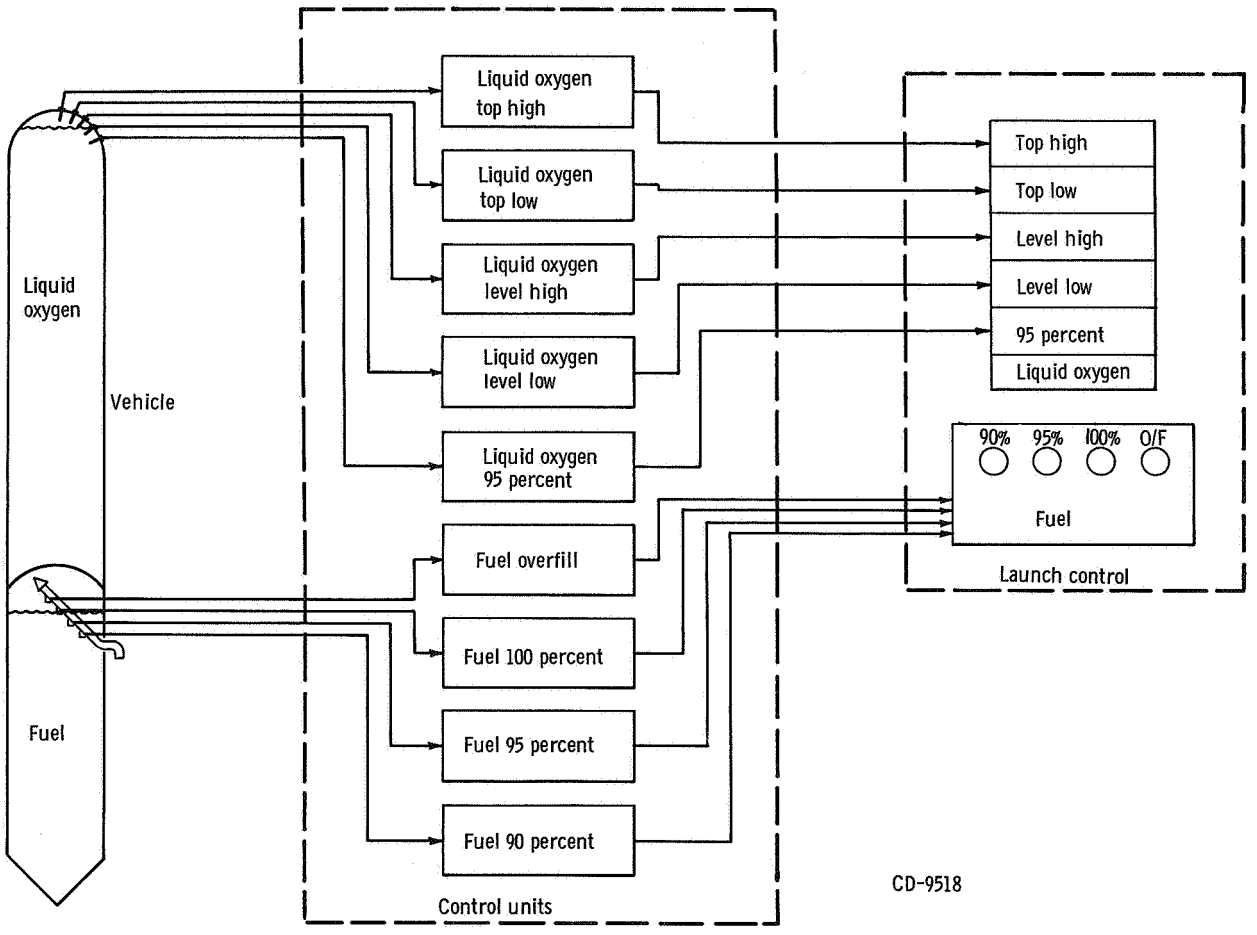

Figure V-45. - Propellant level indicating system for Atlas propellant loading, AC-9. Lights on launch control panel indicate if sensor is wet or dry. (Percent levels are indications of required flights levels and not percent of total tank volume.)

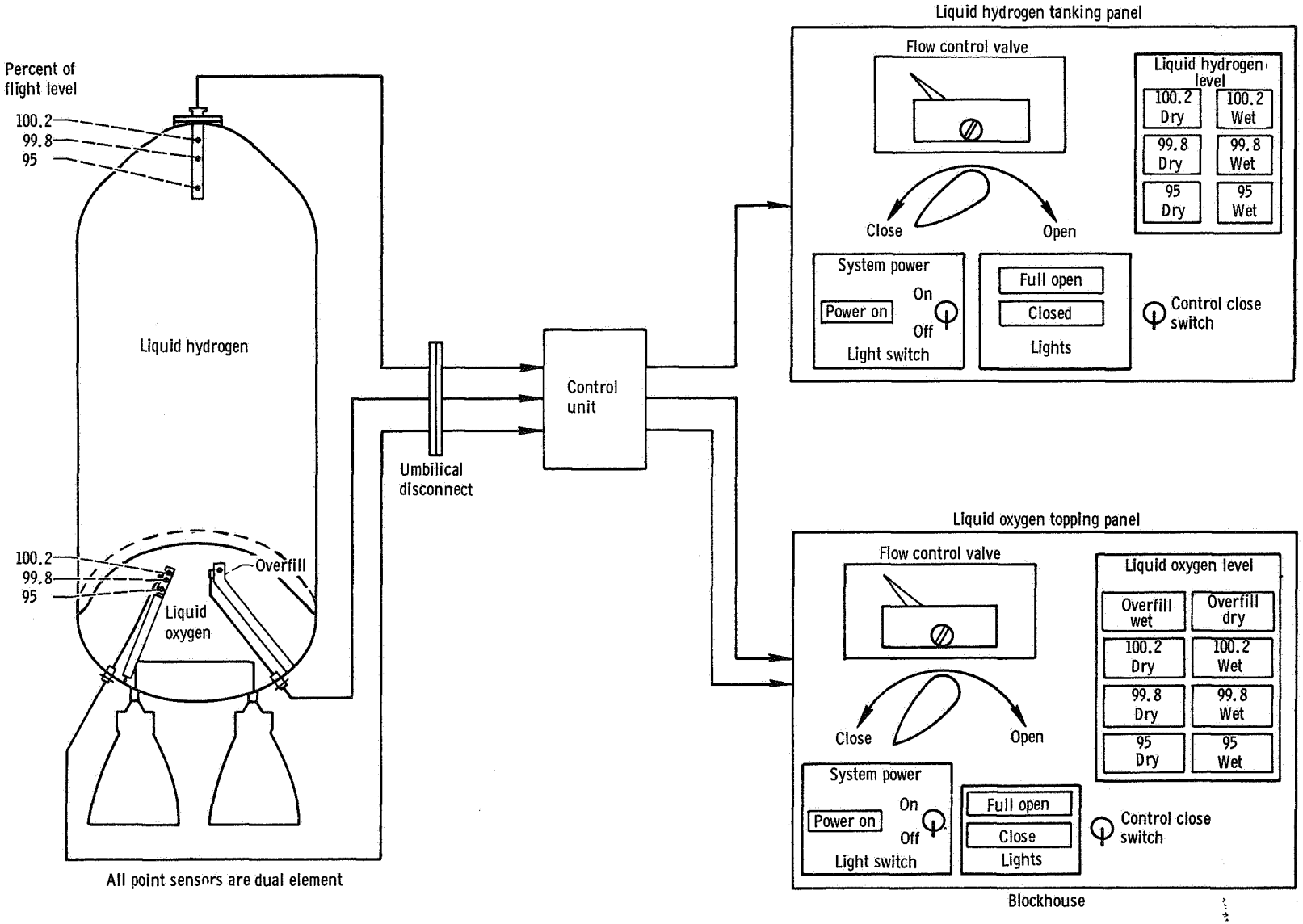

Figure V-46. - Level indicating system for Centaur propellant loading, AC-9.

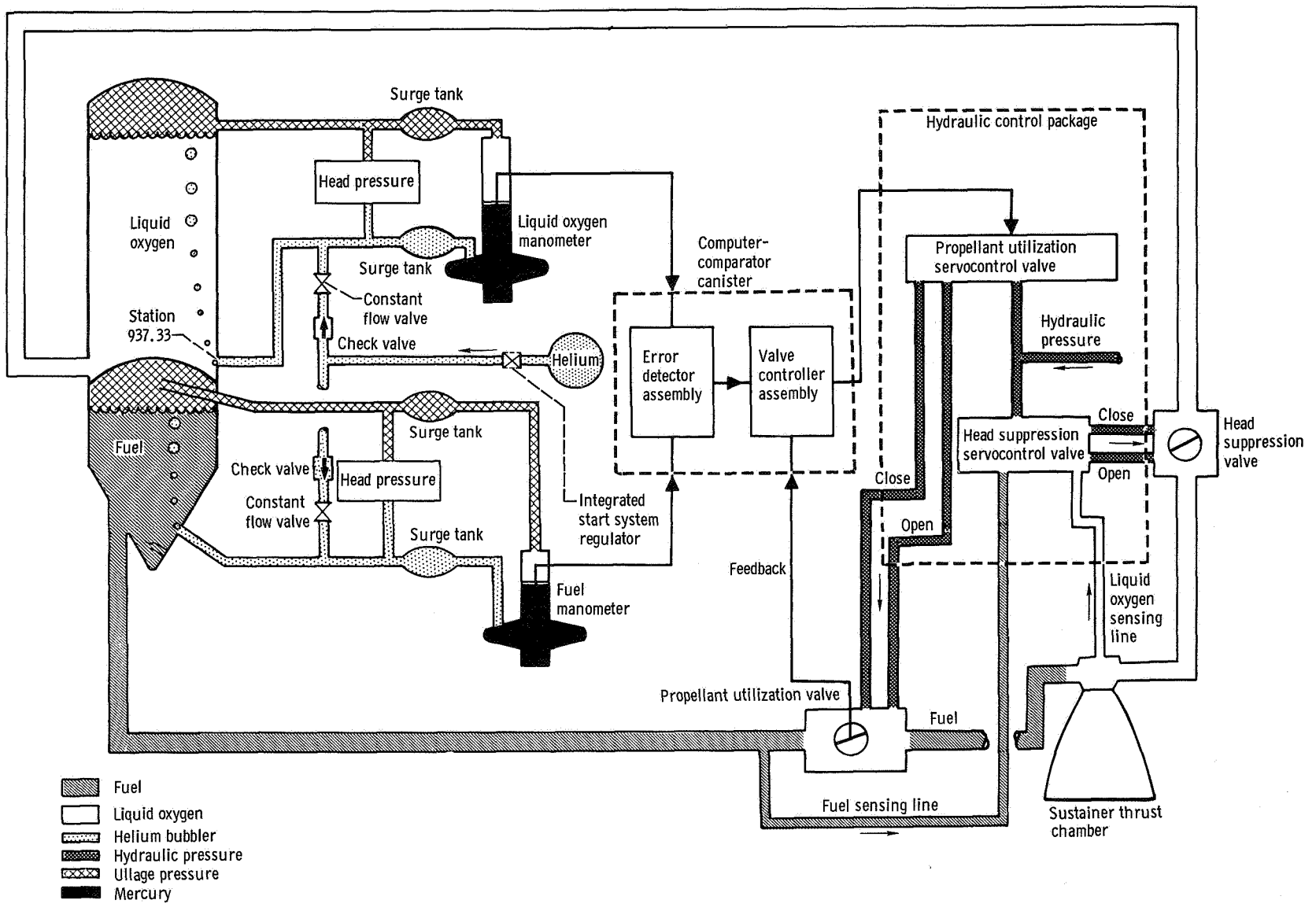

Figure V-47. - Atlas propellant utilization system, AC-9.

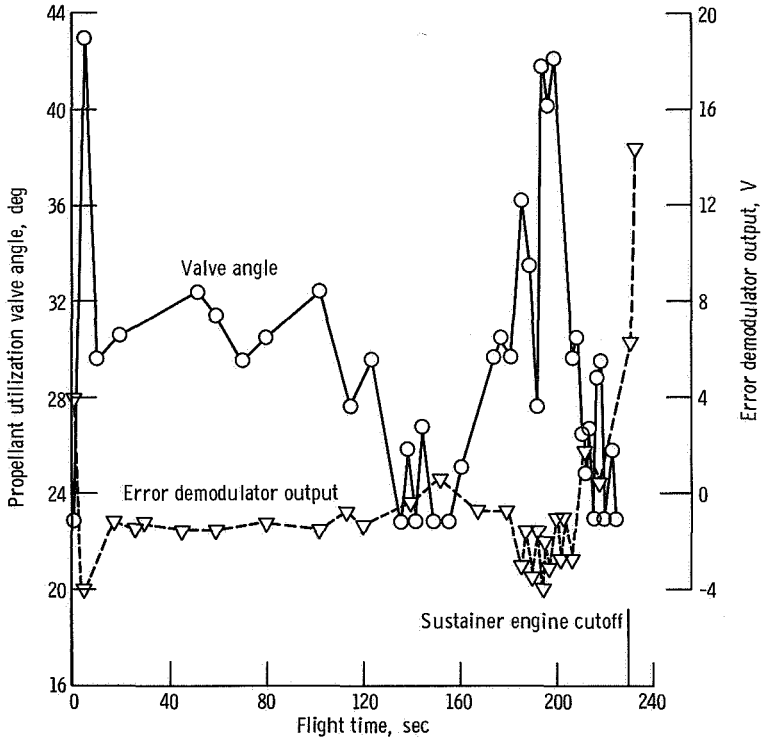

Figure V-48. - Atlas propellant utilization valve angle and error demodulator output, AC-9.

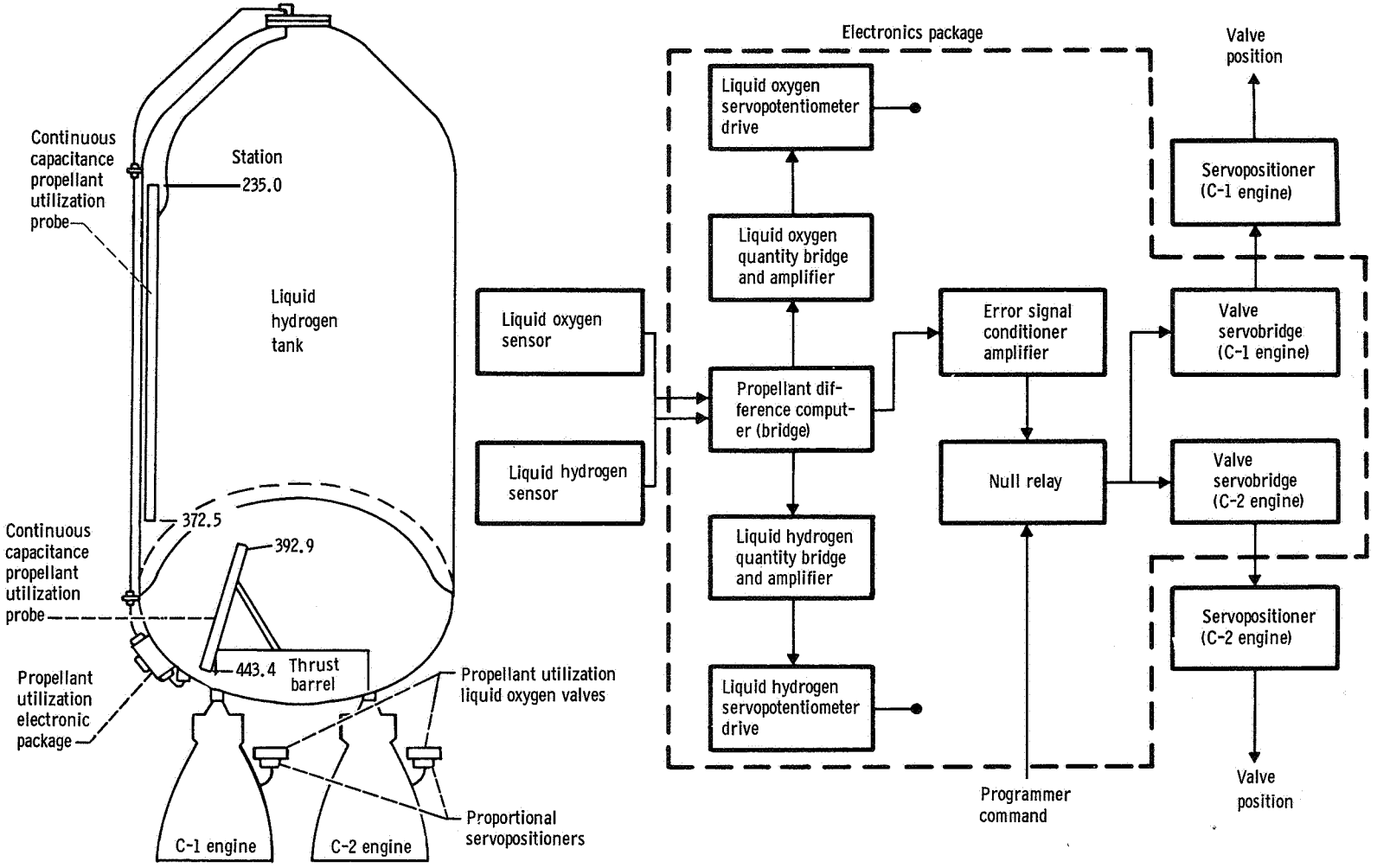

Figure V-49. - Centaur propellant utilization system, AC-9.

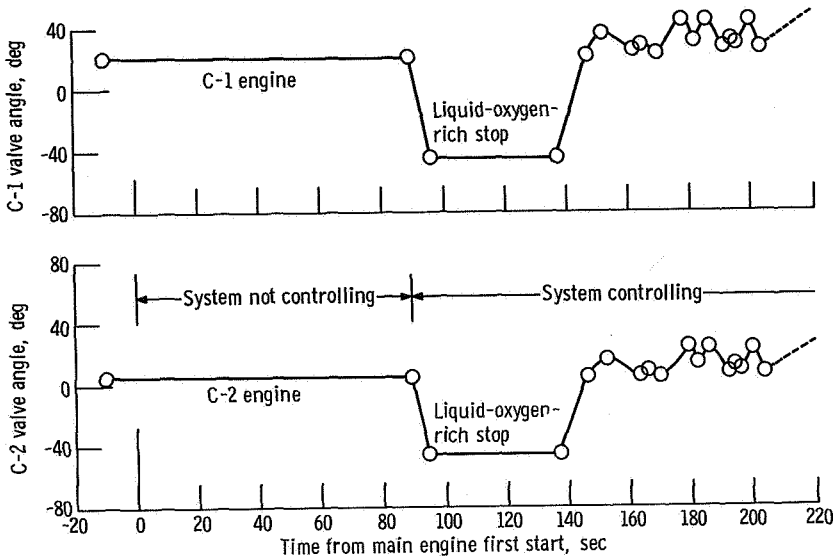

(a) Main engine first firing; T - 20 to T + 220 seconds.

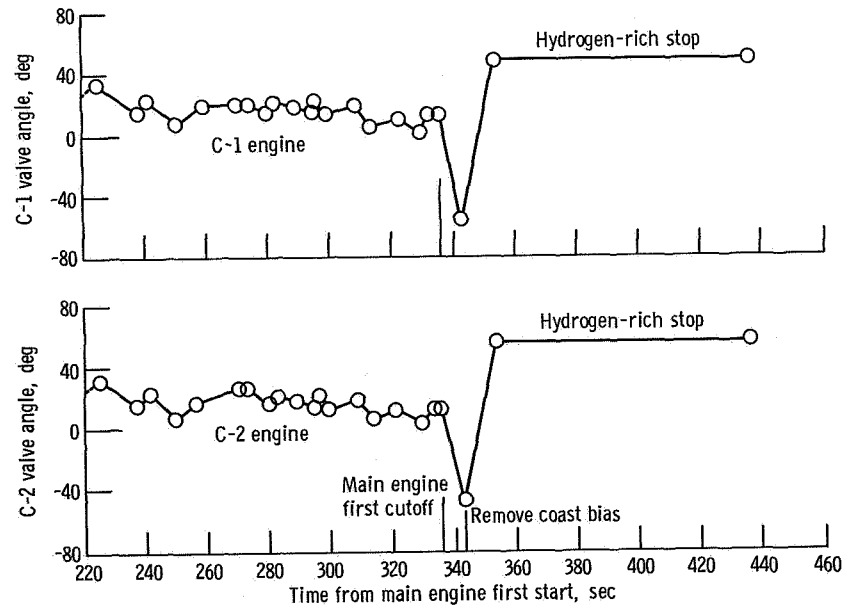

(b) Main engine first firing; T + 220 to T + 440 seconds.

Figure V-50. - Centaur propellant utilization valve angles, AC-9.

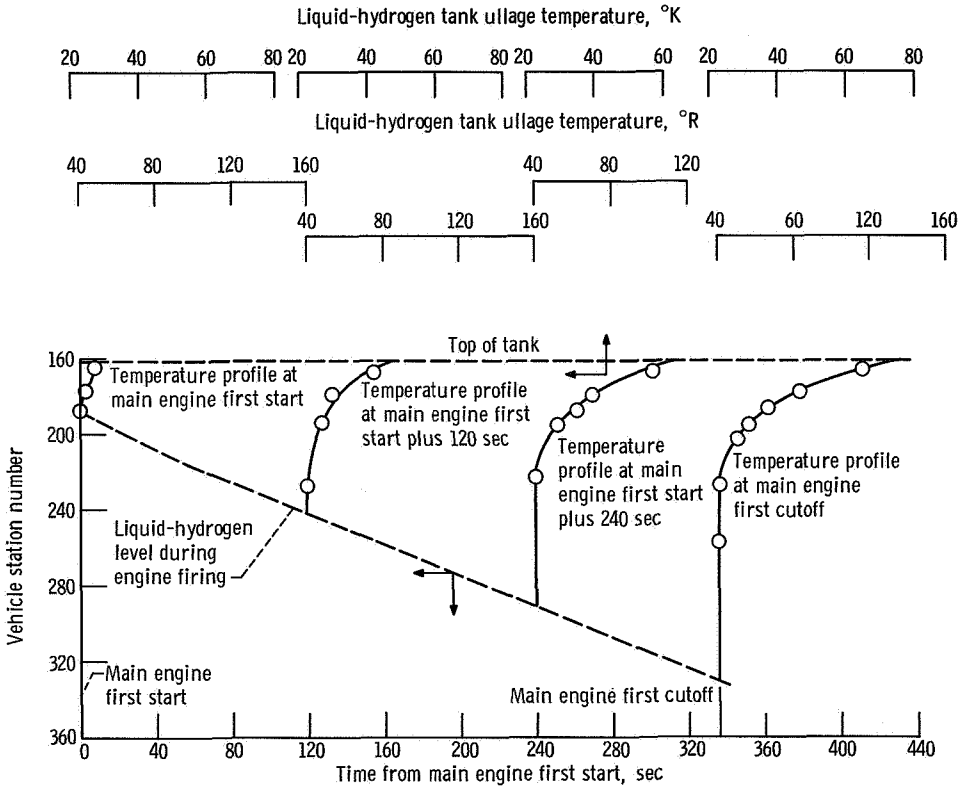

Figure V-51. - Hydrogen ullage temperature profile during engine first firing, AC-9.

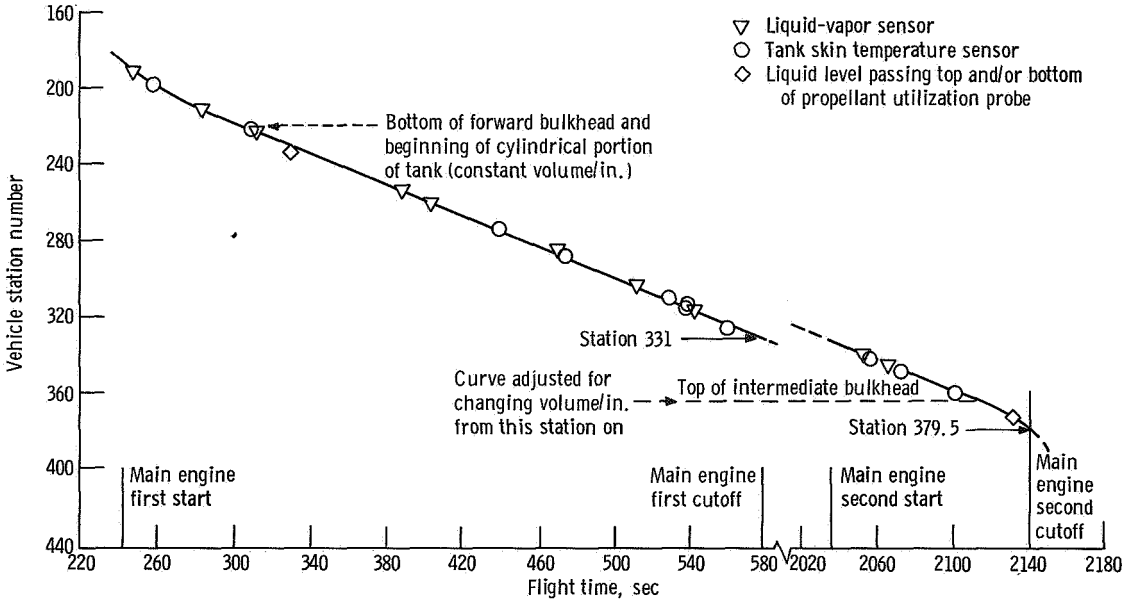

Figure V-52. - Liquid-hydrogen level during main engine first and second firings, AC-9. (See fig. III-2 for relative station number locations.)

COAST PHASE PROPELLANT MANAGEMENT AND PROPELLANT THERMODYNAMICS

by Steven V. Szabo, Jr., and Frederick C. M. Yeh

Coast Phase Propellant Management System

System description. - The AC-9 vehicle propellant management system was identical to that on AC-8 (ref. 1). Energy dissipators, as shown in figure V-53, were installed in the hydrogen tank on

(1) The boost pump volute bleed line

(2) The hydrogen feed duct recirculation line

(3) The hydrogen tank pressurization line

A slosh baffle was installed in the hydrogen tank. The baffle was located at a position which corresponded to the predicted level of the propellant at main engine first cutoff (fig. V-54). Varied thrust levels were also applied to the vehicle during the coast phase. This thrust schedule is shown in figure V-55. At main engine first cutoff, 100 pounds (444 N) of thrust were applied to the vehicle for 76 seconds, suppressing any large propellant disturbances associated with the engine shutdown. Then, 6 pounds (27 N) of thrust were applied to the vehicle until 40 seconds prior to main engine second start. This thrust retained the propellants at the rear of the tanks. Forty seconds prior to main engine second start, the 6 pounds (27 N) of thrust were discontinued and the 100 pounds (444 N) of thrust were reapplied to suppress any propellant disturbances caused by the main engine second prestart sequence.

Coast phase propellant instrumentation. - The AC-9 hydrogen tank was uniquely instrumented with 31 liquid-vapor sensors and ullage temperature sensors, as shown in figure V-56. Although these sensors are part of the overall vehicle instrumentation and telemetry system, the sensors and location are described here for the convenience of the reader. See reference 4 for a detailed description and operation of the liquid-vapor and temperature sensors. These sensors were installed to provide data on liquid-hydrogen motion in the tank and to provide the ullage temperature profile in the hydrogen tank during flight. In addition, the temperature sensors served as liquid-vapor sensors. Also installed on the hydrogen tank were 50 temperature patches to monitor tank skin temperature. The location of the temperature patches is shown in figure V-57.

The liquid-oxygen tank was also instrumented but to a lesser extent. Four skin temperature patches on the tank skin were located as shown in figure V-57.

Liquid-Hydrogen Behavior

Atlas phase of flight. - As shown in figure V-58, the liquid-hydrogen motion during this portion of flight consisted of small surface disturbances. These were in response to hydrogen venting, vehicle acceleration changes at booster and sustainer engine cutoff, and pressurization gas flow during Centaur engine prestart.

Centaur main engine first firing. - During the first Centaur engine firing period, the liquid-vapor sensors responded to the decreasing liquid level, as shown in figure V-58. At main engine first cutoff, minor disturbances were noted in the liquid surface. Sensors located at station 316, approximately 15 inches (38.1 cm) above the liquid surface, were wetted momentarily. However, drying of these sensors occurred within 20 seconds, indicating propellant disturbances were suppressed and the liquid hydrogen was settled.

Coast phase. - Immediately following main engine first cutoff, two 50-pound (222-N) thrust engines were fired for a period of 76 seconds. This thrust level provided an acceleration of 7×10^{-3} g's and settled the propellant in the rear of the tank. For the remainder of the coast, two 3-pound (13-N) thrust engines fired to produced a continuous acceleration of 4×10^{-4} g's on the vehicle. This low, but positive, gravity field retained the propellant in the rear of the tank. No movement of liquid hydrogen was noted throughout the coast phase.

Centaur main engine second firing. - Approximately 40 seconds prior to engine second start, the two 50-pound (222-N) thrust engines were fired to suppress any propellant disturbances caused by the engine prestart sequence. The two 3-pound (13-N) thrust engines were shut off during this time period. The liquid-vapor sensors showed the liquid hydrogen to be completely settled and available for engine start. Engine start occurred as planned, and no unusual propellant motion was observed during this engine firing period. During the firing, the remaining liquid-vapor sensors below the liquid level at engine start became progressively dry as the liquid level decreased.

Post-Centaur main engine second firing. - Following engine second cutoff, various sensors were wetted in the hydrogen tank. This wetting was caused by sprays from the hydrogen boost pump volute bleed and hydrogen feed duct recirculation lines. Liquid motion was also observed in response to vehicle turnaround and beginning of lateral thrust. No liquid motion was observed after the beginning of retrothrust.

Liquid-Oxygen Behavior

Data from the four liquid-oxygen-tank skin temperature patches are presented in figure V-59. The location of these patches is shown in figure V-57. The data reflect the cooling of the Centaur thrust section during the first portion of booster flight. This

cooling was the result of gas outflow from the interstage during ascent. A warming trend was then observed as aerodynamic heating effects became pronounced.

During the Centaur engine first firing, from approximately T + 250 to T + 575 seconds, a cooling trend was observed. This cooling was caused by the decreasing ullage pressure causing bulk fluid boiling with the resultant drop in bulk-liquid-oxygen temperature.

The temperature patches were observed to warm slightly prior to main engine first cutoff because the liquid-oxygen level receded to a level below the temperature patch. The liquid-oxygen level at first engine cutoff was calculated at station 425.8.

Immediately following engine first cutoff, the temperature patches indicated a sharp drop in temperature that was caused by liquid sloshing along the tank walls. During the coast phase, the temperature patches indicated temperatures greater than 210° R (107° K), which were caused mainly by solar heating. The liquid level at this time was below the patches, and no wetting was noted during the coast. This lack of wetting indicated that the liquid oxygen remained settled during the coast phase.

Hydrogen Tank Ullage Temperature Survey

The Centaur hydrogen tank ullage was instrumented with 16 temperature sensors, as shown in figure V-56. These sensors were installed to obtain data on the ullage temperature stratification during flight. These sensors also served as liquid-vapor sensors.

The temperature profile in the hydrogen ullage above station 287 is shown in figure V-60. From main engine start to main engine first cutoff, increasing temperature stratification was indicated in the ullage. The temperature measurement located at station 167, near the forward end of the vehicle, exhibited the largest temperature rise. The temperature increased from 48° R (27° K) at main engine first start to 117° R (65° K) at main engine first cutoff. Other temperature measurements exhibited progressively smaller temperature increases at lower sensor locations in the tank. Temperatures below station 287, which was 44 inches (1.1 m) above the liquid level at main engine first cutoff, remained at saturated hydrogen temperatures throughout main engine first firing.

Shortly after main engine first cutoff, some temperature oscillations occurred in the ullage at the forward end of the tank. These oscillations were caused by transients from main engine first cutoff. However, no sensors indicated liquid-hydrogen temperatures.

The first venting of the hydrogen tank occurred at T + 875 seconds. Two sensors (CF155T and CF158T), located near the forward end of the tank, showed an immediate temperature decrease. This indicated that the warm ullage gas in this area was being vented and being replaced by cooler gas from the lower portion of the tank. Hydrogen

venting continued for the remainder of the coast. The response to hydrogen venting of the sensors located in the forward end of the tank is shown in figure V-60(b). The temperature profile during the venting periods indicated stratification in the ullage. The rate of temperature increase was small, however.

At T + 1995 seconds, the hydrogen tank was pressurized with helium in preparation for engine start. The introduction of warm helium into the tank caused the temperature to increase sharply at several locations. Temperature profiles in the hydrogen tank ullage at main engine second start and main engine second cutoff are shown in figure V-61. During the second engine firing period, temperature stratification was evident. The foremost located temperature sensors again exhibited the largest temperature rise.

At main engine second cutoff, a sudden, sharp temperature drop was noted by all sensors. This indicated the presence of liquid or saturated gas in these areas. After engine shutdown, the temperature pattern became rather erratic. This erratic behavior was expected since the propellants were not controlled after engine second cutoff, and engine shutdown transients caused random motion of the propellants.

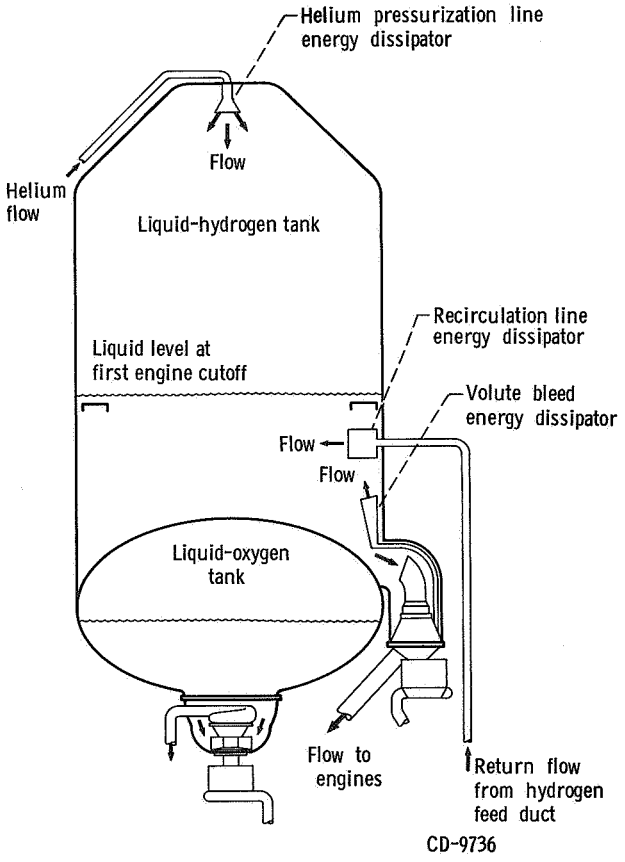

Figure V-53. - Location of energy dissipators, AC-9.

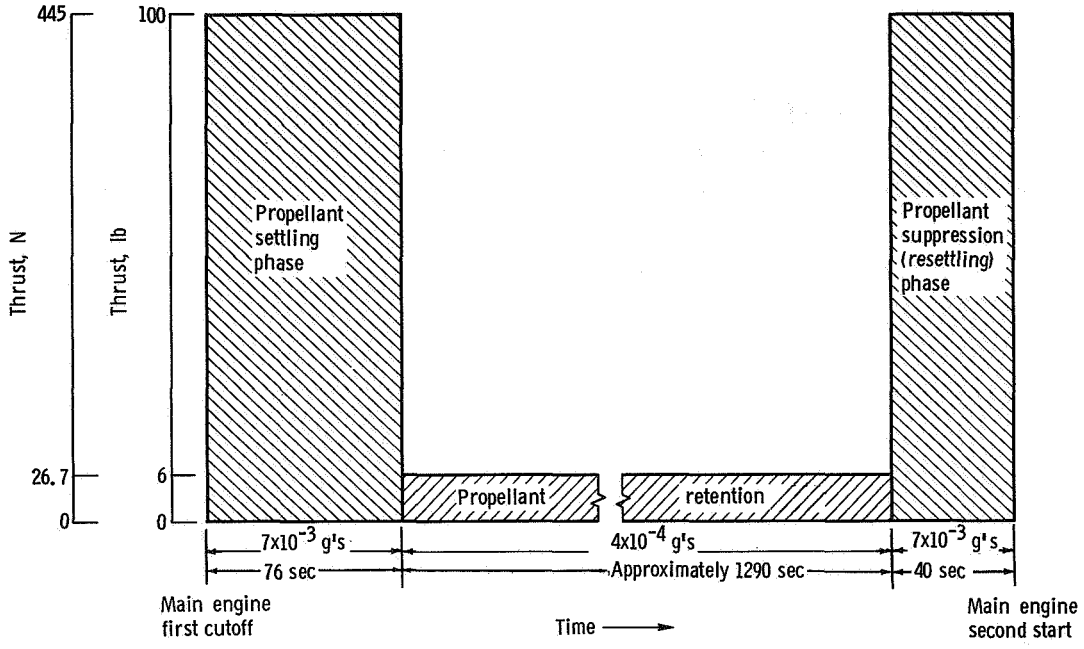

Figure V-55. - Coast phase thrust schedule, AC-9.

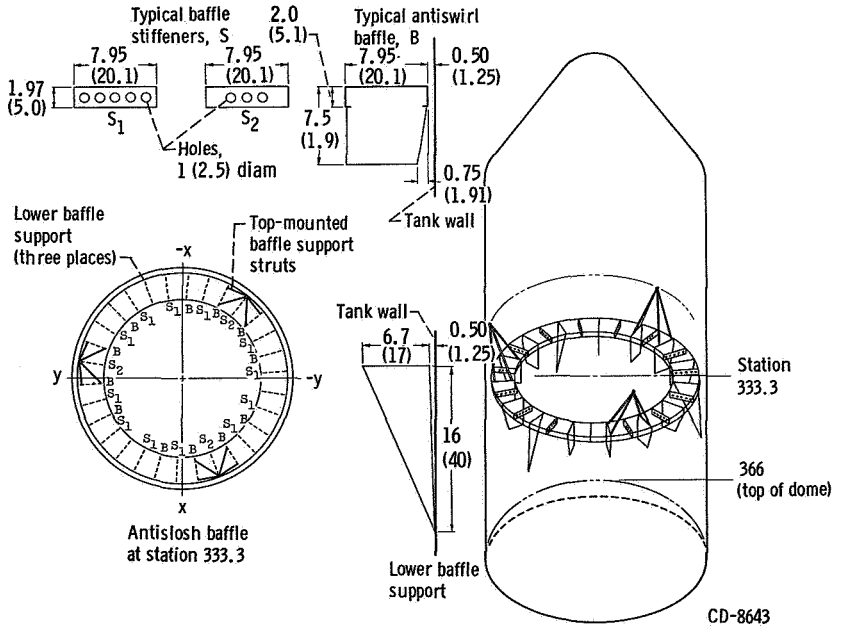

Figure V-54. - Liquid-hydrogen slosh baffle, AC-9. (All dimensions are in inches (cm).)

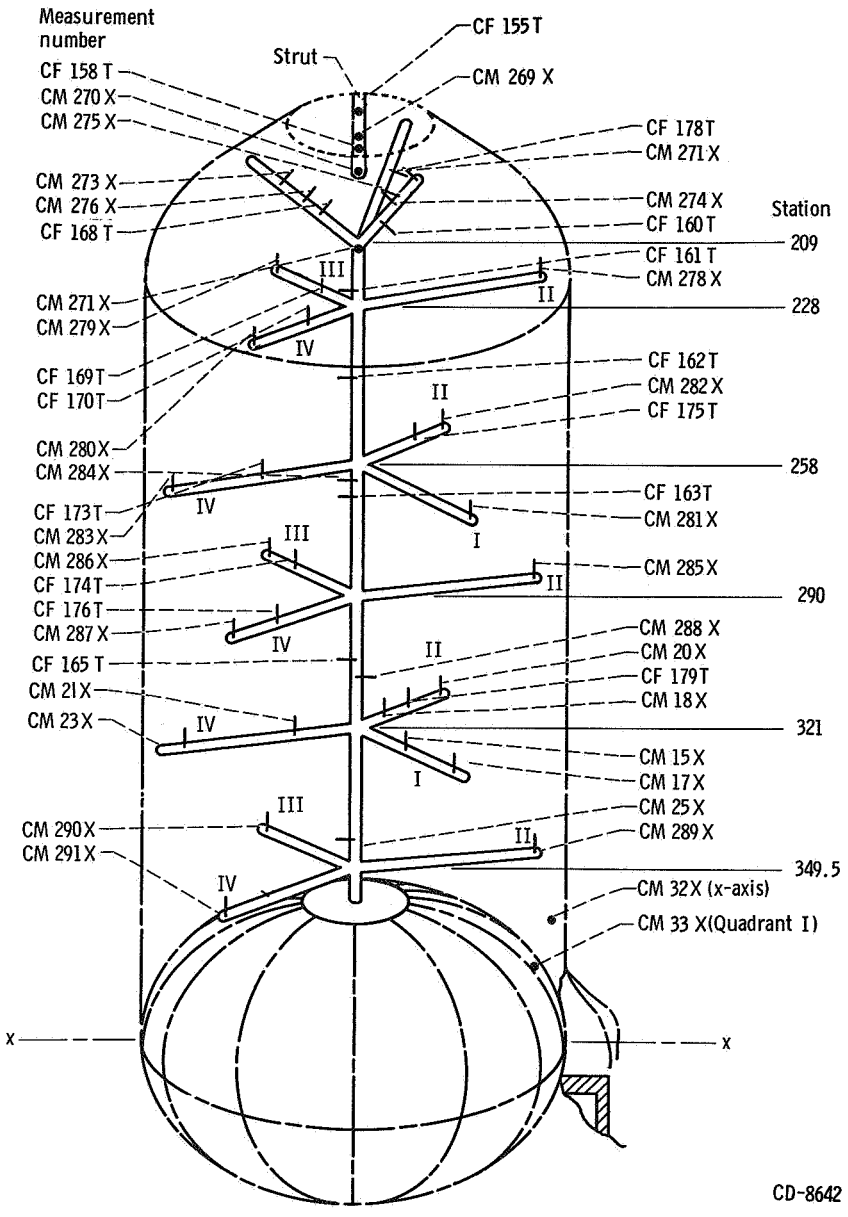

Figure V-56. - Liquid-vapor sensor and ullage gas temperature sensor locations and identification, AC-9. Liquid-vapor sensor denoted by X; temperature sensor denoted by T.

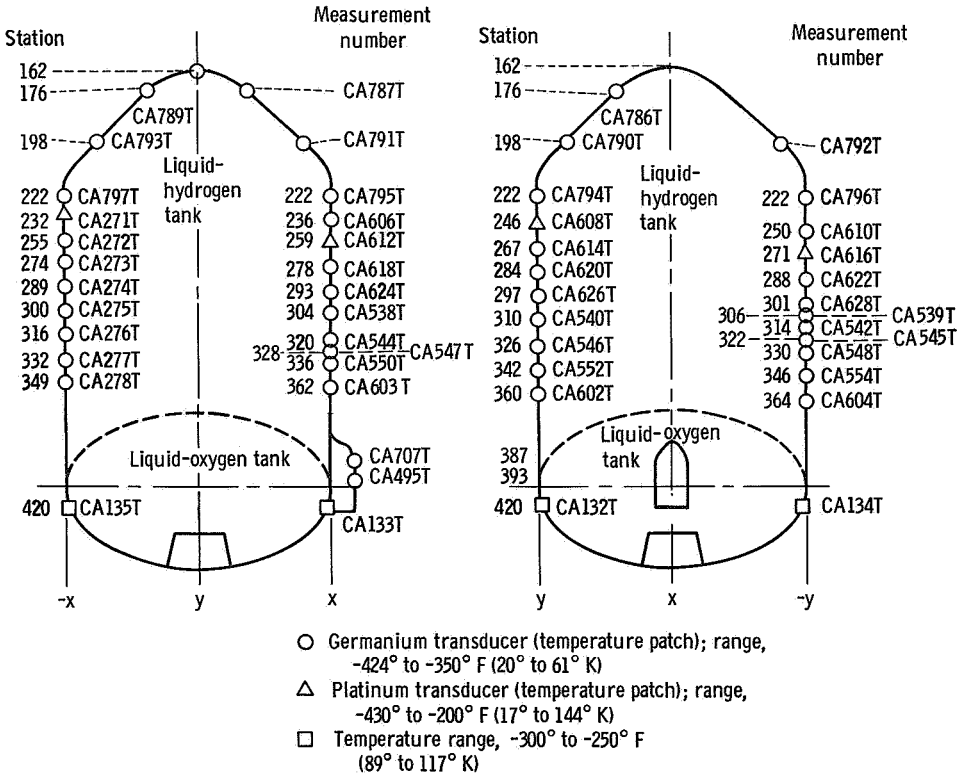

Figure V-57. - Tank-skin temperature instrumentation, AC-9.

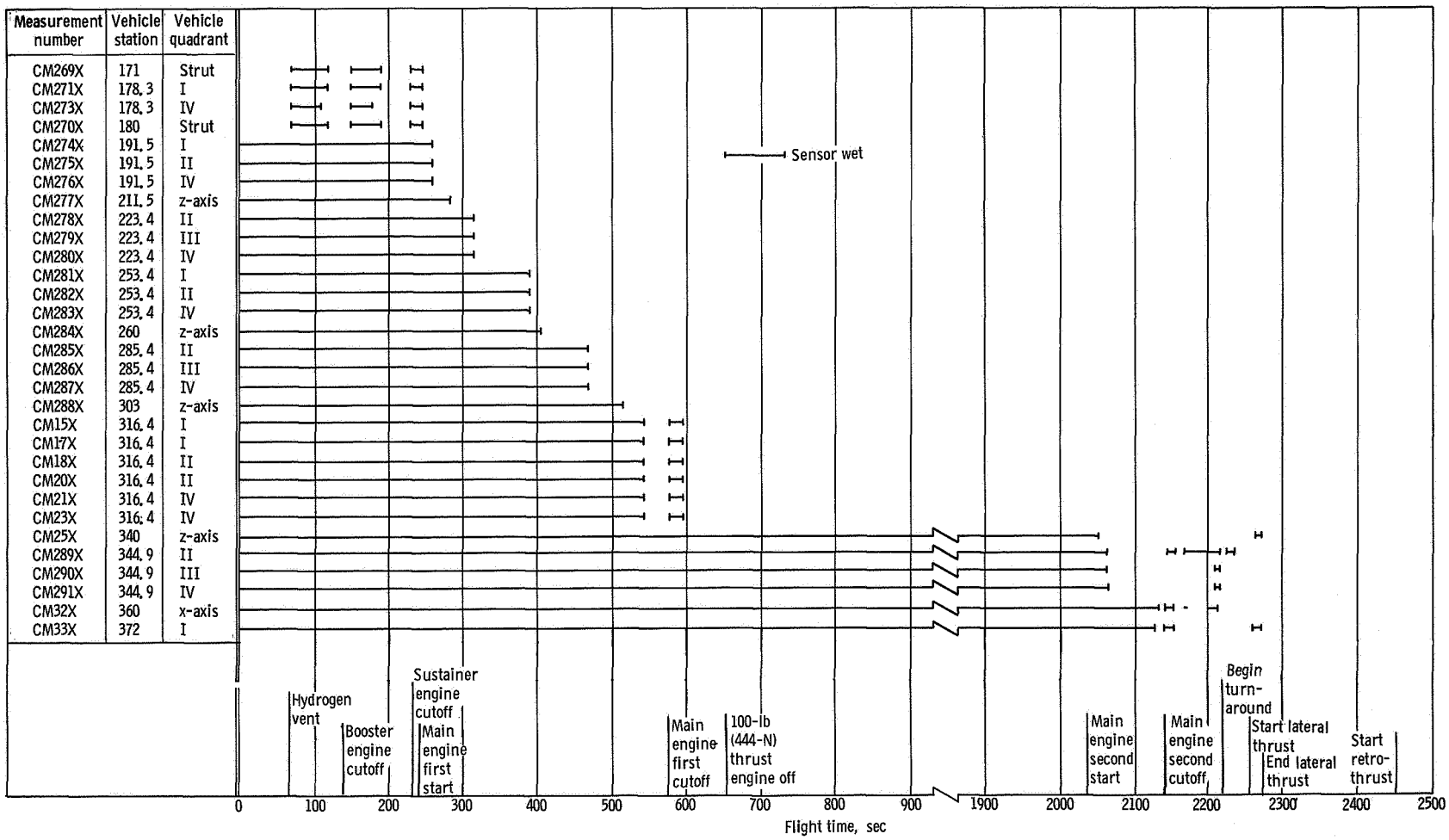

Figure V-58. - Hydrogen liquid-vapor sensor indications, AC-9. (Refer to fig. V-56 for measurement numbers.)

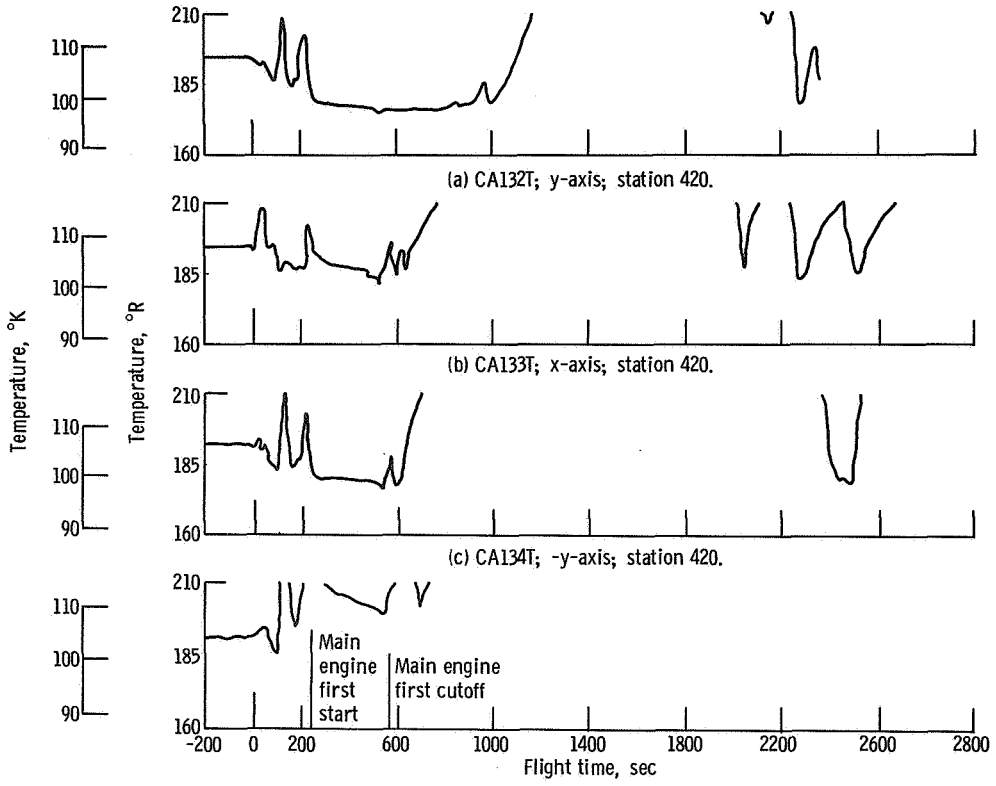

Figure V-59. - Liquid-oxygen-tank skin temperatures, AC-9.

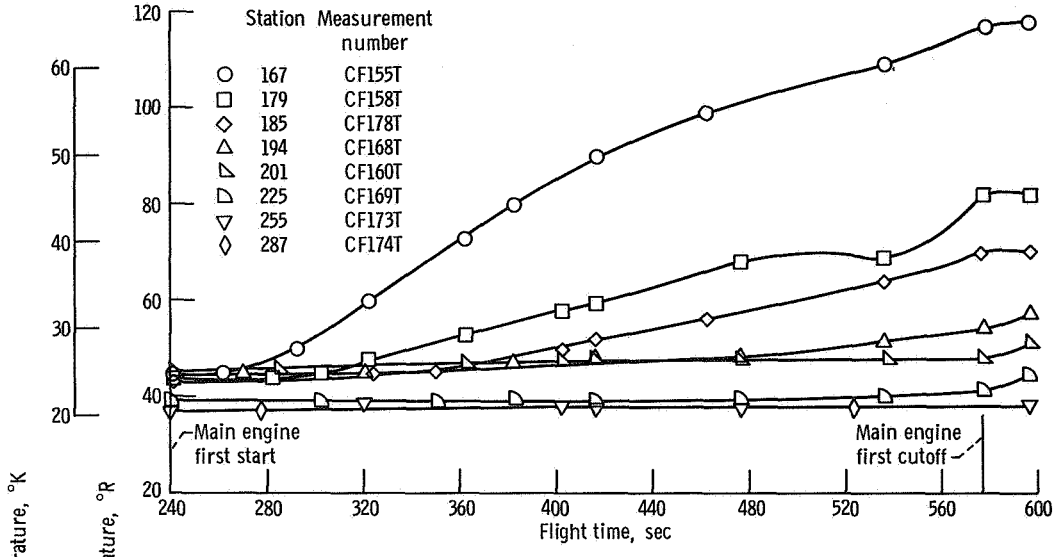

(a) T + 240 to T + 600 seconds.

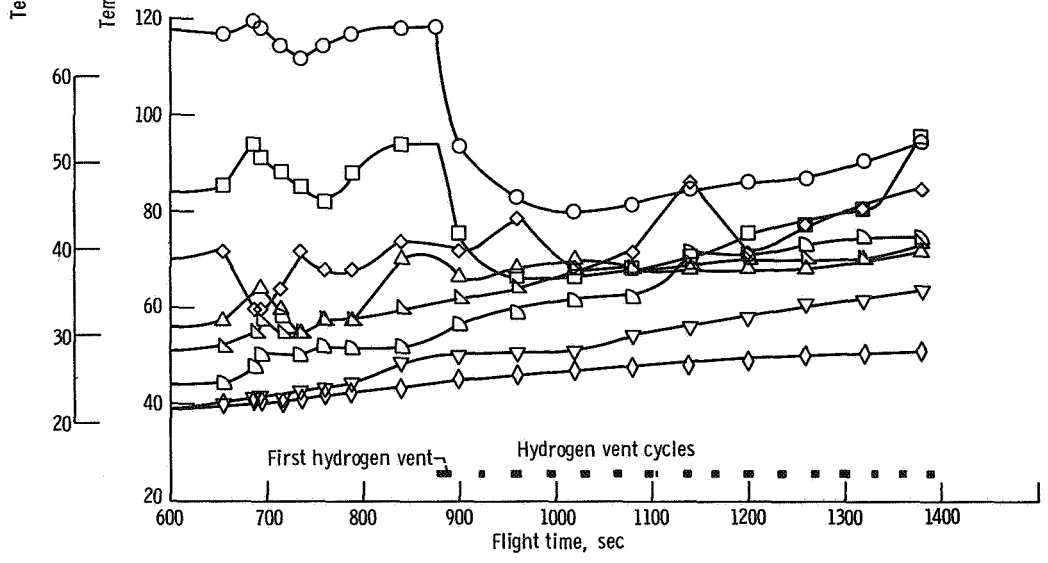

(b) T + 600 to T + 1400 seconds.

Figure V-60. - Hydrogen tank ullage temperatures, AC-9. (Refer to fig. V-56 for measurement locations.)

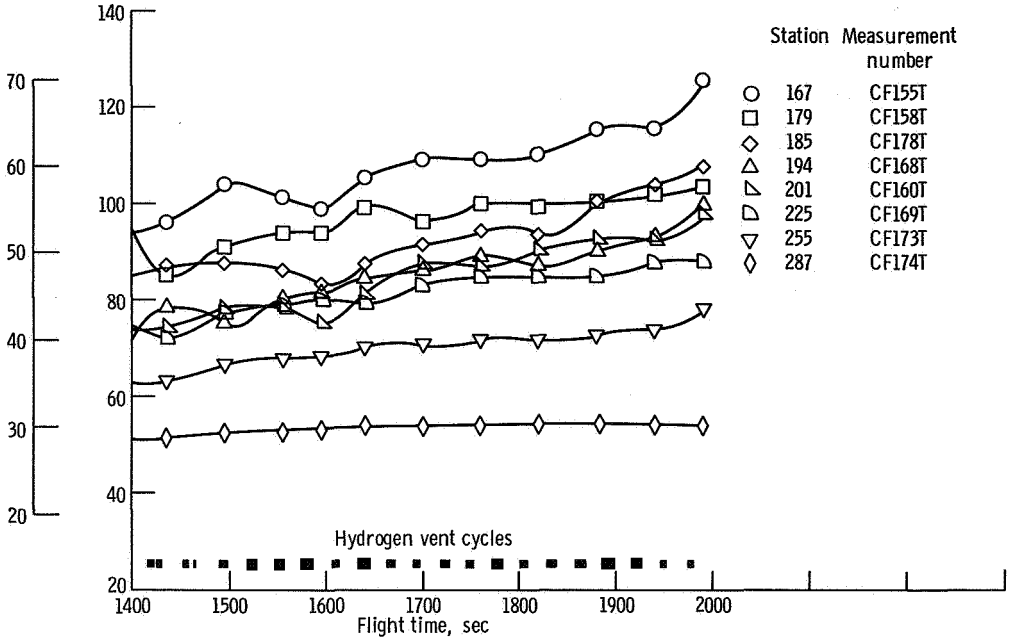

(c) T + 1400 to T + 2000 seconds.

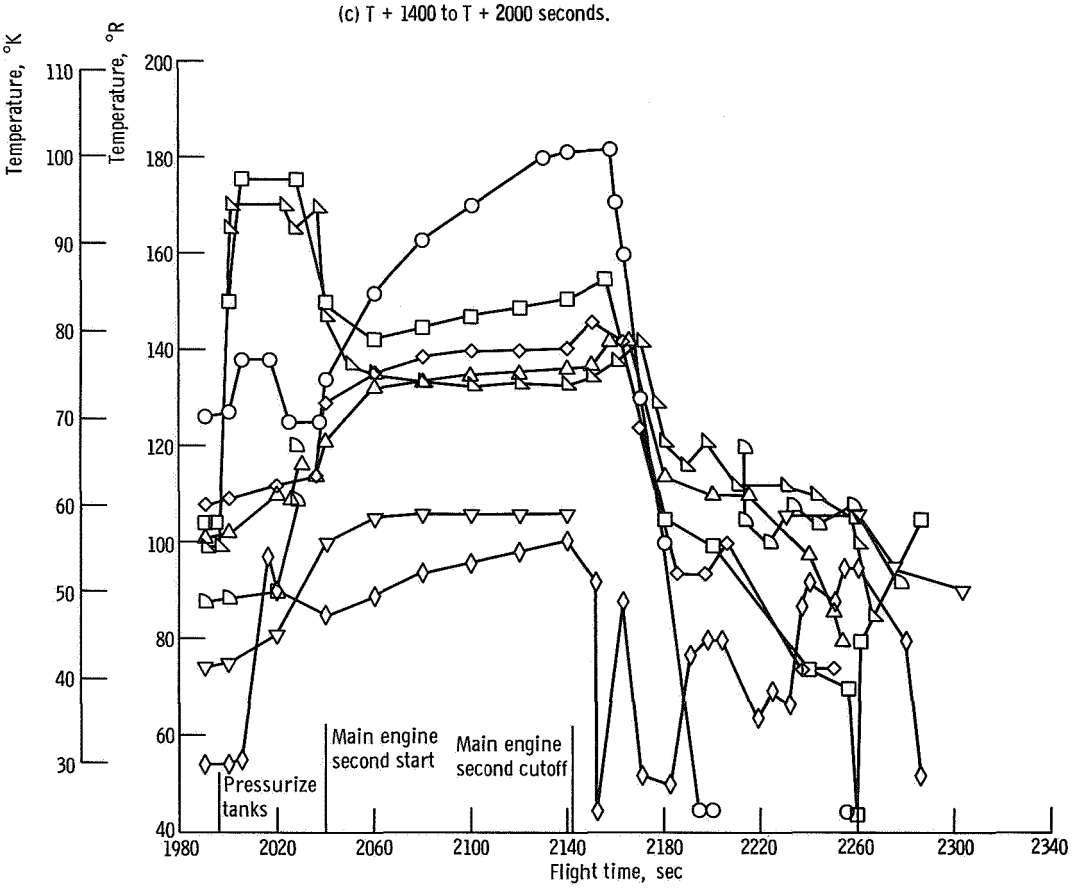

(d) T + 1980 to T + 2340 seconds.

Figure V-60. - Concluded.

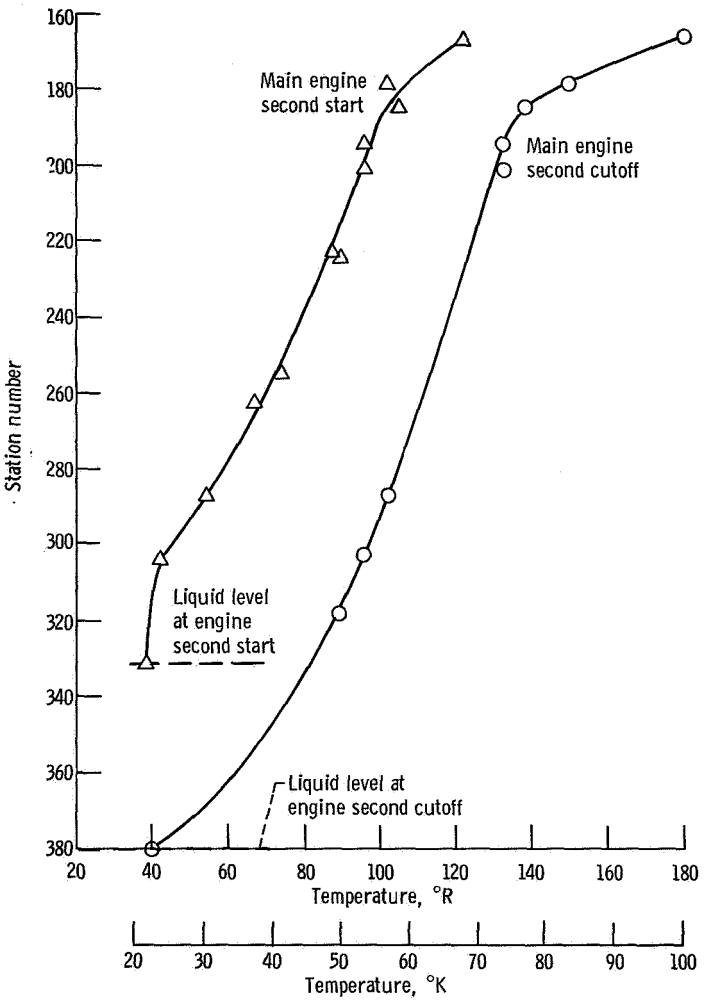

Figure V-61. - Hydrogen ullage temperatures at engine second start and second cutoff.

PNEUMATIC SYSTEMS

by William A. Groesbeck and Merle L. Jones

Atlas

System description. - The Atlas pneumatic system supplied helium gas for tank pressurization and for various vehicle control functions. The system comprised three independent subsystems: propellant tank pressurization, engine control, and booster section jettison. This system schematic is shown in figure V-62.

Propellant tank pressurization subsystem: This system was used to maintain propellant tank pressures at required levels (1) to support the pressure stabilized tank structure, and (2) to satisfy the inlet pressure requirements of the engine turbopumps. In addition, helium was bled from the fuel tank pressurization line to pressurize the hydraulic reservoirs and turbopump lubrication tanks. The system consisted of six shrouded helium storage bottles, a heat exchanger, fuel and oxidizer tank pressure regulators and relief valves, and an explosively actuated "programmed pressure" valve and orifice.

The six shrouded helium storage bottles with a capacity of 44 190 cubic inches (725 000 cm^3) were mounted in the jettisonable booster section. The bottle shrouds were filled with liquid nitrogen during prelaunch operations to chill the helium in order to provide a maximum storage capacity at an absolute pressure of about 3000 psi (2070 N/cm^2). The liquid nitrogen was drained from the shrouds at lift-off. During flight, the cold helium passed through a heat exchanger located in the booster engine turbine exhaust duct before being supplied to the tank pressure regulators.

Functionally, tank pressurization control was switched from the ground system to the airborne system at about T - 60 seconds. Airborne regulators then controlled fuel tank gage pressure between 57 and 60 psi (39.2 and 41.3 N/cm^2) and the oxidizer tank gage pressure between 28.5 and 31.0 psi (19.6 and 21.4 N/cm^2). However, from about T - 2 minutes to T + 20 seconds, the liquid-oxygen regulator was biased by a slight helium bleed flow into the ullage pressure sensing line. The bias caused the tank pressure to be controlled at a lower level than the regulator setting. Depressing the liquid-oxygen-tank pressure allowed increased differential pressure across the intermediate bulkhead to counteract the launch transient loads that act in a direction to cause bulkhead reversal. At T + 20 seconds, the bias was removed and the ullage pressure in the liquid-oxygen tank increased to the normal regulator control range. The increased pressure then provided sufficient vehicle structural stiffness to withstand bending loads during the ascent.

Pneumatic regulation of tank pressure terminated at booster staging. Thereafter, the fuel tank pressure decayed slowly, but the liquid-oxygen tank pressure was sustained by gas boiloff.

Engine controls subsystem: This system supplied helium pressure for actuation of engine control valves, for pressurization of the engine start tanks and booster engine turbopump seals, and the reference pressure regulators which controlled oxidizer flow to the gas generator. Control pressure in the system was maintained through Atlas-Centaur separation. These pneumatic requirements were supplied from a 4650-cubic-inch (76 000-cm^3) storage bottle pressurized to a gage pressure of about 3000 psi (2070 N/cm^2) at lift-off.

Booster section jettison subsystem: This system supplied pressure for release of the pneumatic staging latches to separate the booster engine package. A command from the Atlas flight control system opened two explosively actuated valves to admit helium pressure to the 10 piston-operated staging latches. Helium for the system was supplied by a single 870-cubic-inch (14 260-cm^3) capacity bottle charged to a gage pressure of about 3000 psi (2070 N/cm^2).

System performance. - The Atlas pneumatic system performance was normal throughout the flight. Storage bottle pressure for the engine controls decayed more rapidly than usual as the result of a leak in the propulsion control system. The individual subsystem performance is discussed in the following paragraphs.

Propellant tank pressurization: Control of propellant tank pressures was switched from ground to airborne subsystems at T - 49 seconds. Pressure regulation was normal and ullage pressures were properly controlled throughout the flight. Tank pressurization data for the flight are shown in figure V-63 and table V-7.

The fuel tank pressure regulator controlled gage pressures between 57.2 and 59 psi (39.4 and 40.7 N/cm^2) until termination of pneumatic control at booster staging. During sustainer engine firing the fuel tank gage pressure decreased normally and was 49.7 psi (34.2 N/cm^2) at engine shutdown.

Liquid-oxygen-tank gage pressure on switching to airborne regulation was steady at 26.9 psi (18.5 N/cm^2). The gage pressure dropped to 25 psi (17.2 N/cm^2) at engine start and then showed a gradual increase during the ascent due to reduction in atmospheric pressure. When the regulator bias was terminated at T + 20 seconds, pneumatic regulation stepped the ullage gage pressure abruptly from 26.8 to 29.1 psi (18.4 to 20.0 N/cm^2). At T + 75 seconds, the normal gas boiloff was sufficient to cause the ullage pressure to increase above the regulator control range. The regulator then closed down stopping any further helium flow into the tank. At booster engine shutdown, the ullage pressure increased rather quickly as the result of the sudden decrease in propellant outflow and increase in gas boiloff rate. The boiloff rate increased because of the reduction in hydrostatic pressure caused by the decrease in vehicle acceleration from 5.68 to about 1.1 g's.

TABLE V-7. - ATLAS PNEUMATIC SYSTEM DATA SUMMARY, AC-9

Pneumatic subsystem	Measurement		Units	Time from lift-off, sec			
				Requirement at T - 0	Lift-off, T - 0	Booster engine cutoff, T + 143.1	Sustainer engine cutoff, T + 229.1
Propellant tank pressurization	Liquid-oxygen tank ullage pressure (gage)		psi N/cm^2	23.3 to 28.5 16.1 to 19.7	26.9 18.5	32.0 22.1	31.8 21.9
	Liquid oxygen tank regulator sense line pressure (gage)		psi N/cm^2	---------- ----------	30.4 20.9	---- ----	---- ----
	Fuel tank ullage pressure (gage)		psi N/cm^2	57.8 to 61.5 39.9 to 42.4	58.3 40.2	58.0 40.0	49.7 34.3
	Pressurization bottles helium storage	Pressure (gage)	psi N/cm^2	3100 to 3400 2137 to 2344	3239 2233	924 637	---- ----
		Temperature	^oF ^oR	- 308 (maximum) 85 (maximum)	-316 80	-367 52	---- ----
		Mass	lb kg	---------- ----------	156.5 70.9	73.8 33.4	---- ----
Engine controls	Booster engine pneumatic regulator outlet pressure (gage)		psi N/cm^2	715 to 785 493 to 541	762 525	747 515	---- ----
	Sustainer engine pneumatic regulator outlet pressure (gage)		psi N/cm^2	565 to 635 390 to 438	615 424	610 421	650 448
	Controls bottle helium storage pressure (gage)		psi N/cm^2	2900 to 3400 2000 to 2344	3215 2217	2830 1951	670 462
Booster jettison	Staging bottle helium storage pressure (gage)		psi N/cm^2	2900 to 3400 2000 to 2344	3303 2277	---- ----	---- ----

Engine control regulators: The booster and sustainer pneumatic regulators provided the required helium pressures for engine control throughout the flight. Significant performance values are shown in table V-7. The engine controls bottle pressure decayed at an abnormally high rate following booster engine shutdown but the sustainer pneumatic regulator continued to perform normally. The drop in supply pressure was caused by a helium leak in the vernier engine liquid-oxygen bleed valve in the sustainer engine control system. As a result, helium supply pressure to the engine control system dropped below minimum requirements prior to sustainer engine shutdown. Figure V-64 shows a comparison of the helium bottle supply pressure decrease on AC-9 with that of the AC-7 flight, which was typical of normal system performance. The effect of this helium leak on the engine controls system is discussed in the section PROPULSION SYSTEMS, Atlas (p. 17).

Booster section jettison system: System performance was normal. The explosive actuated valves were opened by the staging command at T + 146.6 seconds allowing high-pressure helium to actuate the 10 booster staging latches.

Centaur

System description. - The Centaur pneumatic system, which is shown schematically in figure V-65, consisted of five subsystems: propellant tank venting, propellant tank pressurization, propulsion pneumatics, helium purge, and nose fairing pneumatics.

The Centaur propellant tanks were self-pressurized by the gas resulting from propellant boiloff. Overboard venting of propellant boiloff gases, in excess of that required for pressure stabilization of the tank, was controlled by a separate vent system on each tank. On the hydrogen tank, this system consisted of two pilot-controlled, pressure-actuated vent valves and ducting. The primary vent valve was fitted with a continuous-duty solenoid valve which, when energized, locked the vent valve preventing operation. The secondary hydrogen vent valve did not have the control solenoid and was always in the enabled-to-relieve mode. The relief range of the secondary valve was above that of the primary valve and prevented overpressurization of the hydrogen tank when the primary vent valve was locked. Until nose fairing jettison, the vent gases were ducted overboard through a single vent. After nose fairing jettison, venting occurred through diametrically opposed nozzles which balanced the vent thrust forces. The oxygen tank vent system used a single vent valve which was fitted with the control solenoid valve. The vented gases were ducted overboard through the interstage adapter. The duct was oriented to aline the venting thrust vector with the vehicle center of gravity.

The vent valves were commanded to the locked mode at specific times to (1) permit the hydrogen tank pressure to increase during the atmospheric ascent to satisfy the structural requirements of the pressure-stabilized tank, (2) permit controlled pressure increases in the tanks to satisfy the boost pump pressure requirements, (3) restrict venting during nonpowered flight to avoid vehicle disturbing torques, and (4) restrict hydrogen venting to nonhazardous times.[1]

The propellant tank pressurization subsystem supplied helium gas in controlled quantities for in-flight pressurization in addition to that provided by the propellant boiloff gases. It consisted of two normally closed solenoid valves and orifices and a pressure

[1]A fire could occur during the early part of the atmospheric ascent if a plume of vented hydrogen washed back over the vehicle and was exposed to an ignition source. A similar hazard could occur at Atlas booster engine staging when residual oxygen envelops a large portion of the vehicle.

switch assembly which sensed oxygen tank pressure. The solenoid valves and orifices provided metered flow of helium to the propellant tanks for step pressurization during both main engine start sequences. The pressure sensing switch controlled the pressure in the oxygen tank from boost pump first start to Centaur main engine first start.

The propulsion pneumatics subsystems supplied helium gas at regulated pressures for actuation of main engine control valves and pressurization of the hydrogen peroxide storage bottle. It consisted of two pressure regulators, which were referenced to ambient pressure, and two relief valves. Pneumatic pressure supplied through the engine controls regulator was used for actuation of the engine inlet valves, the engine cooldown valves, and the main fuel shutoff valve. The second regulator, located downstream of the engine controls regulator, further reduced the pressure to provide expulsion pressurization for the hydrogen peroxide storage bottle. A relief valve downstream of each regulator prevented overpressurization.

A ground-airborne helium purge subsystem was used to prevent air ingestion under the insulation panels and cryopumping into various propulsion system areas. A common airborne distribution system was used for prelaunch purging from a ground helium source and postlaunch purging from an airborne helium storage bottle. This subsystem distributed helium gas for purging the cavity between the hydrogen tank and the insulation panels, the seal between the nose fairing and the forward bulkhead, the propellant feed lines, the boost pumps, the engine chilldown vent ducts, the engine thrust chambers, and the hydraulic power packages. The umbilical charging connection for the airborne bottle could also be used to supply the purge from the ground source should an abort occur after ejection of the aft pneumatic panel.

The nose fairing pneumatic subsystem provided the required thrust for nose fairing jettisoning. It consisted of a nitrogen storage bottle and an explosive actuated valve with an integral thruster nozzle in each fairing half. Release of the gas through the nozzles provided the necessary thrust to propel the fairing halves away from each other and from the vehicle.

Propellant tank pressurization and venting. - The ullage pressures for the hydrogen and oxygen tanks during the flight are shown in figure V-66. The hydrogen tank absolute pressure was 21.9 psi (15.1 N/cm^2) at T - 14 seconds when the primary hydrogen vent valve was locked. After vent valve lockup, the tank absolute pressure increased, at an average rate of 6.67 psi per minute (4.60 (N/cm^2)/min), to 26.4 psi (18.2 N/cm^2) at T + 26.3 seconds. At this time, the secondary vent valve relieved and regulated tank pressure until T + 69.3 seconds when the primary vent valve was enabled. The tank pressure was then reduced and was regulated by the primary vent valve.

At T + 142 seconds, the primary hydrogen vent valve was locked for 9.0 seconds during Atlas booster engine staging. During this period of nonventing, the hydrogen ullage absolute pressure increased to 22.6 psi (15.6 N/cm^2). After booster engine staging, the primary vent valve was enabled and allowed to regulate tank pressure. At

T + 229 seconds, the primary hydrogen vent valve was again locked, and the tank was pressurized with helium for 1 second. The tank absolute pressure increased from 20.0 to 21.2 psi (13.8 to 14.6 N/cm^2). As the warm helium in the tank cooled, the absolute pressure decreased to 20.3 psi (14.0 N/cm^2) at T + 240.5 seconds (Centaur main engine first start). The absolute pressure at engine prestart (T + 232.5 sec) was 20.4 psi (14.1 N/cm^2).

The ullage absolute pressure in the oxygen tank was 30.2 psi (20.8 N/cm^2) at lift-off and then decreased to 29.2 psi (20.1 N/cm^2) at T + 120 seconds, when the vent valve apparently reseated and venting ceased. The absolute pressure then began to increase and continued to increase through Atlas booster engine shutdown to 30.2 psi (20.8 N/cm^2). After Atlas booster engine shutdown, the absolute pressure decreased to 29.5 psi (20.3 N/cm^2).

At T + 205 seconds, the oxygen tank vent valve was locked, and the helium pressurization of the tank began. The tank absolute pressure increased to 39.8 psi (27.4 N/cm^2), which was the upper limit of the pressure switch. As the warm helium gas cooled in the tank, the absolute pressure decreased to 39 psi (26.9 N/cm^2), when the pressure switch closed, and additional helium was injected into the tank. The pressurization cycle occurred three times. After the third cycle, the heat input from the boost pump recirculation flow increased the boiloff and caused the pressure to increase before it reached the lower limit of the pressure switch. The pressure continued to increase until Centaur main engine first start. After Centaur main engine first start, the absolute pressure decreased to its saturation value of approximately 29.6 psi (20.4 N/cm^2).

The ullage pressures in both propellant tanks decreased normally during Centaur main engine first firing. At engine cutoff, the ullage absolute pressures in the hydrogen and oxygen tanks were 15.1 psi (10.4 N/cm^2) and 26.8 psi (18.5 N/cm^2), respectively. The primary hydrogen vent valve was enabled at main engine cutoff, while the oxygen tank vent valve remained locked.

During the coast period following Centaur main engine first cutoff, the hydrogen tank pressure increased at a rate of 0.98 psi per minute (0.68 (N/cm^2)/min). At T + 877 seconds, the tank pressure reached the regulating range of the primary vent valve and was regulated by that valve for the duration of the coast period. The oxygen tank ullage pressure increased gradually throughout the coast period and remained well within the allowable limits.

At T + 1995 seconds, the primary hydrogen vent valve was locked, and helium injection into both propellant tanks was initiated. The pressurizing sequence of the oxygen tank was timed to last 18 seconds. The pressure sensing switch, used prior to the Centaur main engine first start, was bypassed in the circuitry. During this 18-second period, the oxygen tank ullage absolute pressure rose from 29.3 psi (20.2 N/cm^2) to

31.1 psi (21.4 N/cm^2). After engine prestart, the pressure decreased slightly until Centaur main engine second start and decreased more rapidly thereafter. The helium pressurization of the hydrogen tank was also a timed function, lasting 41 seconds until Centaur main engine second start. The absolute pressure increased to 25.8 psi (17.8 N/cm^2) when the relief setting of the secondary vent valve was reached. Tank pressure was then regulated by that valve until Centaur main engine second start. During the engine firing, the oxygen tank ullage pressure decreased to 25.3 psi (17.4 N/cm^2) at main engine cutoff, while the hydrogen tank ullage absolute pressure decreased to 21.3 psi (14.7 N/cm^2).

After Centaur main engine second cutoff, the hydrogen tank ullage pressure increased at a rate of 1.20 psi per minute (0.83 (N/cm^2)/min). The sudden pressure drop at T + 2256 seconds coincided with the start of lateral thrust in the Centaur turnaround maneuver, and it indicated splashing of liquid hydrogen into the ullage. The pressure then increased at approximately the same rate until it reached the relief setting of the secondary vent valve. The pressure was then regulated by that vent valve until the start of retrothrust. During this period following Centaur main engine second cutoff, the oxygen tank ullage pressure increased at a much lower rate than the hydrogen tank ullage pressure. At T + 2440 seconds, the differential pressure across the bulkhead between the two tanks had diminished to 0.4 psi (0.3 N/cm^2). The desired minimum differential pressure is 2.0 psi (1.4 N/cm^2) (see VEHICLE STRUCTURES section).

After the start of retrothrust, the hydrogen tank pressure decreased for approximately 20 seconds, indicating either gaseous or two-phase outflow. The pressure then remained constant for approximately 40 seconds, indicating liquid outflow. After that, the pressure began to decrease, indicating the resumption of gaseous or two-phase outflow. During the period of retrothrust, the oxygen tank pressure remained constant, indicating liquid outflow.

At T + 2701 seconds, the engine valves were closed terminating the retrothrust maneuver. The primary hydrogen and the oxygen vent valves were enabled to prevent ultimate rupture of the tanks in space.

Propulsion pneumatics. - The outlet pressure of the engine controls regulator experienced an abnormal and unexplained increase from 471 psi (324 N/cm^2) at lift-off to 492 psi (339 N/cm^2) at T + 180 seconds. It then leveled off, indicating relief valve opening. The absolute pressure remained steady until boost pump start and then dropped suddenly to the proper level of 455 psi (313 N/cm^2). This level was maintained for the duration of the flight. The hydrogen peroxide bottle pressure regulator maintained a proper system level throughout the flight. The outlet absolute pressure was 323 psi (223 N/cm^2) at lift-off and decreased with a corresponding decrease in ambient pressure to 307 psi (212 N/cm^2).

Helium purge subsystem. - The ground purge system operated normally throughout the countdown. The total helium flow rate to the vehicle after liquid-hydrogen tanking

was approximately 170 pounds per hour (77 kg/hr). The differential pressure across the insulation panels after hydrogen tanking was 0.22 psi (1.5 N/cm^2). The minimum allowable differential pressure is 0.03 psi (0.02 N/cm^2) to prevent air ingestion. At T - 9.6 seconds, the airborne purge system was activated, and at T - 4 seconds the ground purge was terminated. The supply of helium in the airborne purge bottle lasted through most of the atmospheric ascent.

Nose fairing pneumatics. - There is no airborne instrumentation in this system, but proper jettisoning of the nose fairing indicated proper functioning of the nose fairing pneumatics subsystem.

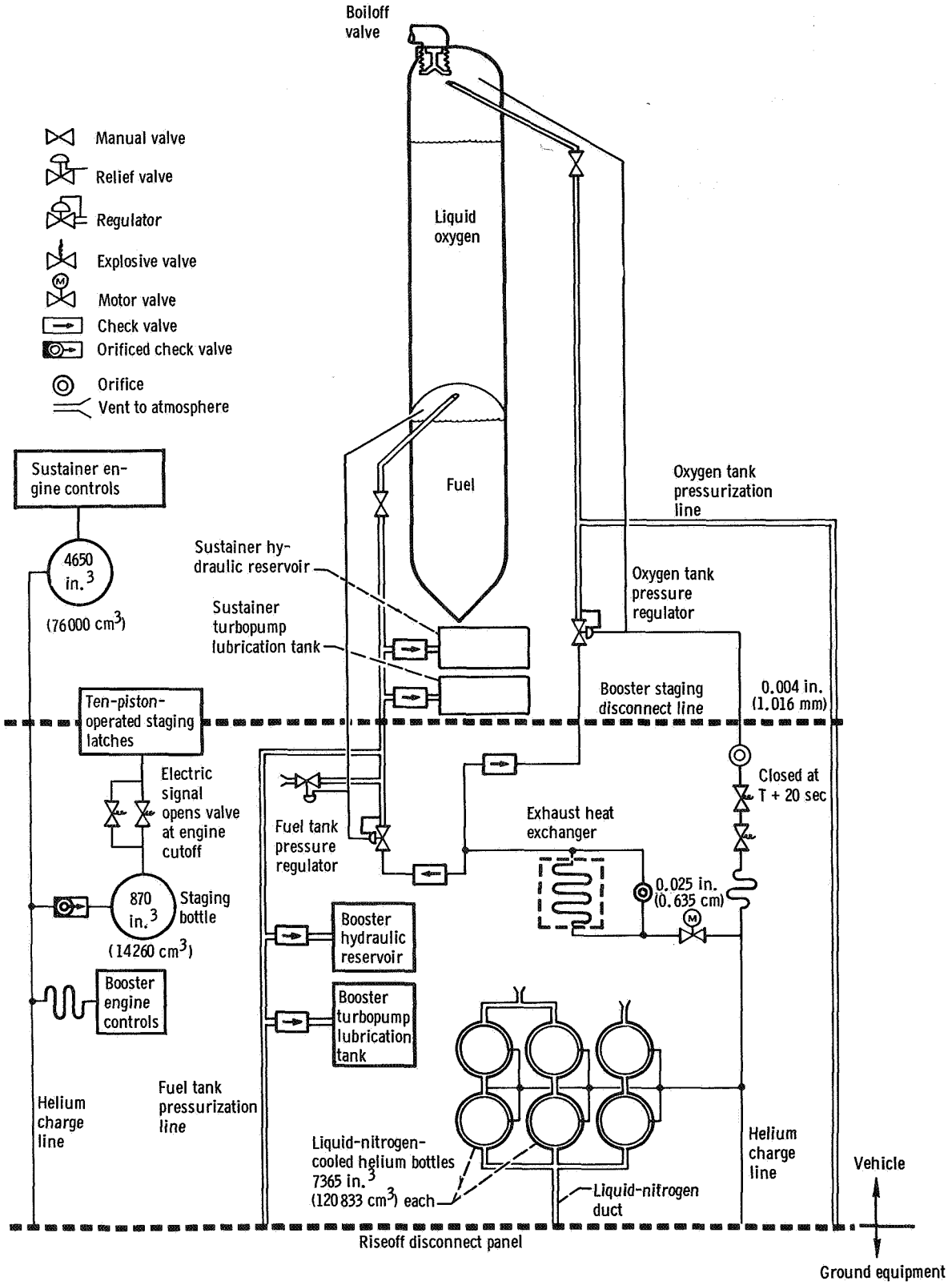

Figure V-62. - Atlas vehicle pneumatic system, AC-9.

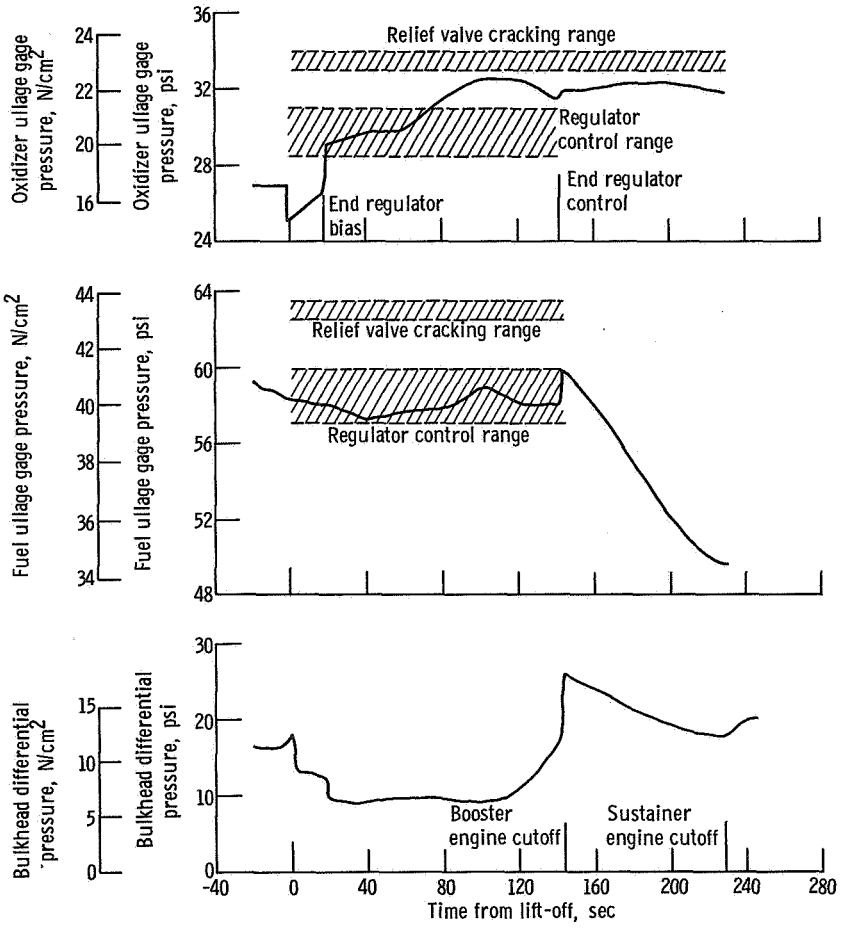

Figure V-63. - Atlas oxidizer and fuel tank ullage pressures, AC-9.

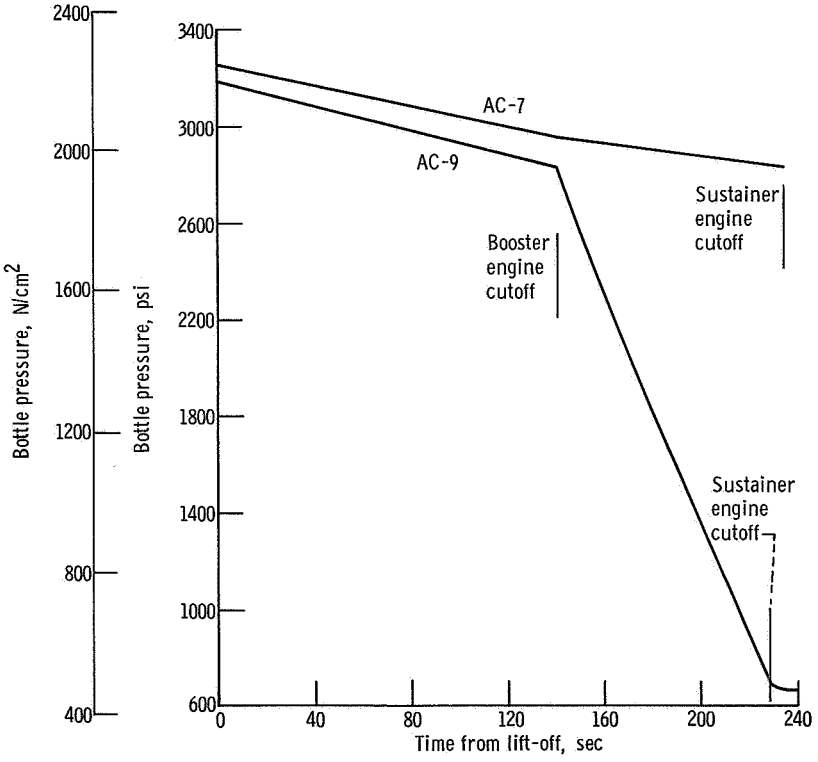

Figure V-64. - Atlas controls bottle pressure, AC-7 and AC-9.

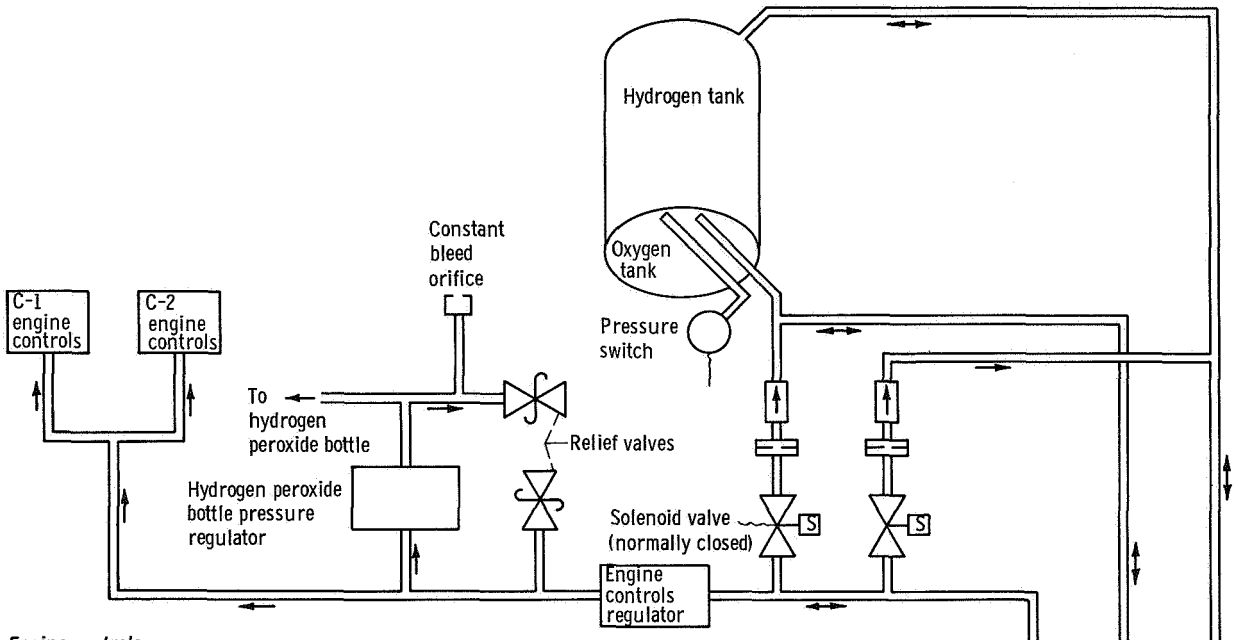

Engine controls
Pressure regulator (gage), 440 to 475 psi (303 to 327 N/cm^2)
Relief valve pressure (gage), 475 to 525 psi (327 to 362 N/cm^2)
Hydrogen peroxide bottle
Pressure regulator (gage), 297 to 315 psi (205 to 217 N/cm^2)
Relief valve pressure (gage), 320 to 354 psi (221 to 244 N/cm^2)
Orifice-tank pressurization
Oxygen tank, 0.043-in. (0.109-cm) diameter
Hydrogen tank, 0.089-in. (0.226-cm) diameter
Constant bleed orifice, 135 standard cu in./min (2211 standard cm^3/min)
Pressure switch (oxygen tank), 38 to 40 psia (26 to 28 N/cm^2 abs)
Helium bottle
Volume, 7365 cu in. (120 639 cm^3)
Initial pressure, 3200 psia (2206 N/cm^2 abs)

(a) Tank pressurization and propulsion pneumatics subsystems.

Figure V-65. - Centaur pneumatics system, AC-9.

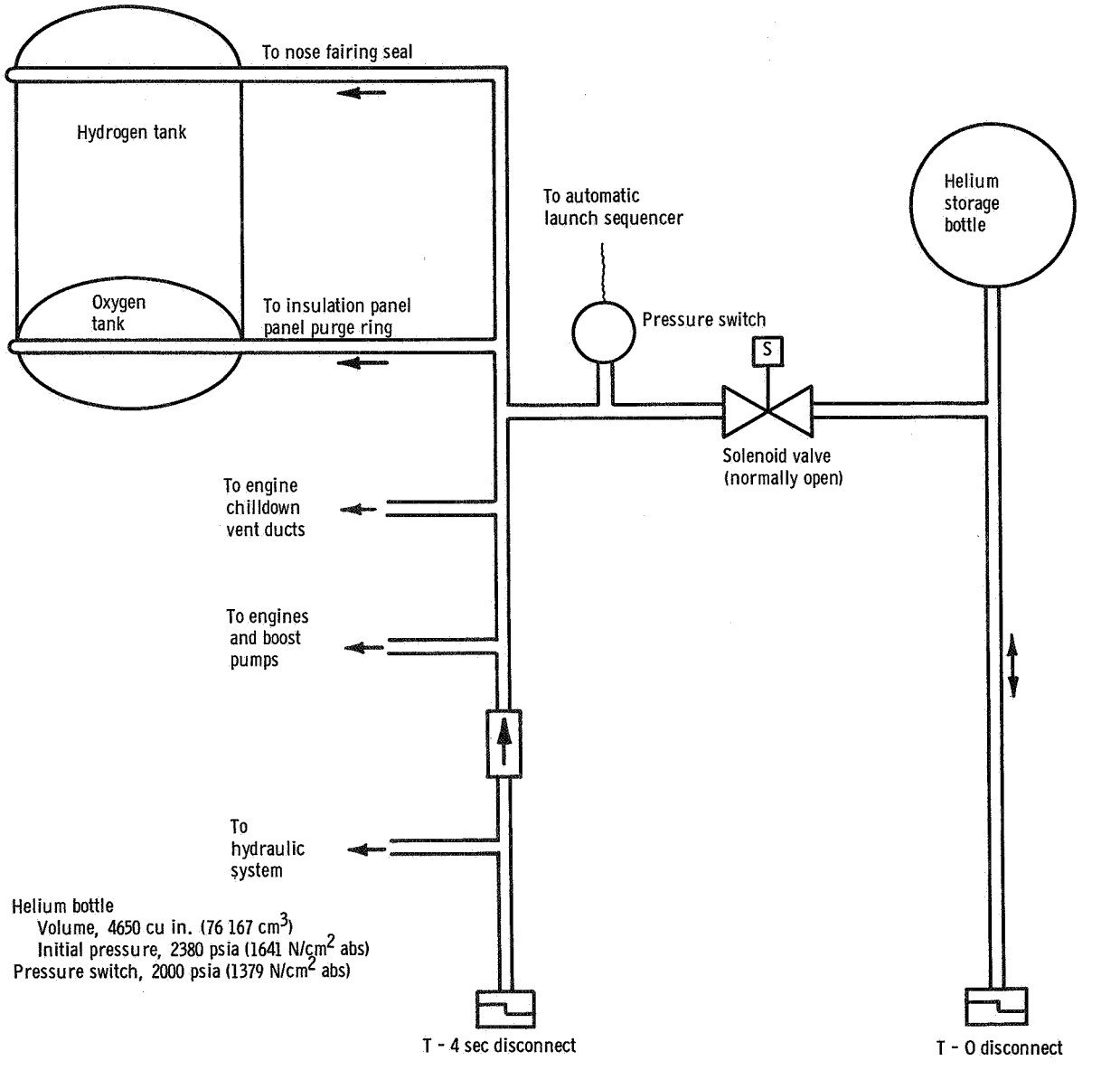

(b) Helium purge subsystem.

Figure V-65. - Continued.

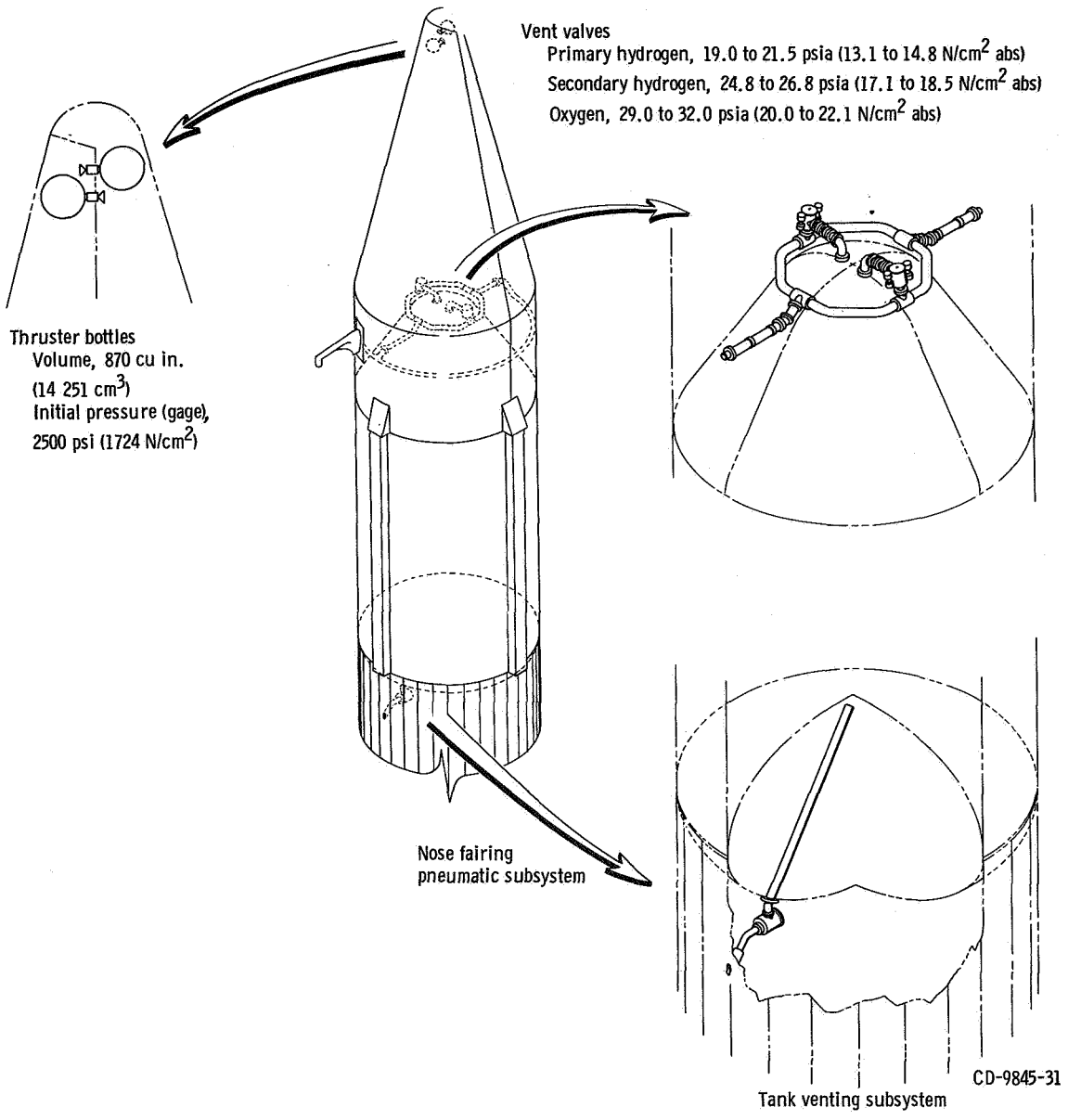

(c) Tank venting and nose fairing pneumatics subsystems.

Figure V-65. - Concluded.

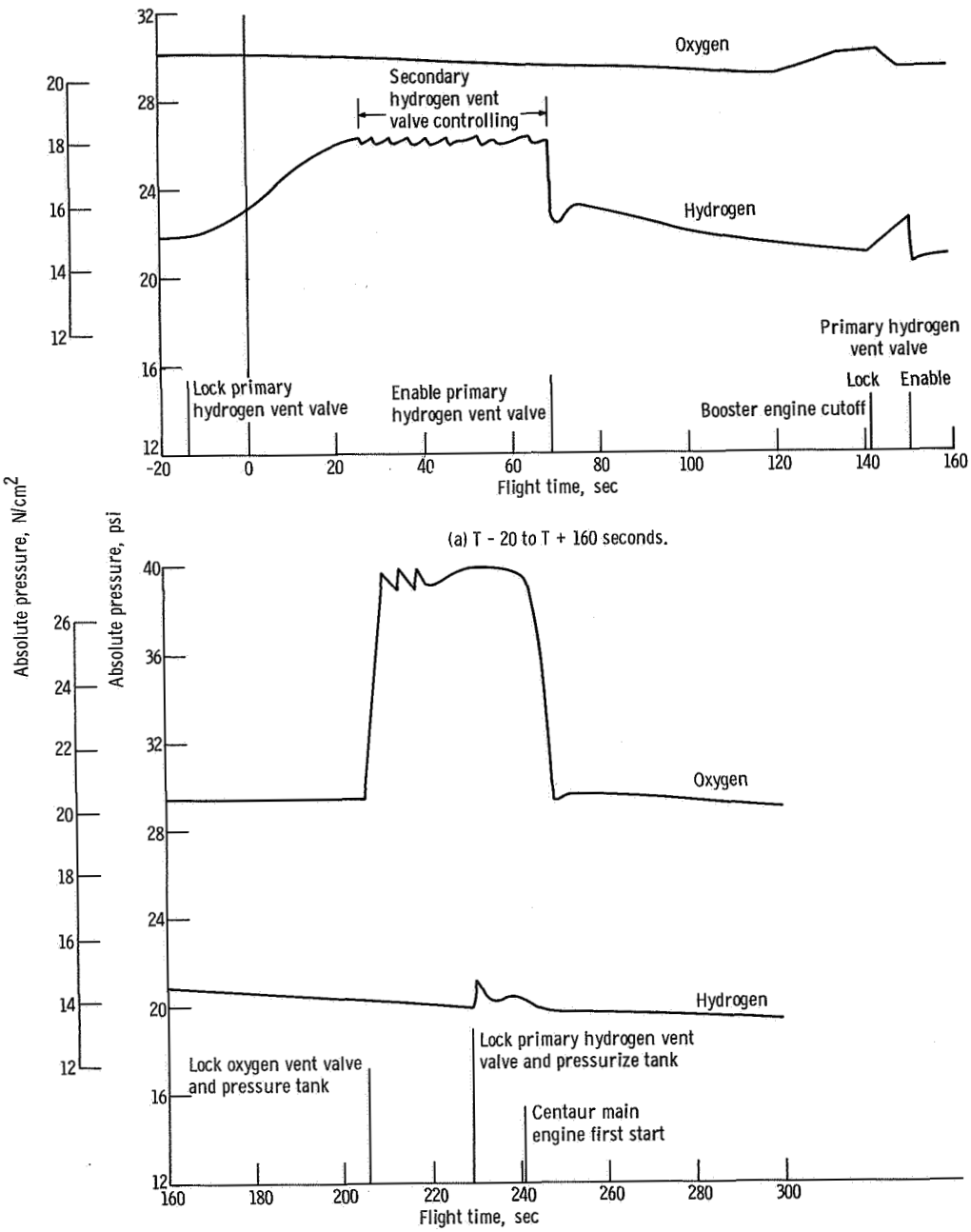

(a) T - 20 to T + 160 seconds.

(b) T + 160 to T + 300 seconds.

Figure V-66. - Centaur tank pressure history, AC-9.

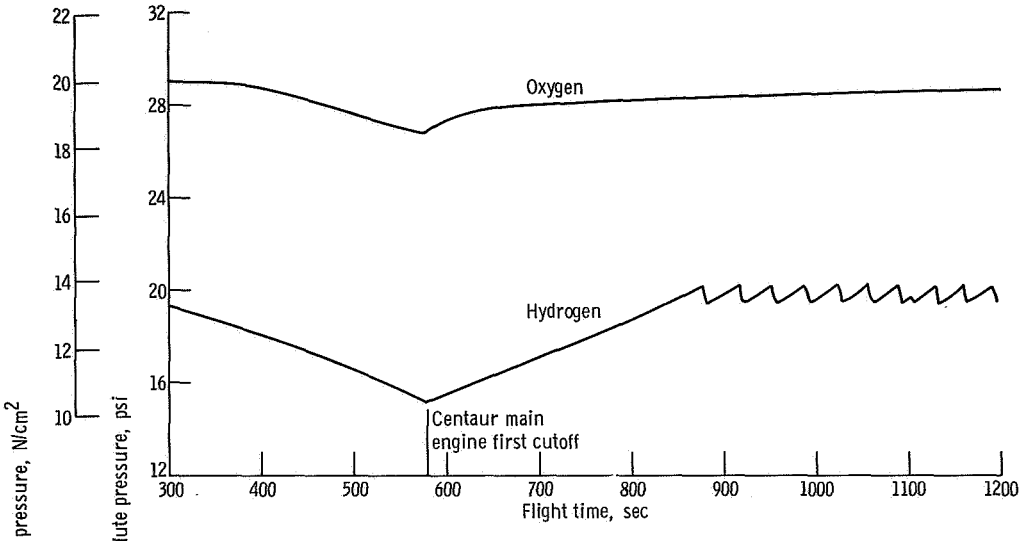

(c) T + 300 to T + 1200 seconds.

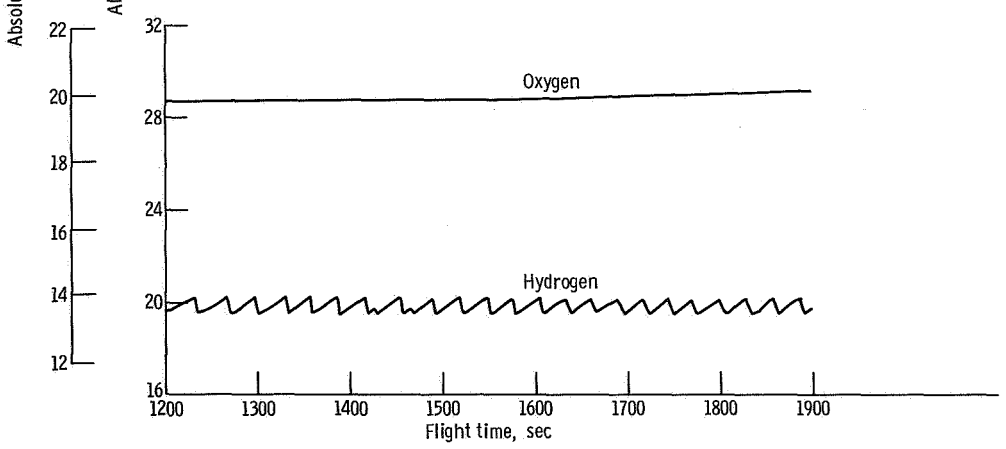

(d) T + 1200 to T + 1900 seconds.

Figure V-66. - Continued.

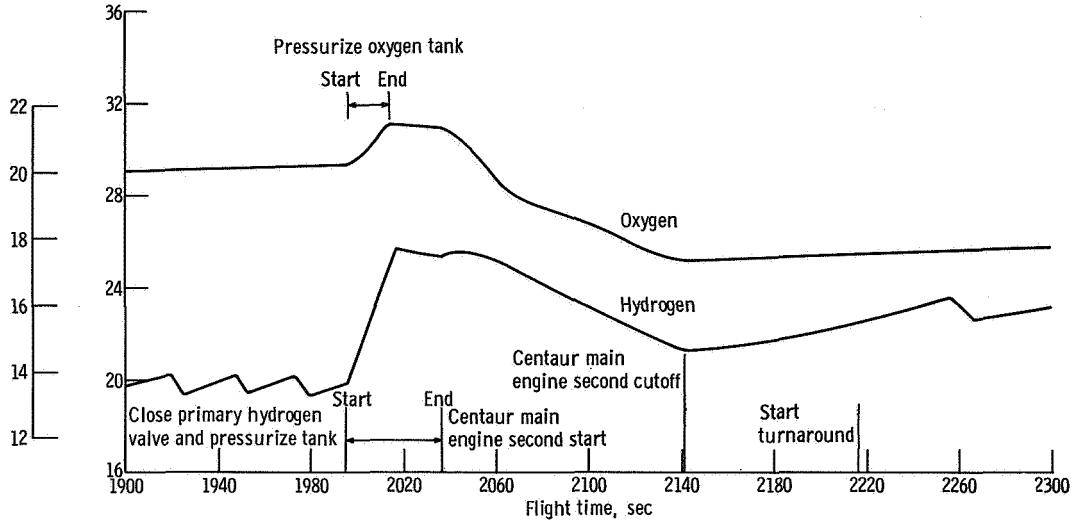

(e) T + 1900 to T + 2300 seconds.

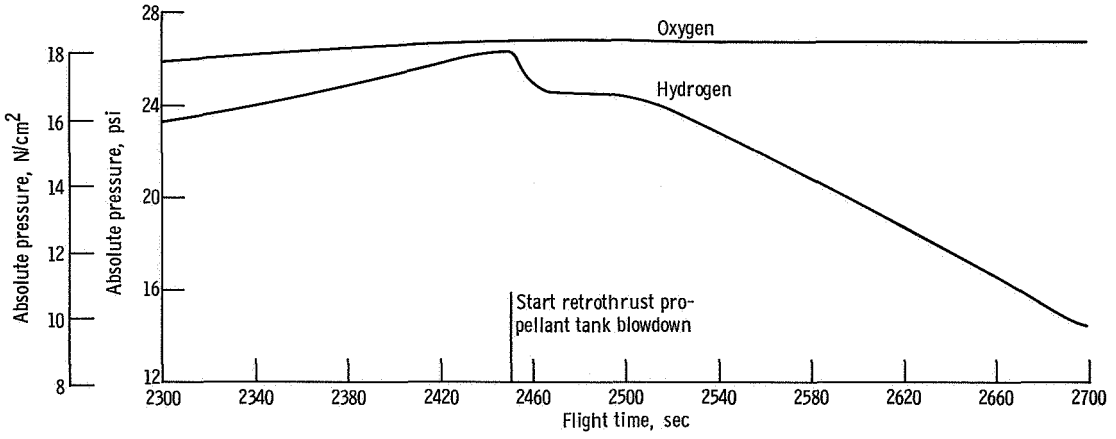

(f) T + 2300 to T + 2700 seconds.

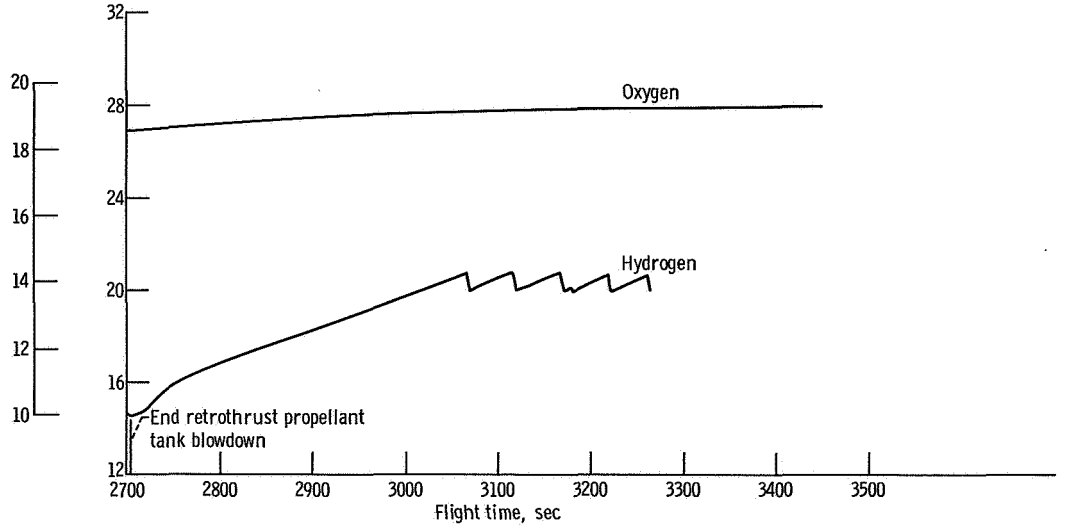

(g) T + 2700 to T + 3500 seconds.

Figure V-66. - Concluded.

HYDRAULIC SYSTEMS

by Eugene J. Cieslewicz

Atlas

System description. - Two hydraulic systems, as shown in figures V-67 and V-68, were used on the Atlas vehicle to supply fluid power for operation of sustainer engine control valves and for thrust vector control of all engines. One system was used for the booster engine and the other for the sustainer engine.

The booster hydraulic system provided power solely for gimbaling the two thrust chambers. System pressure was supplied by a single, pressure-compensated, variable displacement pump driven by the engine turbopump accessory drive. Additional components of the system included four servocylinders, a high-pressure relief valve, two accumulators, and a reservoir. Engine gimbaling in response to flight control commands was accomplished by the servocylinders which provided separate pitch, yaw and roll control during the booster phase of flight. The maximum booster engine gimbal angle capability was $\pm 5^{\circ}$ in the pitch and yaw planes.

The sustainer stage used a system similar to that of the booster but, in addition, provided hydraulic power for sustainer engine control valves and gimbaling of the two vernier engines. Vehicle roll control was accomplished during the sustainer phase by differential gimbaling of the vernier engines. Actuator limit travel of the vernier engines was $\pm 70^{\circ}$, sustainer engine, $\pm 3^{\circ}$.

System performance. - Hydraulic system pressure data for both the booster and sustainer circuits are shown in figure V-69. Pressures were stable throughout the boost flight phase. The transfer of fluid power from ground to airborne hydraulics systems was normal. Pump discharge absolute pressures increased from 1870 psi (1290 N/cm^2) at T - 2 seconds to flight levels of 3050 psi (2100 N/cm^2) in less than 2 seconds. Starting transients produced a normal overshoot of about 10 percent in the pump discharge pressure. Absolute pressure in the sustainer hydraulic circuit stabilized at 3050 psi (2100 N/cm^2) and in the booster circuit at 3060 psi (2110 N/cm^2).

Engine gimbaling requirements during flight were generally less than 1° in the pitch and yaw planes. An exception of 2.36° gimbal occurred in the pitch plane during the period of maximum dynamic pressure. As expected, the excursions were well within the engine gimbal limits.

Centaur

System description. - Two separate but identical hydraulic systems, as shown in figure V-70, were used on the Centaur stage. Each system provided power to gimbal the engine for pitch, yaw, and roll control. Each system consisted of two servocylinders and an engine-coupled power package containing high and low pressure pumps, reservoir, accumulator, pressure-intensifying bootstrap piston, and relief valves for pressure regulation. Hydraulic pressure and flow were provided by a constant-displacement vane-type pump driven by the liquid-oxygen turbopump accessory drive shaft. An electrically powered secondary recirculation pump was also used to provide low pressure for engine gimbaling requirements during prelaunch checkout, to aline the engines prior to main engine start, and for limited thrust vector control during the propellant tank discharge portion of the Centaur retrothrust maneuver. Maximum engine capability was $\pm 3^{\circ}$.

System performance. The hydraulic systems properly performed as commanded throughout the flight. System pressures and temperatures, shown as a function of the flight time, are shown in figures V-71 and V-72.

Activation of the low pressure recirculation pumps provided hydraulic absolute pressures of 125 psi (86 N/cm^2) for the C-1 engine system and 120 psi (83 N/cm^2) for the C-2 engine system These pressures were satisfactory to center the engines prior to main engine first and second starts.

Main system absolute pressure in the C-1 system reached 1165 psi (803.4 N/cm^2) for the first and second firings. Manifold temperatures rose from 53° F (285° K) at main engine first ignition to 157° F (342° K) at main engine cutoff. C-1 hydraulic manifold temperature dropped to a low of 180° F (315° K) just before main engine second ignition. The temperature at main engine second cutoff was 158° F (343° K).

The C-2 system absolute pressure reached 1155 psi (797 N/cm^2) for the first and second firings. Hydraulic manifold temperatures rose from 64° F (29° K) at main engine first ignition to 159° F (344° K) at main engine cutoff. It dropped to a low of 116° F (320° K) just before main engine second start. The temperature at main engine second cutoff was 163° F (346° K).

After main engine second cutoff, the hydraulic system was not powered until the start of propellant tank blowdown. The electrically driven recirculation pumps were then turned on to provide hydraulic power for alining the engines and providing limited thrust vector control during the retromaneuver. This limited control supplemented the hydrogen peroxide attitude control system.

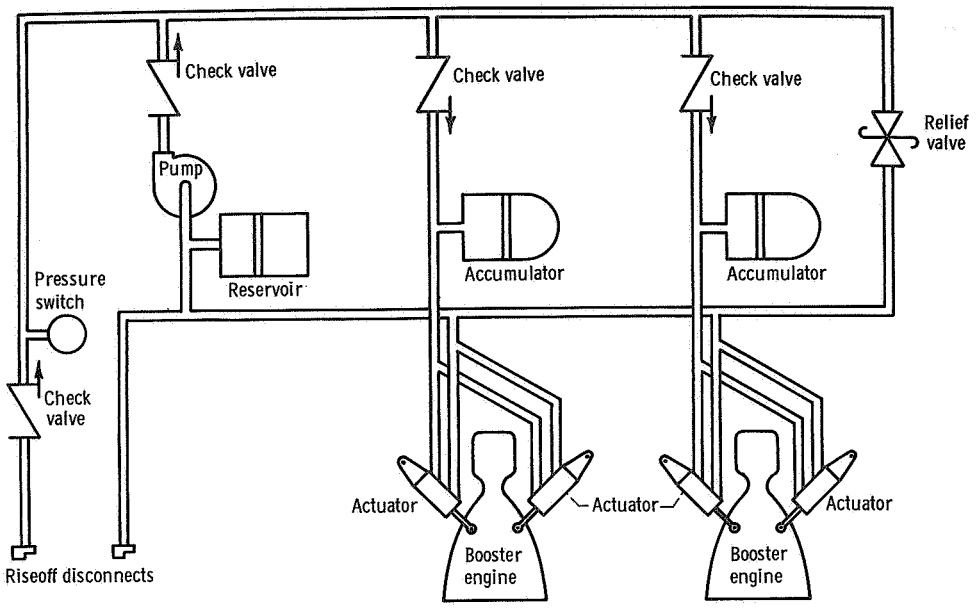

Figure V-67. - Atlas booster hydraulic system, AC-9.

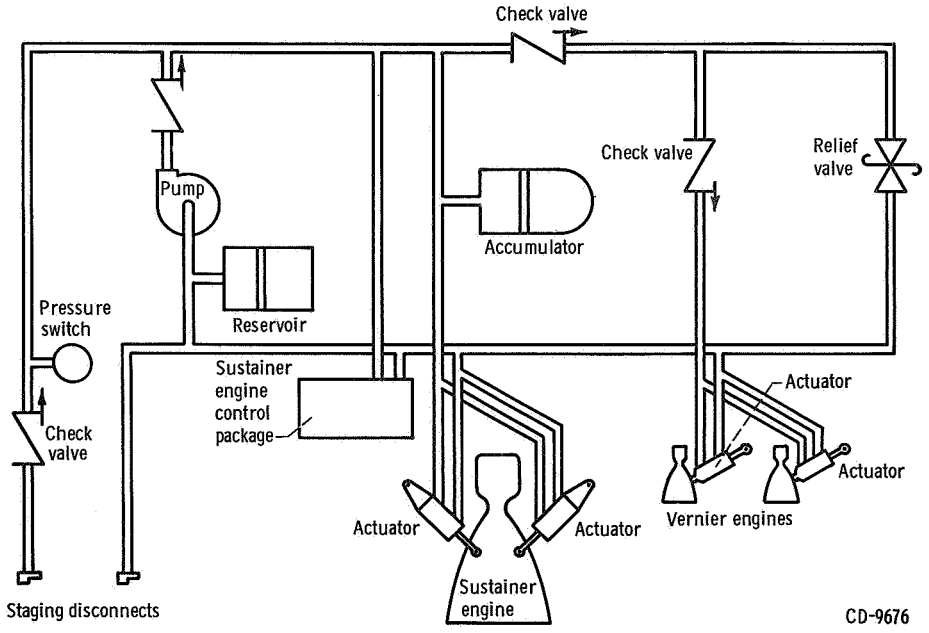

Figure V-68. - Atlas sustainer hydraulic system, AC-9.

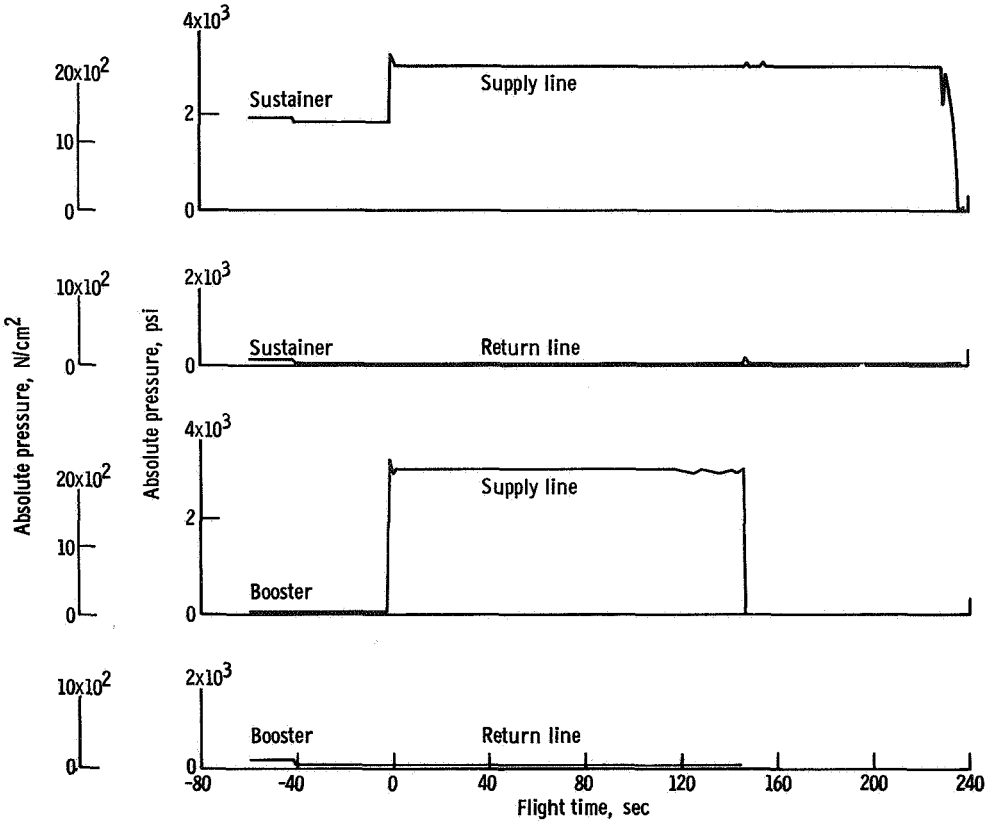

Figure V-69. - Atlas pump line and return system pressures, AC-9.

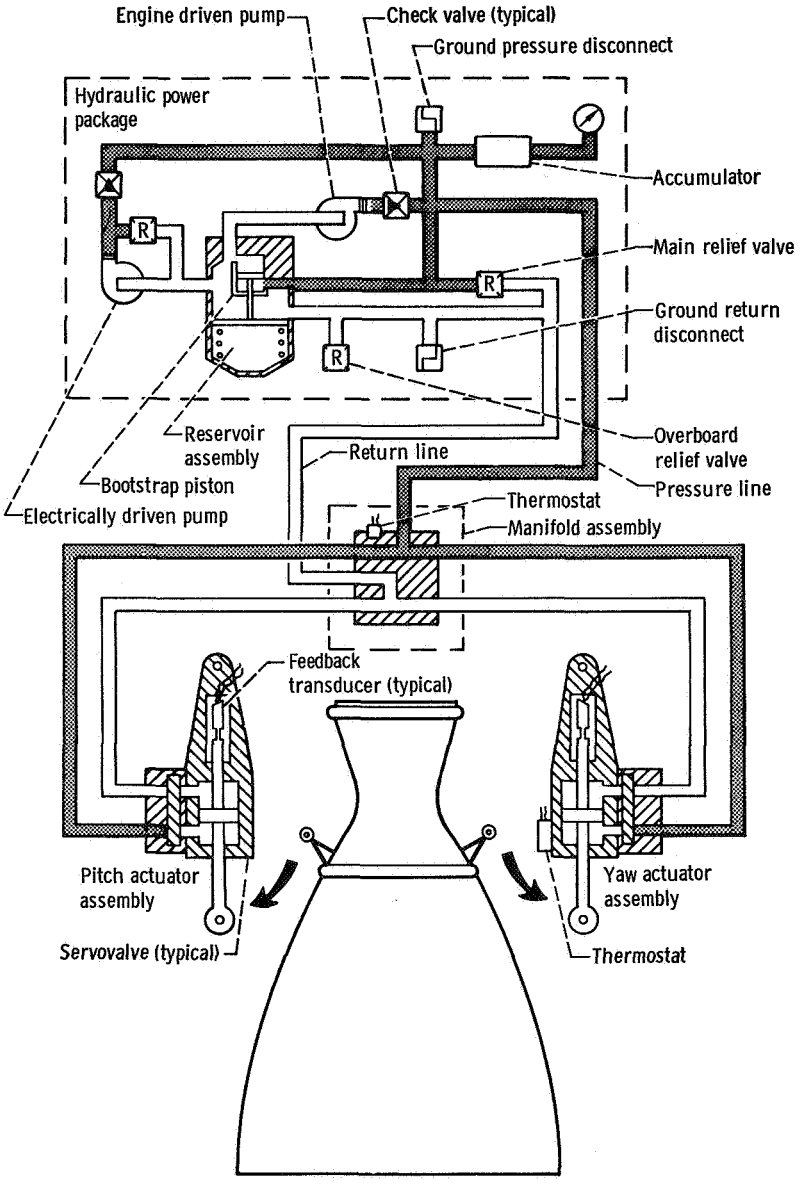

Figure V-70. - Centaur hydraulic system, AC-9. (System shown is typical for each engine.)

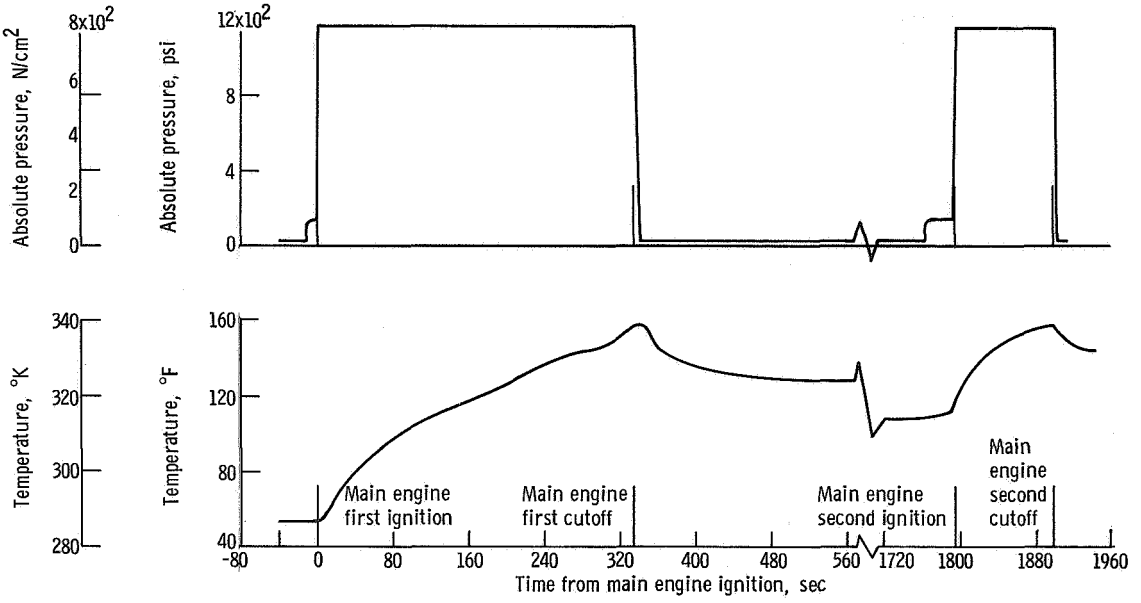

Figure V-71. - C-1 engine hydraulic system pressure and temperature, AC-9.

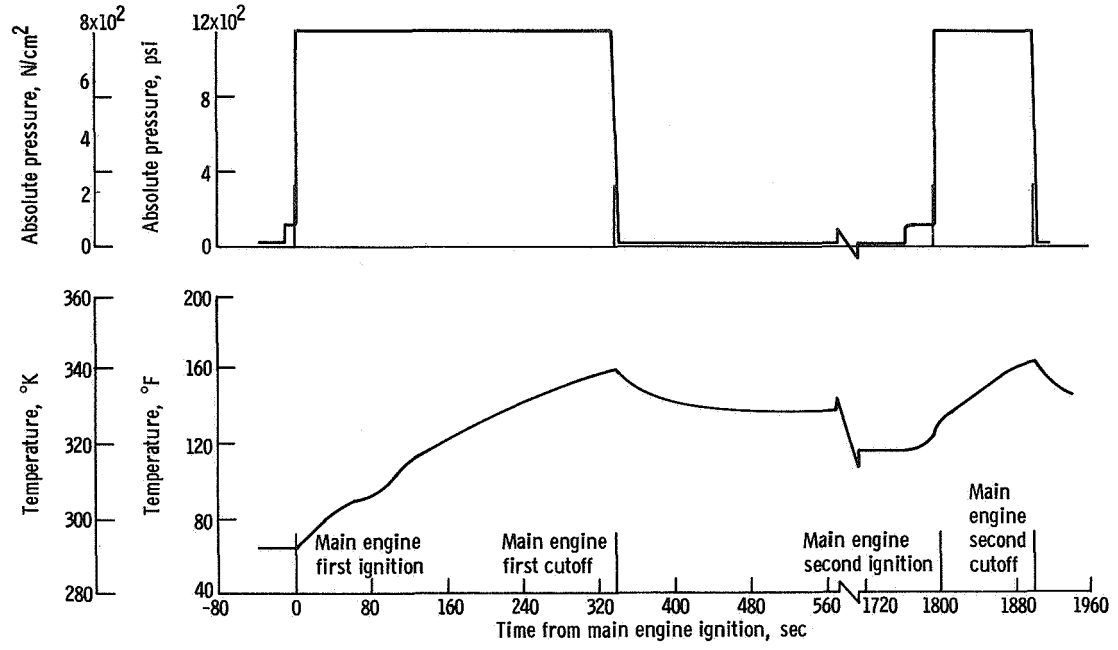

Figure V-72. - C-2 engine hydraulic system pressure and temperature, AC-9.

VEHICLE STRUCTURES

by Robert C. Edwards, Charles W. Eastwood,
Jack C. Humphrey, and Theodore F. Gerus

Atlas Structures

Atlas system description. - The Atlas vehicle structure included the basic tank and all bolt-on hardware. The propellant tanks provided the primary vehicle structure. These tanks were thin-walled pressure-stabilized sections of monocoque construction (see fig. V-73). They required a minimum pressure for various periods of flight in order to maintain structural stability. The structural capability of the tank as a pressure vessel determined the maximum allowable pressure in the propellant tanks.

The Atlas launcher assembly supported and balanced the vehicle in the vertical position prior to launch. This was accomplished by two holddown and release arms and by two auxiliary supports. Figure V-74 shows the launcher assembly. At launch, the assembly restrained the vehicle to prevent release during engine thrust buildup. Pneumatic holddown cylinders applied the restraining force. This force prevented rotation of the release arms and rise of the vehicle. Bleed valves on the cylinders were opened at launch and caused pneumatic pressure to decay thereby reducing the holddown force. When the restraining force decreased to a lower value than the net upward force, the vehicle began to rise. The movement of the vehicle initiated rotation of the holddown and release arms. A kick strut link on each arm engaged a fitting on the vehicle and transmitted force from the vehicle to the support pin retraction mechanism. After approximately 8.7 inches (22.1 cm) of vehicle rise, the pins were fully retracted and the mechanisms locked. The forces supplied by the vehicle through the kick structs were then applied directly to the arms to rotate them clear of the vehicle.

Atlas launcher transients. - The vehicle and its components experienced transient longitudinal and lateral oscillating loads transmitted through the kick structs by launcher mechanism forces at lift-off. Various components of the launcher were instrumented to monitor these loads. The booster fuel staging valve poppet motion and fuel manifold support strut loads were studied through linear motion and strain measurement transducer outputs, respectively.

The maximum kick struct loads and the maximum longitudinal oscillatory acceleration were measured and these data are compared with data from previous flights in table V-8. Accelerometers were installed on the base of the Surveyor mass model to measure lateral acceleration. The maximum acceleration in the YY direction was 1.07 g's, peak to peak, shortly after kick strut third peak load. The maximum acceleration in the XX direction was 0.61 g's, peak to peak, shortly after the kick strut second peak load. These lateral accelerations and the longitudinal accelerations, shown

TABLE V-8. - LOADS ON LAUNCHER KICK STRUTS AT LIFT-OFF, AC-9

Flight	Maximum kick strut loads, lb; N		Loads determined by -	Longitudinal acceleration (peak to peak), g's	Accelerometer location, vehicle station
	B-1 strut	B-2 strut			
AC-9	27 850; 123 800 30 100; 133 800	27 250; 121 000 30 100; 133 800	Strain gages on kick struts Measure of kick strut spring deflection	0.94	173
AC-7	31 200; 138 800	29 600; 131 600	Measure of kick strut spring deflection	0.56	1043
AC-8	29 000; 128 900	30 000; 133 400	Strain gages on kick struts	0.58	173
AC-10	28 000; 124 400	25 600; 113 800	Strain gages on kick struts	0.81	1043

TABLE V-9. - LOADS ON BOOSTER FUEL STAGING VALVE SUPPORT STRUTS AND VALVE POPPET CLEARANCE AT LAUNCH, AC-9

[Loads referenced to pretanking condition.]

Flight	Maximum loads[a] on support struts, lb; N				Valve poppet clearance, in.; cm	
	Fuel manifold support struts				Pretanking measurement	Minimum during launch
	P-2	P-4	P-5	P-6		
AC-9	+2600; +11 550	-990; -4390	-125; -555	-190; -844	1.70; 4.32	1.65; 4.19
AC-7	No data	-1300; -5780	-90; -400	-200; -890	1.77; 4.50	1.77; 4.50
AC-8	+2250; +10 000	-1400; -6230	No data	+650; +2880	1.67; 4.24	1.64; 4.16
AC-10	+2550; +11 330	No data	+150; +667	-150; -667	1.68; 4.27	1.70; 4.32

[a] Tension loads are denoted by plus sign; compression loads are denoted by minus sign.

in table V-8, were all within design allowable limits for the vehicle. The maximum acceleration was approximately 6 percent less than the highest value, 1 g, which occurred on one of the earlier flights.

The fuel staging valve on this vehicle incorporated new design features including a strengthened poppet spider. Poppet motion was normal. The poppet minimum clearance of 1.65 inches (4.19 cm) at kick struct second peak load was within limits. Fuel manifold support strut loads also were normal during the transient period at launch. The four struts which were instrumented are shown in figure V-75. This was the last of four flights on which these parameters were measured. The measured values are compared in table V-9. The minimum poppet clearance and maximum strut loads were well within limits.

Atlas tank pressure criteria. - The Atlas intermediate bulkhead differential pressure, as shown in figure V-76, remained well above the minimum design allowable of 2.0 psi

(1.4 N/cm^2) throughout the critical lift-off period. During this time, the Atlas liquid-oxygen mass was subjected to longitudinal oscillations. Thereafter, the bulkhead differential pressure varied between a minimum of 9.0 psi (6.2 N/cm^2) at T + 100 seconds and a maximum of 25.8 psi (17.8 N/cm^2) at T + 143.1 seconds (booster engine cutoff).

Oxidizer tank pressures during the period of highest bending loads (T + 60 to T + 80 sec) were above the minimum required for resisting the maximum design loads (fig. V-76). The minimum differential between required and actual pressures occurred at T + 70 seconds, when the oxidizer tank absolute pressure was 34.3 psi (23.7 N/cm^2) and the minimum allowable was 33.2 psi (22.9 N/cm^2). The maximum allowable oxidizer tank pressure was most closely approached at T + 200 seconds. At this time, the absolute pressure was 32.4 (22.3 N/cm^2); the allowable maximum absolute pressure was 36.4 (25.1 N/cm^2).

The fuel tank did not approach the maximum allowable or minimum required pressure at any time during the flight.

Quasi-steady-state load factors. - A maximum acceleration of 5.68 g's was reached at booster engine cutoff which was within the ±3 sigma range (5.62 to 5.78 g's; see appendix A). Thus, the longitudinal or axial load factor was within the design limits.

Centaur Structures

Centaur system description. - The Centaur vehicle structure included the basic tank and all bolt-on hardware. The propellant tanks provided the primary vehicle structure. These tanks were thin-walled pressure-stabilized sections of monocoque construction (see fig. V-77). They required a minimum pressure for various periods of flight in order to maintain structural stability. The structural capability of the tank as a pressure vessel determined the maximum allowable pressure in the propellant tanks. The propellant tanks were vented as required during the flight to prevent excessive ullage pressures. (See the PNEUMATIC SYSTEMS section for the sequence of these venting events).

Centaur tank pressure criteria. - Maximum design loads were used to compute maximum allowable and minimum required tank pressures. Appropriate factors of safety were also included. The AC-9 flight pressure profile is compared with the design pressure profile in figure V-78. These pressure profiles are identical to the ones shown in the PNEUMATIC SYSTEMS section with pressure limits added. The tank locations and criteria which determined the maximum allowable and minimum required tank pressures during different phases of flight are described in figure V-79.

The liquid-oxygen-tank pressure was of concern only at booster engine cutoff when the maximum allowable pressure was at a minimum of 33.0 psi (22.7 N/cm^2). At this time, the actual absolute pressure, as shown in figure V-78(a), was 30.2 psi

(20.8 N/cm^2). The liquid-oxygen-tank pressure did not approach the minimum required during any period of the flight.

The strength of the liquid-hydrogen tank was governed by the hoop stress capability of the conical section of the forward bulkhead. Thus, the differential pressure across the forward bulkhead determined the maximum allowable liquid-hydrogen-tank pressure. This allowable differential pressure was 26.8 psi (18.5 N/cm^2). The liquid-hydrogen-tank pressure reached a value near the allowable design maximum just prior to opening of the primary hydrogen vent valve at T + 69.3 seconds (see fig. V-78(a)). The maximum allowable absolute pressure was 26.8 psi (18.5 N/cm^2) plus the nose fairing internal absolute pressure of 3.2 psi (2.2 N/cm^2). Thus, the maximum allowable liquid-hydrogen-tank absolute pressure was 30.0 psi (20.7 N/cm^2). The actual liquid-hydrogen-tank absolute pressure at this time was 26.2 psi (18.0 N/cm^2).

The liquid-hydrogen-tank pressure also reached a value near the allowable design maximum prior to main engine second start at T + 2016 seconds and during the turnaround maneuver at T + 2440 seconds (see figs. V-78(e) and V-78(f)). The liquid-hydrogen-tank absolute pressure at these times was 25.8 psi (17.8 N/cm^2) and 26.4 psi (18.2 N/cm^2), respectively. Since the pressure on the exterior of the forward bulkhead was zero at these times, the maximum allowable tank absolute pressure was 26.8 psi (18.5 N/cm^2).

The liquid-hydrogen-tank pressure approached the minimum required pressure at the following times: prelaunch, launch, primary hydrogen vent valve opening, and nose fairing jettison.

(1) Prior to launch, the insulation panel pretensioning imposed local bending stresses on the liquid-hydrogen-tank cylindrical skin. The minimum required liquid-hydrogen-tank absolute pressure at this time was 19.0 psi (13.1 N/cm^2); the actual tank absolute pressure was 21.8 psi (15.0 N/cm^2), as shown in figure V-78(a).

(2) During the launch phase (T + 0 to T + 10 sec), the payload imposed compression loads on the forward bulkhead due to inertia and lateral vibration. The minimum required liquid-hydrogen-tank absolute pressure, was 20.0 psi (13.8 N/cm^2) at T + 0; at this time, the actual tank absolute pressure was 23.0 psi (15.9 N/cm^2), as shown in figure V-78(a).

(3) Just after the primary hydrogen vent valve was opened at T + 69.3 seconds, the inertia and bending compression loads were critical at station 409.6 on the cylindrical skin. The minimum required liquid-hydrogen-tank absolute pressure was 20.4 psi (14.1 N/cm^2). The tank absolute pressure at this time was 22.4 psi (15.5 N/cm^2), as shown in figure V-78(a).

(4) At nose fairing jettison, the nose fairing exerted inboard radial loads at station 219. The minimum required tank absolute pressure at this time was 18.5 psi (12.8 N/cm^2); the tank absolute pressure was 20.3 psi (14.0 N/cm^2), as shown in figure V-78(b).

The maximum allowable differential pressure between the liquid-oxidizer and liquid-hydrogen tanks was limited by the strength of the Centaur intermediate bulkhead. The liquid-oxygen-tank pressure must always be greater than the liquid-hydrogen-tank pressure to stabilize the bulkhead (prevent bulkhead reversal).

The maximum design allowable differential pressure across the intermediate bulkhead was 23.0 psi (15.9 N/cm^2). During pressurization of the liquid-oxygen tank, the actual differential was 20.0 psi (13.8 N/cm^2) at T + 229 seconds (fig. V-78(b)).

The minimum design allowable differential pressure across the intermediate bulkhead was 2.0 psi (1.4 N/cm^2). Before the primary hydrogen vent valve was opened at T + 69.3 seconds, the actual differential pressure across the intermediate bulkhead was 3.4 psi (2.3 N/cm^2) less a hydrostatic head pressure of 1.0 psi (0.7 N/cm^2), or a net differential pressure of 2.4 psi (1.6 N/cm^2), as shown in figure V-78(a). During main engine second firing at T + 2070 seconds, the differential pressure across the intermediate bulkhead was 3.2 psi (2.2 N/cm^2), as shown in figure V-78(e). During the turnaround maneuver at T + 2440 seconds, the differential pressure across the intermediate bulkhead was indicated to be only 0.4 psi (0.3 N/cm^2), as shown in figure V-78(f) It was anticipated that the differential pressure might be below the minimum design allowable during the turnaround maneuver. However, the possibility of bulkhead reversal was slight, and if the bulkhead did reverse, there was little likelihood that the spacecraft would be subjected to a hazardous condition.

Vehicle Dynamic Loads

The Atlas Centaur launch vehicle receives dynamic loading from several sources. The loads fall into three major categories: (1) external loads from aerodynamic and acoustic sources, (2) transients from engines starting and stopping and from the separation systems, and (3) loads due to dynamic coupling between major systems.

Previous flights of the Atlas-Centaur have shown that these loads were within the structural limits established by ground test and model analysis. For this flight, therefore, only a limited number of dynamic flight measurements were made. With this amount of flight instrumentation, only a limited check of significant launch vehicle dynamic loads and local vibrations could be made. The instruments used and the parameters measured are listed in the following table:

Instruments	Corresponding parameters
Low-frequency-range accelerometer	Launch vehicle longitudinal vibration
Centaur pitch rate gyro	Launch vehicle pitch plane vibration
Centaur yaw rate gyro	Launch vehicle yaw plane vibration
Angle of attack sensor	Vehicle aerodynamic loads
High-frequency accelerometers	Local vibration

Launch vehicle longitudinal vibrations, as measured on the Centaur forward bulkhead, are shown in figure V-80. The frequency and amplitude of the vibrations measured on this flight are compared with three other representative flights.

During launcher release, longitudinal vibrations were excited. (See the previous discussion of Atlas launcher transients, p. 109). The amplitude and frequency of these vibrations were similar to those seen during other launches. Atlas intermediate bulkhead pressure fluctuations were the most significant effects produced by the launcher-induced longitudinal vibrations. The peak pressure fluctuations computed from these vibrations were 6.1 psi (4.2 N/cm^2). Since the bulkhead static differential pressure measured at this time was 18 psi (12.4 N/cm^2, see fig. V-76), the calculated minimum differential pressure was 12 psi (8.3 N/cm^2). The minimum design allowable differential pressure across the bulkhead was 2.0 psi (1.4 N/cm^2).

During Atlas flight between T + 130 and T + 143 seconds, intermittent longitudinal vibrations of 0.11 g's at a frequency of 11.5 hertz were observed on the forward bulkhead . These vibrations are believed to be caused by dynamic coupling between structure, engines, and propellant lines (commonly referred to as "POGO"). The amplitude and frequency of the vibrations were similar for the four vehicles shown in figure V-80, because the controlling parameters had not changed from flight to flight. These vibrations at the measured amplitudes did not produce significant vehicle loads (see ref. 5).

During booster engine thrust decay, short duration transient longitudinal vibrations of 0.62 g's at a frequency of 12 hertz were observed. The analytical models did not indicate significant structural loading due to these vibrations.

During the boost phase of flight, the vehicle vibrates in the pitch and yaw planes as an integral unit of all its natural frequencies. Previous analyses and tests have defined these natural frequencies or modes and the shapes which the vehicle assumes when the modes are excited. The rate gyros on the Centaur provided data for determining the deflection of these modes. The maximum first mode deflection was seen in the pitch plane at T + 139 seconds (fig. V-81). The deflection was less than 7 percent of the allowable deflection. The maximum second mode deflection was seen in the yaw plane at T + 34 seconds (fig. V-82). The yaw deflection was less than 14 percent of the allowable deflection.

Predicted angles of attack were based on upper wind data obtained from a balloon released near the time of launch. Vehicle bending moments were calculated using predicted angles of attack, engine gimbal angle data, vehicle weights, and vehicle stiffnesses. These moments were added to axial load equivalent moments and to moments resulting from random dispersions. The most significant dispersions considered were uncertainties in launch vehicle performance, vehicle center-of-gravity offset, and upper atmosphere wind. The total equivalent moment computed was divided by the design moment allowable to obtain the predicted structural capability ratio as shown in figure V-83. This ratio is expected to be greatest between T + 55 and T + 90 seconds as the result of aerodynamic loads during this period. The maximum structural capability ratio predicted for this period was 0.82.

Differential pressures were measured on the nose fairing cap in the pitch plane and the yaw planes. Total pressure was computed from a trajectory reconstruction. Angles of attack were computed from these data and are compared with predicted angles of attack in figures V-84 and V-85. Since the actual angles of attack were within the expected dispersion values, it follows that the predicted structural capability ratio of 0.82 was not exceeded.

Local shock and vibration were measured by four high-frequency accelerometers. Data from three of these accelerometers were time shared because of data channel limitations. Because of this time sharing, some short duration transients were not measured.

A summary of the most significant shock and vibration levels is shown in table V-10. The steady-state vibration levels were highest near lift-off as expected. The maximum level of the shock loads (13 g's) occurred at Atlas-Centaur separation. These shock levels are of short duration (about 0.025 sec) and do not provide significant loads. An analysis of the data indicates that the levels were well within spacecraft qualification levels.

TABLE V-10. - MAXIMUM SINGLE AMPLITUDE SHOCK AND VIBRATION LEVELS DURING AC-9 FLIGHT

[Bandwidth of all channels was 1000 Hz. Accelerometer data were time shared. Each signal was active for 1 sec and inactive for 3 sec.]

Accelerometer location	Station	Quadrant	Sensitive axis	Flight events							
				Launch			Boost phase		Booster engine cutoff		Insulation panel jettison
				Time, sec	Frequency, Hz	Acceleration, g's	Frequency, Hz	Acceleration, g's	Frequency, Hz	Acceler- g's	
Hydrogen vent valve	160	IV	X	T + 0.35	100	7.9	High	5.25	(a)	(a)	(a)
Near hydrogen peroxide bottle	459	IV	X	T + 2	Random spectrum	1.25	Random spectrum	1.56	50	0.625	(a)
C-1 gimbal mount	453	---	Z	-------	Random spectrum	1.56	Random spectrum	1.56	(a)	(a)	(a)
Guidance platform mount (upper tier)	---	II	Y	T + 3	Random spectrum	2.25	Random spectrum	1.13	(a)	(a)	(a)

Accelerometer location	Station	Quadrant	Sensitive axis	Flight events								
				Nose fairing jettison		Atlas-Centaur separation		Main engine first start		Main engine first cutoff	Main engine second start	Main engine second cutoff
				Frequency, Hz	Acceleration, g's	Frequency, Hz	Acceleration, g's	Frequency, Hz	Acceleration, g's			
Hydrogen vent valve	160	IV	X	Channel segment saturated by opening and shutting hydrogen valve						No detectable response	No detectable response	(a)
Near hydrogen peroxide bottle	459	IV	X	(a)	(a)	(a)	(a)	200 21.4	1.88 .375	(a)	(a)	(a)
C-1 gimbal mount	453	---	Z	28.6	0.94	(a)	(a)	(a)	(a)	(a)	(a)	Abrupt bias shift exhibited
Guidance platform mount (upper tier)	---	II	Y	(a)	(a)	[b]High	13	No detectable response	No detectable response	(a)	No detectable response	(a)

[a] Not sampled.

[b] Shock transient, 0.025-sec duration.

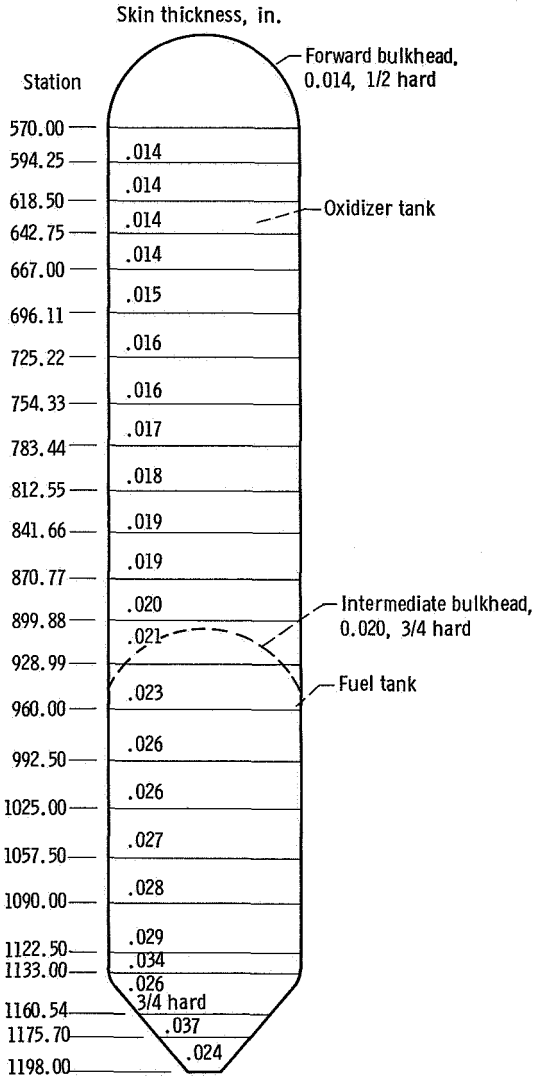

Figure V-73. - Atlas propellant tanks, AC-9. (Unless noted otherwise, all material is 301 extra-full-hard stainless steel.)

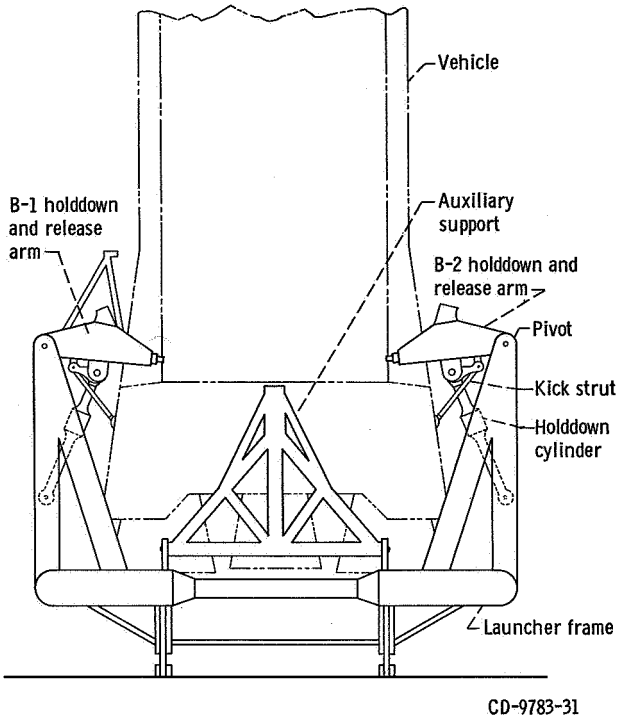

Figure V-74. - Launcher assembly, AC-9.

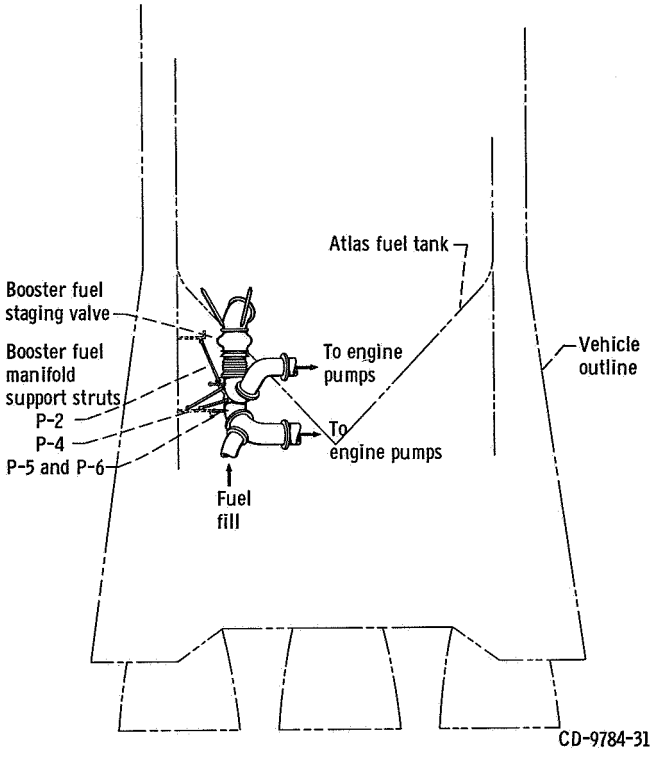

Figure V-75. - Booster staging valve and booster manifold support struts, AC-9.

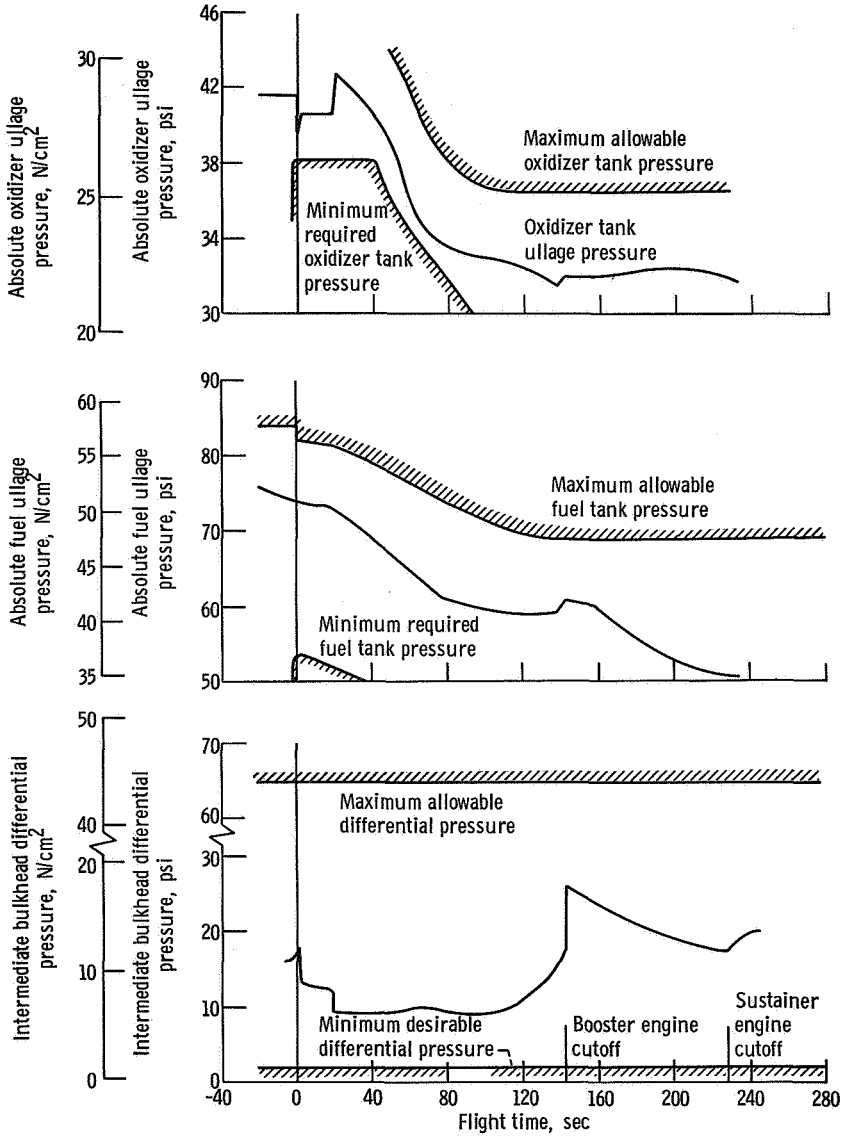

Figure V-76. - Atlas fuel and oxidizer tank pressures, AC-9.

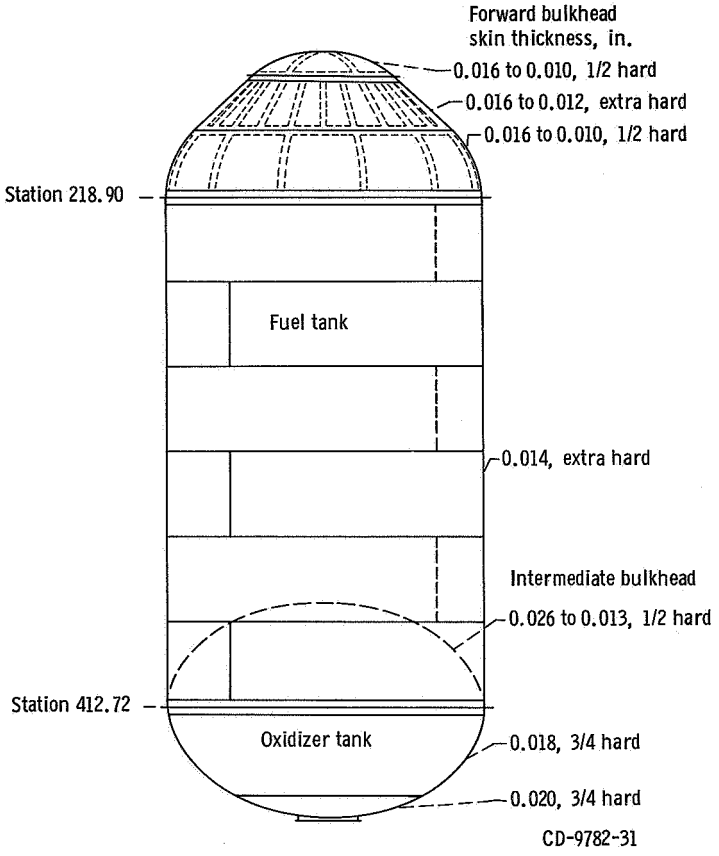

Figure V-77. - Centaur propellant tanks, AC-9. (All material 301 stainless steel of hardness indicated.)

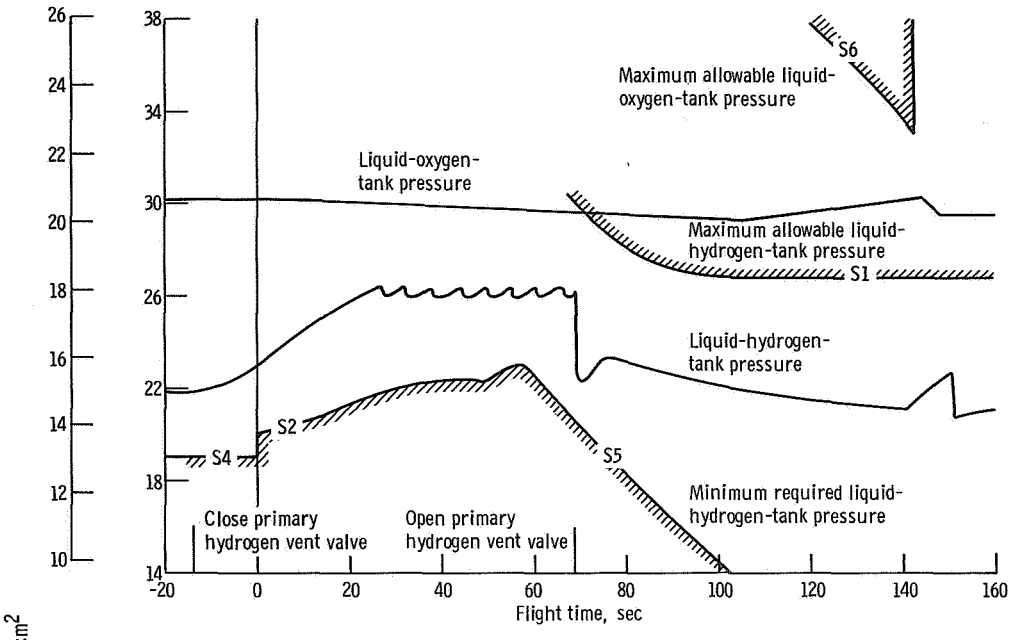

(a) T - 20 to T + 160 seconds.

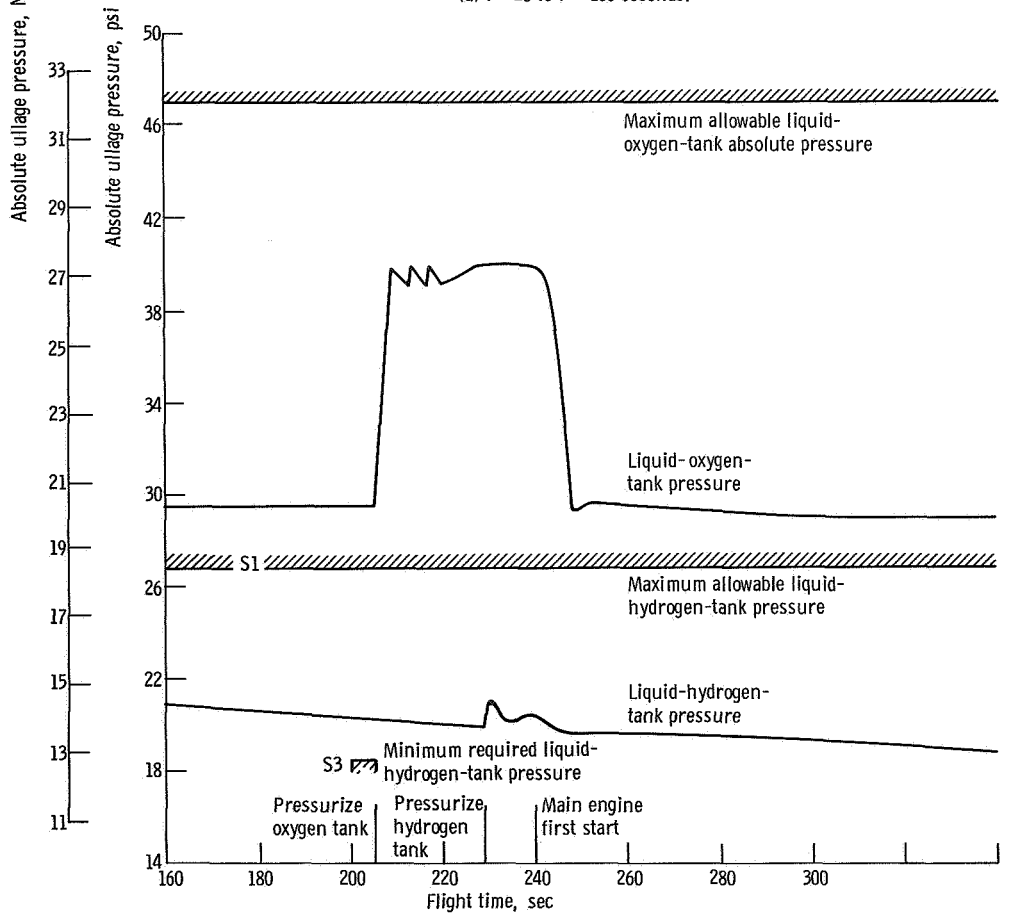

(b) T + 160 to T + 300 seconds.

Figure V-78. - Centaur tank pressure profiles, AC-9. (S1, S2, etc., indicate tank locations and criteria which determine the allowable pressure and are defined in fig. V-79.)

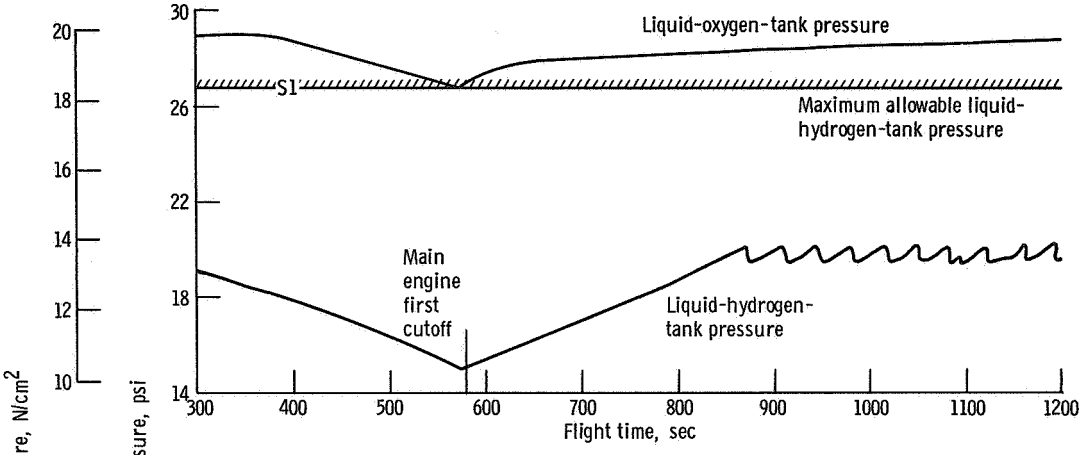

(c) T + 300 to T + 1200 seconds.

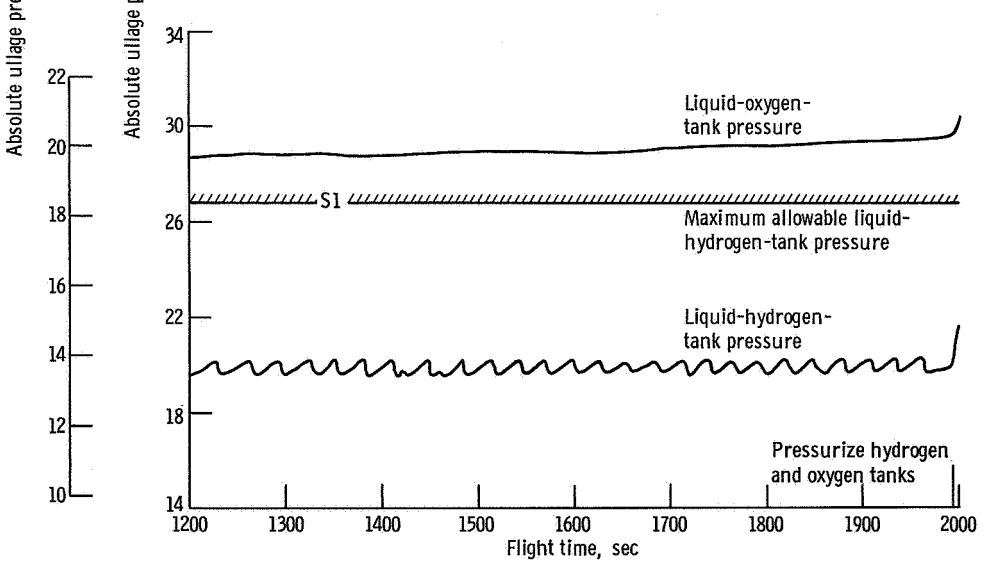

(d) T + 1200 to T + 2000 seconds.

Figure V-78. - Continued.

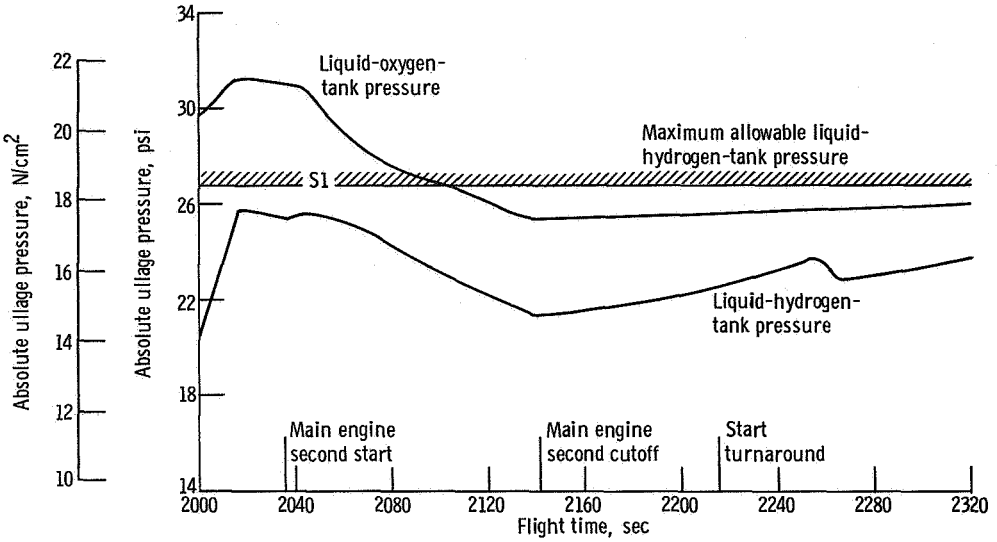

(e) T + 2000 to T + 2320 seconds.

Figure V-78. - Continued.

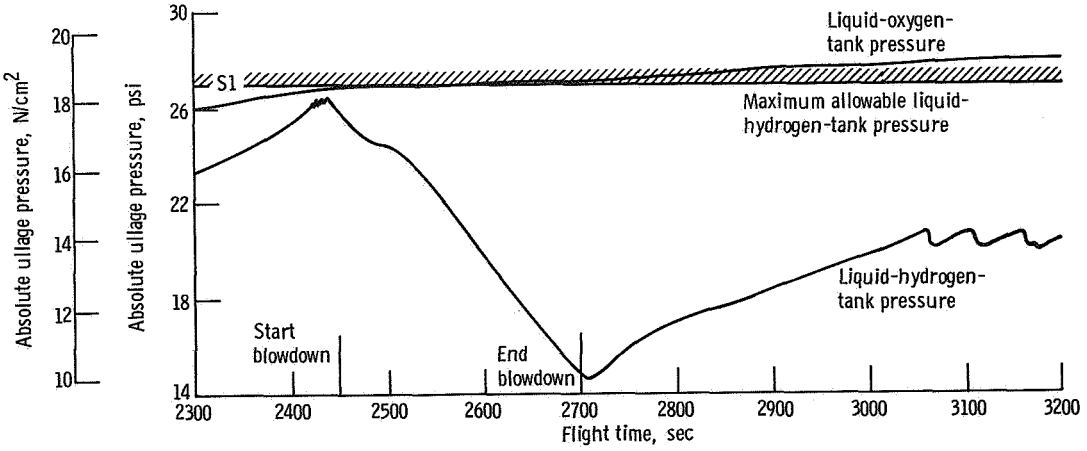

(f) T + 2300 to T + 2320 seconds.

Figure V-78. - Concluded.

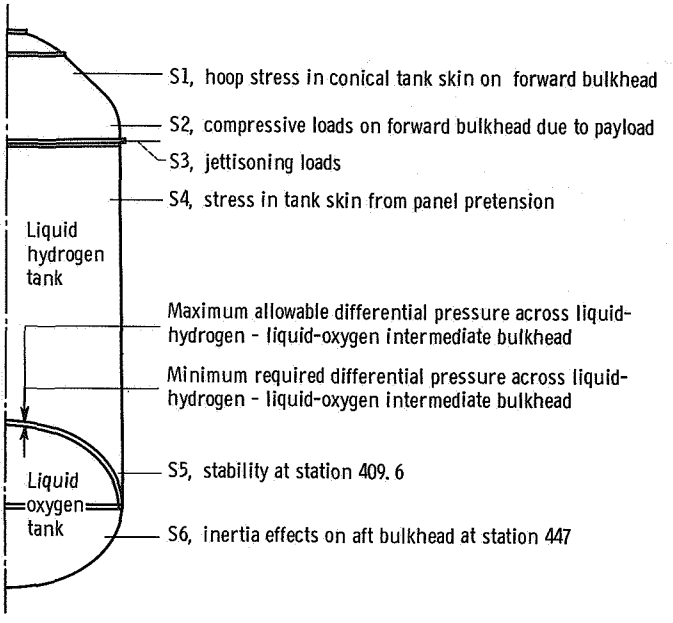

Figure V-79. - Tank locations and criteria which determine allowable pressures, AC-9.

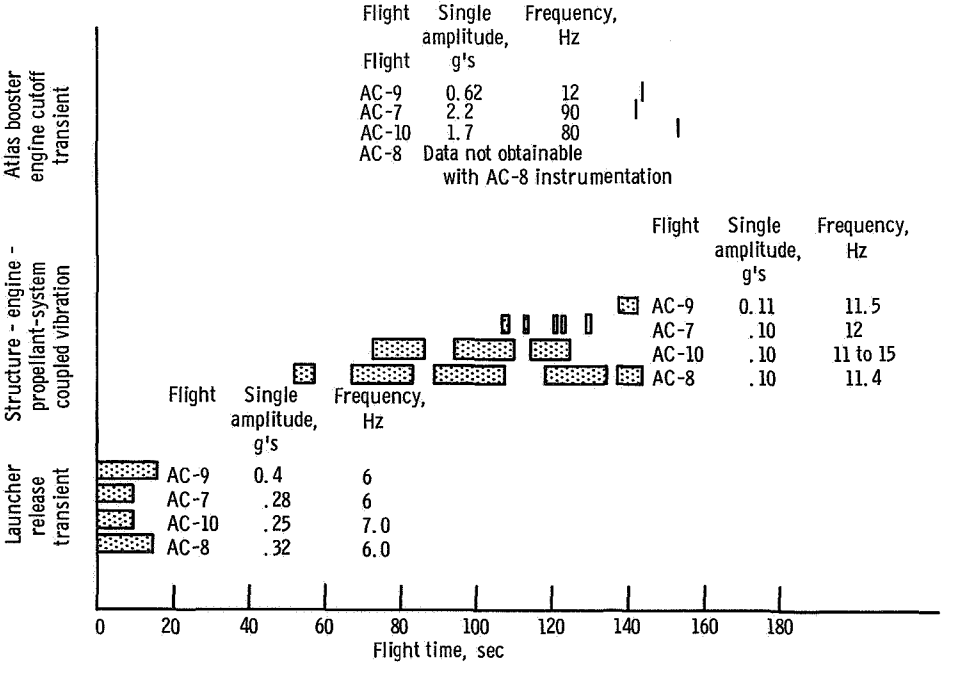

Figure V-80. - Comparison of longitudinal vibrations for Atlas-Centaur flights. (Length of bars indicates duration of vibration.)

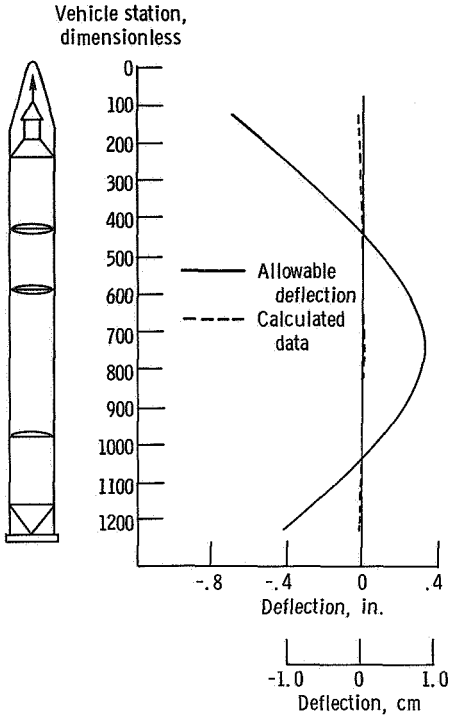

Figure V-81. - Maximum pitch plane first bending mode amplitudes, AC-9 (T + 139 sec).

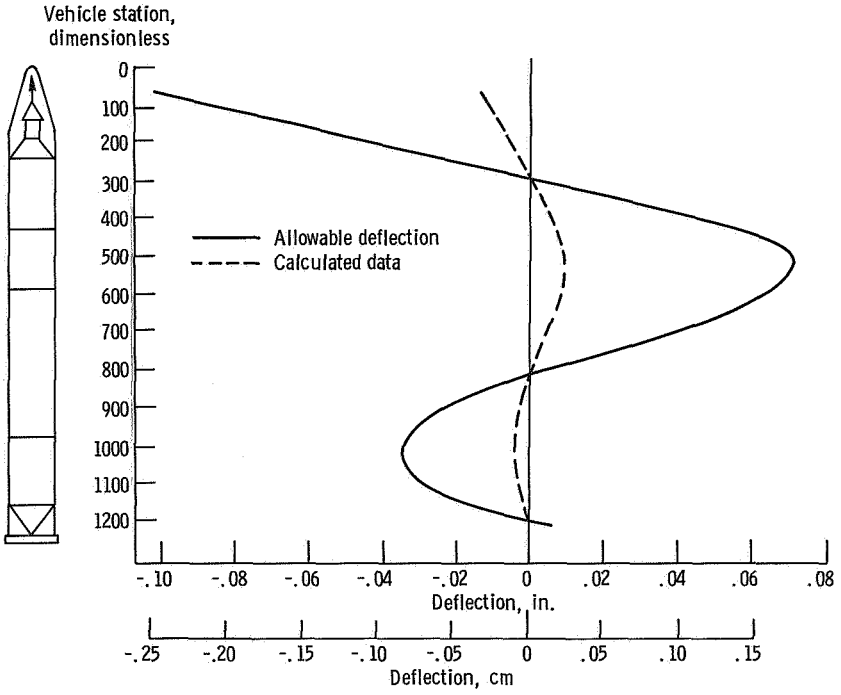

Figure V-82. - Maximum yaw plane second bending mode amplitudes, AC-9 (T + 34 sec).

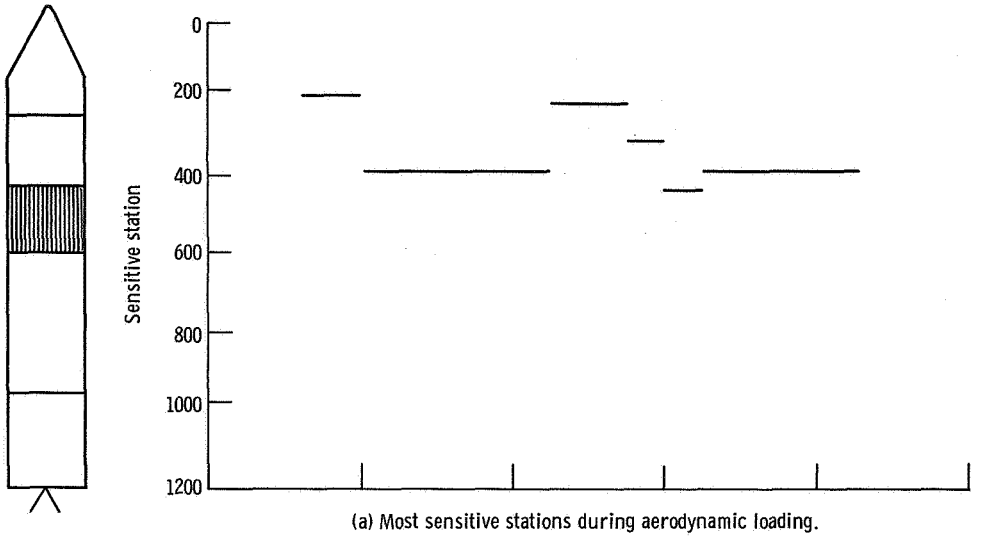

(a) Most sensitive stations during aerodynamic loading.

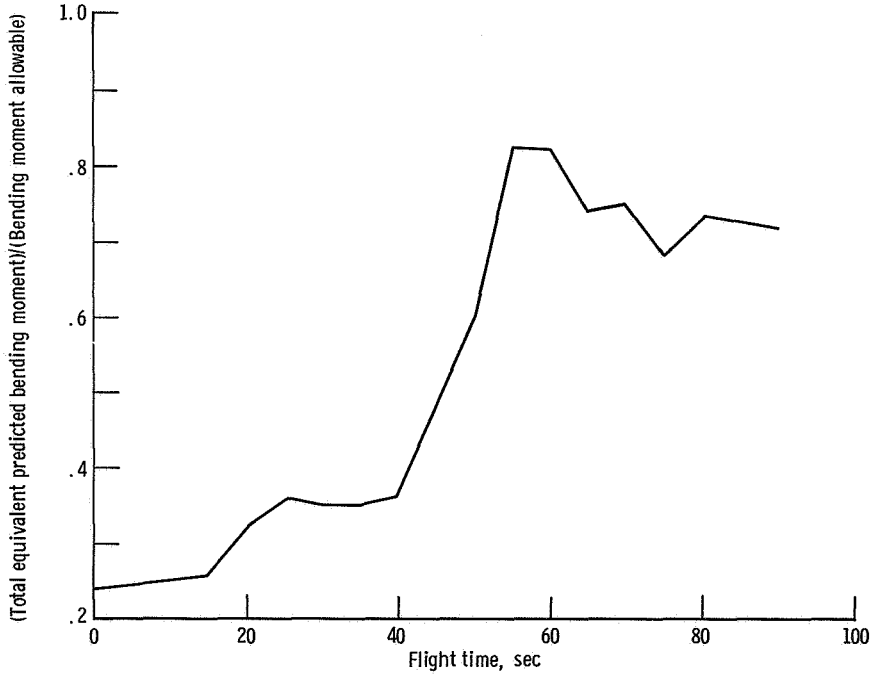

(b) Structural capability ratio during aerodynamic loading.

Figure V-83. - Maximum predicted structural capability ratio and most sensitive stations during aerodynamic loading, AC-9.

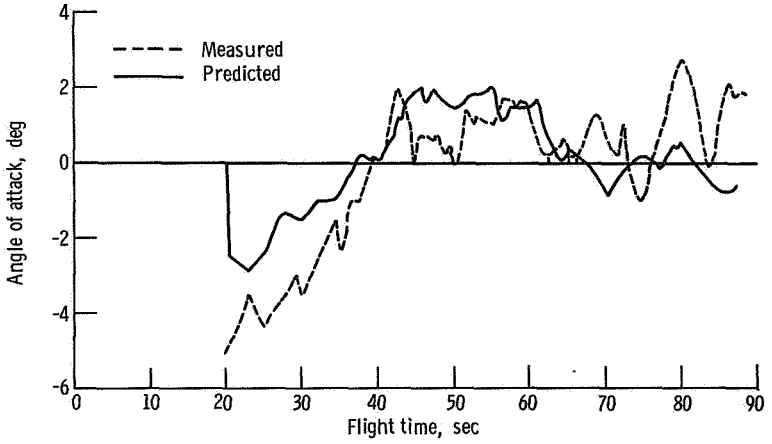

Figure V-84. - Pitch angles of attack, AC-9.

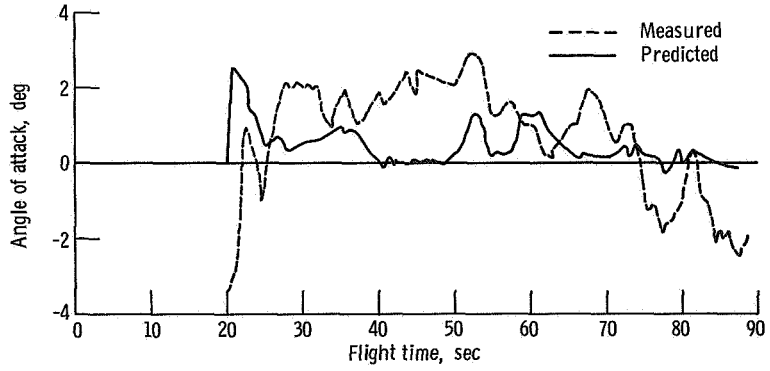

Figure V-85. - Yaw angles of attack, AC-9.

SEPARATION SYSTEM AND THERMAL ENVIRONMENTS

by Thomas L. Seeholzer and Raymond F. Lacovic

Separation Systems

System description. - The Atlas-Centaur AC-9 vehicle required systems for the following: (1) Centaur hydrogen tank insulation panels jettison, (2) nose fairing jettison, (3) Atlas-Centaur Staging, (4) Centaur spacecraft staging.

A general description of the insulation panels, nose fairing, spacecraft mass model, and all separation systems follows. (A description of the Atlas and Centaur tanks is given in the VEHICLE STRUCTURES section of this report).

The hydrogen tank insulation was made up of four fiberglass honeycomb panels bolted together along the longitudinal axis to form a cylindrical cover over the Centaur tank. The panels were tied circumferentially at their aft end by a metal ring to the Centaur stage. At the forward end, a circumferential Teflon and fiberglass cloth seal connected the panels to the base of the nose fairing at station 219.

The four insulation panels were separated by firing flexible, linear, shaped charges located at the forward, aft, and longitudinal seams. After shaped-charge firing, the panels were forced to rotate about hinge points by (1) center-of-gravity offset, (2) in-flight purge pressure, and (3) elasticity of the panels due to hoop tension. Each panel was hinged about two points located on the interstage adapter (fig. V-86). After approximately 45^{o} of rotation, the panels were freed from the Centaur vehicle.

The nose fairing was a fiberglass honeycomb structure consisting of a cylindrical section approximately 6 feet (1.83 m) long bolted to a conical section approximately 16 feet (4.87 m) long. It was assembled in two jettisonable halves, with the split line along the X-X axis as shown in figure V-87. During the boost phase of flight (0 to T + 143 sec), the nose fairing was subjected to bending loads, axial loads, and high temperatures as the vehicle passed through the atmosphere. Thermal protection, in the form of a subliming agent called Thermolag, was applied to both cone and cylindrical sections of the fairing in order to maintain necessary strength at high temperatures.

The nose fairing was jettisoned by nitrogen gas thrusters located in the forward end, one in each fairing cone half. The thrusters, when fired, forced the fairing halves to pivot outboard around their respective hinge points. After approximately 35^{o} rotation, the fairings separated from the Centaur vehicle. Prior to thruster actuation, the aft circumferential connection to the Centaur tank was severed by firing a flexible, linear, shaped charge. The nose fairing split line was opened by release of eight pyrotechnically operated pin puller latches (fig. V-87).

Atlas-Centaur staging, as shown in figure V-88, was accomplished by firing a flexible, linear, shaped charge which cut the interstage adapter circumferentially near

its forward end. The Atlas and interstage adapters were then separated from the Centaur by firing retrorockets on the Atlas approximately 0.1 second after shaped-charge firing.

The spacecraft mass model consisted of a steel structure which simulated an actual Surveyor spacecraft in mass and center-of-gravity location. As shown in figure V-89, an S-band transponder was also incorporated to allow tracking of the spacecraft mass model on its simulated lunar trajectory.

The mass model was separated from Centaur by actuation of three pyrotechnically operated pin puller latches mounted on the forward payload adapter, as shown in figure V-89. Separation force was provided by three mechanical spring assemblies, each having a 1-inch (2.54-cm) stroke, mounted adjacent to each separation latch on the forward adapter.

Insulation panel jettison system performance. - Flight data indicated that the four insulation panels were jettisoned satisfactorily. Four breakwires, as shown in figure V-90, attached between the insulation panel hinge arms and the interstage adapter, indicated panel rotational velocities of approximately 85 degrees per second. These velocities are comparable to the 80 degrees per second on AC-7. A summary of breakwire times is shown in the following table:

Breakwire	Panel in quadrant-	Hinge arm in quadrant-	Break time, sec
A	II and III	III	T + 177.30
B	IV and I	I	T + 177.30
C	I and II	I	T + 177.29
D	III and IV	III	T + 177.29

Nose fairing jettison system performance. - Separation of the nose fairing occurred at T + 203.8 seconds. This event was verified by cessation of data (from instrumentation) transmitted through the electrical connectors. These connectors separated when the fairing halves were jettisoned.

Measurements of nose fairing hinge fitting longitudinal loads were obtained during flight by strain gages (see fig. V-87 for location). The nose fairing hinge fitting is designed to take loads only at fairing jettison and ensure that nose fairing inertia, pressure, and drag loads will be taken by the Centaur nose fairing attachment ring rather than by the hinge fitting. At the time of jettison, the nose fairing hinge fittings support the two fairing sections as each section pivots away from the Centaur tank.

At nose fairing jettison, the maximum aft compression load in the hinge fittings was 3200 pounds (14 250 N), and the maximum forward tension was 950 pounds (4230 N), as shown in figure V-91. These loads were within the design allowable load of 10 000 pounds (44 500 N). AC-9 values were comparable to the AC-8 hinge loads of 3475 pounds (15 450 N) aft compression and 3090 pounds (13 750 N) forward tension.

Atlas-Centaur staging system performance. - Vehicle staging was initiated at T + 230.9 seconds by the firing of the shaped charge which severed the interstage adapter at station 413. Eight retrorockets mounted around the aft end of the Atlas fired 0.1 second later to decelerate the Atlas and provide separation between it and the Centaur stage. Accelerometer and other recorded data indicated that all retrorockets fired properly.

The vehicle rate gyros indicated that the Atlas rotated 0.37° about its yaw axis at the time it cleared the Centaur. This rotation created a 3.7-inch (9.4-cm) movement of the forward end of the interstage adapter reducing the total clearance to 27.3 inches (69.1 cm). The vehicle rate gyros indicated 0.06° pitch rotation by the time the Atlas cleared the Centaur. The resulting vertical motion at the forward end of the interstage adapter was approximately 0.6 inch (1.52 cm), reducing the clearance to 10.4 inches (26.4 cm).

Spacecraft staging system performance. - The Surveyor mass model separated from the Centaur at T + 2210.8 seconds. Extensometers located on the separation spring assemblies indicated that all three separation latches actuated within 0.001 second of each other. The three jettison spring assemblies operated normally and yielded almost identical displacement time data (see fig. V-93). The separation was normal, producing no spring induced tipoff rate in the spacecraft. Vehicle tracking data indicated that the spacecraft tumbled at a rate of 0.5 degree per second shortly after separation. The allowable rate is 3 degrees per second.

Vehicle Thermal Environment During Ascent

Nose fairing. - An inner and outer surface temperature study similar to that performed on AC-8 was also performed on AC-9. A summary and comparison of the maximum AC-8 and AC-9 nose fairing temperatures are shown in table V-11. The AC-9 temperatures indicated moderate heating of the fairing surfaces. A subliming material (Thermolag T230) was used to limit the temperature of the nose fairing to less than 230° F (383° K). The design temperature allowable for the nose fairing is 300° F (422° K). The reduction in the external temperatures achieved by the application of Thermolag is given for two points on the fairing in table V-11(a). The aerodynamic heating curves for the stagnation point, 30° from the stagnation point, and 60° from the stagnation point are presented in figure V-93. These curves present the heating profile of the nose cap portion of the fairing. The maximum temperature recorded on the fairing was 784° F (692° K) at the stagnation point and occurred at T + 151 seconds.

Insulation panels. - Aerodynamic heating of the external flat panel surface was moderate. The internal temperatures increased from an average of -340° F (66° K) at

TABLE V-11. - NOSE FAIRING TEMPERATURES

(a) External

Location	Maximum indicated temperature, ^{o}F; ^{o}K	
	[a]AC-8	[b]AC-9
Y-axis, station 19	240; 389	262; 401
-Y-axis, station 19	275; 408	266; 403
Y-axis, station 72	220; 377	296; 419
-Y-axis, station 72	305; 425	272; 409
X-axis, station 72	[b]180; 355	[b]147; 337
-X-axis, station 72	[b]155; 342	[b]165; 347
Y-axis, station 125	275; 408	271; 405
-Y-axis, station 125	315; 430	305; 425
-X-axis, station 125	265; 402	297; 419
-Y-axis, station 185	135; 330	166; 348
Stagnation point	Invalid	784; 692
30^{o} from stagnation point at 135^{o} on Y-axis	475; 519	570; 572
60^{o} from stagnation point at 135^{o} on Y-axis	370; 461	381; 466

(b) Internal

Location	Measured temperature, ^{o}F; ^{o}K			
	AC-8		AC-9	
	Lift-off	Jettison	Lift-off	Jettison
-Y-axis, station 19	68; 293	80; 300	75.0; 297	95.3; 308
Y-axis, station 72	65; 291	78; 299	75.0; 297	86.2; 303
X-axis, station 72	66; 292	71; 295	76.0; 297	75.5; 297
-Y-axis, station 125	66; 292	70; 294	68.6; 293	76.8; 298
-X-axis, station 125	64; 291	68; 293	72.6; 296	76.8; 298
-Y-axis, station 185	48; 282	31; 272	51.3; 284	49.2; 283
30^{o} stagnation point	66; 292	85; 302	78.4; 299	123.9; 324

[a]Temperature transducers were located in a 4-in. - (10.16-cm-) diameter area void of Thermolag except where noted.

[b]Temperature transducers covered with Thermolag T230.

lift-off to an average of -317° F (79° K) at panel jettison. Selected areas of the insulation panels were covered with Thermolag; temperature measurements were taken at selected locations on the panels but not in Thermolag coated areas. A summary and comparison of insulation panel temperatures between AC-8 and AC-9 are presented in table V-12.

Protuberance heating. - The temperature obtained from the Centaur vehicle airframe protuberances defined a moderate aerodynamic heating profile. The maximum temperature levels of the protuberances are summarized and compared with corresponding AC-8 data in table V-13. The hydrogen vent stack experienced the maximum heating to a temperature of 706° F (647° K) at T + 152 seconds.

Interstage adapter. - The interstage adapter internal skin temperature survey on AC-9 defined a uniform and moderate surface temperature profile throughout the boost phase. A summary and comparison of the maximum temperatures observed for AC-8 and AC-9 are presented in table V-14. A small reduction in temperature of the interstage adapter achieved by the application of a thin coat of Thermolag is indicated in the table.

TABLE V-12. - INSULATION PANEL TEMPERATURES

(a) External

Location	Flight					
	AC-8			AC-9		
	Maximum measured temperature		Time, sec	Maximum measured temperature		Time, sec
	°F	°K		°F	°K	
Station 256, 115° from Y-axis	270	406	130	Invalid		
Station 280, 115° from Y-axis	225	381	127	230	383	136
Station 321, 115° from Y-axis	230	383	127	253	396	136

(b) Internal

Condition	Measured temperatures, °F, °K	
	AC-8	AC-9
Average temperature at lift-off	-360; 55	-340; 66
Average temperature at panel jettison (T + 177.3 sec)	-340; 66	-317; 79

TABLE V-13. - PROTUBERANCE TEMPERATURES DURING ASCENT

Location	Flight					
	AC-8			AC-9		
	Maximum temperature		Time, sec	Maximum temperature		Time, sec
	°F	°K		°F	°K	
Wiring fairing, station 198 at X-axis	80	300	[a]203.8	85	302	129
Wiring fairing, station 214 at X-axis	80	300	[a]203.8	99	311	129
Telemetry tunnel, station 314 at X-axis	160	345	128	167	349	131
Destruct fairing, station 392 at Y-axis	165	348	129	126	325	131
Telemetry tunnel, station 400 at X-axis	310	428	133	270	406	139
Fuel outlet fairing, station 400 at X-axis	310	428	145	312	429	147
Destruct fairing, station 381 at Y-axis	180	356	127	135	331	129
Fuel outlet fairing, station 389 at 79° from Y-axis	125	325	145	170	350	129
Hydrogen vent stack	750	674	145	706	647	152

[a]Nose fairing jettison.

TABLE V-14. - INTERSTAGE ADAPTER EXTERNAL SKIN TEMPERATURES

Location	Flight						
	AC-8			AC-9			
	Maximum temperature		Time, sec	Maximum temperature		Time, sec	Temperature transducer coated with Thermolag T230
	°F	°K		°F	°K		
Station 418 at 290° from Y-axis	170	350	115	84	303	106	✓
Station 431 at 291° from Y-axis	255	397	128	217	376	126	✓
Station 446 at 291° from Y-axis	225	381	115	220	377	121	✓
Station 461 at 291° from Y-axis	265	403	118	221	377	121	✓
Station 490 at 291° from Y-axis	270	406	122	244	392	122	✓
Station 519 at 291° from Y-axis	250	394	118	238	388	121	✓
Station 533 at 291° from Y-axis	265	403	119	246	393	123	✓
Station 503 at -Y-axis	235	387	137	285	414	132	
Station 533 at -Y-axis	235	387	137	254	397	133	

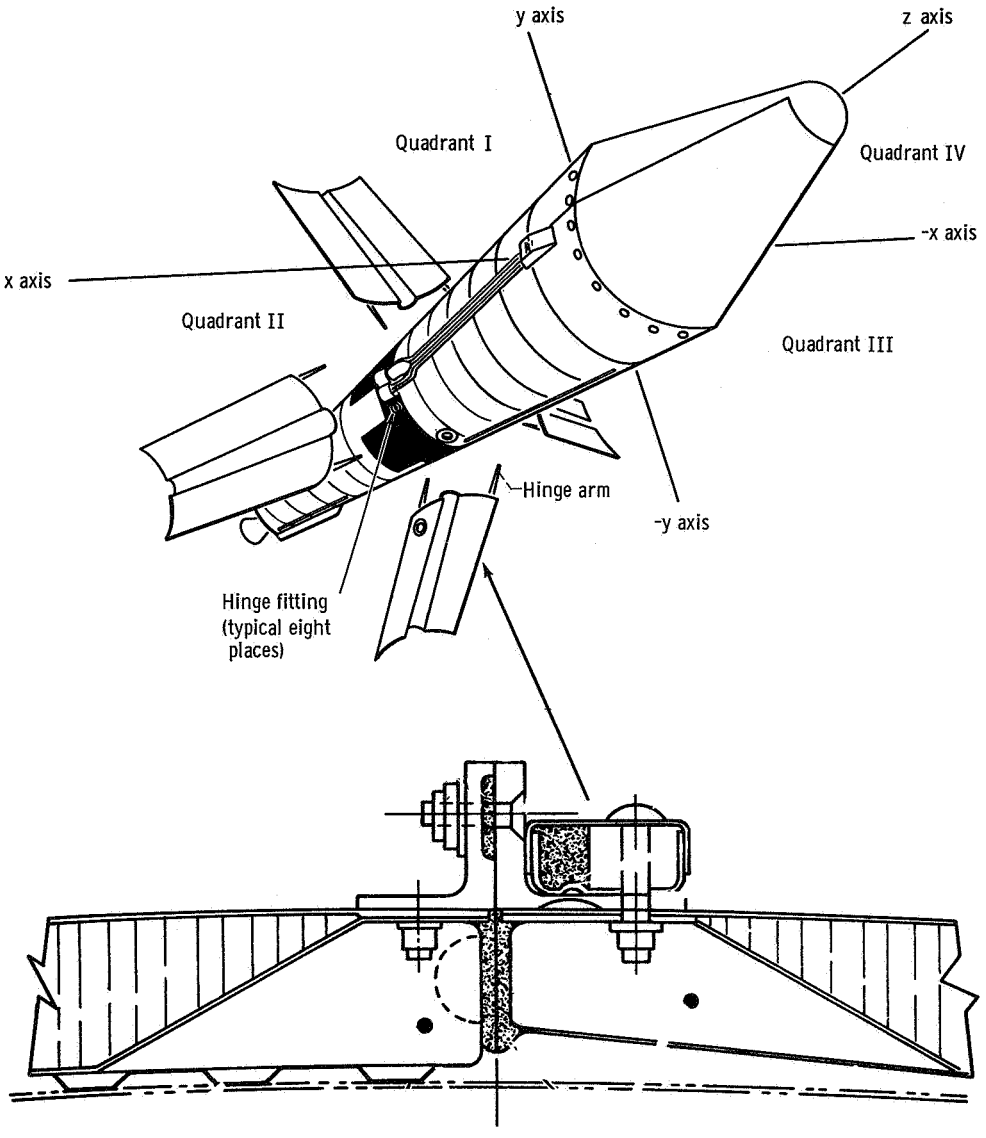

Figure V-86. - Hydrogen tank insulation jettison system, AC-9.

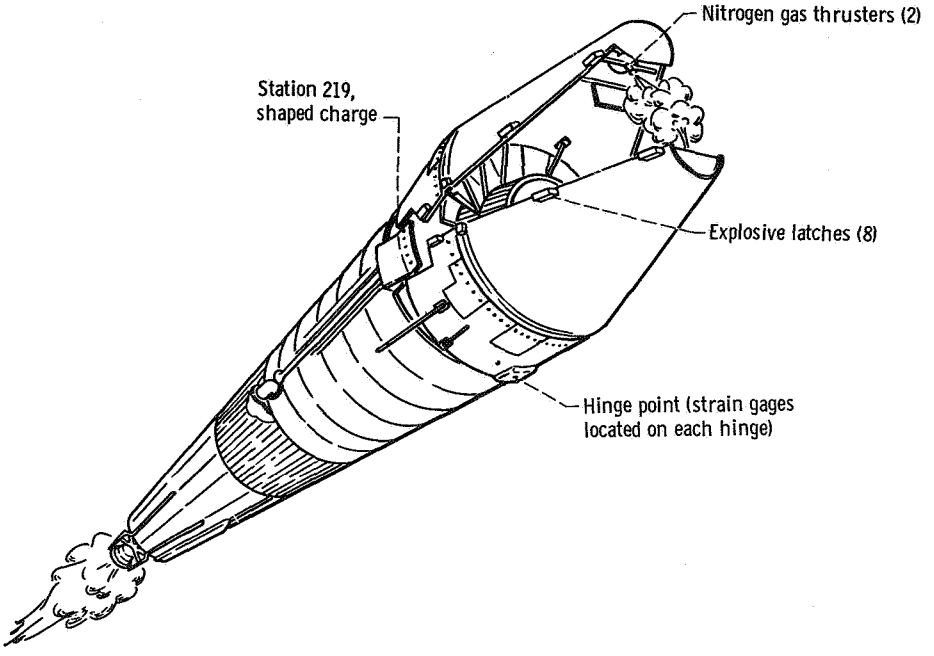

Figure V-87. - Nose fairing jettison, AC-9.

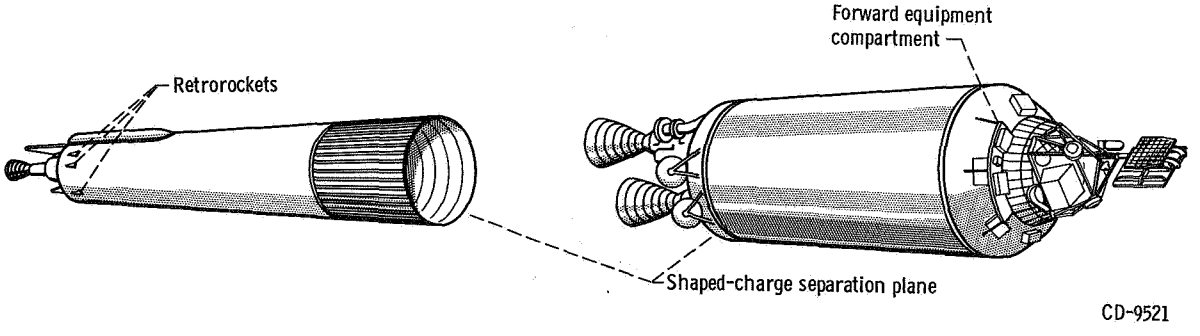

Figure V-88. - Atlas-Centaur separation system, AC-9.

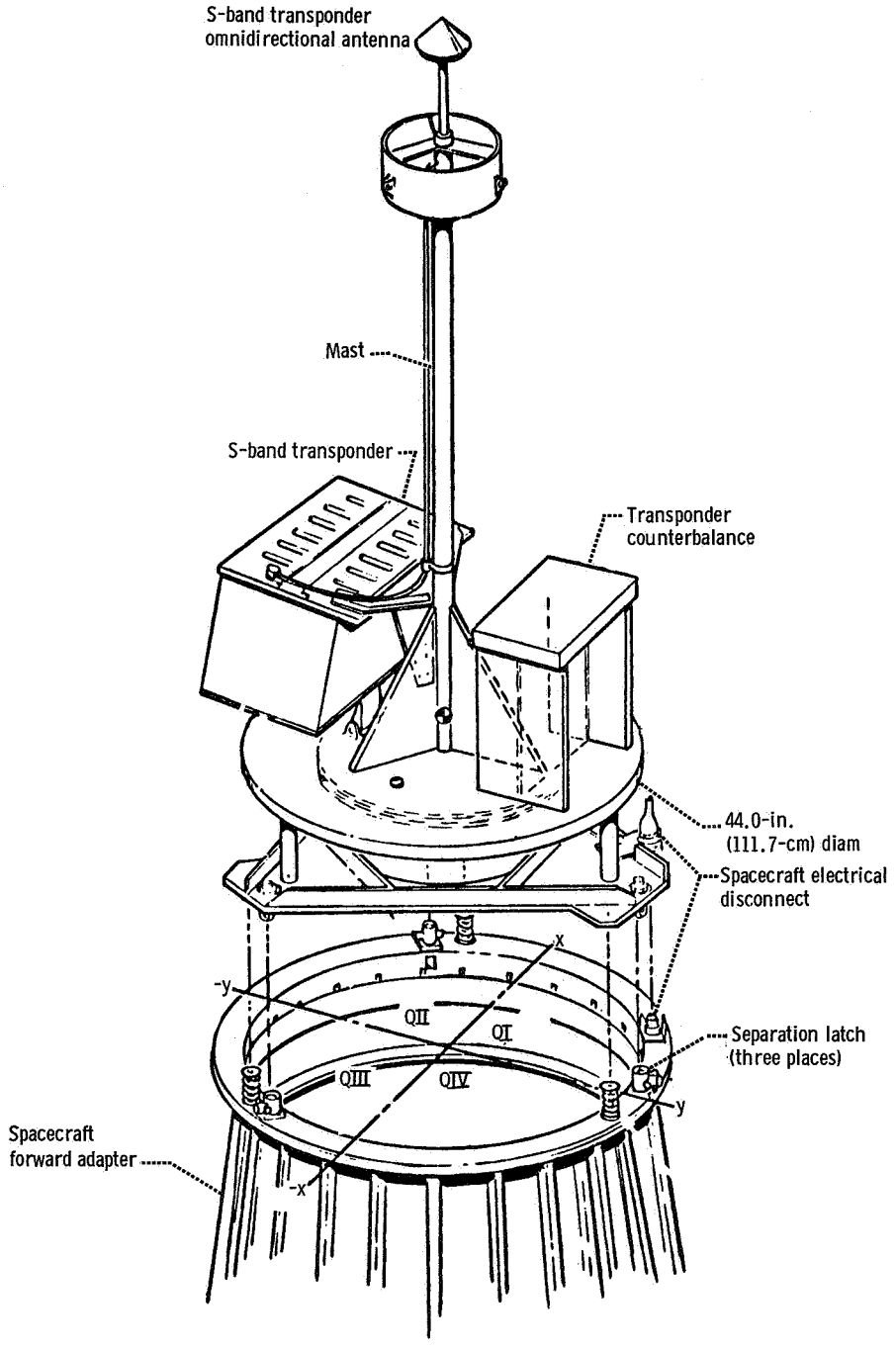

Figure V-89. - Spacecraft (Surveyor mass model) separation system, AC-9.

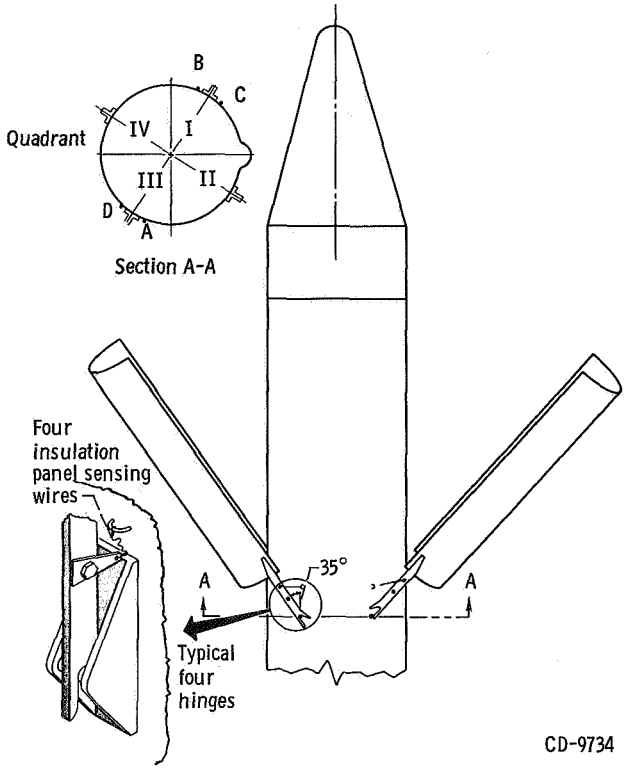

Figure V-90. - Insulation panel breakwire locations, AC-9.

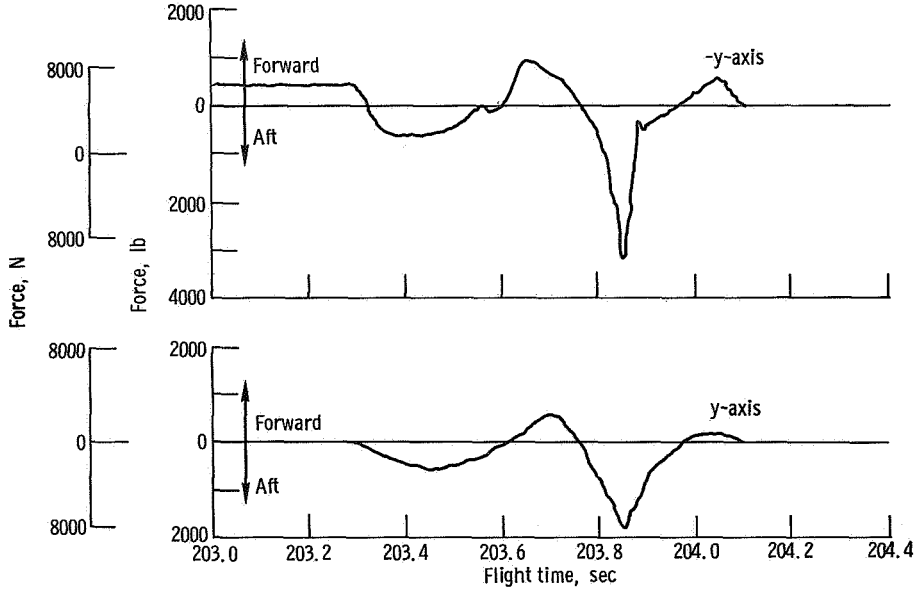

Figure V-91. - Nose fairing hinge fitting longitudinal jettison force, AC-9.

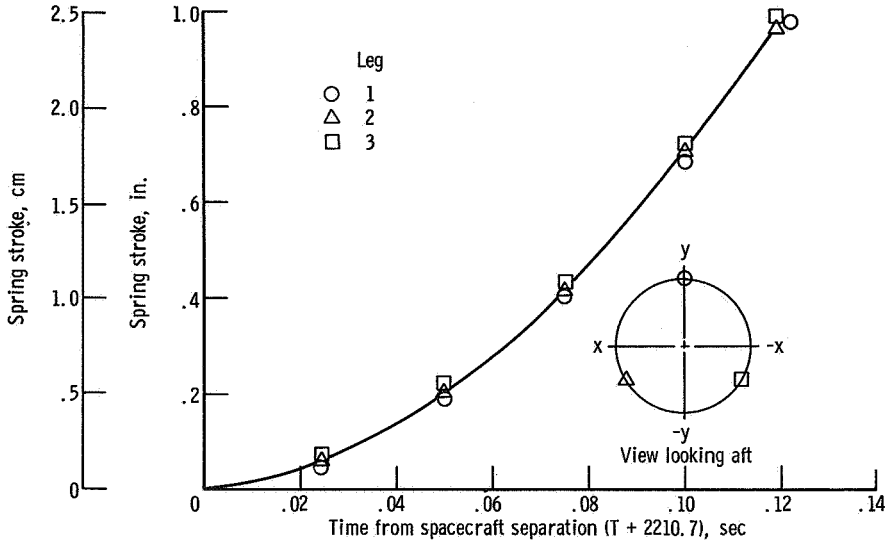

Figure V-92. - Centaur-Surveyor separation spring displacement, AC-9.

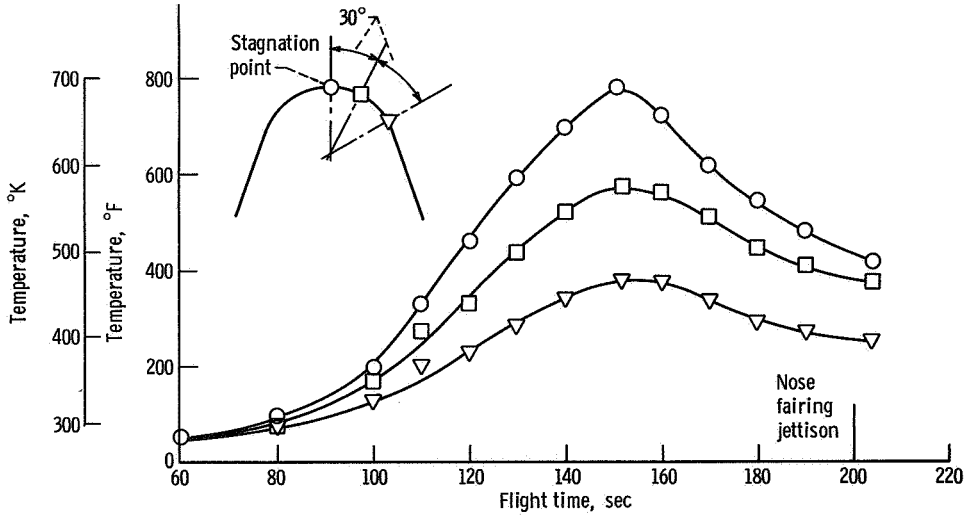

Figure V-93. - Nose cap temperatures, AC-9.

ELECTRICAL SYSTEMS

by John M. Bulloch, John E. Moss, and John B. Nechvatal

Power Sources and Distribution

Atlas system description. - The Atlas power requirements were supplied by a main power battery, a telemetry battery, two range safety command vehicle destruct system batteries, and a 400-hertz rotary inverter. Transfer of the Atlas electrical load from the external ground power supply to internal battery was accomplished by the main power changeover switch at T - 2 minutes. (See fig. V-94 for the system block diagram.)

Atlas system performance. - The Atlas main power battery supplied the requirements of all loads at nearly normal voltage levels. The battery voltage was 28.1 volts at lift-off; it rose to 28.4 volts at sustainer engine cutoff, then dropped to a low of 26.6 volts at retrorocket firing. The telemetry battery voltage was 28.8 volts at lift-off.

The rotary inverter, supplying the airborne 400-hertz power, operated within established voltage and frequency parameters. The voltage at lift-off was 115.2 volts; it reached a maximum of 115.4 volts at booster engine cutoff. The inverter frequency at lift-off was 401.5 hertz and rose to 402.4 hertz at end of programmed Atlas flight. The gradual rise in frequency is typical for this component, as noted on earlier flights and during ground testing. The required difference of 1.3 to 3.7 hertz between Atlas and Centaur inverter frequencies was properly maintained to avoid generation of undesirable beat frequencies in the autopilot system. If a beat frequency occurred in resonance with the slosh or natural frequencies of the vehicle, false commands would be given to the autopilot resulting in possible degradation of vehicle stability.

Centaur system description. - The Centaur electric power system included four separate subsystems, powered by a main battery, a telemetry battery, two range safety vehicle destruct subsystem batteries, and two pyrotechnic subsystem batteries. A three-phase 400-hertz solid-state inverter was used to provide alternating current in the main power subsystem. This inverter had been improved over earlier ones by incorporating more reliable parts and by improved mechanical and thermal design. AC-9 was the first flight for this component. Efficiency was increased from 67 to 70 percent. This subsystem included a power changeover switch which served to transfer the Centaur electrical system to internal power at T - 4 minutes. A second power changeover switch served to transfer the telemetry subsystem to internal at T - 4 minutes.

Centaur system performance. - The Centaur electric system voltage and currents were normal at lift-off and satisfactorily supplied power to all loads throughout the flight.

The main battery voltage was 28.4 volts at lift-off. A low of 27.9 volts was recorded

during the main engine first start sequence, and a high of 29 volts was reached during the coast phase. The voltage dropped to 28.5 volts at main engine second start and recovered to 29.0 volts by final power turnoff.

Main battery current was 43 amperes at lift-off. It peaked at 59 amperes at main engine first and second starts. The flight current profile was consistent with ground test values and is shown in figure V-95.

The telemetry battery voltage at lift-off was 29.1 volts and remained normal throughout the flight. The expected flight load of 21 amperes was measured.

The pyrotechnic battery voltages were 35.5 and 35.2 volts at lift-off. Minimum specification limit is 34.7 volts. Proper operation of the pyrotechnic subsystem was verified by the successful jettison of the insulation panels and nose fairing.

Performance of the range safety vehicle destruct subsystem batteries was satisfactory as verified by telemetered data of receiver operation during launch and flight. The battery voltages at lift-off were 32.7 and 32.8 volts with receivers on. The minimum specification limit is 30 volts.

The Centaur solid-state inverter, supplying 400-hertz power to the guidance, autopilot, and propellant utilization systems, operated satisfactorily throughout the flight. Telemetered voltage levels compared closely with the values recorded during preflight testing. Inverter voltages at lift-off were: phase A, 116.7 volts; phase B, 116.2 volts; phase C, 116 volts. Voltage levels rose slightly during flight (0.9 V for phase A, 1.1 V for phase B, and 1.2 V for phase C). The inverter frequency remained constant at 400.0 hertz throughout the flight.

Inverter temperature was 100° F (311° K) prior to hydrogen tanking and then cooled to 83° F (303° K) at lift-off. The temperature was 95° F (308° K) at T + 540 seconds, and rose to 144° F (335° K) at T + 2246 seconds. The inverter temperature measurement had been relocated from the external skin, as on earlier flights, to a point closer to the internal heat sources.

Instrumentation and Telemetry

Atlas system description. - The Atlas telemetry system consisted of a single PAM/FM/FM unit. A block diagram of this system is shown in figure V-96. This system transmitted at 229.9 megahertz. This flight package was a heavyweight cannister design which is being phased out and will not be used in the future. The latter designation PAM refers to Pulse Amplitude Modulation, a technique of sampling data to allow better utilization of the data handling capacity of the telemetry system. The designation FM/FM (Frequency Modulation/Frequency Modulation) refers to the combination of a frequency modulated radio frequency carrier upon which has been superimposed a number of fre-

quency modulated subcarriers. All operational measurements were transmitted with two antennas, one in each Atlas equipment pod.

Locations of ground and ship stations used in AC-9 flight are shown in figure V-97. Telemetry coverage was obtained as shown in figure V-98.

Atlas system performance. - A summary of 121 Atlas instrumentation measurements transmitted is given in table V-15. Of these measurements, the following four failures occurred:

(1) Booster engine 2 thrust chamber pressure measurement (AP59P) produced data of poor quality from T + 10 seconds to the end of booster engine operation. This is characteristic of a wiper arm lift-off condition caused by intermittent contact between the potentiometer wiper and the resistance element of the transducer. This failure mode is is encountered under certain conditions of vibration.

(2) Skin temperature measurement at station 576 (AA923T), quadrant IV, failed at T + 67 seconds. It is believed that the thermocouple separated from the liquid-oxygen tank at that time. This thermocouple has separated from the liquid-oxygen tank on previous flights.

(3) Ambient temperature measurement (AA743T) at the sustainer instrument panel

TABLE V-15. - ATLAS MEASUREMENT SUMMARY, AC-9

Airborne systems	Number and type of measurement										
	Acceleration	Rotation rate	Deflection	Vibration	Pressure	Frequency	Rate	Temperature	Voltage	Discrete	Totals
Airframe	-	-	--	1	9	-	-	19	-	8	37
Range Safety	-	-	--	-	--	-	-	--	2	1	3
Electrical	-	-	--	-	--	1	-	--	2	--	3
Pneumatics	-	-	--	-	7	-	-	--	2	--	9
Hydraulics	-	-	--	-	6	-	-	--	-	--	6
Dynamics	1	-	--	-	--	-	-	--	-	--	1
Propulsion	-	3	2	-	20	-	-	2	-	10	37
Flight control	-	-	11	-	--	-	3	--	-	7	21
Telemetry	-	-	--	-	--	-	-	1	-	--	1
Propellants	-	-	--	-	2	-	-	--	1	--	3
Totals	1	3	13	1	44	1	3	22	7	26	121

failed during the booster jettison sequence. The period of primary interest for this measurement terminated at booster jettison.

(4) The adapter skin temperature measurement (AA244T) at 290° station 418, failed at Atlas-Centaur separation. This measurement is located 5 inches (12.7 cm) from the mechanical separation line and the shaped charge. It is believed that the transducer was damaged by shaped-charge firing during the separation sequence. No significant data were lost as the primary period of interest was prior to separation.

Centaur system description. - Three telemetry subsystems, identified as 1, 2, and 5, were used to telemeter the two-burn vehicle performance data. These PAM/FM/FM modulated systems transmitted from a single telemetry antenna mounted on a ground plane atop the umbilical island. Figure V-99 shows antenna locations on the Centaur. Location of ground and ship receiving stations are shown in figure V-97. A block diagram of the Centaur telemetry system is shown in figure V-100. The three telemetry subsystems operated at the frequencies and power levels shown in the following table:

Subsystem	Frequency, MHz	Radiated power output, W
1	225.7	4
2	230.0	3
5	259.7	3

Measurements common to all Centaur flights were telemetered from telemetry subsystems 2 and 5. This instrumentation was provided on the AC-9 vehicle to observe during the coast phase. (Refer to the COAST PHASE PROPELLANT MANAGEMENT AND PROPELLANT THERMODYNAMICS section for the description and location of these instruments.)

Several telemetry improvements were incorporated on AC-9. These improvements included

(1) A solid-state transmitter to replace the vacuum tube configuration

(2) An improved transducer power supply and demodulator

(3) Improved subcarrier oscillators

Centaur system performance. - Telemetry coverage was virtually continuous through T + 3550 seconds, as shown in figure V-101. Low signal levels, however, to the Tananarive and Carnarvon receiving stations did not allow proper data processing during several periods of time.

Data quality, commutator speed, and signal strength parameters were within satisfactory limits, except for subsystem 5, channel 9. The commutator for this channel

TABLE V-16. - CENTAUR MEASUREMENT SUMMARY, AC-9

Airborne systems	Number and measurement type														
	Acceleration	Rotation rate	Current	Deflection	Power	Vibration	Pressure	Frequency	Rate	Strain	Temperature	Voltage	Discrete	Digital	Totals
Dynamics	8	-	-	1	-	-	--	-	-	-	---	--	--	-	9
Airframe	--	-	-	-	-	4	2	-	-	2	162	--	1	-	171
Range safety	--	-	-	-	-	-	--	-	-	-	---	2	8	-	10
Electrical	--	-	4	-	-	-	--	1	-	-	3	4	--	-	12
Pneumatics	--	-	-	-	-	-	11	-	-	-	23	--	2	-	36
Hydraulics	--	-	-	-	-	-	2	-	-	-	6	--	--	-	8
Guidance	3	-	-	-	-	-	--	-	-	-	6	25	1	1	36
Miscellaneous	--	-	-	-	-	-	--	-	-	-	---	1	--	-	1
Propulsion	--	4	-	-	-	-	22	-	-	-	46	--	20	-	92
Flight control	--	-	-	-	-	-	--	-	6	-	2	4	35	-	47
Telemetry	--	-	1	-	-	-	--	-	-	-	6	2	--	-	9
Propellants	--	-	-	2	-	-	--	-	-	-	1	2	32	-	37
Azusa	--	-	-	-	1	-	--	-	-	-	1	--	--	-	2
Spacecraft	--	-	-	3	-	-	1	-	-	-	1	--	--	-	5
Totals	11	4	5	6	1	4	38	1	6	2	257	40	99	1	475

failed prior to launch. This type of commutator will not be flown on future missions.

A total of 475 Centaur instrumentation measurements were transmitted. A summary of these measurements is given in table V-16. Over 90 percent of the data was successfully obtained. The following data were not obtained:

(1) Twenty-five measurements were lost because of the failure of channel 9 in subsystem 5. These data consisted of 15 calorimeter measurements located at the forward end of the hydrogen tank, nine temperature measurements at the engine bell gimbal trunnion and hydrogen boost pump housing, and one voltage measurement used to calibrate the calorimeter measurements.

(2) The following three measurements were inoperative prior to launch:

CA4T forward bulkhead skin temperature

CA352T forward bulkhead skin temperature

CA797T tank skin forward temperature

(3) The C-1 engine gimbal mount vibration measurement on the Z-axis (CA310) exhibited abrupt bias shifts from main engine second start to main engine cutoff.

(4) Liquid-hydrogen vent valve vibration measurement (CA1360) exhibited bias level shifts which started prior to launch and continued to the end of recorded data.

(5) Liquid-hydrogen boost pump inlet temperature measurement (CP32T) exhibited an erratic increase in temperature from T + 370 to T + 460 seconds. The data were valid before and after this period. The cause of this increase is unknown.

(6) Ambient temperature measurement (CA12T) aft of the hydrogen peroxide supply bottle became erratic at T + 233 seconds. This measurement exhibited an 8 percent information bandwidth step, at this time, followed by a ±6 percent information bandwidth low-frequency variation. No data were retrieved after T + 233 seconds.

(7) Hydrogen tank skin temperature measurement (CA622T) located at station 288 exceeded the upper instrumentation limit at Atlas-Centaur separation. This failure indicated an open circuit. No valid data were obtained from this measurement after Atlas-Centaur separation.

(8) Fine X-axis acceleration measurement (CM13A) and X-axis acceleration measurement (CM39A) exhibited random bias level shifts from T + 1550 seconds to the end of data acquisition. The shifts reached 20 percent of the information bandwidth on measurement CM13A and 2 percent of the information bandwidth on measurement CM39A. These measurements use the same type transducer. The two measurements differ only in sensitivity measurement CM13A being 10 times as sensitive as measurement CM39A. As a result of these shifts (qualitative only), data were obtained from these measurements after T + 1550 seconds.

(9) The liquid-hydrogen pump-inlet C-1 engine pressure measurement (CP52P) did not return to zero after main engine first cutoff. An offset of 15 percent information bandwidth was noted thereafter, coincident with the expected large pressure transient.

This transient exceeded the upper instrumentation range. It is believed that the transducer was damaged at this time causing the 15 percent offset for this shift. No information was lost.

(10) The liquid-oxygen-pump discharge pressure measurement for the C-1 engine exhibited negative transients throughout the flight. No data were lost as a result of these 10 percent transients.

(11) The C-2 liquid-oxygen pump-case temperature measurement (CP125T) exhibited a slow response to temperature changes during engine first and second start sequences. The frequency response of this channel was not adequate for precise transient definition.

(12) The pump speed C-1 engine and pump speed C-2 engine measurements CP1B and CP2B exhibited transients up to 40 percent information bandwidth at both main engine starts. This discrepancy has been seen before and is believed to be caused by the noise susceptibility of the signal converter at low pump speeds.

(13) Intermediate bulkhead pressure measurement (CA885P) indicated pressures up to 50 microns of mercury (6.66 N/m^2) between T + 40 and T + 100 seconds. The expected pressure is less than 10 microns of mercury (1.33 N/m^2). It is believed that induced aerodynamic vibration caused the degradation in the transducer.

Tracking Subsystems

C-band beacon description. - A C-band radar subsystem with associated ground stations provided real-time position and velocity data to the range safety tracking system impact predictor. These data were also used by the Deep Space Network for acquisition of the spacecraft and for guidance and flight trajectory analvsis. The airborne equipment included a lightweight transponder, circulator (to channel receiving and sending signals), power divider, and two antennas located on opposite sides of the tank. The locations of the Centaur antennas are shown in figure V-99. The ground and ship stations are standard radar sets and are located as shown in figure V-97. A block diagram of the C-band system is shown in figure V-102.

C-band system performance. - C-band radar tracking was satisfactory. Complete coverage was obtained to T + 7186 seconds. Although individual ground stations experienced occasional malfunctions, no data were lost because of overlapping and redundant coverage. For example, Grand Turk radar acquired only after switching from circular polarization mode to linear polarization mode. Actual coverage extended from T + 409 to T + 609 seconds instead of the committed period from T + 218 to T + 542 seconds. Continental United States, Grand Bahama Island, and Bermuda radars provided redundant tracking coverage early in the flight. Antigua, Pretoria, and Carnarvon radars provided later data for near-real-time orbit calculations. C-band radar cover-

age is shown in figure V-103.

Azusa beacon system description. - An Azusa transponder was installed on the Centaur stage. A block diagram of the Azusa system is shown in figure V-104. An antenna mounted on the interstage adapter was used for transmission while the insulation panels remained in place, since the insulation panels covered the Centaur mounted antenna. Subsequently, the transponder output was switched to the Centaur mounted antenna. The antenna locations are shown in figure V-99. Associated ground tracking stations used the Glotrac system.

Azusa beacon system performance. - The airborne Azusa subsystem performed satisfactorily throughout flight. Data provided by the Azusa-Glotrac system provided precise flight position and velocity data used to evaluate the guidance system. These data supplement that of the C-band system early in flight. Azusa system tracking periods are shown in figure V-105.

S-band beacon subsystem description. - The Surveyor mass model contained an S-band transponder assembly and omnidirectional antenna mounted on top of the forward mast. The transponder is capable of operating at two power output levels (100 mW and 10 W).

S-band beacon subsystem performance. - The S-band beacon performed satisfactorily. The transponder operated on low power (100 mW) until 10 seconds prior to spacecraft separation (T + 2200.8 sec). The Centaur programmer then initiated a switchover by Woomera Deep Space Instrumentation Facility at T + 50 minutes. Tracking continued to T + 21 hours by Goldstone.

Range Safety Command Subsystem

(Vehicle Destruct Subsystem)

Airborne subsystem description. - The Atlas and Centaur stages each contained independent vehicle destruct subsystems. These subsystems were designed to function simultaneously on command from the ground stations. These subsystems included redundant receivers, power control units, destructors, and batteries which operated independently of the main vehicle power subsystems. Block diagrams of the Atlas and Centaur vehicle destruct subsystems are shown in figures V-106 and V-107, respectively.

The Atlas and Centaur vehicle destruct subsystem provided a means of shutting down the engines only, or shutting down the engines and destroying the vehicle. To destroy a vehicle in the event of a flight malfunction, the propellant tanks would be ruptured with a shaped charge and the liquid propellants of the first and second stages dispersed. The spacecraft destruct portion of the Centaur vehicle destruct subsystem

was inert since an actual Surveyor spacecraft was not carried on AC-9.

Subsystem performance. - The Atlas and Centaur range safety command vehicle destruct subsystems were prepared to execute destruct commands throughout the flight. No engine cutoff or destruct commands were sent by the range transmitters, nor were inadvertent commands generated by other vehicle systems. The command from Antigua ground station to disable the range safety command system shortly after Centaur main engine cutoff was properly received and executed. Figure V-108 shows ground transmitter coverage to support the vehicle destruct systems.

Signal strength at the Atlas and Centaur range safety command receivers was excellent throughout the flight, as indicated by telemetry measurements. Telemetered data indicated that both the Centaur receivers were deactuated at approximately T + 587 seconds, thus confirming that the disable command was transmitted from the Antigua station.

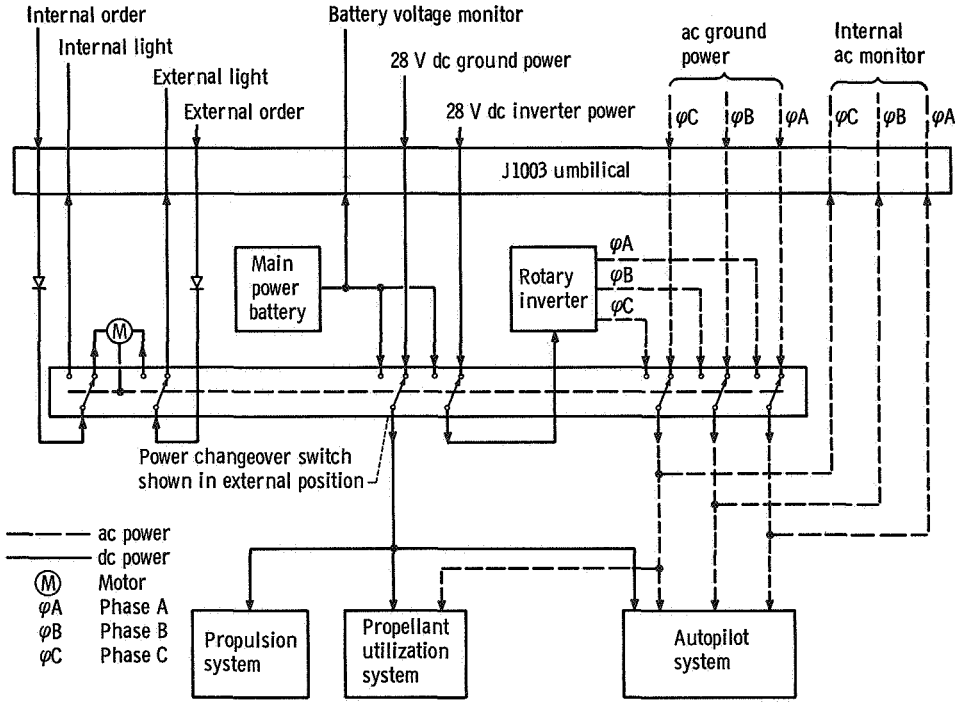

Figure V-94. - Atlas electrical system block diagram, AC-9.

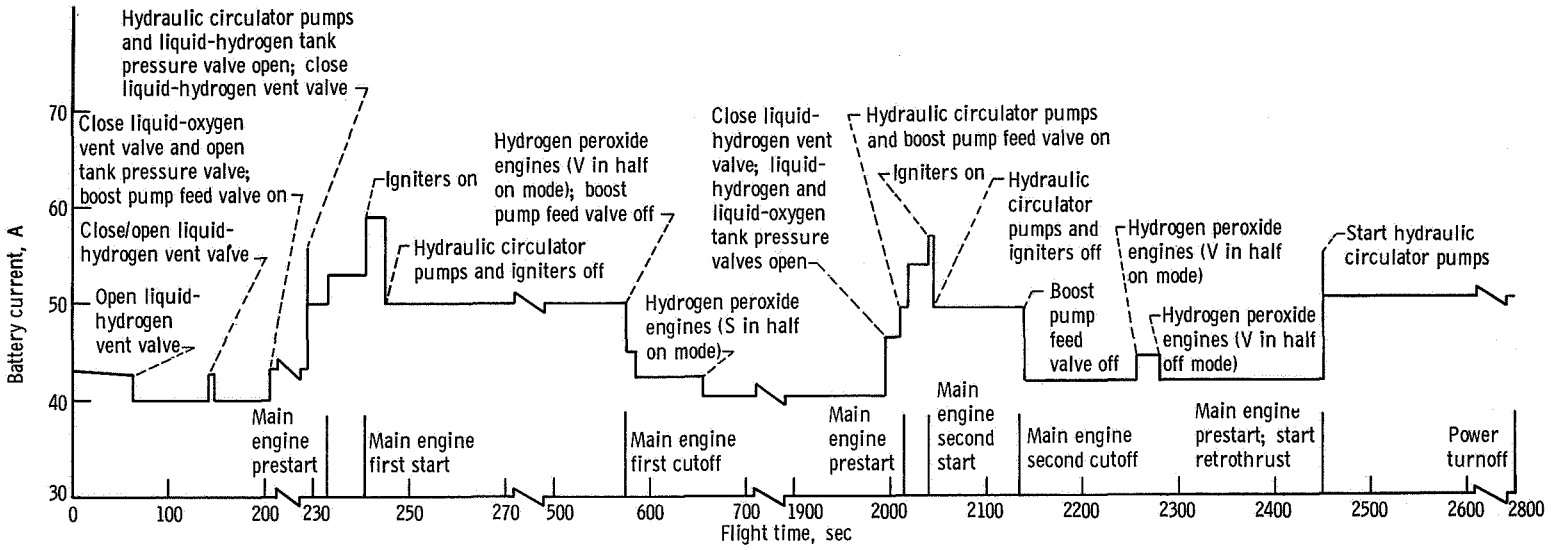

Figure V-95. - Main battery load profile, AC-9.

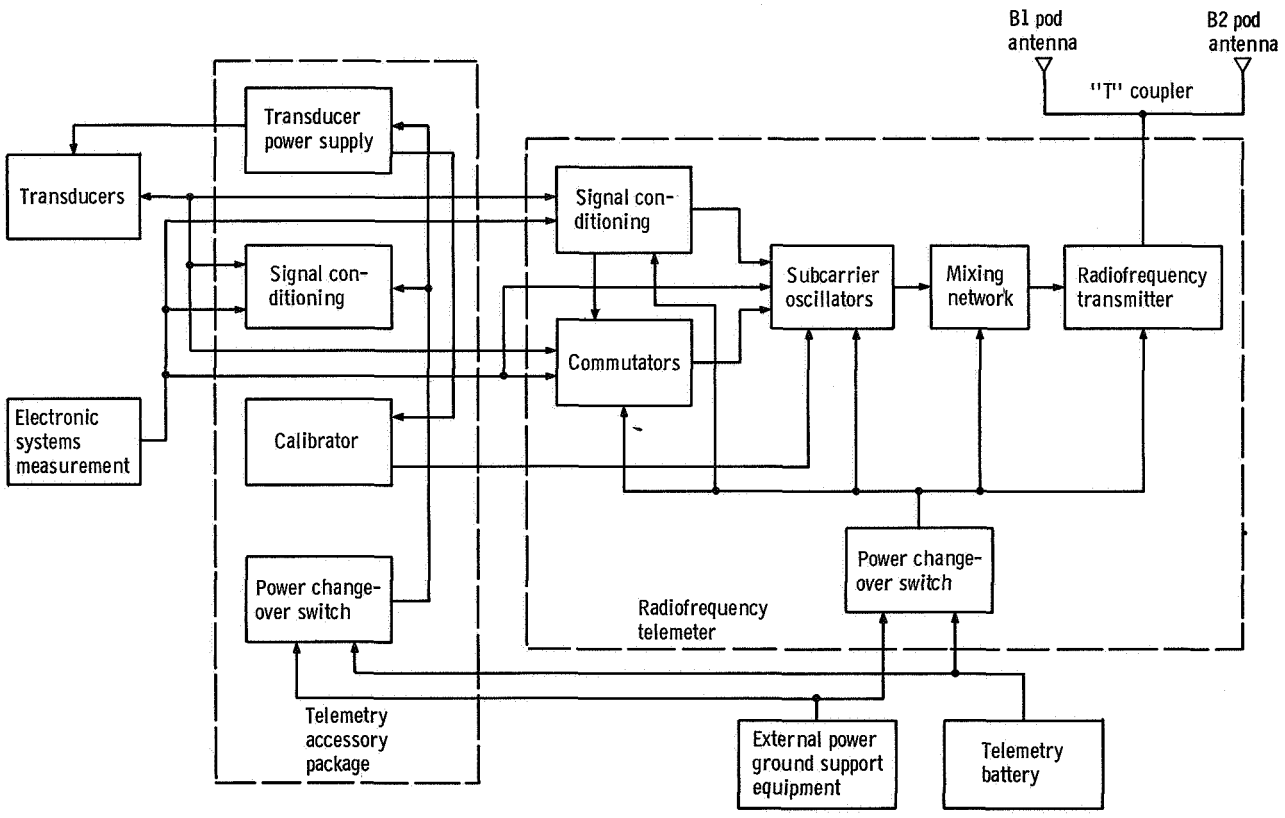

Figure V-96. - Atlas telemetry system block diagram, AC-9.

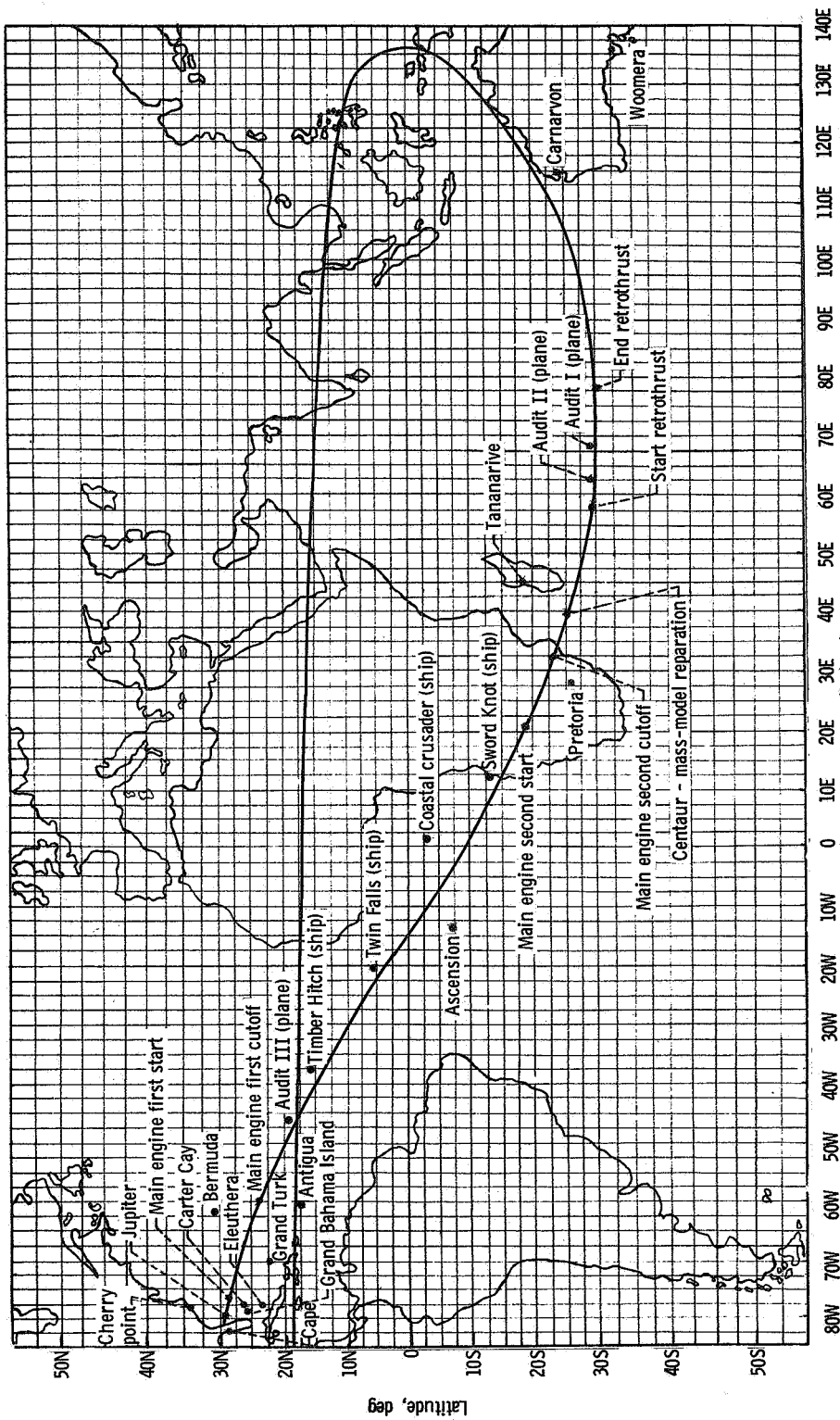

Figure V-97. - Tracking station locations and vehicle trajectory Earth track, AC-9.

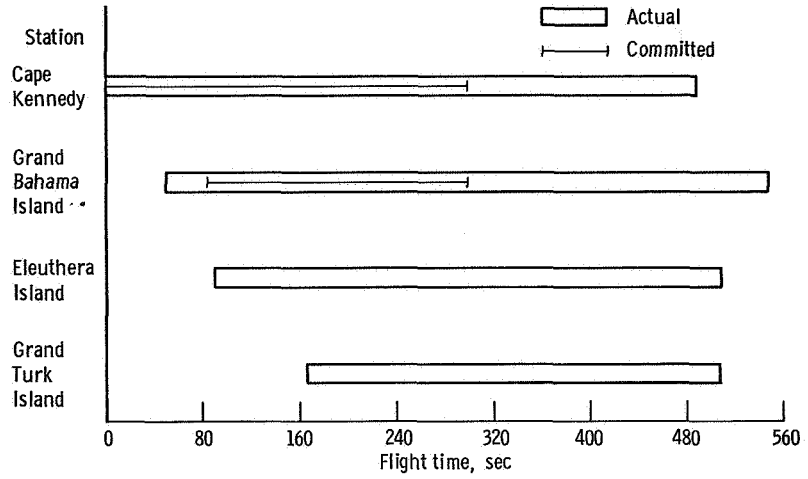

Figure V-98. - Atlas telemetry coverage, AC-9.

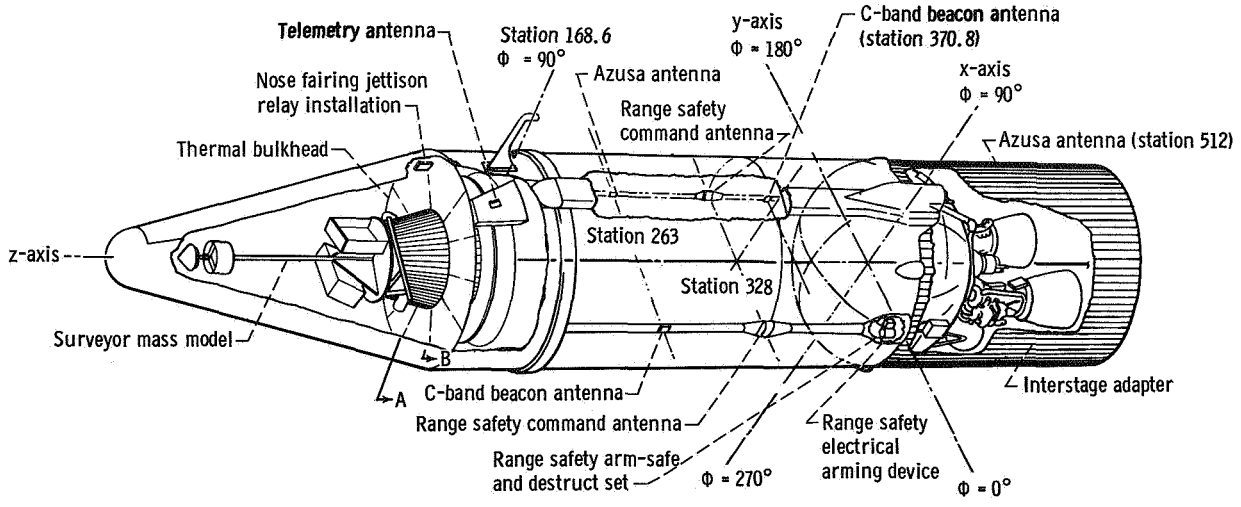

Figure V-99. - Centaur antenna locations and radiofrequency subsystem, AC-9.

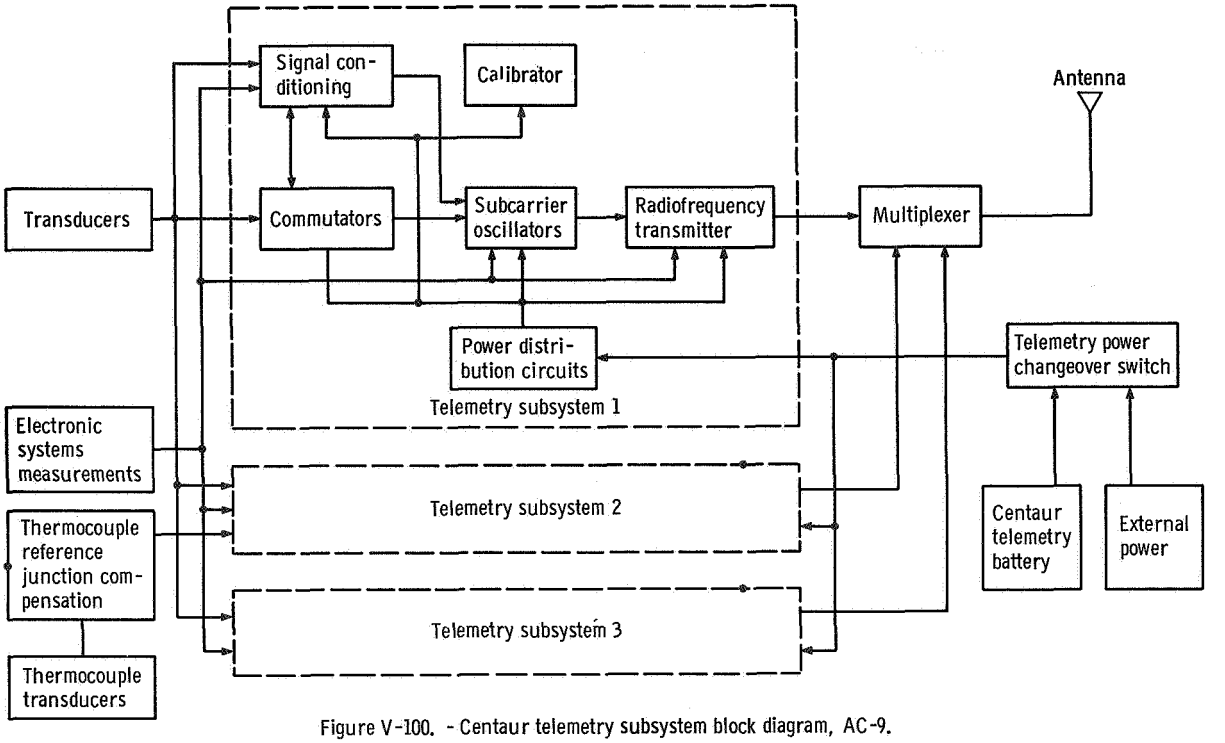

Figure V-100. - Centaur telemetry subsystem block diagram, AC-9.

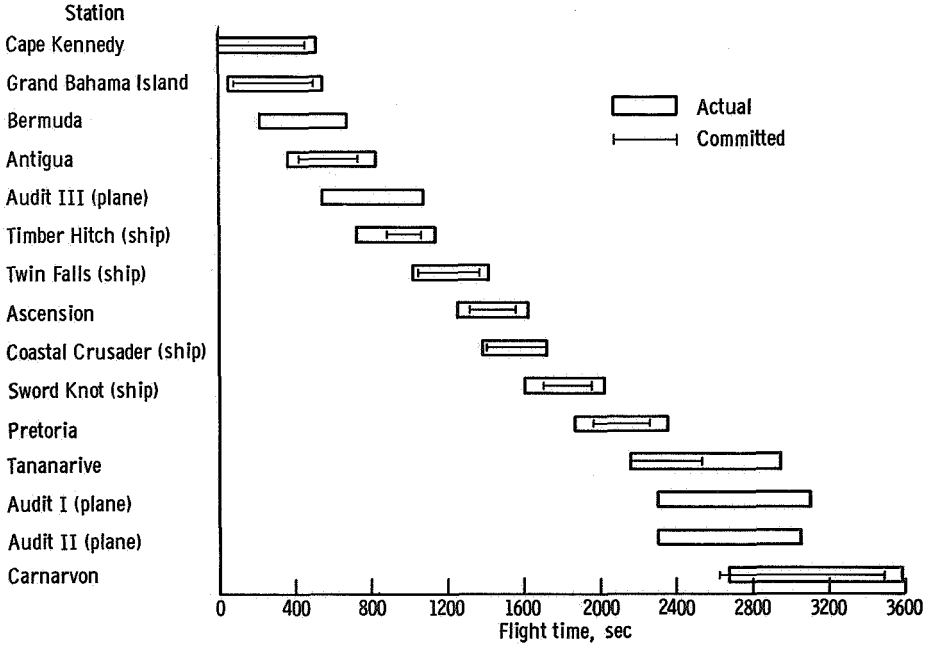

Figure V-101. - Centaur telemetry coverage, AC-9.

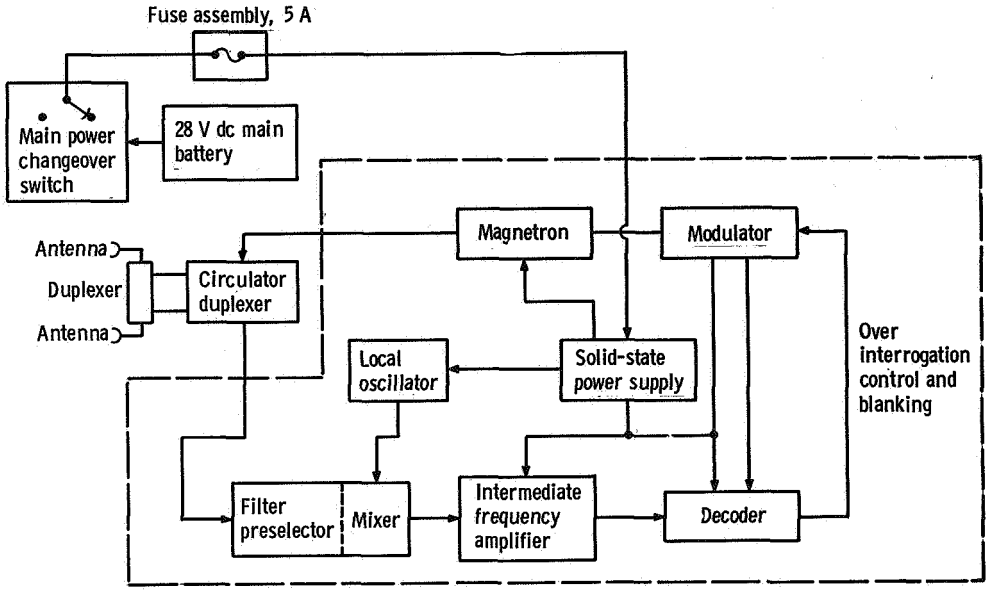

Figure V-102. - Centaur C-band beacon subsystem, AC-9.

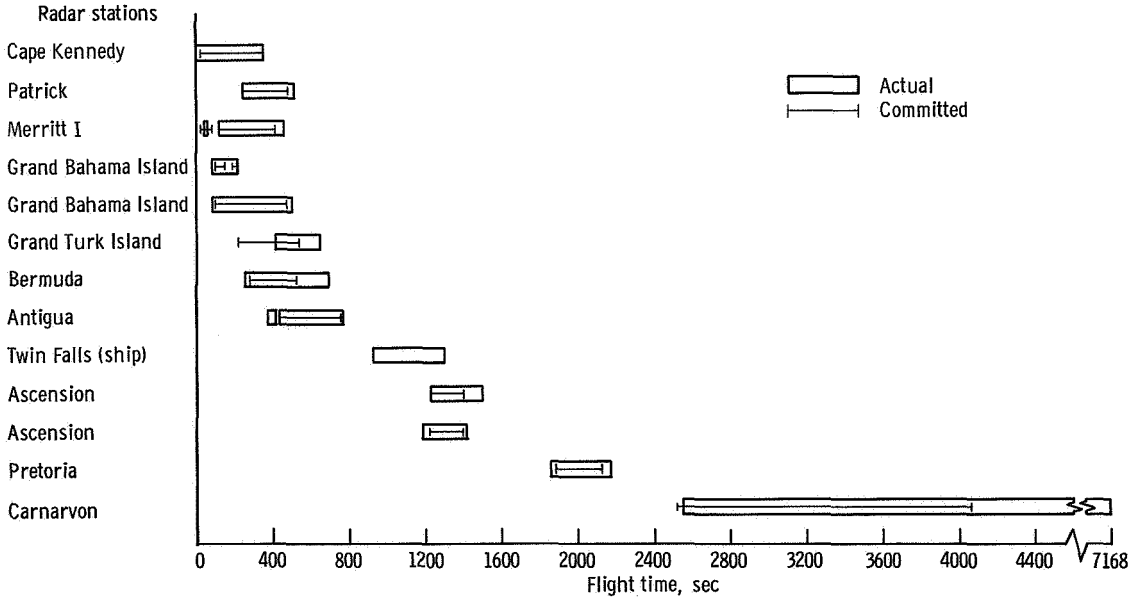

Figure V-103. - C-band radar coverage (autobeacon track only), AC-9.

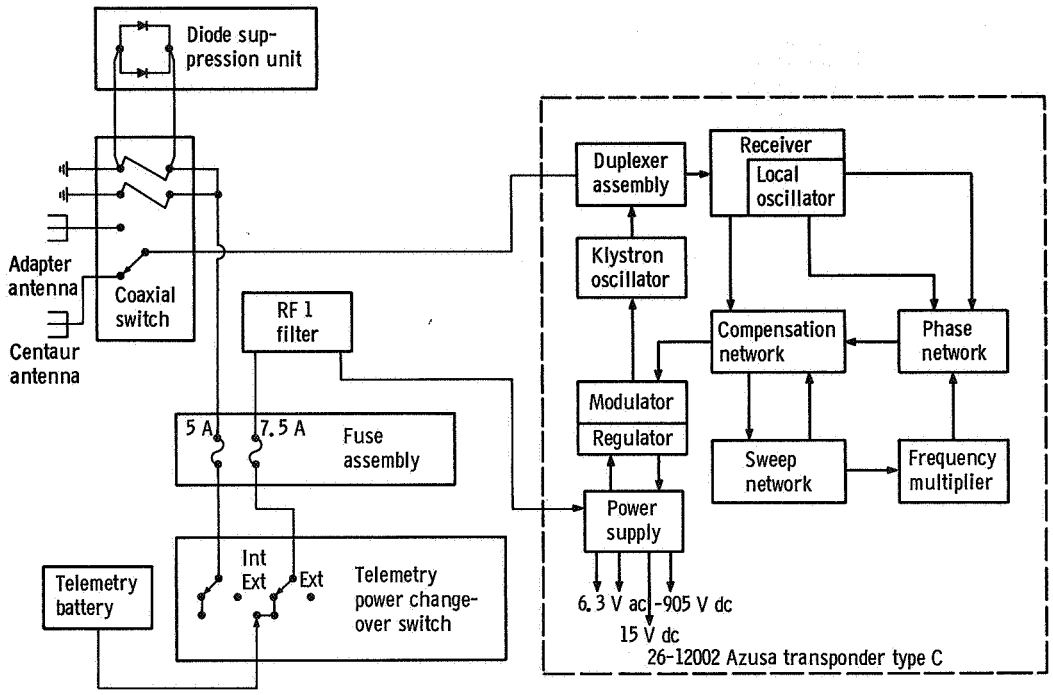

Figure V-104. Azusa beacon subsystem block diagram, AC-9.

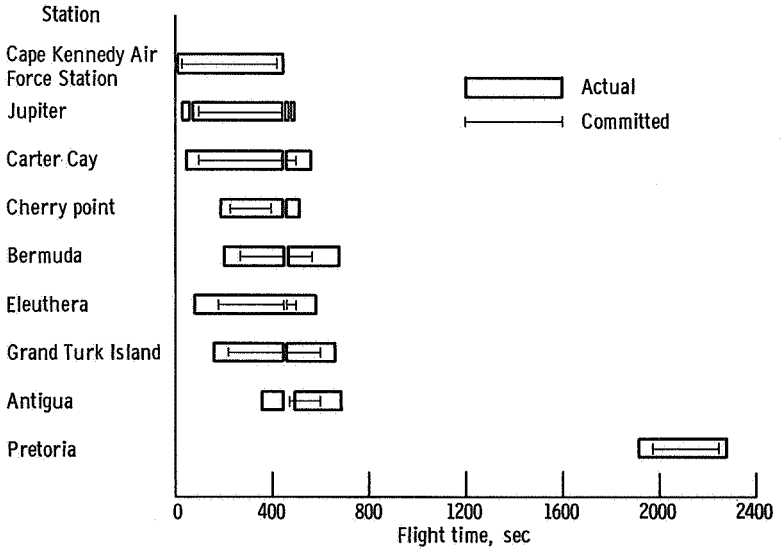

Figure V-105. - Glotrac coverage, AC-9.

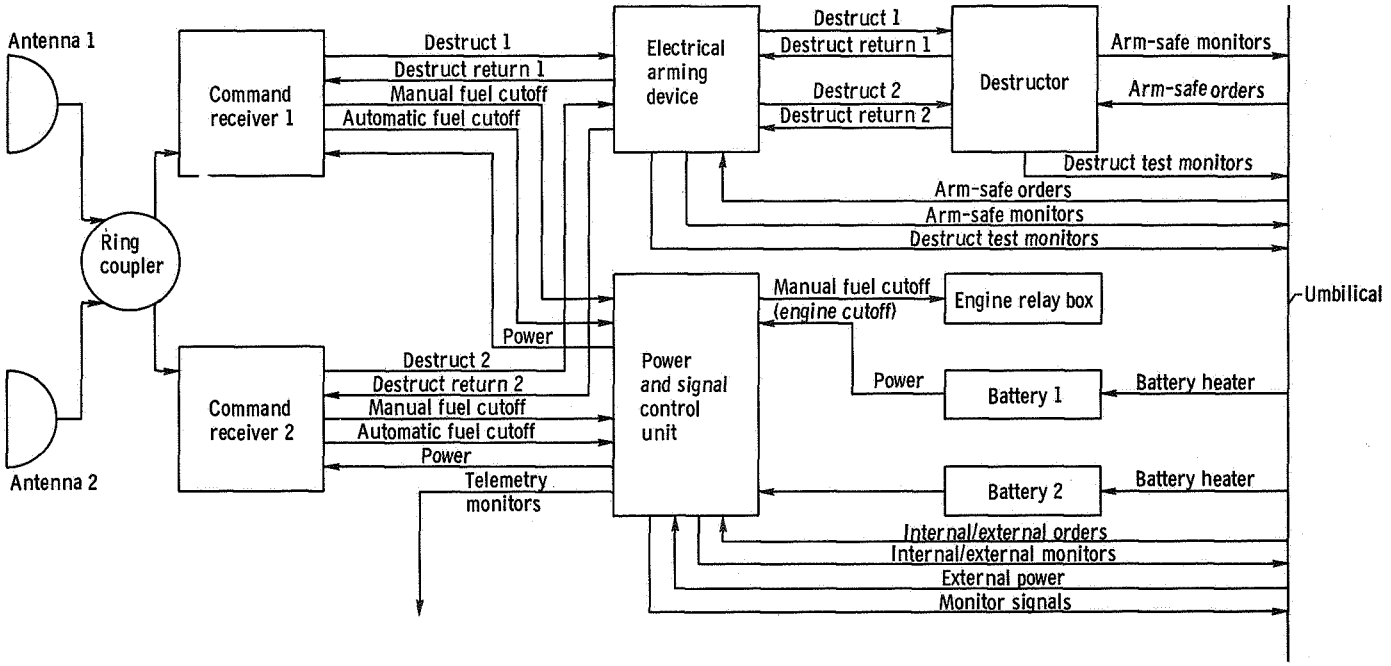

Figure V-106. - Atlas vehicle destruct subsystem block diagram, AC-9.

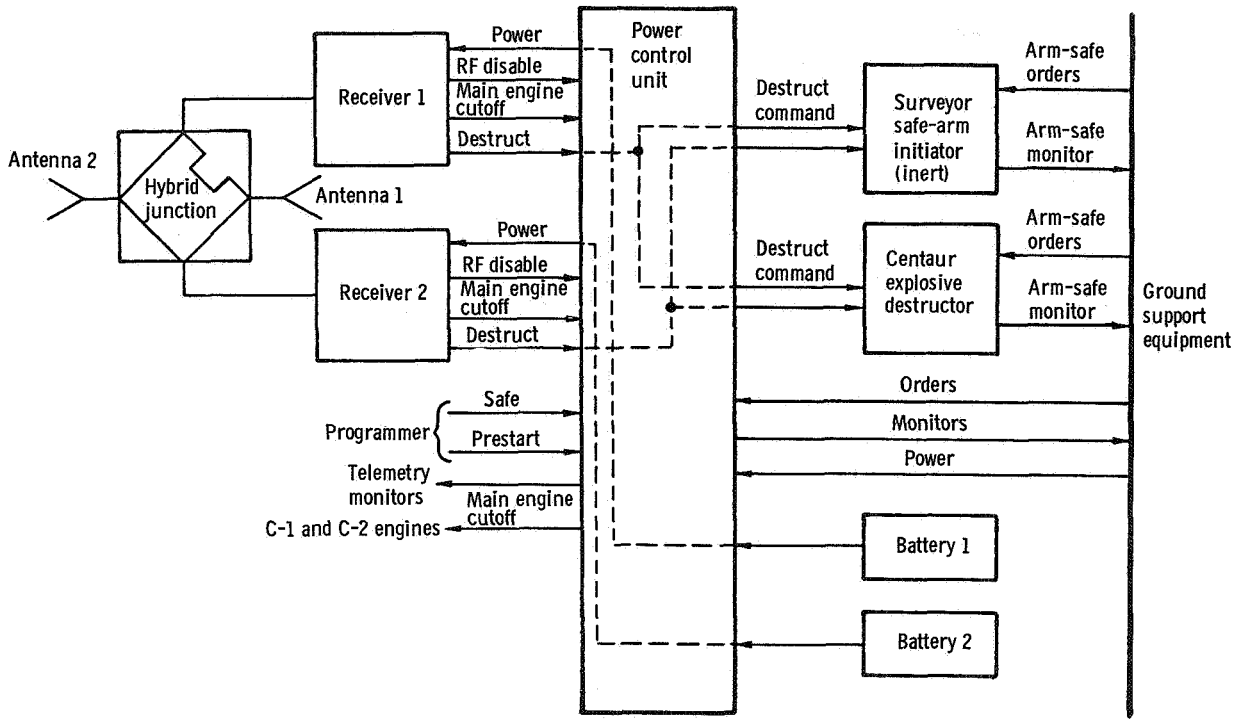

Figure V-107. - Centaur vehicle destruct subsystem block diagram, AC-9.

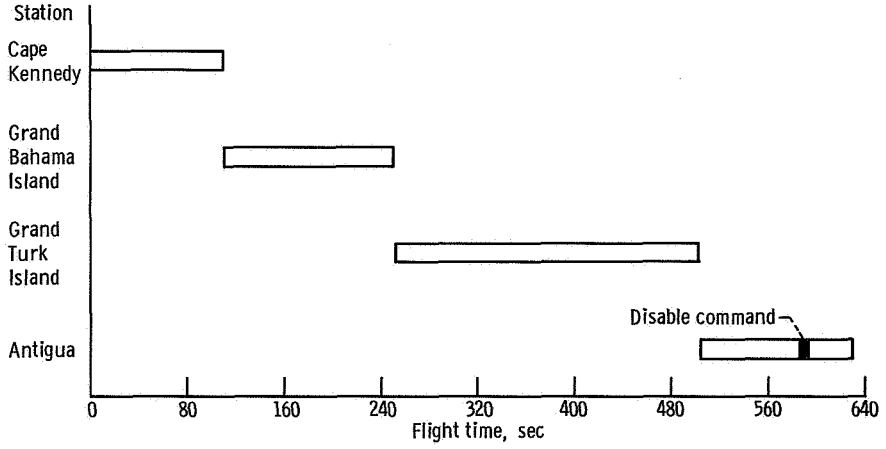

Figure V-108. - Range safety command system transmitter utilization, AC-9.

GUIDANCE AND FLIGHT CONTROL SYSTEMS

by John L. Feagan, Donald F. Garman, Paul W. Kuebeler,
and Corrine Rawlin

The general objective of the guidance and flight control systems was to guide the vehicle into the proper simulated lunar-transfer orbit. Achieving the proper orbit required precise velocity and position correlation at the time of injection. An indirect (parking-orbit) mode of ascent was used for the AC-9 flight. An inertial guidance system was installed on the Centaur stage, and separate flight control systems were installed on the Atlas and on the Centaur stages. These systems stabilized, controlled, guided, and sequenced flight events from lift-off through completion of the Centaur retromaneuver after spacecraft separation. Trajectory dispersions resulting from thrust misalinement, winds, and performance variations in the Atlas and Centaur stages were compensated for by these systems.

Three modes of operation were used for stabilization or stabilization and control of the launch vehicle. These modes were rate stabilization, stabilization and open-loop control, and stabilization and closed-loop control (fig. V-109). The periods of operation of the different modes and the modes of operation of the hydrogen peroxide attitude control system, which are discussed later in this section, are shown in figure V-110. The purpose of the rate stabilization mode was to maintain the vehicle with near-zero angular rates about the vehicle pitch, yaw, and roll axes. Angular rates were sensed with rate gyros, one for each axis. These rates were minimized either by gimbaling the main engines during powered phases of flight or by using the hydrogen peroxide attitude control system during coast phases of flight. The stabilization and open-loop control mode was used only during the Atlas booster phase of flight. This mode is termed open-loop control because the displacement gyros (one each for pitch, yaw, and roll axes) provided a reference attitude. If the reference attitude did not result in the desired flight path, there was no means of determining the difference to correct the flight path. The reference attitude was programmed to vary in discrete steps as a function of time. These changes in reference attitude caused the vehicle to roll to the initial flight azimuth angle and to pitch downward. Stabilization of the vehicle was accomplished by algebraically summing the rate gyro output with displacement gyro output. Gimbaling the engines provided directional thrust which resulted in stabilizing the vehicle and positioning the vehicle to the referenced attitude.

Closed-loop control was used during the Atlas sustainer and Centaur phases of flight. The term "closed-loop control" denotes a method of operation where the guidance system provided the attitude and direction reference. Directional thrust of the engines controlled the vehicle in accordance with steering signals from the guidance system.

Therefore, if the flight path, as measured by the guidance system, was not the desired flight path, the guidance system issued steering signals to direct the vehicle to the desired flight path. Stabilization of the vehicle was accomplished by algebraically summing the rate gyro output with the steering signals. Closed-loop control was used for only the pitch and yaw axes. The third axis, roll, was open-loop-controlled during the Atlas sustainer phase by using the Atlas roll displacement gyro. During Centaur phase, the roll axis was in the rate stabilization mode. Figure V-111 is a simplified diagram of the guidance and flight control system interface.

The sequencing of some flight events was a cooperative function of the flight control systems and the guidance system. This means that one system initiates a period of performance and another system terminates that period. Table V-17 lists the cooperative functions commanded by these systems and identifies the system that originated the discrete command for the flight event.

TABLE V-17. - GUIDANCE AND FLIGHT CONTROL SYSTEMS COOPERATIVE DISCRETE COMMANDS, AC-9

Event	Originating source of discrete command
Guidance to flight condition	Guidance launch equipment
Enable Atlas flight control system	42-in. (1.1-m) rise umbilical ejection
Start roll program	Atlas flight control
Start pitch program	Atlas flight control
Booster engine cutoff	Guidance
Start guidance steering	Atlas flight control
Sustainer engine cutoff	Atlas flight control
Atlas-Centaur separation	Atlas flight control
Centaur main engine first start sequence	Atlas flight control
Start guidance steering	Centaur flight control
Accept a main engine cutoff command	Centaur flight control
Centaur main engine first cutoff	Guidance
Centaur main engine second start sequence	Guidance
Start guidance steering	Centaur flight control
Centaur main engine second cutoff	Guidance
Separate spacecraft	Centaur flight control
Provide retromaneuver steering vector	Guidance
Start guidance steering	Centaur flight control
Telemetry calibration on	Guidance
Telemetry calibration off	Guidance
Centaur electrical power off	Centaur flight control

Guidance

System description. - The AC-9 Centaur guidance system was an inertial system which was completely independent of ground control after entering flight conditions approximately 8 seconds before lift-off of the vehicle. The guidance system performed the following functions:

(1) Measured vehicle acceleration in fixed inertial coordinates
(2) Computed the values of vehicle velocity, actual position and direction, and the desired vehicle attitude to attain the trajectory injection point
(3) Compared actual position to the desired position and issued steering signals
(4) Issued discrete commands

A simplified block diagram of the guidance system is shown in figure V-112.

Inertial measuring units: Vehicle acceleration was measured by the following three units:

(1) The inertial platform unit which contained the platform assembly, gyros, and accelerometers
(2) The pulse rebalance, gyro torquer, and power supply unit, which contained the electronics associated with the accelerometers
(3) The platform electronics unit, which contained the electronics associated with the gyros

The platform assembly used four gimbals to provide a three-axis coordinate system. The use of four gimbals, instead of three, allowed complete rotation of all three vehicle axes about the platform without gimbal lock. Gimbal lock is a condition in which two axes coincide causing loss of 1 degree of freedom. A gimbal diagram is shown in figure V-113. The azimuth gimbal was isolated from movements of the vehicle airframe by the other three gimbals. The inertial components (three gyros and three accelerometers) were mounted on the azimuth gimbal. A gyro and an accelerometer were mounted as a pair with the sensing axes of each pair parallel. These gyro and accelerometer pairs were also alined on three mutually perpendicular (orthogonal) axes corresponding to the three axes of the platform.

The three gyros were identical and were of the single-degree-of freedom, floated-gimbal, rate-integrating type. Each gyro monitored one of the three axes of the platform. These gyros were elements of control loops, the sole purpose of which was to maintain each axis fixed in inertial space. Each gyro signal was connected to a servo-amplifier whose output controlled a direct-drive gimbal torque motor. The orientation of the azimuth gimbal was fixed in inertial space while the outer roll gimbal was attached to the vehicle. The angles between these gimbals provided a means for transforming steering signals from inertial coordinates to vehicle coordinates. The transformation was accomplished by electromechanical resolvers, mounted between gimbals,

which produced analog electrical signals proportional to the sine and cosine functions of the gimbal angles. These electrical signals were used to provide an analog solution of the mathematical equations for coordinate transformation by interconnecting the resolvers in a multiple resolver chain.

The three accelerometers were identical and were of the single axis, viscous-damped, hinged-pendulum type. The accelerometer associated with each axis measured the change in vehicle velocity along that axis by responding to acceleration. Acceleration of the vehicle caused the pendulum to move off center. The associated electronics then produced precise current pulses to recenter the pendulum. The rebalance pulses were either positive or negative pulses depending on an increase or decrease in vehicle velocity. These pulses representing changes in velocity (incremental velocity) were then routed to the navigation computer unit for further processing.

For proper flight operation, it was necessary to aline and calibrate the inertial measuring units during launch countdown. The azimuth axis of the platform, to which the desired flight trajectory was referenced, was alined by ground based optical equipment. The remaining two axes of the platform were alined perpendicular to the local vertical by using the two accelerometers in the horizontal plane. Each gyro was calibrated to determine its characteristic constant torque drift rate and mass unbalance along the input axis. The scale factor and zero bias offset of each accelerometer were determined. These prelaunch determined calibration constants and scale factors were stored in the navigation computer for use during flight.

Navigation computer unit: The navigation computer unit was a serial, binary, digital machine with a magnetic drum memory. The memory drum had a capacity of 2816 words (25 bits per word) of permanent storage, 256 words of temporary storage, and six special purpose tracks. Permanent storage was prerecorded and could not be altered by the computer. The temporary storage was the working storage of the computer.

Incremental velocity pulses from the accelerometers were the information inputs to the navigation computer. The operation of the navigation computer was controlled by the prerecorded program. This program directed the computer to perform three basic operations which are described by the prelaunch equations, navigation equations, and guidance equations.

The prelaunch equations established the initial conditions for the navigation and guidance equations. The initial conditions included (1) a reference trajectory, (2) launch site values of geographical position, and (3) initial values of navigation and guidance functions. Based on these initial conditions, the guidance system started flight operation approximately 8 seconds prior to lift-off.

The navigation equations were used to compute vehicle velocity and actual position.

The velocity was determined by algebraically summing the incremental velocity pulses from the accelerometers. An integration was then performed on the computed velocity to determine actual position. Corrections for the prelaunch-determined gyro and accelerometer constants were also made during the velocity and position computation to improve the navigation accuracy. As an example, the velocity data derived from the accelerometer measurements were adjusted to compensate for the accelerometer scale factors and zero offset biases measured during the launch countdown. The direction of the velocity vector was also adjusted to compensate for the gyro constant torque drift rates measured during the launch countdown.

The guidance equations were used to compare actual position and velocity with the position and velocity desired at the time of injection. In addition, the equations had modifications to optimize other mission constraints. Based on this position comparison, steering signals were generated to guide the vehicle along an optimized flight path to obtain the desired injection conditions. The guidance equations were used to generate eight discrete commands: (1) booster engine cutoff, (2) sustainer engine cutoff backup, (3) Centaur main engine first cutoff, (4) hydrogen peroxide settling engines cutoff, (5) B timer start (Centaur main engine second start sequence) (6) Centaur main engine second cutoff (7) telemetry calibration on, and (8) telemetry calibration off. The booster engine cutoff command and the sustainer engine cutoff backup command were issued when the measured vehicle acceleration equaled predetermined values. The Centaur main engine first cutoff command was issued when the vehicle orbital energy equaled the energy required for injection into the parking orbit. The hydrogen peroxide settling engines cutoff command was issued at a predetermined time interval after main engine first cutoff. The B timer start command was issued when the angle between the position and target vectors, as computed by the guidance system, equaled a prelaunch determined angle. When the measured vehicle orbital energy equaled the predetermined value required for injection into the lunar trajectory, the Centaur main engine second cutoff command was issued. The telemetry calibration commands were issued at fixed time intervals after the B timer start command.

During the booster phase of flight, the navigation computer supplied an incremental pitch signal and the total yaw signal for steering the Atlas stage. From a series of predetermined programs, one pitch program and one yaw program were selected based on prelaunch upper wind soundings. The selected programs were entered and stored in the computer during launch countdown. The programs consisted of discrete pitch and yaw turning rates for specified time intervals from T + 15 seconds until booster engine cutoff. These programs permitted changes to be made in the flight reference trajectory during countdown to reduce anticipated aerodynamic heating and structural loading conditions on the vehicle.

Signal conditioner unit: The signal conditioner unit was the link between the guidance system and the vehicle telemetry system. This unit modified and scaled guidance system parameters to match the input range of the telemetry system.

System performance. - The performance of the AC-9 guidance system was excellent. The system performance was evaluated in terms of resultant flight trajectory and the midcourse correction that would have been required by a spacecraft. In addition, the issuance of discrete commands, operation of the guidance steering loop, gyro control loops, accelerometer loops, and other measurements were evaluated in terms of available data.

Trajectory and midcourse requirements: The overall accuracy of the AC-9 guidance system was excellent. The parking orbit altitude was designed to be 90±5 nautical miles (166.7±9.3 km), based on the spacecraft heating and payload considerations. The Centaur spacecraft was injected into the parking orbit at an altitude of 89.8 nautical miles (166.3 km). The perigee and apogee altitudes were 86.1 nautical miles (159.5 km) and 90.0 nautical miles (166.7 km), respectively. After coasting for 24.28 minutes, the Centaur engines were restarted and the vehicle-spacecraft was successfully injected into the proper simulated transfer ellipse.

The AC-9 vehicle carried a mass model instead of an actual Surveyor spacecraft. In addition, a hypothetical target was selected to avoid intercepting the real Moon. The guidance system accuracy was evaluated and is presented in terms of midcourse correction capability.

Data from tracking information indicated that a midcourse correction, 20 hours after injection, of 6.5 meters per second (miss only[2]) or 7.5 meters per second (miss plus time of flight[3]) would have been required to hit the designed target. These corrections were well within the established specification that a Surveyor spacecraft not be required to perform a midcourse correction greater than 50 meters per second.

The slight inaccurracies at injection were primarily introducted by three main sources:

(1) An error due to the computational limitations

(2) An error between predicted and actual engine shutdown impulse

(3) An error related to the guidance equipment limitations and to dispersions from the predicted values of the thrust producted by the hydrogen peroxide engines.

---

[2]Miss only is the velocity correction required to hit the aiming point.

[3]Miss plus time of flight is the velocity correction required to hit the aiming point at the specified time.

The contribution of these sources to the midcourse correction required 20 hours after injection is shown in the following table:

Error	Miss only, m/sec	Miss plus time of flight, m/sec
Computational limitations	2.6	3.1
Engine shutdown impulse dispersion	2.5	2.9
Guidance equipment and hydrogen peroxide engines	1.4	1.5
Total error (vector summation)	6.5	7.5

In each of these cases, the errors were in the same direction and thus were added algebraically for the total error.

A true lunar trajectory was actually flown, but to a point in space where the Moon would have been on another day. The true lunar trajectory was designed for January 24, 1967, instead of the actual AC-9 launch day of October 26, 1966. If the launch had taken place on the day for which the trajectory was designed, the landing conditions which would have resulted had no midcourse maneuver been made are listed in the following table:

Landing conditions	Designed	No midcourse correction
Selenographic latitude	0^{o}	15.60^{o} N
Selenographic longitude	0.67^{o} W	35.38^{o} E
Unbraked impact velocity, m/sec	2648.0	2644.1
Flight time to Moon	2 days 17 hr 39 min 23.3 sec	2 days 18 hr 4 min 52.2 sec

The preceding data reflect a projected miss of the designed target of about 546 nautical miles (1012 km), an unbraked impact velocity error of 128 feet per second (3.9 m/sec) low, and a flight time difference of 25 minutes, 28.9 seconds late.

Discrete commands: All eight discrete commands were issued within the expected range. Table V-18 lists the discretes, the criteria that had to be solved by the navigation computer for the issuance of the discrete, and the computed value at time of issuance of the discrete. Actual and predicted times from lift-off are also shown for reference.

Guidance steering loop: Guidance steering was activated 8 seconds after the booster engine cutoff command. At this time, a 13^{o} pitchdown maneuver was commanded. A yaw maneuver was not required. This vehicle attitude change was required to correct for errors accumulated during the booster phase of flight when the vehicle was under open-loop control. After correcting this error, the steering signals were less than 1^{o} throughout the remainder of the sustainer phase of flight. Guidance steering was deactivated at sustainer engine cutoff in preparation for staging. When guidance steering was

TABLE V-18. - DISCRETE COMMANDS

Discrete command	Discrete issued at this computed value	Criteria for discrete to be issued	Actual time, sec	Predicted time, sec
Booster engine cutoff	32.72 $(g's)^2$	When the square of vehicle thrust acceleration is greater than 29.72 $(g's)^2$	142.9	140.6 to 145.0
Sustainer engine cutoff backup	0.002 $(g's)^2$	When the square of vehicle thrust acceleration is less than 0.53 $(g's)^2$	231.7	233.3 to 250.8
Centaur main engine first cutoff	62 000 $(ft/sec)^2$ (5766 $(m/sec)^2$)	When extrapolated orbital energy to be gained is equal to zero	577.7	563.9 to 581.7
Hydrogen peroxide settling engines cutoff	75.9 sec after Centaur main engine first cutoff discrete	When time from main engine first cutoff discrete is greater than 74.45 sec	653.6	639.4 to 658.4
B timer start Centaur main engine second start sequence)	-0.052573	When sine of angle between position and target vectors is greater than -0.052587	1974.6	1973.8
Centaur main engine second cutoff	221 000 $(ft/sec)^2$ (20 553 $(m/sec)^2$)	When extrapolated orbital energy to be gained is equal to 148 000 $(ft/sec)^2$ (13 764 $(m/sec)^2$)	2140.9	2138.63 to 2144.23
Telemetry calibration on	261.0 sec after B timer start discrete	When time from B timer start discrete is greater than 260.5 sec	2235.6	2233.8 to 2235.8
Telemetry calibration off	265.3 sec after B timer start discrete	When time from B timer start discrete is greater than 264.5 sec	2239.9	2237.8 to 2239.8

reactivated, 4 seconds after Centaur main engine first start, a 3^{o} pitchdown maneuver was commanded. Again, a yaw maneuver was not required. During the remainder of the first Centaur powered phase of flight, the steering signals were less than 1^{o}. During the coast phase of flight the maximum steering signals were 4^{o} in pitch and 3^{o} in yaw. Table V-19 lists the magnitude of the steering signals after each period of guidance system deactivation.

Guidance steering was deactivated at Centaur main engine second start and was reactivated 4 seconds later. At this time, 3^{o} pitchdown and 4^{o} yaw-left maneuvers were commanded. The steering signals were negligible during the remainder of the second Centaur powered phase of flight.

Guidance steering was deactivated at Centaur main engine second cutoff and was reactivated at T + 2215.8 seconds for the retromaneuver. At this time, the steering signals corresponded to the negative of the vehicle velocity vector. The signals caused the vehicle to pitch up and yaw to the right to accomplish the turnaround maneuver.

Gyro control loops: The inertial platform was stable throughout the flight. The platform gyro control loops operated satisfactorily. The maximum displacement errors were less than 11 arc-seconds (the dynamic accuracy tolerance was 60 arc-sec). Normal low frequency oscillations (less than 2 Hz) observed in all four loops were attributed to vehicle dynamics.

Accelerometer loops: The accelerometer loops operated satisfactorily throughout the flight. The maximum accelerometer-pendulum excursions were approximately 5 arc-seconds peak to peak.

TABLE V-19. - ATTITUDE COMMAND AT START OF GUIDANCE STEERING AFTER EACH PERIOD OF SYSTEM DEACTIVATION, AC-9

Event	Time since end of last period of steering, sec	Flight time at start of steering, T + sec	Pitch command magnitude and direction, deg	Yaw command magnitude and direction, deg
Atlas sustainer phase enable guidance steering	Lift-off	T + 151.1	13, nose down	0
Centaur main engine first start enable guidance steering	16.7	T + 245.8	3, nose down	0
Centaur main engine second start enable guidance steering	4	T + 2040	3, nose down	4, nose left

Other measurements: All the guidance system signals and measurements which were monitored during flight were normal and indicated satisfactory operation of the guidance system.

Flight Control Systems

Atlas system description.- The Atlas flight control system provided the primary functions required for vehicle stabilization, control, execution of guidance steering signals, and timed switching sequences.

The Atlas flight control system comprised the following principal units.

(1) The displacement gyro unit, which consisted of three single-degree-of-freedom, floated, rate-integrating gyros and associated electronic circuitry for gain selection and signal amplification. These gyros were mounted to the vehicle airframe in an orthogonal triad configuration, alining the input axis of a gyro to its respective vehicle axis of pitch, yaw, or roll. Each gyro provided an electrical output signal proportional to the difference in angular position of the measured axis from the gyro reference axis.

(2) The rate gyro unit, which contained three single-degree-of-freedom, floated, rate gyros and associated electronic circuitry. These gyros were mounted in the same manner as the displacement gyro unit. Each gyro provided an electrical output signal proportional to the angular rate of rotation of the vehicle about the gyro input (reference) axis.

(3) The servoamplifier unit, which contained electronic circuitry to amplify, filter, integrate, and algebraically sum engine position feedback signals with position and rate signals. The electrical outputs of this unit were sent to hydraulic actuators which controlled the gimbaling of the engines.

(4) The programmer unit, which contained an electronic timer, arm-safe switch, high, low, and medium power electronic switches, the fixed pitch program, and circuitry to set the roll program from launch ground equipment. The programmer issued discrete commands to the following systems: other units of the Atlas flight control system, Atlas propulsion, Atlas pneumatics, vehicle separation systems, Centaur flight control, and Centaur propulsion.

Atlas system performance. - The flight control system performed satisfactorily throughout the Atlas phase of flight. The corrections required to control the vehicle because of disturbances were well within the system capability. The vehicle dynamic response resulting from each flight event was evaluated in terms of amplitude, frequency, and duration, as observed from rate gyro data (see table V-20). In this table, control capability is the ratio of engine gimbal angle used to the available total engine gimbal angle, in percent. The control used at all times of the flight events includes that neces-

TABLE V-20. - VEHICLE DYNAMIC RESPONSE TO FLIGHT DISTURBANCES, AC-9

Event	Time[a], sec	Measurement	Rate gyro peak-to-peak amplitude, deg/sec	Transient frequency, Hz	Transient duration, sec	Required percent control capability
Lift-off	T + 0	Pitch	1.02	6.67	2.0	(b)
		Yaw	.51	10.00	(b)	(b)
		Roll	2.21	10.00	1.0	(b)
42-in. (1.1-m) rise	T + 1	Pitch	1.28	6.67	1.7	6
		Yaw	.85	(b)	(b)	4
		Roll	1.96	2.50	1	4
Maximum dynamic pressure	Data reviewed from T + 72 to T + 90	Pitch	2.04	0.30	15	50
		Yaw	1.36	.40	15	24
		Roll	.68	1.00	10	24
Booster engine cutoff	T + 143.1	Pitch	1.02	5.00	1.0	14
		Yaw	.68	5.00	1.5	7
		Roll	1.62	.58	3.0	7
Booster engine jettison	T + 146.6	Pitch	0.76	5.00	1.0	(b)
		Yaw	2.04	.67	3.0	(b)
		Roll	1.70	.91	5.0	(b)
Admit guidance	T + 151.1	Pitch	3.06	1.00	2.0	68
		Yaw	.51	.50	2.0	22
		Roll	1.87	1.00	2.5	22
Insulation panel jettison	T + 177.3	Pitch	1.02	(b)	(b)	12
		Yaw	.68	(b)	(b)	12
		Roll	1.19	4.0	1	8
Nose fairing jettison	T + 203.8	Pitch	2.30	20	(b)	18
		Yaw	1.02	10	10	12
		Roll	1.62	3.3	6	4
Sustainer engine cutoff	T + 229.1	Pitch	No significant transients			
		Yaw				
		Roll				
Atlas-Centaur separation	T + 231.0	Pitch	Smooth separation; no noticeable transients			
		Yaw				
		Roll				
Main engine first start	T + 240.5	Pitch	2.08	0.25	7	20
		Yaw	.34	(b)	(b)	14
		Roll	2.30	.5	9	14
Admit guidance	T + 245.8	Pitch	(b)	(b)	(b)	10
		Yaw	(b)	(b)	(b)	6
		Roll	(b)	(b)	(b)	6
Main engine first cutoff	T + 577.7	Pitch	1.28	(b)	(b)	10
		Yaw	.34	(b)	(b)	24
		Roll	.85	0.83	2	24
Main engine second start	T + 2036	Pitch	1.44	0.5	3	22
		Yaw	1.12	.5	3	16
		Roll	2.32	1.43	3	16
Admit guidance	T + 2040	Pitch	1.44	0.77	7	8
		Yaw	1.44	.77	8	6
		Roll	.64	1.00	9	6
Main engine second cutoff	T + 2141	Pitch	1.92	50	0.5	24
		Yaw	.64	50	.2	32
		Roll	.72	1	1.2	32

[a]Initiation of disturbances as seen on rate gyro data.
[b]Indicates no measurable data.

sary for correction of the vehicle transient disturbances and for steady-state requirements.

The programmer was started at 42-inch (1.1-m) rise which occurred at approximately T + 1 second. This permitted the flight control system to gimbal the engines and thereafter control the vehicle. The vehicle lift-off transients were damped out by T + 1.7 seconds and required 6 percent of the control capability. The roll program was initiated at approximately T + 2.2 seconds to roll the vehicle to the desired flight azimuth of 99.7^{o}. An average rate of 1.23 degrees per second clockwise was sensed. The pitch program was observed to start at T + 15 seconds with a pitch rate of -0.72 degree per second nose down.

Rate gyro data indicated that the period of maximum aerodynamic loading for this flight was approximately from T + 72 to T + 90 seconds. During this period, a maximum of 50 percent of the control capability was required to overcome both steady-state and transient loading.

The sustainer engine was held in the centered position until booster engine cutoff at T + 143.1 seconds. At this time, disturbances created by differential cutoff impulse of the booster engine were damped by gimbaling the sustainer and vernier engines. This correction required 14 percent of the sustainer engine gimbal capability. The sustainer engine was centered a second time for 0.7 second during booster stage jettison at T + 146.6 seconds. The rates imparted to the vehicle by this disturbance (booster engine jettison) were nearly damped out by the time Centaur guidance was admitted at T + 151.1 seconds.

During Atlas booster phase of flight, the Atlas flight control system provided the vehicle attitude reference. After T + 151.1 seconds, the Centaur guidance system was required to move the vehicle to the new reference. The maximum vehicle rate during this change was 3.06 degrees per second peak to peak. The vehicle was stabilized on the new reference within 2.5 seconds.

Insulation panels and nose fairings were jettisoned at T + 177.3 and T + 203.8 seconds, respectively. The maximum vehicle transient observed due to these disturbances was a pitch rate of 2.3 degrees per second peak to peak. The maximum control capability used to overcome these disturbances was 18 percent.

Centaur system description. - The Centaur flight control system provided the primary means for vehicle stabilization and control, execution of guidance steering signals, and timed switching sequences for programmed flight events. A simplified block diagram of the Centaur flight control system is shown in figure V-114.

The Centaur flight control system comprised the following principal units:

(1) The rate gyro unit contained three single-degree-of-freedom, floated, rate gyros with associated electronics for signal amplification. These gyros were mounted to the vehicle in an orthogonal triad configuration alining the input axis of each gyro to its respective vehicle axis of pitch, yaw, or roll. Each gyro provided an electrical

output signal proportional to the angular rate of rotation of the vehicle about the gyro input (reference) axis.

(2) The servoamplifier unit contained electronics to amplify, integrate, and algebraically sum engine position feedback signals with position and rate signals. The electrical outputs of this unit were sent to hydraulic actuators, which controlled the gimbaling of the engines. In addition, this unit contained the logic circuitry for controlling the engines of the hydrogen peroxide attitude control system.

(3) The electromechanical timer unit contained a 400-hertz synchronous motor to provide the time reference. The motor drove a mechanical arrangement of shafts and cams which activated switch contacts. The switches were used as control inputs for the auxiliary electronics unit. Two timer units designated A and B were needed because of the large number of discrete commands required for the parking-orbit mission.

(4) The auxiliary electronics unit contained logic relay switches, transistor power switches, power supplies, and an arm-safe switch. The arm-safe switch electrically isolated valves and pyrotechnic devices from control switches. The combination of the electromechanical timer units and the auxiliary electronics unit issued discretes to the following systems: other units of the flight control system, propulsion, pneumatic, hydraulic, separation system, propellant utilization, telemetry, spacecraft, and electrical.

Vehicle steering during Centaur powered flight was by thrust vector control provided by gimbaling the two main engines. There were two actuators for each engine to provide pitch, yaw, and roll control. Pitch control was accomplished by moving both engines together in the pitch plane. Yaw control was accomplished by moving both engines together in the yaw plane, and roll control was accomplished by moving the engines differentially in the yaw plane. Thus, the yaw actuator responded to an algebraically summed yaw-roll command. By controlling the direction of thrust of the main engines, the flight control system maintained the flight of the vehicle on a trajectory directed by the guidance system. After main engine cutoff, control of the vehicle was maintained by the flight control system using selected constant thrust hydrogen peroxide engines in on-off modes of operation.

During the coast phases of flight the hydrogen peroxide attitude control system provided the required thrust to stabilize, control, and guide the vehicle. A more complete description of the engines and the propellant supply for the attitude control system is presented in the PROPULSION SYSTEMS section of this report.

The logic circuitry which commands the hydrogen peroxide engines, either on or off, was contained in the servoamplifier unit of the flight control system. The 14 engines were commanded and figure V-115 shows their alphanumeric designations and locations on the aft end of the vehicle.

Algebraically summed position and rate signals were the inputs to the logic cir-

cuitry. The logic circuitry provided five modes of operation designated all off, separate on, A and P separate on, V half on, and S half on. These modes of operation were used during different periods of the flight which were controlled by the timer unit. A summary of the modes of operation is presented in table V-21. In this table, "threshold" designates the vehicle rate in degrees per second that had to be exceeded before the engines were commanded on.

Centaur system performance. - The Centaur flight control system performance was satisfactory. Vehicle stabilization and control were maintained throughout the flight. All events sequenced by the timer(s) were executed at the required times. The following evaluation is presented in paragraphs related to timed-sequenced portions of flight. For the guidance - flight-control mode of operation for each portion of flight, refer to figure V-110 and table V-21. The dynamic response for all portions of flight is tabulated in table V-20 and the firing times for the attitude control engines are shown in figure V-116.

Sustainer engine cutoff through main engine first cutoff (T + 229.05 to T + 577.8 sec): The Centaur A timer was started at sustainer engine cutoff by a discrete command from the Atlas programmer. Appropriate commands were issued to separate the Centaur stage from the Atlas stage and to initiate the first main engine firing sequence. Disturbing torques were created prior to main engine start by boost pump exhaust and chilldown flow through the main engines. Vehicle control was maintained by gimbaling the main engines.

Centaur main engine first start was commanded at T + 240.5 seconds. The maximum angular rates due to engine start transients were 2.3 degrees per second and were corrected by gimbaling the engines less than 1^{o}. When guidance steering was enabled 4 seconds after main engine start, the Centaur vehicle was oriented 3^{o} nose high of the steering vector. This difference was corrected within 9 seconds. No yaw correction was required Vehicle steady-state angular rates during the period of closed-loop control were too small to be measured. Angular rates imparted to the vehicle due to main engine cutoff transients were low, indicating a small differential cutoff impulse. The maximum rate measured was 1.28 degrees per second in pitch.

Main engine first cutoff to main engine second prestart (T + 577.8 to T + 2008 sec): After main engine first cutoff, the hydrogen peroxide attitude control system was activated. During the 24.28-minute coast period, the control requirements were well within the capability of the attitude control system. The rate gyros indicated maximum rates of 0.48 degree per second about the roll axis.

Main engine second prestart through main engine second cutoff (T + 2008 to T + 2141 sec): The hydraulic recirculating pumps were activated 28 seconds prior to main engine second start, and the Centaur main engines were centered. Main guidance steering was disabled at engine second start (T + 2034.7 sec). The maximum angular

TABLE V-21. - ATTITUDE CONTROL SYSTEM MODES OF OPERATION, AC-9

[V engines, 50 lb (222.4 N) thrust; S engines, 3.0 lb (13.3 N) thrust; A engines, 3.5 lb (15.6 N) thrust; P engines, 6.0 lb (26.7 N) thrust.]

Mode	Flight period	Description
All off	1. Powered phases 2. 5 sec during spacecraft separation sequence	This mode prevents the operation of all attitude control engines regardless of error signals.
Separate on	1. Main engine second cutoff until start of spacecraft separation sequence 2. End of lateral thrust during turnaround until end of retrothrust	When in the separate on mode, a maximum of 2 A and 2 V engines and 1 P engine fire. These engines fire only when appropriate error signals surpass their respective thresholds. A engines: when 0.2 deg/sec threshold is exceeded, suitable A engines fire to control in yaw and roll. A_1A_4 and A_2A_3 combinations are inhibited. P engines: when 0.2 deg/sec threshold is exceeded, suitable P engine fires to control in pitch. P_1P_2 combination is inhibited. S engines: off V engines: when 0.3 deg/sec threshold is exceeded, suitable engines fire (as a backup for higher rates). V_1V_3 and V_2V_4 combinations are inhibited.
A and P separate on	End of spacecraft separation sequence until start of lateral thrust	This mode is the same as separate on mode, except V engines are inhibited.
V half on	1. Main engine first cutoff until main engine first cutoff plus 75 sec 2. Main engine second start minus 40 sec until main engine second start 3. During lateral thrust phase 4. Last 100 sec prior to Centaur power turnoff	In the V half on mode, only the V engines are in the half on mode. A engines: when 0.2 deg/sec threshold is exceeded, suitable A engines fire to control in roll only. P engines: off S engines: off V engines: when there are no error signals, V_2V_4 combination fires continuously. This continuous firing serves various purposes: to settle propellants in flight periods 1 and 2, to provide lateral and added longitudinal separation between Centaur and spacecraft in flight period 3, and in order to deplete hydrogen peroxide supply to determine the amount of usable propellant remaining at end of mission in flight period 4. When 0.2 deg/sec threshold is exceeded, a minimum of 2 and a maximum of 3 V engines fire to control in pitch and yaw.
S half on	1. Main engine first cutoff plus 76 sec until main engine second start minus 40 sec	This mode is described as follows: A engines: when 0.2 deg/sec threshold is exceeded, suitable A engines fire to control in roll only. P engines: off S engines: when there are no error signals, S_2S_4 combination fires continuously for propellant retention purposes. When 0.2 deg/sec threshold is exceeded, a minimum of 2 and a maximum of 3 S engines fire to control in pitch and yaw. V engines: when 0.3 deg/sec threshold is exceeded, a minimum of 1 and a maximum of 2 V engines fire to control in pitch and yaw. When a V engine fires, a corresponding S engine is commanded off.

rate observed at this time was 2.32 degree per second about the roll axis. Prestart and ignition sequences resulted in an attitude 3^{o} nose high and 4^{o} nose right of the desired orientation when guidance steering was reenabled (approximately T + 2040 sec). The maximum control capability used to control these disturbances was 22 percent. Angular rates were low during the second powered phase which ended with main engine second cutoff (T + 2141 sec).

Main engine cutoff (T + 2141 to T + 2760.7 sec): At the time of Centaur main engine cutoff, guidance-generated steering signals were temporarily discontinued. The hydrogen peroxide attitude control system damped the low angular rates created by the main engine cutoff transient to within the 0.2 degree per second control threshold. At T + 2210.8 seconds, the hydrogen peroxide system was deactivated for 5 seconds, and the mass model was successfully separated from Centaur. The deactivation of the hydrogen peroxide system during this time was to preclude a possibility of the Centaur interfering with the mass model during the separation phase.

The retromaneuver sequence was initiated at T + 2215.9 seconds. The Centaur was commanded to turn approximately 180^{o} to the guidance steering vector which was fixed at the time of injection. The attitude control system was activated which started the vehicle to turn to the new vector. Approximately half way (90^{o}) through the turnaround, the V engines were commanded to the V half on mode to provide 100 pounds (445 N) of thrust for 20 seconds. This maneuver increased the lateral separation between Centaur and the spacecraft and minimized impingement of the residual propellants on the spacecraft during the period of retrothrust. Guidance gimbal resolver data indicated that the vehicle turned through a total angle of 167^{o} in approximately 105 seconds.

At T + 2450.8 seconds, the engine prestart valves were opened to allow the residual propellants to discharge through the main engines. Coincident with this propellant discharge, the engine thrust chambers were gimbaled to aline the thrust vector through the vehicle center of gravity. Thrust from the propellant discharge provided adequate separation between Centaur and the Surveyor mass model. Separation distance at the end of 5 hours was 1194 kilometers. This was more than 3.5 times the separation distance required for a real Surveyor mission.

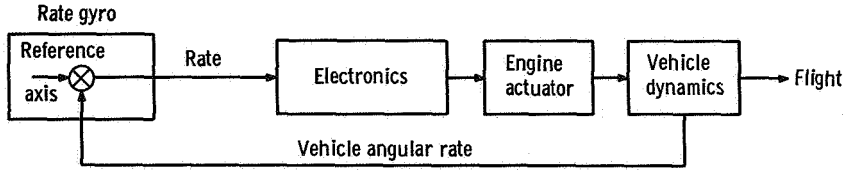

(a) Rate stabilization mode.

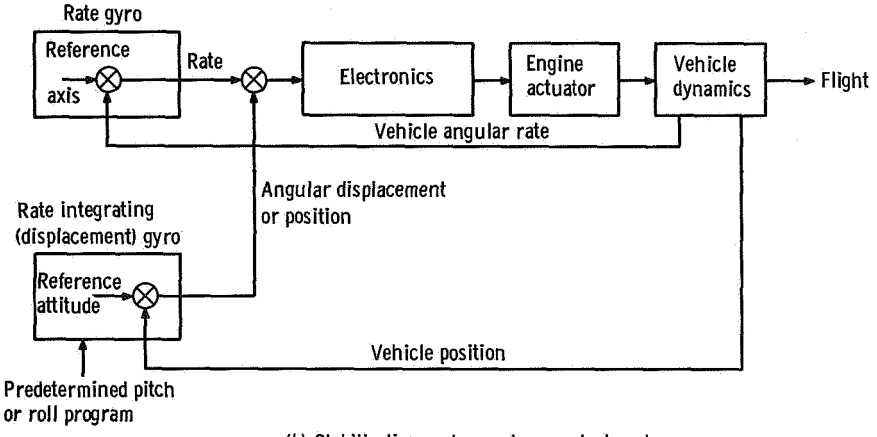

(b) Stabilization and open-loop control mode.

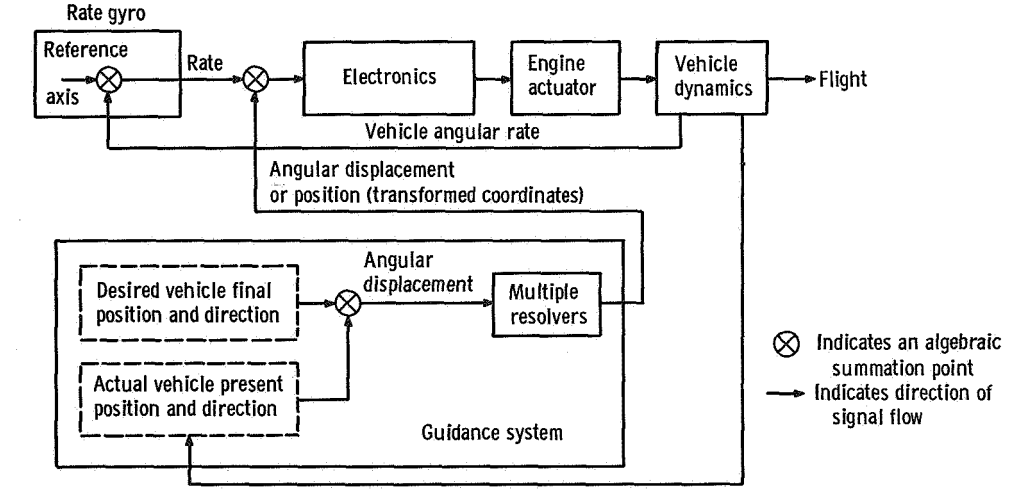

(c) Stabilization and closed-loop control mode.

Figure V-109. - Guidance and flight control modes of operation, AC-9.

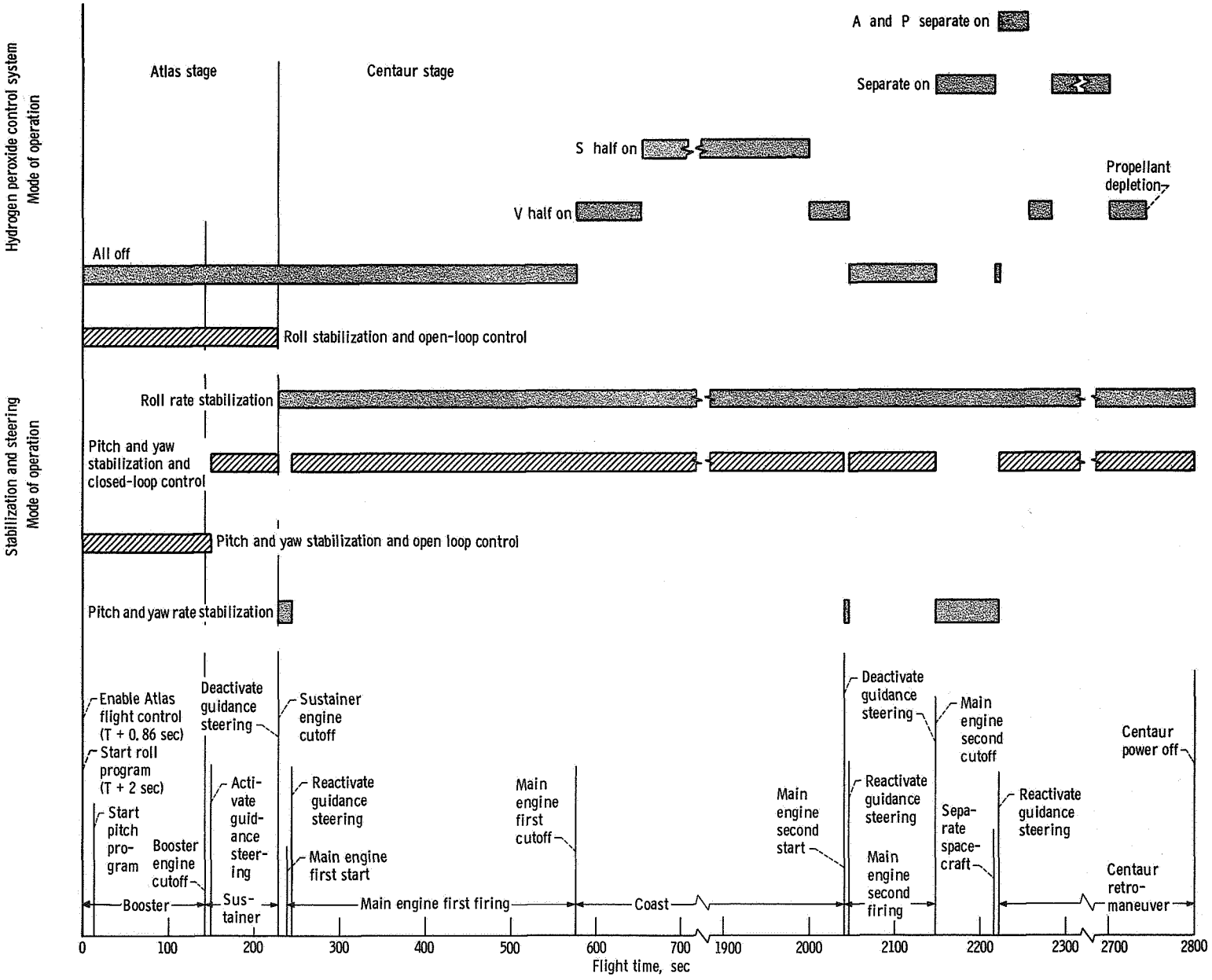

Figure 110. - Guidance and flight control modes of operation, AC-9.

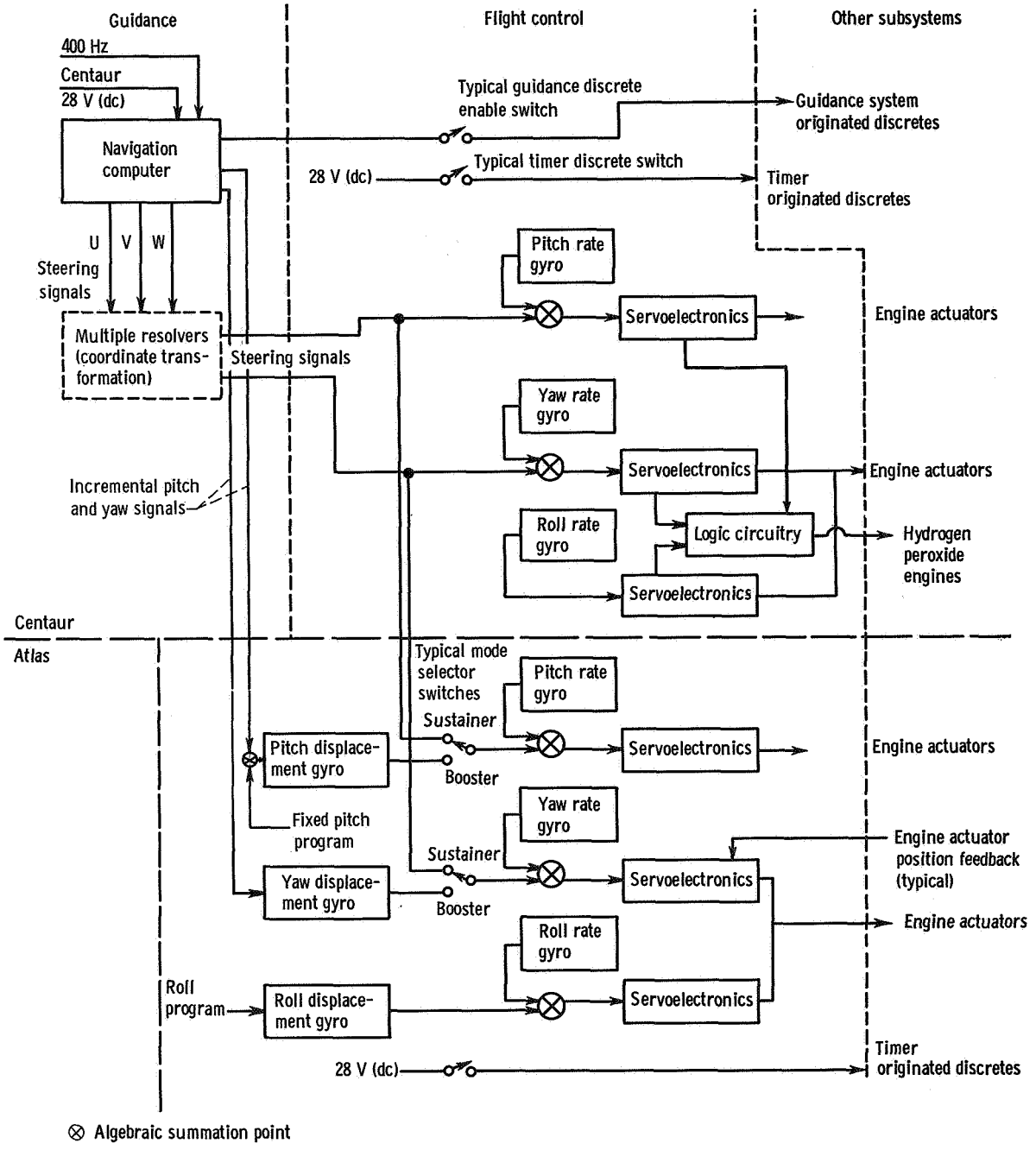

Figure V-111. - Simplified guidance and flight control systems interface, AC-9.

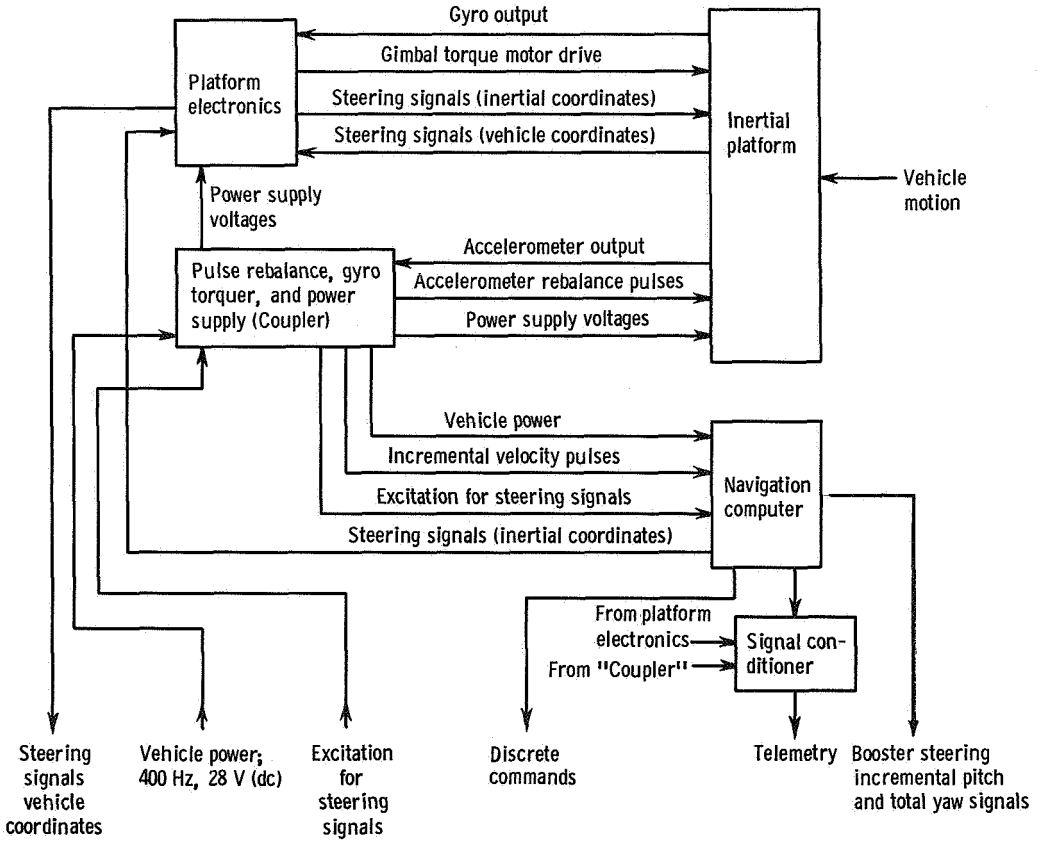

Figure V-112. - Simplified block diagram of Centaur guidance system, AC-9.

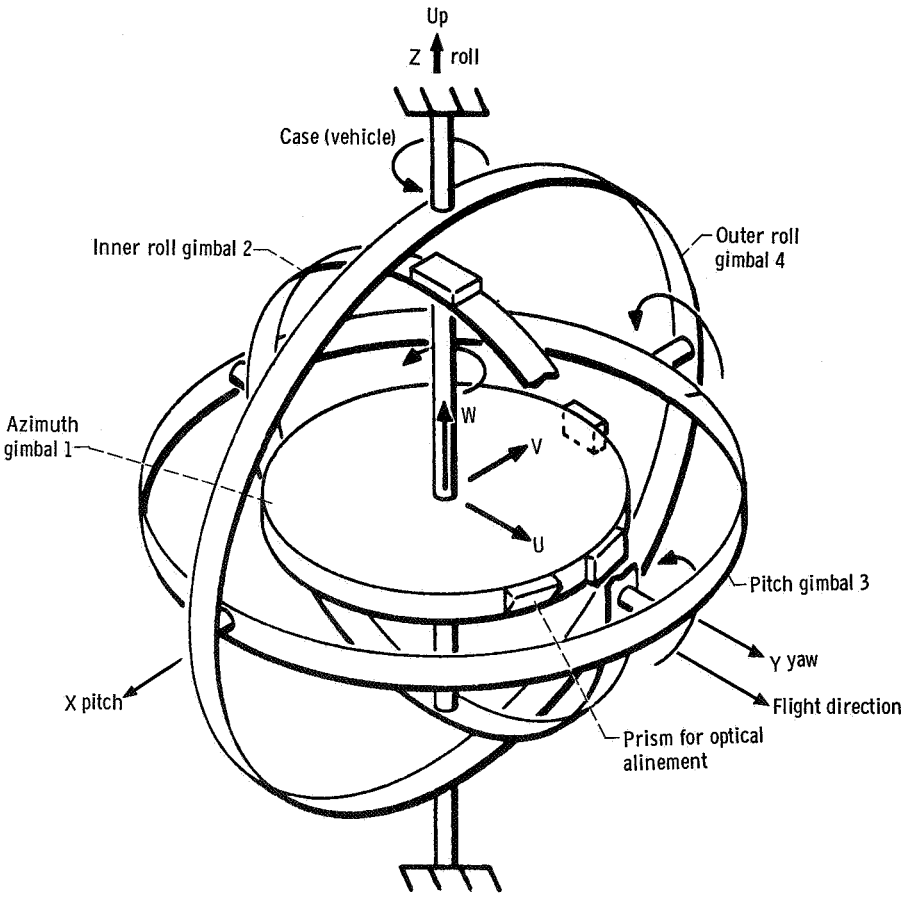

Figure V-113. - Gimbal diagram, AC-9. Launch orientation: inertial platform coordinated, U, V, and W; vehicle coordinates, X, Y, and Z.

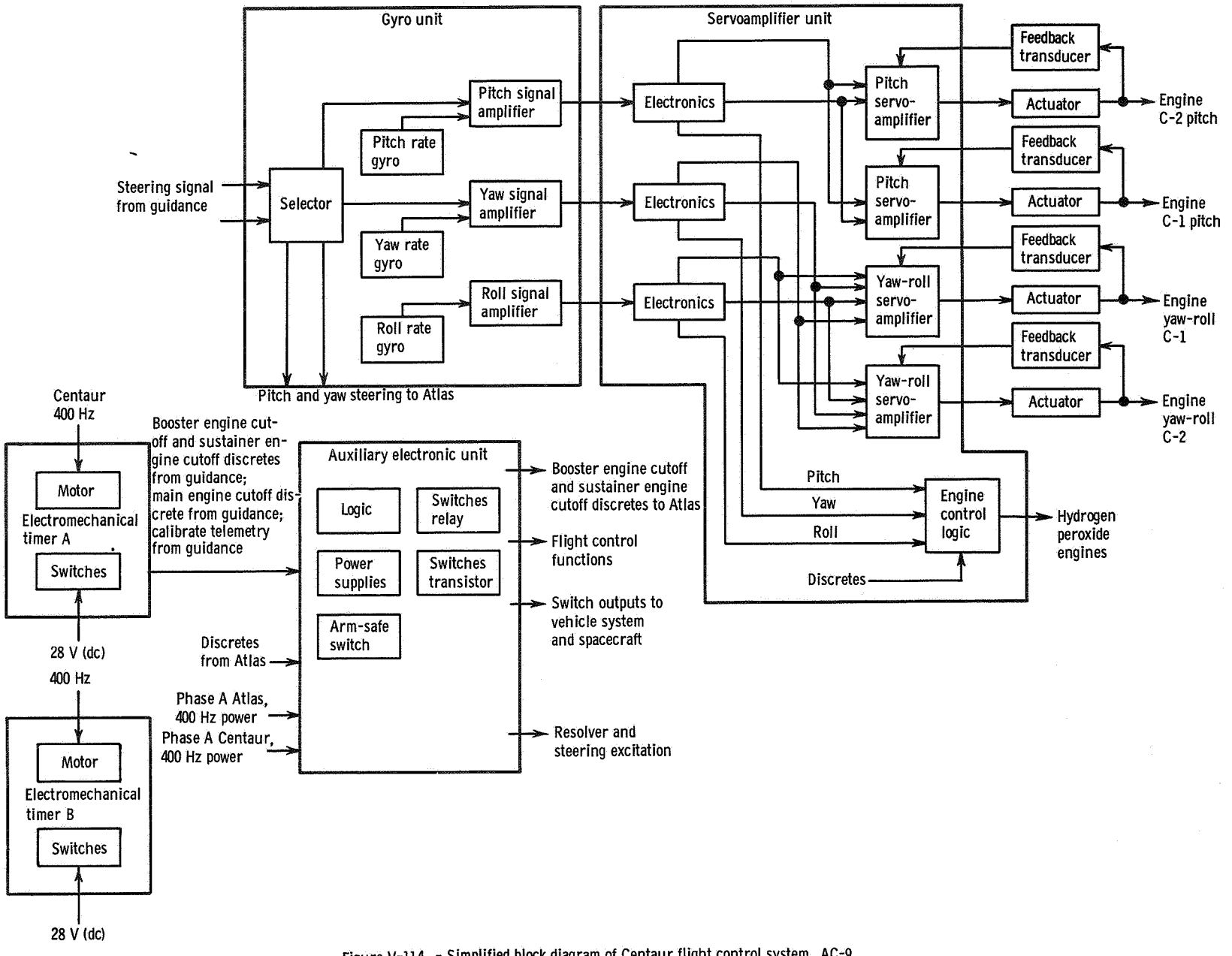

Figure V-114. - Simplified block diagram of Centaur flight control system, AC-9.

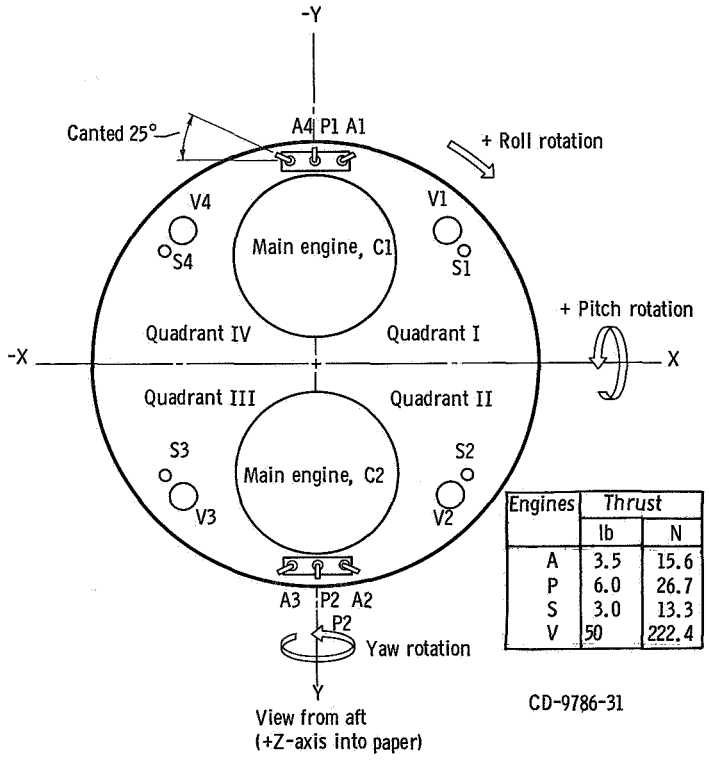

Engines	Thrust	
	lb	N
A	3.5	15.6
P	6.0	26.7
S	3.0	13.3
V	50	222.4

Figure V-115. - Attitude engines alphanumeric designations and locations, AC-9. Signs of axes are convention for flight control system.

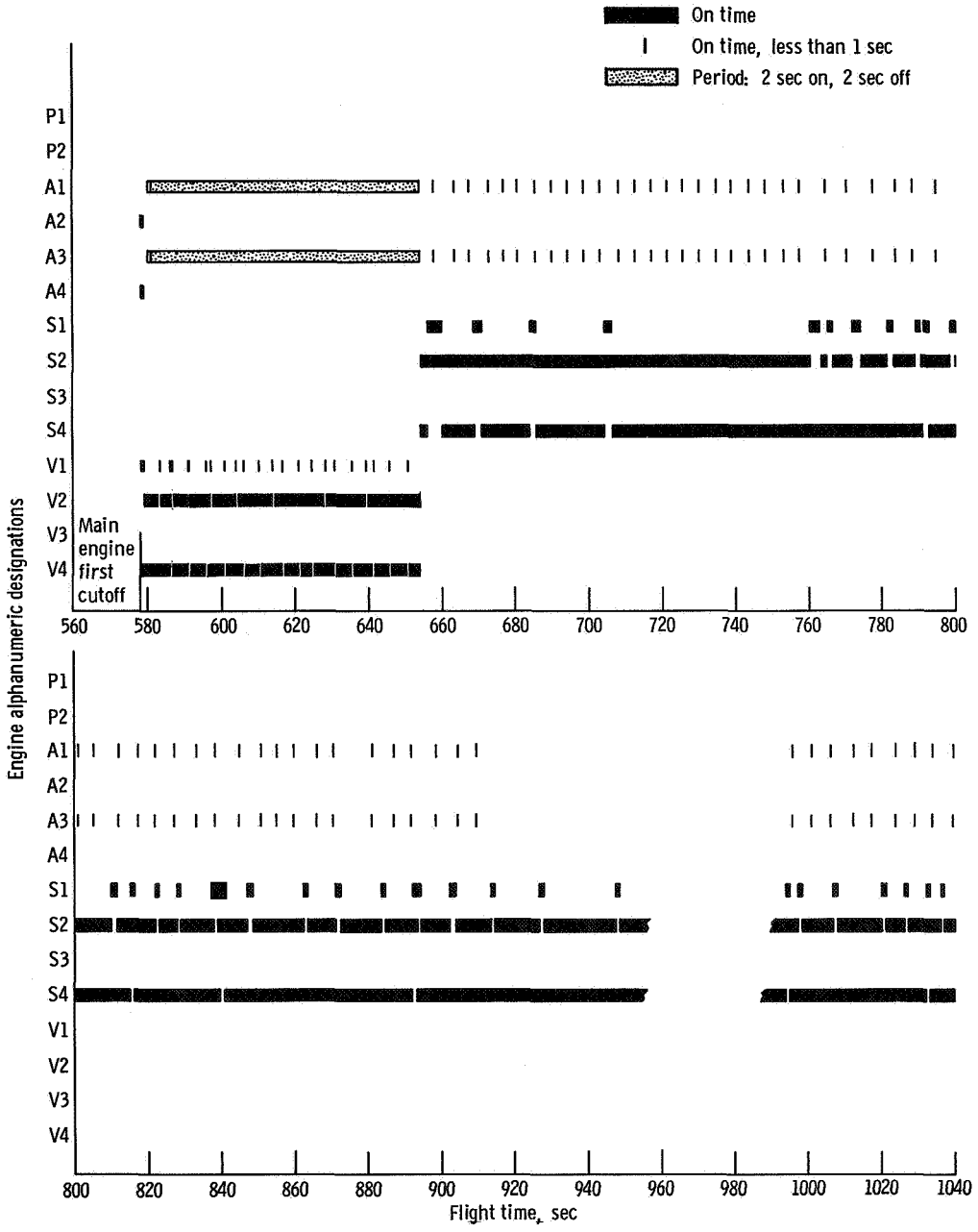

(a) T + 560 to T + 1040 seconds.

Figure V-116. - Attitude control engines operating times, AC-9.

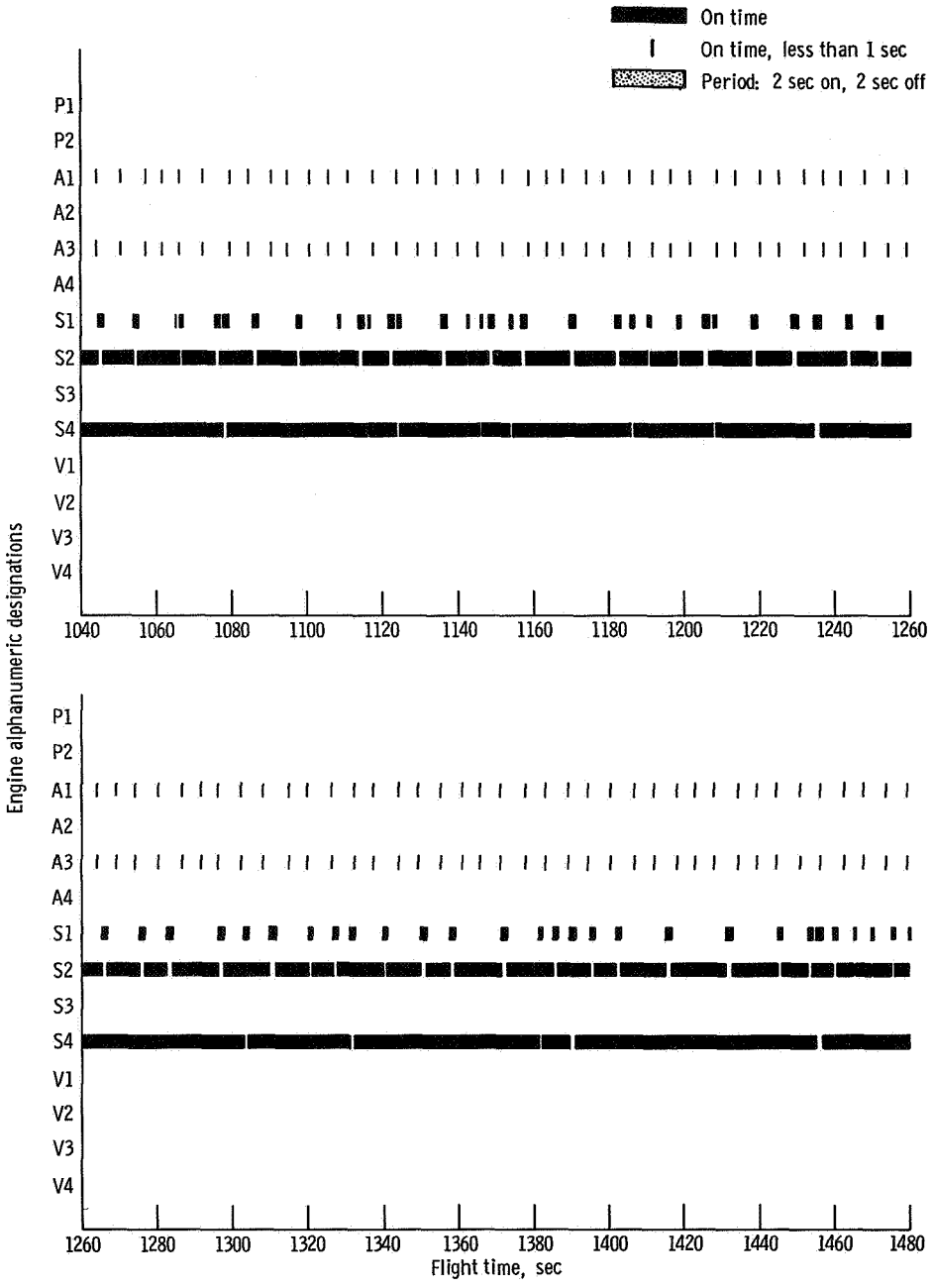

(b) T + 1040 to T + 1480 seconds.

Figure V-116. - Continued.

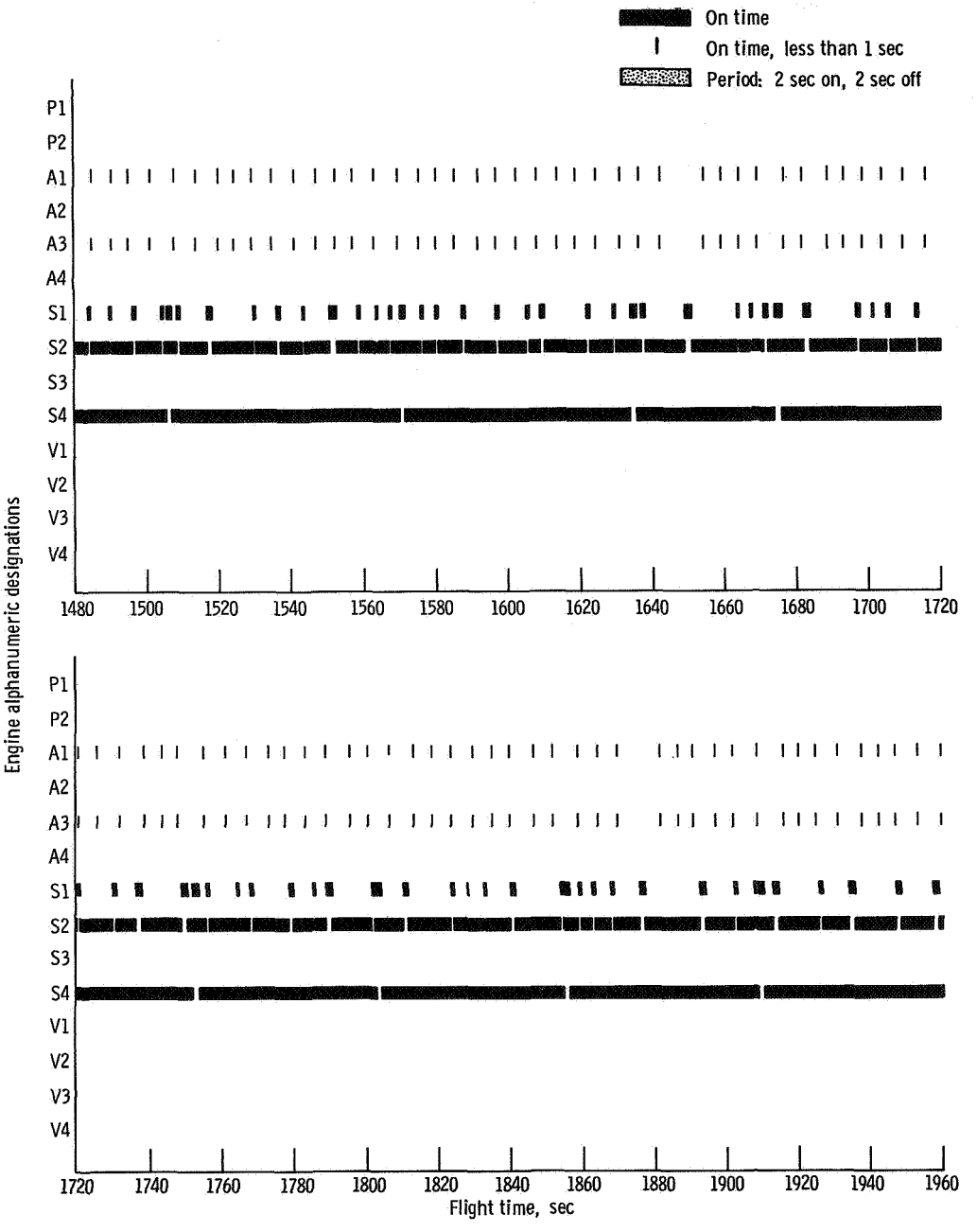

(c) T + 1480 to T + 1960 seconds.

Figure V-116. - Continued.

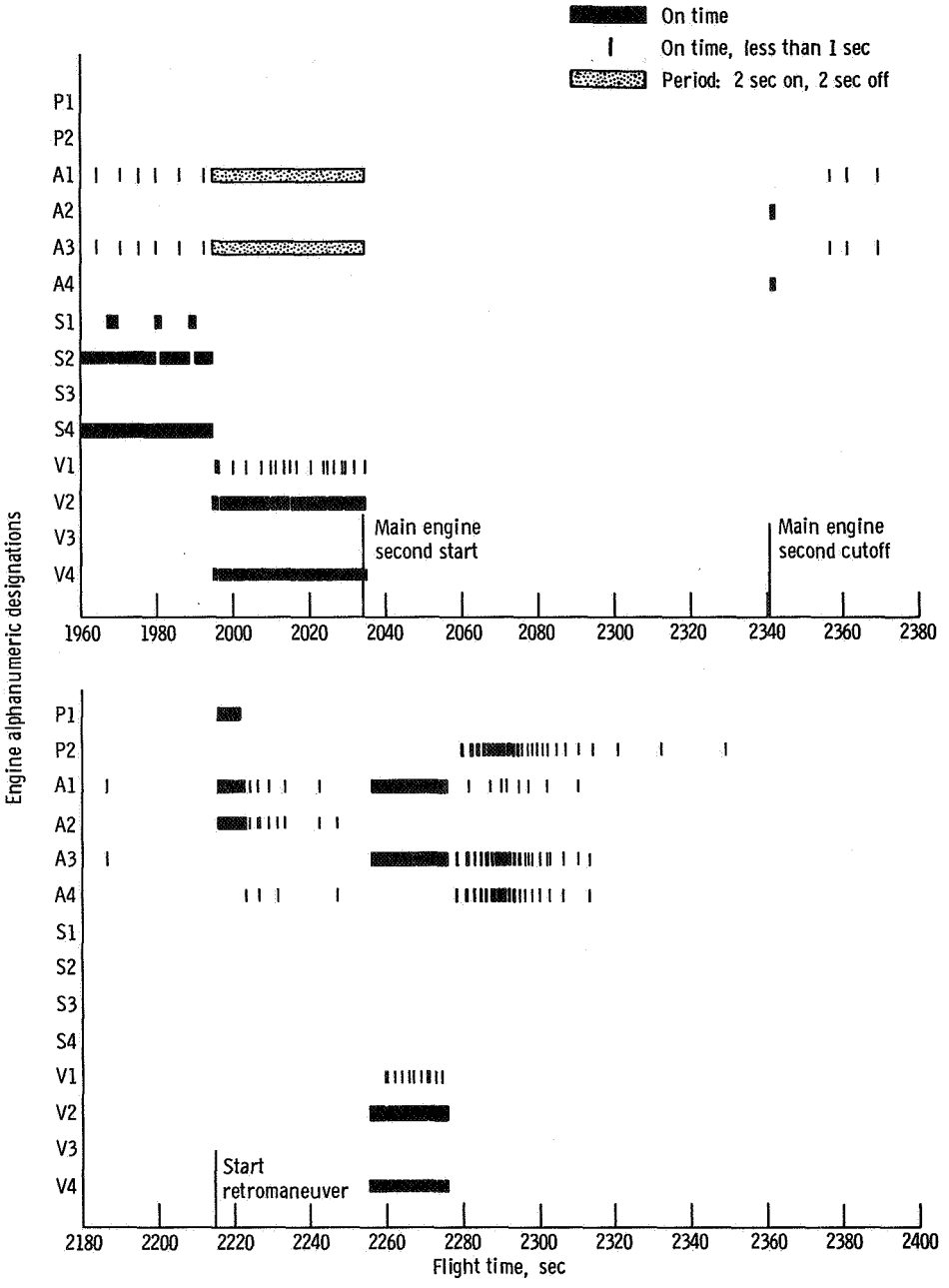

(d) T + 1960 to T + 2400 seconds.

Figure V-116. - Continued.

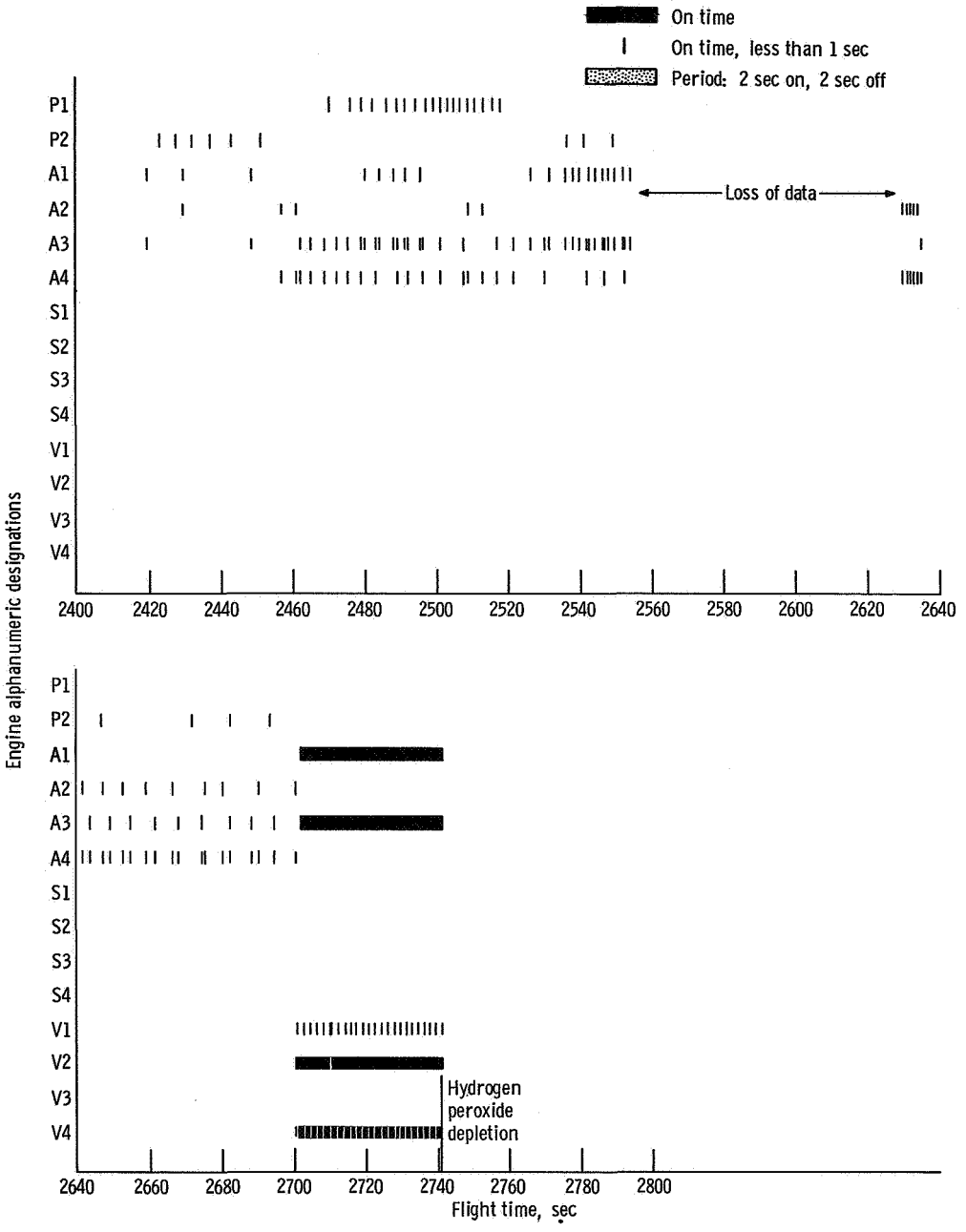

(e) T + 2400 to T + 2800 seconds.

Figure V-116. - Concluded.

VI. CONCLUSIONS

The Atlas-Centaur AC-9 launch vehicle successfully injected a Surveyor mass model into the proper lunar-transfer orbit following an indirect (parking-orbit) mode of ascent. This was the final research and development vehicle in the Centaur program. In addition to demonstrating the capability of this vehicle to support space missions requiring parking-orbit two-burn operation, extensive data concerning cryogenic propellant settling and retention during low-gravity coast in space and engine restart in space were obtained. The data verify results of analyses and ground tests that were used to establish the vehicle configuration for this flight.

Lewis Research Center,
National Aeronautics and Space Administration,
Cleveland, Ohio, March 26, 1968,
491-05-00-02-22.

APPENDIX A

SUPPLEMENTAL FLIGHT, TRAJECTORY, AND PERFORMANCE DATA

by John J. Nieberding

ATMOSPHERIC SOUNDING DATA

Ambient Temperature and Pressure

The atmospheric conditions at the launch site were determined from data obtained by several Rawinsonde sounding balloons sent aloft on the day of launch up until approximately 06:15 hours eastern standard time. Profiles of measured temperature and pressure are compared with the values predicted on the basis of characteristic weather for the Cape Kennedy area. Temperature data, as shown by figure A-1, were nearly normal at all altitudes. The largest dispersion between predicted and actual temperatures oc-

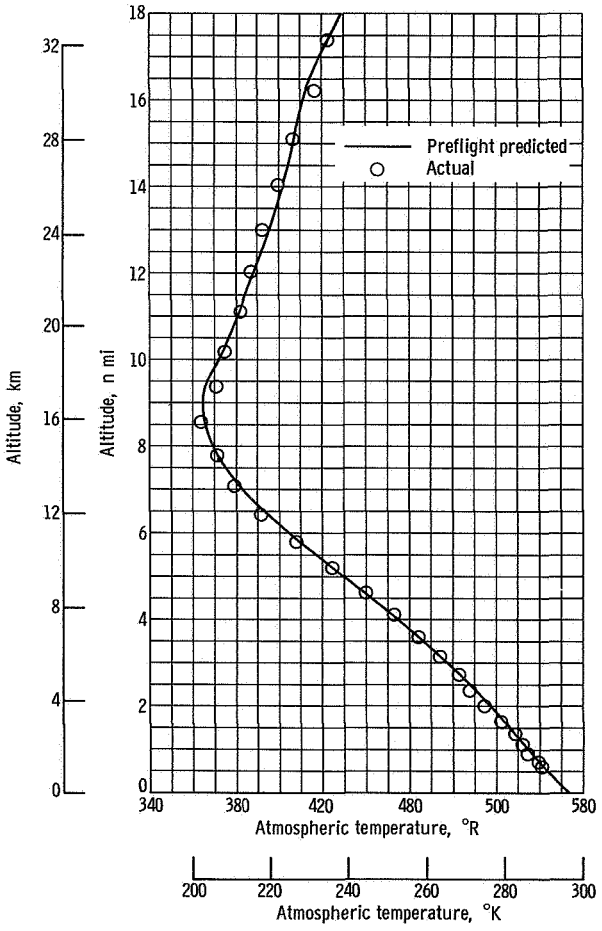

Figure A-1. - Altitude as function of temperature, AC-9.

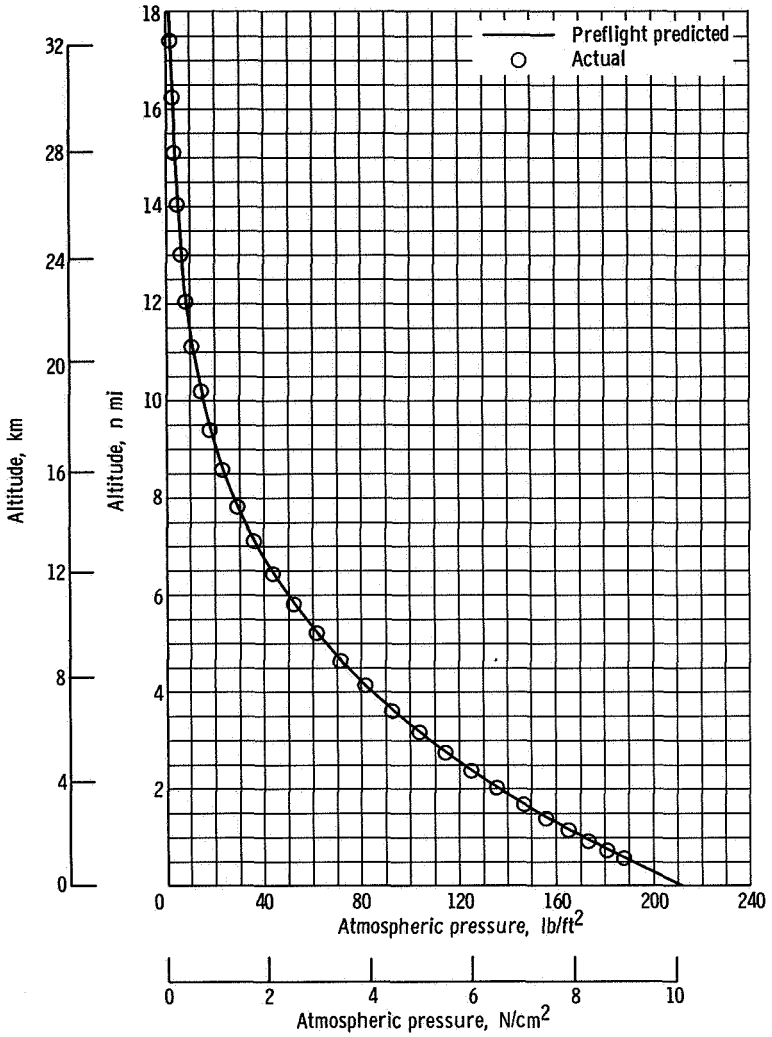

Figure A-2. - Altitude as function of pressure, AC-9.

curred at an altitude of about 9.4 nautical miles (17.4 km). At this altitude, the actual temperature was only about 5^{o} R (2.8^{o} K) higher than expected. The measured pressures in figure A-2 were in close agreement with the predicted values at all altitudes. Consequently, atmospheric temperatures and pressures had no adverse affects on the Centaur flight.

Atmospheric Winds

Wind speed and azimuth data as a function of altitude are compared with the normal October wind data for the Cape Kennedy area in figures A-3 and A-4, respectively. The erratic pattern of the wind data curves actually occurred. The data should not be

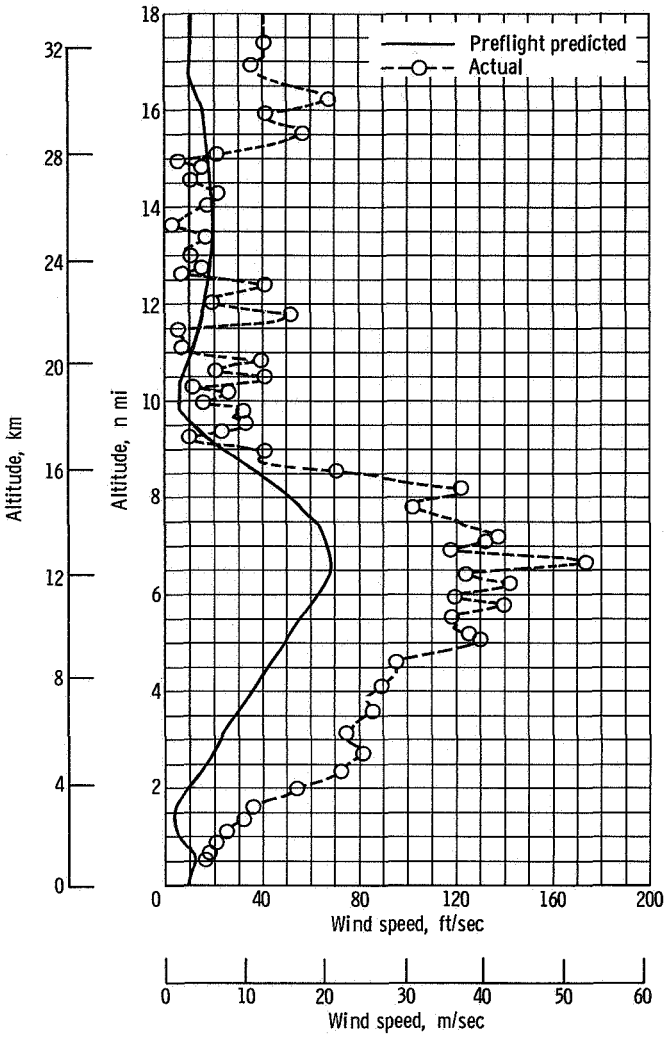

Figure A-3. - Altitude as function of wind speed, AC-9.

smoothed. Wind azimuth is the direction toward which the wind is blowing. Although the magnitudes of the actual wind speeds up to an altitude of about 9 nautical miles (16.7 km) are larger than predicted, the characteristics of the predicted and actual data curves in this region are similar. The maximum wind speed measured was 174 feet per second (53.0 m/sec) at an altitude of 6.7 nautical miles (12.4 km). This measured maximum occurred only 0.10 nautical mile (0.18 km) higher than the predicted maximum of 69 feet per second (21.0 m/sec). Between 9 and 15 nautical miles (16.7 and 27.8 km), the average measured wind speed was nearly normal. At higher altitudes, the actual wind speeds averaged about 30 feet per second (9.8 m/sec) higher than predicted.

At altitudes below 9.8 nautical miles (18.1 km), the actual wind azimuths were more northerly than predicted. The characteristics of the actual and predicted curves in this

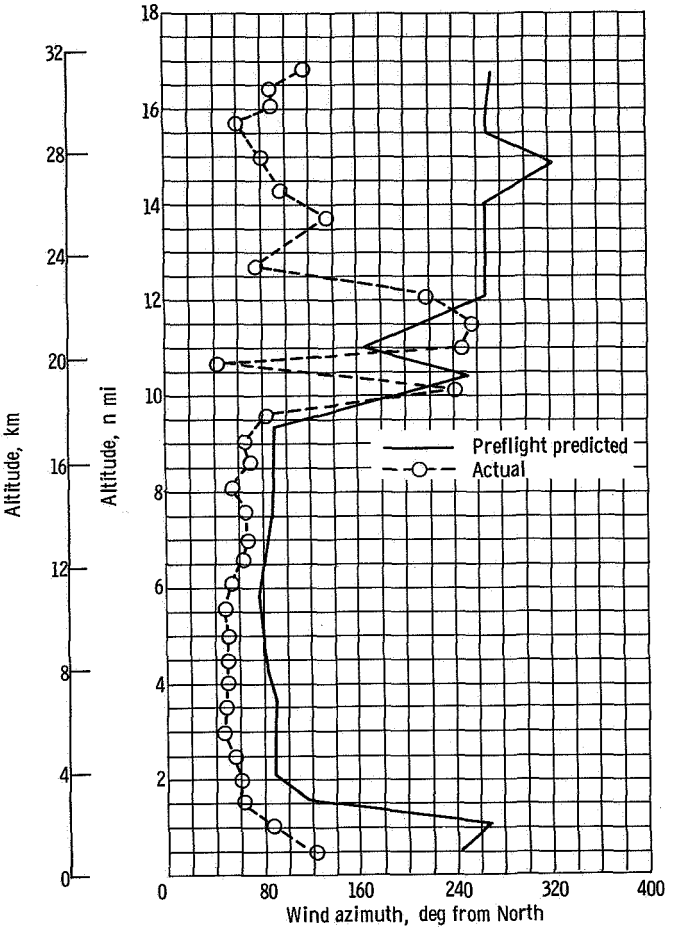

Figure A-4. - Altitude as function of wind azimuth, AC-9.

altitude region are, however, similar. Erratic data occurred, as predicted, between approximately 10 and 12 nautical miles (18.5 and 22.2 km). Above 12 nautical miles (22.2 km), the actual azimuths averaged about 94^{o} from North. The predicted azimuths in this region averaged approximately 279^{o} from North. No wind data were available above about 17.2 nautical miles (31.8 km).

TRAJECTORY DATA

Dynamic Pressure and Mach Number

Dynamic pressure and Mach number data for AC-9 are presented in figures A-5 and A-6, respectively. These data were calculated from downrange tracking data obtained during flight and from atmospheric sounding data taken approximately 3 minutes after launch. The agreement between actual and predicted values of dynamic pressure was

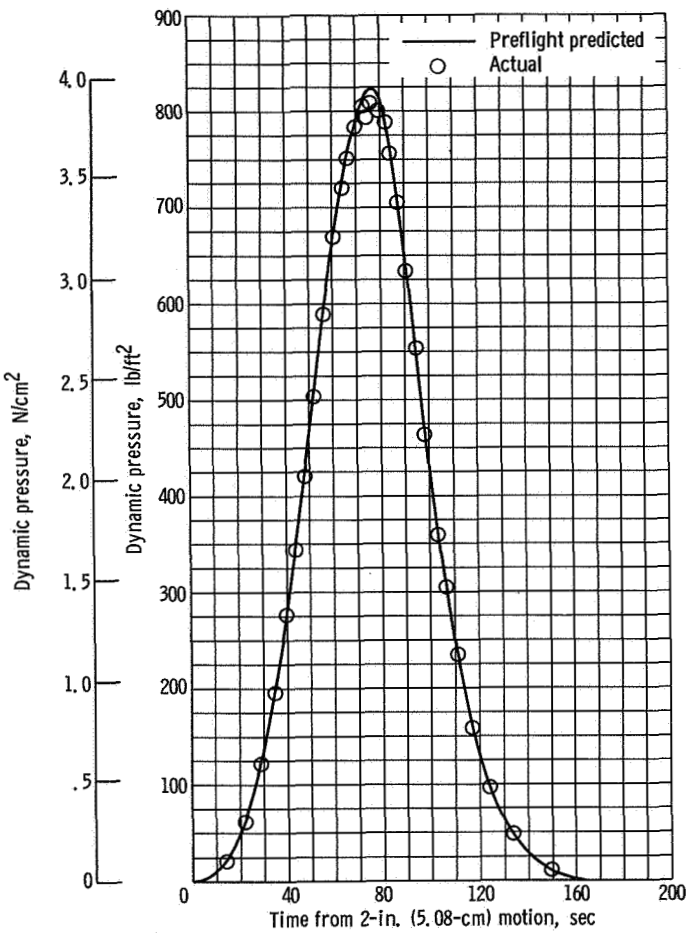

Figure A-5. - Dynamic pressure as function of time, AC-9.

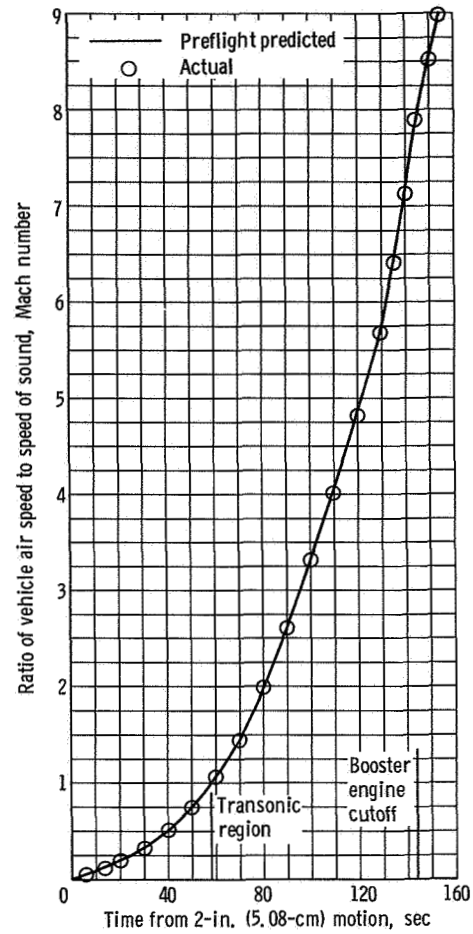

Figure A-6. - Mach number as function of time, AC-9.

good except for the time interval from T + 74 to T + 79 seconds when slight discrepancies were present. All actual data points in this interval are lower than predicted. A peak value of 824 pounds per square foot (3.95 N/cm^2) was predicted at T + 76 seconds. But an actual peak of 808 pounds per square foot (3.88 N/cm^2) was measured at this time. Thus, although the predicted and actual peak values occurred at the same time, the values were different. This difference in peak values, 16 pounds per square foot (0.077 N/cm^2), represents a dispersion of only 1.94 percent. The maximum dispersion between predicted and actual values occurred at T + 74 seconds when the actual value was 21 pounds per square foot (0.101 N/cm^2) lower than predicted. Even this maximum dispersion represented an error of only 2.55 percent.

Dynamic pressure Q is defined as $1/2\ \rho V^2$, where ρ is the atmospheric density and V is the vehicle velocity relative to the atmosphere. Since ρ depends on atmospheric pressure P and on atmospheric temperature T, dispersions in Q can only re-

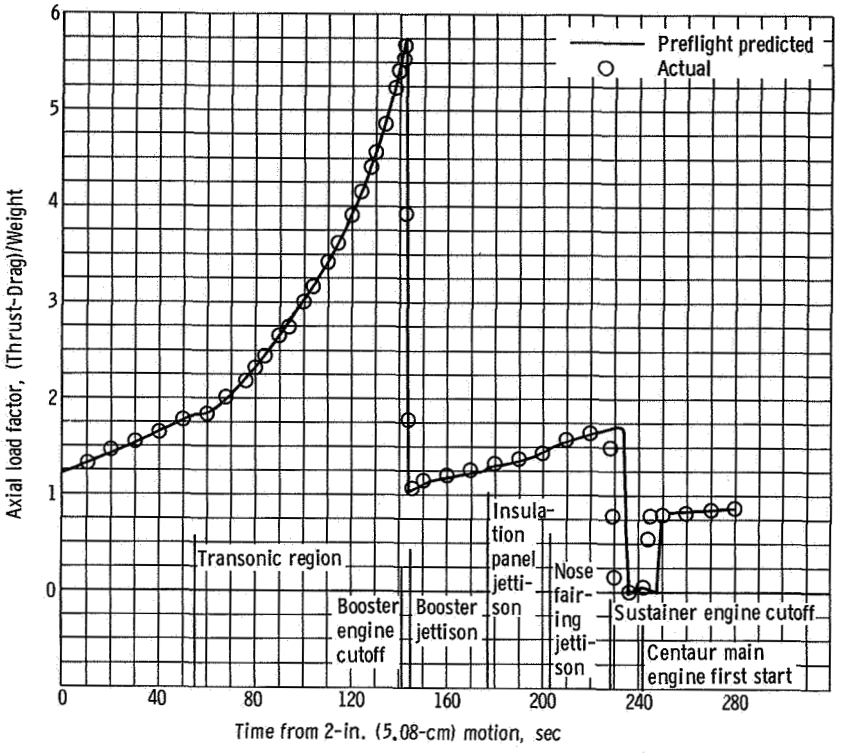

(a) T + 0 to T + 280 seconds.

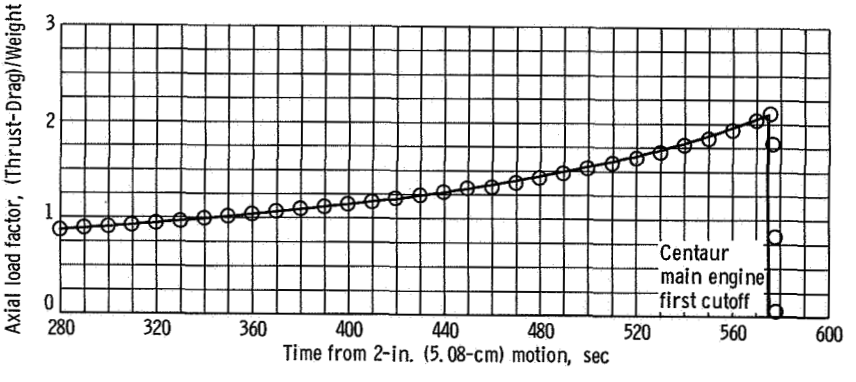

(b) T + 280 to T + 600 seconds.

Figure A-7. - Axial load factor as function of time, AC-9.

sult from dispersions in P, T, or V. Deviations of actual from predicted values of these three parameters completely explain all dynamic pressure dispersions. Every actual data point which disagreed with the value predicted at that time can be precisely correlated with this predicted value if known dispersions in ambient pressure and temperature and vehicle relative velocity (air speed) are considered. Analysis of the data indicates that no single parameter was responsible for the low Q values in the time interval from T + 74 to T + 79 seconds.

Variation of the actual Mach number values (velocity ratios) from the expected

values was negligible over the entire time interval shown in figure A-6. At about T + 58 seconds, the vehicle reached a relative velocity of Mach 1 and thus entered the transonic region (see fig. A-7(a)). The decrease in acceleration, or change in slope, at T + 143.1 seconds was a result of the loss of booster thrust at booster engine cutoff.

Axial Load Factor

The axial load factor for the Atlas and Centaur powered phases of flight is shown in figure A-7. Axial load factor is defined as the ratio of vehicle thrust minus drag over vehicle weight. A plot of the axial load factor is equivalent to a plot of the acceleration, in g's, supplied by thrust alone (thrust acceleration). Actual and predicted data showed good agreement at all times except in the intervals between about T + 230 and T + 250.0 seconds, and between T + 574 and T + 578 seconds.

A flattening of the curve occurs from approximately T + 54 to T + 60 seconds. This interval of constant acceleration reflects the severe vibrations experienced by the vehicle when it passed through Mach 1 (fig. A-6). An abrupt decrease in acceleration from 5.68 to 1.08 g's occurred, as expected, at booster engine cutoff at T + 143.1 seconds. A small but sudden increase in acceleration occurred about 3.5 seconds later to reflect the sudden loss of the booster weight at booster jettison. Following booster jettison, the constantly decreasing vehicle propellant weight caused the acceleration to increase smoothly, except for small perturbations caused by sudden weight losses at insulation panel and nose fairing jettison (T + 177.3 and 203.8 sec, respectively). Sustainer engine cutoff was expected to occur at T + 235.8 seconds; it actually occurred at T + 229.1 seconds. This 6.7-second early shutdown is discussed in the Atlas System Performance section. Since Centaur main engine first start is a timed function from sustainer engine cutoff, the Centaur main engines fired earlier than expected. Consequently, the sudden rise in the axial load factor curve reflecting the Centaur main engine thrust occurred at T + 240.5 seconds, 6.8 seconds earlier than predicted. After the Centaur main engines started, the uniformly decreasing Centaur propellant weight caused the axial load factor to increase again smoothly until termination of the Centaur main engine first burn at T + 577.7 seconds. This firing period was 10.3 seconds longer than predicted. (See Centaur Main Engines System, Performance section.)

Inertial Velocity

Inertial velocity data for the AC-9 flight are presented in figure A-8. Inertial velocity is referenced to a coordinate system which does not rotate with the Earth.

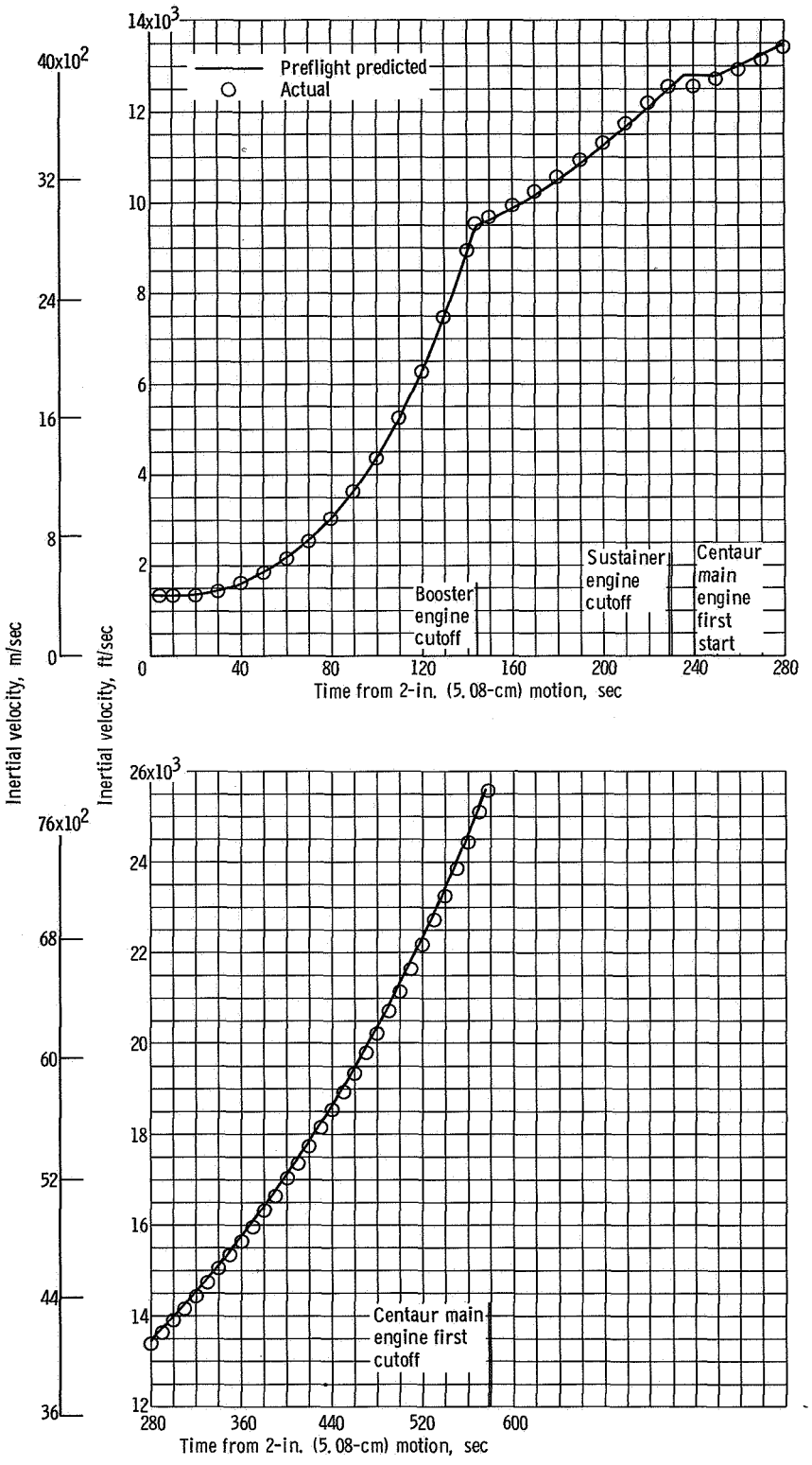

Figure A-8. - Inertial velocity as function of time, AC-9.

Predicted and actual results were in good agreement. As expected, abrupt changes in the vehicle total acceleration, the slope of the inertial velocity curve, coincided with the sharp changes in axial load factor, or thrust acceleration in g's (fig. A-7). From lift-off to booster engine cutoff the agreement between actual and predicted data is excellent. Between booster engine cutoff and sustainer engine cutoff, actual inertial velocities averaged about 1 percent high. The sudden flattening of the curve at sustainer engine cutoff indicates the loss of all thrust. The actual curve shows that the sustainer engine shut off approximately 6.7 seconds earlier than expected. Consequently, the inertial velocities again began to increase approximately 7 seconds sooner than expected when the Centaur main engines started for the first time. From this time until the main engines first shut down, the actual inertial velocities were less than 1 percent lower than predicted. The average deviation between actual and predicted data in this period was approximately 100 feet per second (30.5 m/sec). By Centaur main engine first cutoff, however, the guidance system had compensated for these slightly lower velocities so that the deviation was reduced to only 4 feet per second (1.2 m/sec). This close agreement was essential at this time to ensure the proper energy for the parking orbit.

Altitude and Range Tracking Data

Altitude ground range data are shown in figures A-9 and A-10, respectively. The Earth trace or ground track of the vehicle subpoint, latitude against longitude, is given in figure A-11.

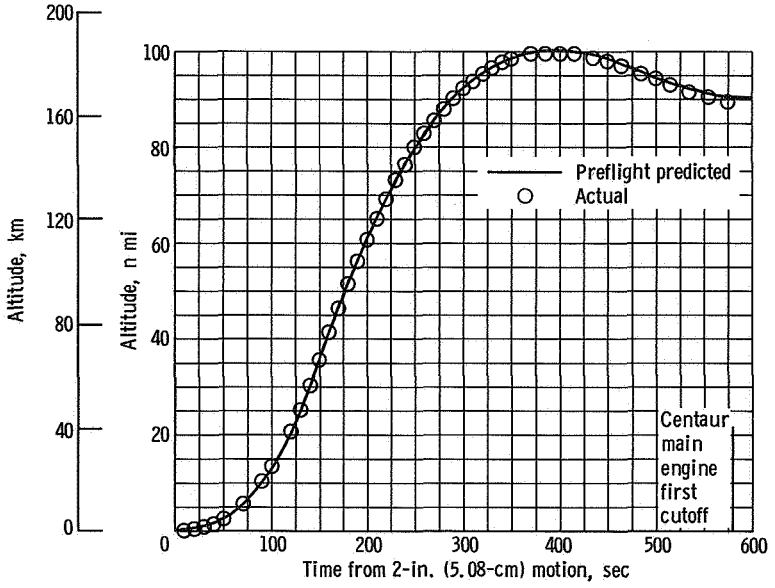

Figure A-9. - Altitude as function of time, AC-9.

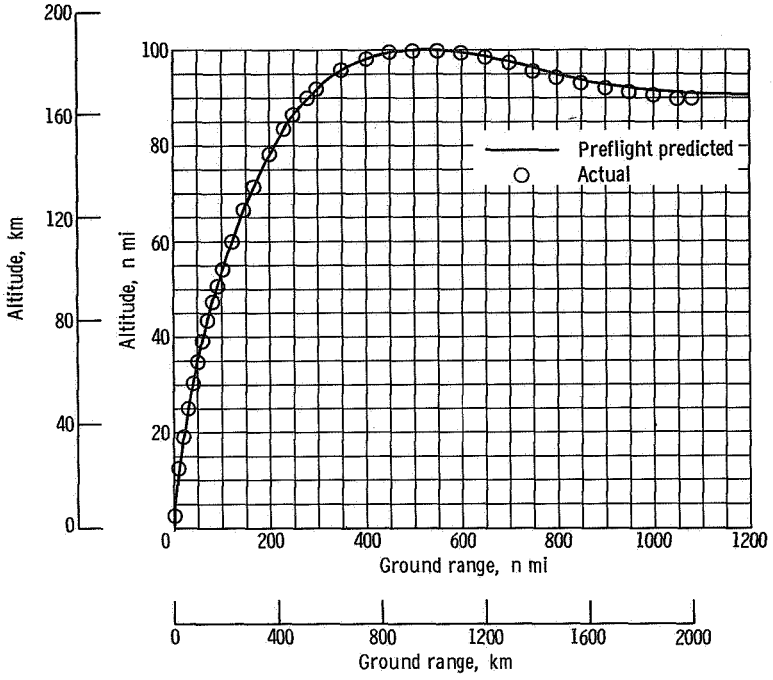

Figure A-10. - Altitude as function of ground range, AC-9.

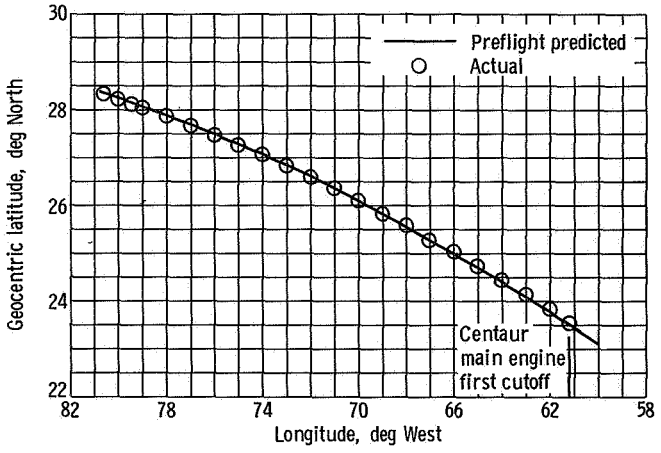

Figure A-11. - Ground trace of vehicle subpoint, AC-9.

Actual and predicted altitudes were in close agreement until approximately T + 375 seconds. Beyond this time, actual altitudes were lower than expected. The maximum deviation was 1.12 nautical miles (2.07 km) at Centaur main engine first cutoff. At this time, the altitude was 89.8 nautical miles (166.1 km). This deviation was well within the designed specification of 90±5 nautical miles (166±9.25 km). The slope of the curve for altitude as a function of time at this time is nearly zero. Thus, because the altitude did not change much after this time, a nearly circular parking orbit was indicated.

The plot of altitude as a function of ground range in figure A-10 shows good agreemei between actual and predicted data until the vehicle was approximately 470 nautical miles (870 km) down range. Beyond this range, the altitudes are slightly lower than expected. This deviation is consistent with that observed in figure A-9.

Geocentric latitude against longitude in figure A-11 shows good agreement between actual and predicted data. At Centaur main engine first cutoff, both the latitude and longitude dispersions were less than 0.1 degree.

Orbital Parameters

Orbital parameters for the Surveyor mass model transfer orbit, the Centaur parking orbit, and the Centaur postretromaneuver orbit are presented in tables A-1

TABLE A-1. - SURVEYOR MASS MODEL ORBIT PARAMETERS, AC-9

Parameter	Value
Time from 2-in. (5.08-cm)	2140.9
Greenwich mean time, hr	11:47:43.8
Apogee altitude, n mi; km	250 921; 465 005
Perigee altitude, n mi; km	89.1; 165.0
Injection energy, C3, km^2/sec^2	-1.66802
Semimajor axis, n mi; km	128 948; 238 966
Eccentricity	0.97262
Orbital inclination, deg	29.64041
Injection true anomaly, deg	4.80185
Injection flight path angle, deg	2.46068
Period, days	13.4
Longitude of ascending node, deg	135.725
Argument of perigee, deg	229.56691
Geocentric latitude at Centaur main engine second cutoff, deg South	23.70
Longitude at Centaur main engine second cutoff, deg East	32.73

TABLE A-2. - CENTAUR PARKING ORBIT PARAMETERS, AC-9

Parameter	Value
Time from 2-in. (5.08-cm) motion, sec	1634.2
Greenwich mean time, hr	1139:16.794
Apogee altitude, n mi; km	89.97; 166.73
Perigee altitude, n mi; km	86.13; 159.61
Injection energy, C_3, km^2/sec^2	-60.937
Semimajor axis, n mi; km	3532; 6545
Eccentricity	0.000544
Orbital inclination, deg	29.6506
Period, min	87.75
Inertial velocity at Centaur main engine first cutoff, ft/sec; m/sec	25 575; 7795
Earth relative velocity at Centaur main engine first cutoff, ft/sec; m/sec	24 175; 7368
Geocentric latitude at Centaur main engine first cutoff, deg North	23.57
Longitude at Centaur main engine first cutoff, deg West	61.22

TABLE A-3. CENTAUR POSTRETROORBITAL PARAMETERS, AC-9

Parameter	Value
Time from 2-in. (5.08-cm) motion, sec	20 211.1
Greenwich mean time, hr	1648:53.7
Apogee altitude, n mi; km	188 570; 349 455
Perigee altitude, n mi; km	91.28; 169.16
Injection energy, C_3, km^2/sec^2	-2.201
Semimajor axis, n mi; km	97 709; 181 073
Eccentricity	0.963844
Orbital inclination, deg	29.6244
Period, days	8.8

to A-3, respectively. The reference time for the data defining the mass model orbit is that time when Centaur main engine second cutoff occurred. The Centaur parking orbit is based on guidance data obtained during the coast phase, 1056.5 seconds after Centaur main engine first cutoff. The postretroorbit is based on Eastern Test Range tracking data.

LAUNCH WINDOWS AND COUNTDOWN HISTORY

No actual lunar intercept was intended for the Surveyor mass model launched by AC-9 on October 26, 1966. In order to simulate an actual lunar-intercept trajectory for this mission, the Earth-Moon geometry for a January 24, 1967 launch day was assumed. Consequently, the geometric constraints which limit an actual lunar-intercept-mission launch opportunity to a specified number of days were not present for the launch of AC-9.

The duration of the launch window on any specific day was, however, limited by a coast time constraint. Flight experience with a Centaur coast period between 23 and 25 minutes was desired. As a result, the daily launch window duration was limited to 38 minutes. The coast was also required to occur in sunlight. Therefore, the earliest possible launch time was 0600 eastern standard time.

The countdown for the first attempt to launch AC-9 on October 25, 1966 proceeded normally down to T - 5 minutes. At this time, the launch was aborted because of an unacceptable liquid-oxygen-pump inlet-temperature indication. This temperature was considered to be a prime measurement for a research and development flight.

The second launch attempt resulted in a successfull lift-off at 0612:02.6 eastern standard time on October 26, 1966, about 12 minutes into the window. The slight delay was caused by a temporary problem encountered in arming the mass model inert destruct unit.

VEHICLE WEIGHT SUMMARIES

The postflight weight summaries for the Centaur and Atlas are presented in tables A-4 and A-5, respectively.

TABLE A-4 CENTAUR WEIGHTS SUMMARY, AC-9

	Weight	
	lb	kg
Basic hardware:		
Body	994	451
Propulsion group	1 235	559
Guidance group	339	154
Control group	148	67
Pressurization group	201	91
Electrical group	276	125
Separation group	77	35
Flight instrumentation	547	248
Miscellaneous equipment	338	153
Total	4 155	1 883
Jettisonable hardware:		
Nose fairing	2 033	921
Insulation panels	1 218	552
Ablated ice	50	23
Total	3 301	1 496
Centaur residuals:		
Liquid-hydrogen residual	150	68
Liquid-oxygen residual	290	131
Gaseous hydrogen	116	52
Gaseous oxygen	170	77
Hydrogen peroxide	33	15
Helium	4	2
Ice	12	5
Total	775	350
Centaur expendables:		
Main impulse hydrogen	4 805	2 177
Main impulse oxygen	24 794	11 232
Gas boiloff on ground hydrogen	6	3
Gas boiloff on ground oxygen	21	9
In-flight chill hydrogen	65	29
In-flight chill oxygen	77	35
Booster phase vent hydrogen	40	18
Booster phase vent oxygen	80	36
Sustainer phase vent hydrogen	18	8
Sustainer phase vent oxygen	30	14
Engine shutdown loss hydrogen:		
First shutdown loss	6	3
Second shutdown loss	6	3
Engine shutdown loss oxygen:		
First shutdown loss	18	8
Second shutdown loss	18	8
Parking orbit vent hydrogen	47	21
Parking orbit vent oxygen	0	0
Parking orbit leakage hydrogen	0	0
Parking orbit leakage oxygen	0	0
Hydrogen peroxide	202	91
Helium	6	3
Total	30 239	13 698
Total tanked weight	38 470	17 427
Minus ground vent	-27	-12
Total Centaur weight at lift-off	38 443	17 415

TABLE A-5. - ATLAS WEIGHTS SUMMARY, AC-9

	Weight	
	lb	kg
Booster jettison weight:		
Booster dry weight	6 220	2 818
Booster residuals	1 117	506
Unburned lubrication oil	28	13
Total	7 365	3 337
Sustainer jettison weight:		
Sustainer dry weight	5 600	2 537
Sustainer residuals	1 778	805
Interstage adapter	1 023	463
Unburned lubrication oil	28	13
Total	8 429	3 818
Flight expendables:		
Main impulse RP-1	75 502	34 202
Main impulse oxygen	171 526	77 701
Helium-panel purge	6	3
Oxygen vent loss	15	7
Lubrication oil	3	1
Total	247 052	111 914
Ground expendables:		
Fuel	550	249
Oxidizer	1 731	784
Lubrication oil	3	1
Exterior ice	50	23
Liquid nitrogen in helium shrouds	140	63
Pre-ignition gaseous oxygen loss	450	204
Total	2 924	1 324
Total tanked weight	265 770	120 393
Minus ground run	-2 924	-1 324
Total Atlas weight at lift-off	262 846	119 069
Spacecraft[a]	1 741	788
Total Atlas-Centaur-spacecraft lift-off weight	303 030	137 272

[a]See MISSION PERFORMANCE section, p. 15.

FLIGHT TIMES

A comparison of preflight and actual times is presented in table A-6.

TABLE A-6. - EVENT TIMES, AC-9

Event	Programmer time, sec	Preflight time, sec	Actual time, sec
Lift-off (2-in. (5.08-cm) motion)	T + 0.0	T + 0.0	T + 0.0
Start roll	T + 2.0	T + 2.0	T + 2.0
End roll	T + 15.0	T + 15.0	T + 15.4
Start pitchover	T + 15.0	T + 15.0	T + 15.4
Booster engine cutoff	BECO	T + 142.8	T + 143.1
Jettison booster package	BECO + 3.1	T + 145.9	T + 146.6
Jettison insulation panels	BECO + 34.0	T + 176.8	T + 177.3
Jettison nose fairing	BECO + 61.0	T + 203.8	T + 203.8
Start Centaur boost pumps	BECO + 62.0	T + 204.8	T + 204.8
Sustainer engine cutoff; vernier engine cutoff; start Centaur programmer	SECO	T + 235.8	T + 229.1
Atlas-Centaur separation	SECO + 1.9	T + 237.7	T + 231.0
Centaur main engine first start	SECO + 11.5	T + 247.3	T + 240.5
Centaur main engine first cutoff	MECO 1	T + 574.2	T + 577.7
Start propellant settling engines	MECO 1	T + 574.2	T + 577.7
Stop propellant settling engines; start propellant settling engines	MECO 1 + 76.0	T + 650.2	T + 653.6
Stop propellant retention engines; start propellant retention engines	MES 2 - 40.0	T + 1993.5	T + 1994.8
Start Centaur boost pumps	MES 2 - 28.0	T + 2005.5	T + 2007.0
Centaur main engine second start	MES 2	T + 2033.5	T + 2034.7
Stop propellant settling engines	MES 2	T + 2033.5	T + 2034.7
Centaur main engine second cutoff	MECO 2	T + 2140.6	T + 2140.9
Mass model separate	MES 2 + 176.0	T + 2209.5	T + 2210.8
Start turnaround	MES 2 + 181.0	T + 2214.5	T + 2216.0
Start propellant settling engines[a]	MES 2 + 219.0	T + 2254.5	T + 2251.0
Stop propellant settling engines[a]	MES 2 + 238.0	T + 2274.5	T + 2271.0
Start discharge of Centaur residual propellants	MES 2 + 416	T + 2449.5	T + 2451.0
End discharge of Centaur residual propellants	MES 2 + 666	T + 2699.5	T + 2701.0
Energize power changeover	MES 2 + 766	T + 2799.5	T + 2801.0

[a]Lateral thrust imparted to Centaur for additional longitudinal separation from spacecraft.

APPENDIX B

CENTAUR PERFORMANCE CALCULATIONS

by William A. Groesbeck, Ronald W. Ruedele, and John J. Nieberding

Flight values of engine thrust, engine specific impulse, and oxidizer to fuel mixture ratio were calculated using the Pratt & Whitney characteristic velocity (C*) iteration and the Pratt & Whitney regression methods. In addition, vehicle specific impulse was calculated by the guidance thrust velocity method. The Pratt & Whitney techniques calculate individual engine performance at discrete times. In contrast, the guidance thrust velocity method calculates average vehicle performance over an interval of time. The calculated engine specific impulse using the C* method was approximately 443 seconds.

The guidance thrust velocity method gave an average vehicle specific impulse of approximately 441 seconds. These values are considered to be in good agreement. A comparison of the specific engine data calculated by the Pratt & Whitney C* and the regression methods is shown in figure V-7. The Pratt & Whitney and guidance thrust velocity calculation techniques are discussed in the following sections.

Methods of Calculation

Pratt & Whitney C* Iteration Technique

This technique is an iteration process for determining engine performance parameters. Flight data are used with calibration coefficients obtained from the engine acceptance tests. Calculations are made to determine C*, individual propellant weight flow rates, and subsequently specific impulse and engine thrust. The procedure is as follows:

(1) Calculate hydrogen flow rate by using acceptance test calibration data and venturi measurements of pressure and temperature as obtained from telemetry.

(2) Assume a given mixture ratio and calculate corresponding oxidizer flow rate and total propellant flow rate.

(3) Obtain C* ideal from performance curve as a function of mixture ratio.

(4) Correct to C* actual by using C* efficiency factor obtained from acceptance test results.

(5)Calculate total propellant flow rate by using C* actual

$$\dot{w}_t = \frac{p_o A_t g}{C^*}$$

where $\dot{w}_t$ is the total engine propellant flow rate, p_o is the measured chamber pressure from telemetry, A_t is the thrust chamber throat area, g is the gravitational acceleration at the Earth's surface, and C* is characteristic velocity.

(6) Determine mixture ratio by using calculated total propellant flow rate and measured hydrogen flow rate.

(7) Compare calculated mixture ratio with that assumed in step (2).

(8) If the two values of mixture ratio do not agree, assume a new value of the mixture ratio and repeat the process until agreement is obtained.

(9) When the correct mixture ratio is determined, obtain the ideal specific impulse from performance data as a function of actual mixture ratio.

(10) Correct to the actual specific impulse by using specific impulse efficiency factor determined from acceptance test results.

(11) Calculate the engine thrust as the product of propellant flow rate and specific impulse.

Pratt & Whitney Aircraft Regression Technique

This program determines engine thrust, specific impulse, and propellant mixture ratio from flight values of engine inlet pressures, engine inlet temperatures, and propellant utilization valve angle. The program is strongly dependent on engine ground testing. The method in which ground testing is correlated with the flight is as follows.

A large group of RL10A-3-3 engines were ground tested. An average level of engine performance was obtained as a function of engine pump inlet pressures, inlet temperatures, and the propellant utilization valve angle. During any specific engine acceptance test, the differences in performance from this average level are noted.

Flight performance is then determined in two steps: (1) the average engine level of performance is obtained for flight values of engine inlet conditions and propellant utilization valve angle, and (2) corrections are made for the difference between the average engine level and the specific engine level, as noted during the engine acceptance testing.

Guidance Thrust Velocity Method

The guidance thrust velocity method computes Centaur vehicle specific impulse by using guidance-computed inertial thrust velocities. Vehicle specific impulse is defined as

$$\left(I_{sp}\right)_v = \frac{|\vec{F}|}{\dot{W}} \tag{B1}$$

where $|\vec{F}|$ is the magnitude of the total Centaur thrust vector, and $\dot{W}$ is the time rate of change of instantaneous total Centaur weight (total instantaneous weight flow).

It should be noted that vehicle specific impulse differs from the engine specific impulse which is defined as

$$\left(I_{SP}\right)_e = \frac{|\vec{F}|}{\dot{w}_t} \tag{B2}$$

where $\dot{w}_t$ is the total Centaur main engine propellant flow rate. The time rate of change of total Centaur weight in equation (B1) includes weight losses, due to hydrogen peroxide used to drive the boost pumps, and all other losses in addition to the total propellant flow rate through the engines. Consequently, the vehicle specific impulse would be less than the engine specific impulse. Vehicle specific impulse is a measure of total vehicle performance, whereas engine specific impulse is an index of engine performance only.

The derivation of vehicle specific impulse is based on the Centaur vehicle vector equation of motion

$$\vec{F} + M\vec{G} - \vec{X} = M\vec{A} \tag{B3}$$

where $\vec{F}$ is the Centaur total instantaneous thrust vector, M is the Centaur instantaneous mass, $\vec{G}$ is the Centaur instantaneous acceleration vector due to gravity, $\vec{X}$ is the instantaneous force vector due to drag or other perturbing forces, and $\vec{A}$ is the Centaur total instantaneous acceleration vector. It was assumed that drag and other perturbing forces are negligible over the time interval of interest, that the time rate of change of total Centaur weight is either constant or at least varies symmetrically about a mean value over this invertal, and that only a negligible amount of axial thrust is lost as the result of engine gimbaling. Based on these assumptions, the equation of motion can be rewritten as

$$\vec{F} = M(\vec{A} - \vec{G})$$

or

$$\frac{\vec{F}}{M} = (\vec{A} - \vec{G}) \tag{B4}$$

The acceleration $\vec{A} - \vec{G}$, designated as the thrust acceleration, is the acceleration imparted to the Centaur by thrust alone. It is obtained as the time rate of change of the inertial thrust velocity which is computed by the guidance system.

The thrust acceleration is used in a computer program to calculate the vehicle axial load factor, and this load factor is then used to determine the total vehicle specific impulse. Axial load factor, which is defined as the ratio of vehicle thrust minus drag

over vehicle weight, is obtained by dividing the magnitude of the thrust acceleration in equation (B4) by g

$$\frac{|\vec{F}|}{Mg} = \frac{|\vec{A} - \vec{G}|}{g} \tag{B5}$$

where g is the gravitational acceleration at the Earth's surface. But

$$\frac{|\vec{F}|}{Mg} = \frac{|\vec{F}|}{W} \equiv \alpha \tag{B6}$$

where $W = Mg$ is the instantaneous total Centaur weight and α is the axial load factor. If the instantaneous Centaur weight is written as

$$W = W_o - \dot{W}(t - t_o) = W_o - \dot{W}\Delta t \tag{B7}$$

where W_o is the total Centaur weight at main engine first start, t_o is the time of main engine first start (measured from lift-off), t is instantaneous time from lift-off, and $\Delta t = t - t_o$ and this substitution is made in equation (B6), the result is

$$\alpha = \frac{|\vec{F}|}{W} = \frac{|\vec{F}|}{W_o - \dot{W}\Delta t} \tag{B8}$$

The reciprocal of this equation is

$$\frac{1}{\alpha} = \frac{W_o - \dot{W}\Delta t}{|\vec{F}|} = \frac{W_o}{|\vec{F}|} - \frac{\dot{W}\Delta t}{|\vec{F}|} \tag{B9}$$

If W and F are constant, a plot of $1/\alpha$ as a function of Δt is a straight line with a slope equal to $-(\dot{W}/|\vec{F}|)$. Since by definition, the vehicle specific impulse is

$$\left(I_{sp}\right)_v = \frac{|\vec{F}|}{\dot{W}}$$

the slope $-(\dot{W}/|\vec{F}|)$ is the negative reciprocal of the vehicle specific impulse. The computer program therefore determined the specific impulse by

(1) Calculating thrust acceleration based on guidance-computed inertial thrust velocities

(2) Computing axial load factor from equation (B5)

(3) Plotting the reciprocal of the axial load factor as a function of time

(4) Curve fitting the reciprocal of axial load factor as a function of time with a straight line by using the method of least squares

(5) Taking the negative reciprocal of line slope to obtain the average value of vehicle specific impulse for the time interval considered

The time interval for calculating the Centaur vehicle specific impulse on AC-9 was from T + 400 to T + 570 seconds. During this interval, the propellant utilization valve motion was approximately symmetrical about a mean value; consequently, the mean values of thrust and weight flow could be assumed constant. Calculations were made for 171 data points, and the resultant vehicle specific impulse was 441.3 seconds.

REFERENCES

1. Staff of the Lewis Research Center: Postflight Evaluation of Atlas-Centaur AC-8 (Launched April 7, 1966). NASA TM X-1343, 1967.

2. Foushee, B. R.: Liquid Hydrogen and Liquid Oxygen Density Data for Use in Centaur Propellant Loading Analysis. Rep. AE62-0471, General Dynamics Corp., May 1, 1962.

3. Pennington, K., Jr.: Liquid Oxygen Tanking Density for the Atlas-Centaur Vehicles. Rep. BTD 65-103, General Dynamics Corp., June 3, 1965.

4. Groesbeck, William A.: Design of Coast-Phase Propellant Management System for Two-Burn Atlas-Centaur Flight AC-8. NASA TM X-1318, 1966.

5. Gerus, Theodore F.; Housely, John A.; and Kusic, George: Atlas-Centaur-Surveyor Longitudinal Dynamics Tests. NASA TM X-1459, 1967.

"The aeronautical and space activities of the United States shall be conducted so as to contribute . . . to the expansion of human knowledge of phenomena in the atmosphere and space. The Administration shall provide for the widest practicable and appropriate dissemination of information concerning its activities and the results thereof."

—NATIONAL AERONAUTICS AND SPACE ACT OF 1958

NASA SCIENTIFIC AND TECHNICAL PUBLICATIONS

TECHNICAL REPORTS: Scientific and technical information considered important, complete, and a lasting contribution to existing knowledge.

TECHNICAL NOTES: Information less broad in scope but nevertheless of importance as a contribution to existing knowledge.

TECHNICAL MEMORANDUMS: Information receiving limited distribution because of preliminary data, security classification, or other reasons.

CONTRACTOR REPORTS: Scientific and technical information generated under a NASA contract or grant and considered an important contribution to existing knowledge.

TECHNICAL TRANSLATIONS: Information published in a foreign language considered to merit NASA distribution in English.

SPECIAL PUBLICATIONS: Information derived from or of value to NASA activities. Publications include conference proceedings, monographs, data compilations, handbooks, sourcebooks, and special bibliographies.

TECHNOLOGY UTILIZATION PUBLICATIONS: Information on technology used by NASA that may be of particular interest in commercial and other non-aerospace applications. Publications include Tech Briefs, Technology Utilization Reports and Notes, and Technology Surveys.

Details on the availability of these publications may be obtained from:

SCIENTIFIC AND TECHNICAL INFORMATION DIVISION

NATIONAL AERONAUTICS AND SPACE ADMINISTRATION

Washington, D.C. 20546